UNIVERSITY OF CALIFORNIA SAN DIEGO

Extracellular vesicles from endothelial colony forming cells in the repair of ischemic retinal disease

A dissertation submitted in partial satisfaction of the requirements for the degree Doctor of Philosophy

in

Bioengineering

by

Kyle Marra

Committee in charge:

Professor Adam Engler, Chair
Professor Martin Friedlander, Co-Chair
Professor Daniel Chao
Professor Brian Eliceiri
Professor Gabriel Silva
Professor Emily Wang

2021

The Dissertation of Kyle Marra is approved, and it is acceptable in quality and form for publication on microfilm and electronically.

University of California San Diego

2021

DEDICATION

This doctoral dissertation is dedicated to my mother Rosemarie Marra, a teacher and mother to all those around her.

Thanks mom for teaching us all to love to learn, to develop our individual arts, to be present, to absorb experiences, to speak up, to be confident, to care about others, to radiate cheerfulness, to share what we have without expectations, to love without doubt, to celebrate those who are happy and to listen to those who are sad, to give praise to those who've achieved and empower those who are trying, to substitute frustration with patience, to wear a smile, to "just buy it!," to instill others with willpower, to introduce ourselves, to go the above and beyond, to dress for success, to never quit, to ask, and to laugh louder and harder.

EPIGRAPH

The road to wisdom? — Well, it's plain and simple to express:
Err
and err
and err again
but less
and less
and less.

~ Piet Hein

TABLE OF CONTENTS

LIST OF ABBREVIATIONS

AAV.COMP-Ang1	Adeno-associated virus serotype 2 encoding a more stable, soluble, and potent formulation of angiopoietin 1
AKI	Acute kidney injury
α-SMA	Alpha-smooth muscle actin
Ang	Angiopoietin
BRMVEs	Bovine retinal microvessel endothelial cells
CACs	Circulating angiogenic cells
CD144/VE	Vascular endothelial-cadherin
$CD44^{hi}$ ECFCs	Endothelial colony forming cells with high CD44 expression
$CD44^{lo}$ ECFCs	Endothelial colony forming cells with low CD44 expression
CECs	Circulating endothelial cells
CFU-Hill	Colony forming unit-Hill
CM	Conditioned media
CNV	Choroidal neovascularization
ECFCs	Endothelial colony forming cells
ECM	Extracellular matrix
ECs	Endothelial cells
eNO	Endothelial nitric oxide
eNOS	Endothelial nitrous oxide synthase
EPCs	Endothelial progenitor cells
ERG	Electroretinography
ERK	Extracellular signal-regulated kinase

ESCRT	Endosomal sorting complexes required for transport
EVs	Extracellular vesicles
EVs^{ECFCs}	Extracellular vesicles from endothelial colony forming cells
EVs^{HCAECs}	Extracellular vesicles from HCAECs
FGF	Fibroblast growth factor
GFP	Green fluorescent protein
H/R	Hypoxia-reperfusion
HA	Hyaluronic acid
HAECs	Human aortic endothelial cells
HBMECs	Human brain microvascular endothelial cells
HCAECs	Human coronary artery endothelial cells
HCAECs	Human coronary artery endothelial cells
HGF	Hepatocyte growth factor
HGS	Hepatocyte growth factor-regulated tyrosine kinase substrate
HIF-1α	Hypoxia-inducible factor 1-alpha
hiPSCs	Induced pluripotent stem cells
HITA	Human internal thoracic artery
HLA	Human leukocyte antigens
HMECs	Human microvascular endothelial cells
HMGB1	High mobility group box-1
HPP	High proliferative potential
hRMECs	Human retinal microvascular endothelial cells
HSCs	Hematopoietic stem cells

HUVECs	Human umbilical vein cells
IA	Immunoaffinity isolation
ICAM-1	Intercellular adhesion molecule-1
IGFBP	Insulin-like binding protein
IGFs	Insulin-like growth factors
IL	Interleukin
ILVs	Intraluminal vesicles
INL	Inner nuclear layer
iNOS	Inducible nitrous oxide synthase
IPL	Inner plexiform layer
LIF	Leukemia inhibiting factor
LPS	Lipopolysaccharide
MACs	Myeloid angiogenic cells
MIP	Macrophage inflammatory protein
miR	MicroRNA
MMPs	Matrix metalloproteinases
MNCs	Mononuclear cells
MSCs	Mesenchymal stem cells
MVB	Multivesicular bodies
NO	Nitric oxide
NOD/SCID	Nonobese diabetic/severe combined immunodeficiency
OIR	Oxygen-induced retinopathy
PARP	Poly ADP ribose polymerase

PB	Peripheral blood
PDGF-BB	Platelet derived growth factor-BB
PDGFR-β	Platelet derived growth factor receptor
PDR	Proliferative diabetic retinopathy
PEG	Poly-ethylene glycol
PIK3R2	Phosphoinositide-3-kinase regulatory subunit 2
PIK3R2	Phosphoinositol-3 kinase regulatory subunit 2
PIP2	Phosphatidylinositol 4,5-bisphosphate
PIP3	Phosphatidylinositol (3,4,5)-trisphophates
PSGL-1	P-selectin glycoprotein ligand-1
PTEN	Phosphatase and tensin homolog
RBMECs	Rat brain microvascular endothelial cells
RD10, Pde6brd10/rd10	Retinal degeneration 10 mouse model
RG16	Regulator of G protein signaling 16
RISC	RNA-induced silencing complex
ROP	Retinopathy of prematurity
SAECs	Human small airway epithelial cells
SASP	Senescence-associated secretory phenotype
SDF	Stromal derived factor
SEC	Size exclusion chromatography
sECFCs	Endothelial colony forming cells subjected to starvation
SMCs	Smooth muscle cells
SP	Side population

SPRED1	Sprouty-related protein-1
STAT-3	Signal transducer and activator transcription-3
STZ	Streptozotocin
TBI	Traumatic brain injury
TEnCs	Peritubular endothelial cell
TEpCs	Tubular epithelial cells
Th-17 cells	T-helper-17 cells
TIMP-1	Tissue inhibitor of metalloproteinase-1
TLRs	Toll-like receptors
UC	Ultracentrifugation
UCB	Umbilical cord blood
UF	Ultrafiltration
UF-SEC-UF	Serial ultrafiltration, size exclusion chromatography, then repeated UF
VCAM	Vascular cell adhesion molecule
VEGF	Vascular endothelial growth factor
VEGFR-2, KDR, Flk-1 (in mice)	Vascular endothelial growth factor receptor-2
VLA-4; CD49d/CD29	Very-late antigen 4
VO	Vaso-obliteration
vWF	von Willebrand factor
ZO	Zonula occludens

LIST OF FIGURES

LIST OF SCHEMES

LIST OF TABLES

ACKNOWLEDGEMENTS

I'd like to acknowledge my family for their endless support of my personal, educational, and career goals throughout my life. I offer my deepest gratitude to my parents, Rosemarie and Vincent Marra, as well as my sister, Lauren Marra, whose love and sacrifice have provided me with endless opportunities. My family encouraged me to live with excitement and passion, and through their example I have learned to live a healthy, balanced life of happiness and purpose. My friends have been another source of unending support, and I'm grateful for their camaraderie and community. I also wish to acknowledge my high school physics and music teacher Mr. Gregory Devine, who's support and inspirational teaching inspired me at a young age to pursue an undergraduate B.S. in Physics and this Ph.D. in Bioengineering.

It is my pleasure to acknowledge the roles of several individuals and institutions that were instrumental to the completion of my dissertation research. First, I would like to express gratitude to my PhD Advisor and Committee Co-chair Martin Friedlander, MD, PhD, who was an incredible source of support. Marty encouraged me to push the boundaries of my projects and created a sociable and hard-working environment that catered to the sharing of ideas and enhancement of science. In addition to providing me with the resources and connections to pursue my research goals, Dr. Friedlander exposed me to the wide spectrum of opportunities presented by a career in academic medicine. I was privileged with numerous and varied opportunities to pursue my passion for this field of research.

I'd like to acknowledge current and former colleagues that were instrumental throughout my training. Edith Aguilar is a research associate for the Friedlander lab whose expertise in lab techniques for retina research was absolutely instrumental in the completion of this work. Guoqin Wei and Ayumi Ouchi were post-docs in Dr. Friedlander's lab at Scripps Research

during the latter years of my PhD and provided critical assistance with experimental design and feedback on results. Alex Ideguchi is the animal technetium for the Friedlander lab and was extremely helpful in overseeing our mice colonies and animal models. Edith, Guoqin, Ayumi, and Alex created an open and friendly work environment that encouraged the exchange of ideas. Outside of lab, I enjoyed our lab's dinners while learning more about Chinese and Japanese cuisine and culture. When I arrived at Scripps Research, Felicitas Bucher and Susumu Sakimoto were post-docs in Dr. Friedlander's lab who helped train me in wet lab techniques. Susumu specifically trained me on many cell culture techniques needed for this dissertation. I'd also like to acknowledge Marin Gantner and Kevin Eade, staff scientists at Dr. Friedlander's laboratory at the Lowy Medical Research Institute (LMRI), as well as Rebecca Berlow, a Staff Scientist in the Wright laboratory at Scripps Research, who also assisted training me and provided important feedback during our joint lab meetings. I would also like to thank other members of Dr. Friedlander's labs at Scripps Research and LMRI including Jennifer Trombley, Sarah Harkins-Perry, Simone Tzaridis, Regis Fallon, Sarah Gillies, Michael Dorrell, Lea Schepke, Katherina Nado, Marti Lynn Moon, and Jessica Orozco.

I must acknowledge those outside of the Friedlander labs who provided input and/or direct assistance on experiments and techniques used in this dissertation. Throughout my PhD, Brian Seegers and Brian Monteverna in the Flow Cytometry Core facility at Scripps Research trained me on flow cytometry and helped run and oversee my cell sorts. Scott Henderson and Theresa Fassel in the Microscopy Core at Scripps Research assisted my use of transmission electron microscopy to image my samples. Dr. Louise Laurent and Dr. Peter DeHoff at the Sanford Consortium for Regenerative Medicine were instrumental in assisting with the experimental design and execution of RNA sequencing experiments. John Nolan and researchers

at Cellarcus Biosciences assisted by performing single particle flow cytometry experiments. Measurements using nanoparticle tracking analysis on the ViewSizer3000 were performed by the helpful employees of HORIBA Inc. and MANTA (which was acquired by HORIBA) including Cindy Rosal, Anderson Bonon, Kuba Tatarkiewicz, and Rick Cooper. Wonjun Yim also assisted with nanoparticle tracking analysis measurements using a MANTA ViewSizer3000 afforded to the lab of Dr. Jesse Jokerst by grant S10 OD023555. I also sincerely appreciate all the feedback and advice provided by my committee members: Drs. Daniel Chao, Brian Eliceiri, Adam Engler, Gabriel Silva, and Emily Wang.

This research would not have been possible without generous funding. I'd like to thank the National Eye Institute at the National Institute of Health for awarding me with an F30 grant (EY029141), the Medical Scientist Training Program at the University of San Diego, California for supporting me with a T32 grant (GM007198-40), and the Frank Lowy and the Lowy family for their overwhelming generosity in funding provided to the Friedlander lab.

Chapters 1 and 2 are currently being prepared for submission for publication of the material. Marra, KV; Friedlander, M. The dissertation author was the primary investigator and author of this material.

Chapter 3, in part, has been submitted for publication of the material as it may appear in Nature Medicine, 2021, Marra, KV; Aguilar, E; Usui-Ouchi A; Wei, G; Ideguchi, A; Sakimoto, S; Friedlander, MF. "Bioactive extracellular vesicles from a subset of endothelial progenitor cells rescue retinal ischemia and neurodegeneration." The dissertation author was the primary investigator and author of this material.

Chapter 4, in full, is a reprint of the materials as it appears in The Journal of Clinical Investigation Insight, 2017. Xiao, S; Bucher, F; Wu, Y; Rokem, A; Lee, CS; Marra, KV; Fallon,

R; Diaz-Aguilar, S; Aguilar, E; Friedlander, M; Lee AY. The dissertation author was a co-investigator and co-author of this material.

Chapter 5, in full, is a reprint of the materials as it appears in Investigative Ophthalmology & Visual Science, 2020. Bucher, F; Aguilar, E; Marra, KV; Rapp, J; Arnold, J; Diaz-Aguilar, S; Lange, C; Agostini, H; Schlunck, G; Stahl, A; Friedlander, M. The dissertation author was a co-investigator and co-author of this material. Work completed by the dissertation author contributed to generation of Figure 1 and Figure 4.

VITA

EDUCATION:

2012	Bachelor of Science, Physics. Boston College, Boston MA *Magna cum Laude*. Scholar of the College, Honors Thesis: "Implementation of a Peltier-based cooling device for localized deep cortical deactivation during in vivo object recognition testing"
2021	Doctor of Philosophy, Bioengineering. University of California San Diego. Dissertation: "Extracellular vesicles from endothelial colony forming cells in the repair of ischemic retinal disease"
2014-Present	Medical Student, University of California San Diego

POSITIONS:

2008-2009	Research Intern, Boston College, Boston MA (Ellen Walker, PhD)
2009	Research Associate, Electricity Generating Authority of Thailand, Bangkok, Thailand
2010-2011	Research Associate/Student Liaison, Boston College's Research Experience for Undergraduates Program, Nanofabrication Cleanroom, Newton MA (Michael Naughton, PhD)
2011-2012	Research Associate, Harvard's Rowland Institute for Science, Visual Neuroscience Group, Cambridge MA (David Cox, PhD)
2012-2014	Research Coordinator/Clinical Assistant, Beth Israel Deaconess Medical Center, Division of Ophthalmology, Boston MA (Jorge Arroyo, MD, MPH)
2016-Present	Research Associate, Scripps Research, La Jolla CA (Martin Friedlander, MD, PhD)

HONORS AND AWARDS:

2008-2012	Presidential Scholar (merit-based full scholarship), Boston College
2010	Sophomore Scholar, Boston College
2011	First Place, Undergraduate Research Symposium, Boston College
2011,2012	Deans Scholar, Boston College
2012	Scholar of the College, Boston College
2012-Present	Phi Beta Kappa
2012-2014	Grimshaw-Gudewicz Charitable Foundation Research Grant
2015	UCSD Travel Grant Recipient
2017	Honorable Mention, UCSD MSTP Research Symposium
2018	Knights Templar Eye Foundation Travel Grant Recipient
2018	F30 EY029141-01, Ruth L. Kirschstein National Research Service Award

PUBLICATIONS:

1. Bucher F, Aguilar E, **Marra KV**, Rapp J, Arnold J, Diaz-Aguilar S, Lange C, Agostini H, Schlunck G, Stahl A, Friedlander MF. Ciliary Neurotrophic Factor prevents development of outer retinal neovascularization through upregulation of CxCl10. IOVS. 2020 Aug 3;61(10):20.

2. Xiao S, Bucher F, Wu Y, Rokem A, Lee C, **Marra KV**, Fallon R, Diaz-Aguilar S, Aguilar E, Friedlander M, Lee A. Fully automated, deep learning segmentation of oxygen-induced retinopathy images. JCI Insight. 2017;2(24): e97585.

3. Chang JS, **Marra KV**, Flynn HW, Berrocal AM, Arroyo JG. Scleral Buckling in the Treatment of Retinal Detachment due to Retinal Dialysis. Ophthalmic Surg Lasers Imaging Retina. 2016 Apr; 47(4):336-40.

4. **Marra KV**, Wagley S, Kuperwaser M, Campo R, Arroyo JG. Care of the Aging Patient: Role of the Primary Care Physician in the Treatment of Cataracts and Macular Degeneration. J Am Geriatr Soc. 2016 Feb; 64(2):369-77.

5. Yu G, Duguay J, **Marra KV**, Gautam S, Le Guern G, Begum S, Sharifzadeh A, Arroyo JG. Efficacy and Safety of Pneumatic Vitreolysis, Intravitreal Ocriplasmin, and Vitrectomy for Vitreomacular Traction: A Case Series and Meta-Analysis. Retina 2016 Jan 17. [Epub ahead of print]

6. Kovacs K, **Marra KV**, Wagley S, Akella S, Ma J, Teague G, Johnson W, Lashkari K, Arroyo JG. Angiogenic and Inflammatory Biomarkers Associated with Ischemic Retinopathy: Vitreous Protein Analysis. Invest Ophthalmol Vis Sci. 2015 Oct; 56(11):6523-30.

7. Wagley S, **Marra KV**, Salhi R, Gautam S, Campo R, Veal P, Veale J, Arroyo JG. Periodontal Disease and Age-related Macular Degeneration: Results from the National Health and Nutrition Examination Survey III. Retina 2015 May; 35(5):982-8.

8. **Marra KV**, Wagley S, Omar A, Kinoshita T, Kovacs K, Silva P, Kuperwaser M, Arroyo JG. Case-matched comparison of vitrectomy, peripheral retinal endolaser, and endocyclophotocoagulation versus standard care in neovascular glaucoma. Retina 2015 Jun;35(6):1072-83.

9. Hernandez-Siman J, **Marra KV**, Arroyo JG. Sub-Conjunctival Lidocaine Injection before Intravitreal Injection. Surv Ophthalmol 2014 Nov-Dec;59(6):672-3

10. Thanos A, Hernandez-Siman J, **Marra KV**, Arroyo JG. Reversible Vision Loss and Outer Retinal Abnormalities Following Intravitreal Ocriplasmin Injection. Retin Cases Brief Rep. 2014;8(4):330-2

11. **Marra KV**, Yanekawa Y, Papakostas T, Arroyo JG. Indications and techniques of endoscope-assisted vitrectomy. JOVR 2013;8(3):282-290.

12. Yiu G, **Marra KV**, Wagley S, Krishnan S, Sandhu H, Kovacs K, Kuperwaser M, Arroyo JG. Surgical outcomes after epiretinal membrane peeling combined with phacoemulsification and intraocular lens implantation versus membrane peeling alone. Br J Ophthalmol 2013;97(9):1197-201.

13. Yiu G, **Marra KV**, Arroyo JG. Authors' response: Surgical outcomes after epiretinal membrane peeling combined with phacoemulsification and intraocular lens implantation versus membrane peeling alone. Br J Ophthalmol 2013 [Published online first: 3 October 2013].

14. Yonekawa Y, Papakostas TD, **Marra KV**, Arroyo JG. Endoscopic Pars Plana Vitrectomy for the Management of Severe Ocular Trauma. Int Ophthalmol Clin. 2013 Fall;53(4):139-148.

INVITED SYMPOSIA TALKS AND INSTITUTIONAL SEMINARS
(Presenter Underlined):

2013

- Retina Society, Los Angeles, California

Yonekawa Y, Papakostas TD, **Marra KV** Arroyo JG. Endoscopic Pars Plana Vitrectomy for the Management of Severe Ocular Trauma.

- Harvard's Resident Lecture Series, Boston Massachusetts

2014

Kovacs K, **Marra KV**, Wagley S, Arroyo JG. Increased Placental Growth Factor Associated with Retinal Ischemia.

- Macula Society, Key Largo, Florida

Marra KV, Arroyo JG. Nonsurgical Treatment of Symptomatic Vitreomacular Adhesions.

- American Society of Retina Specialists, San Francisco, California

Wagley SW, **Marra KV**, Arroyo JG. Periodontal Disease Associated with AMD.

- Retina Society, Los Angeles, California
- Macula Society Meeting, Los Angeles, California
- American Society of Retina Specialists, Toronto

2018

Marra KV, Aguilar E, Ouchi AO, Sakimoto S, Friedlander MF. Extracellular vesicles from endothelial colony forming cells (ECFCs) as paracrine mediators of neurovasculotrophic repair of the retina.

- Feinberg School of Medicine, Northwestern University, Chicago, Illinois

2019

- The Association for Research in Vision and Ophthalmology Annual Meeting. Vancouver, Canada.
- Neurotech USA, Inc., Cumberland, RI

Marra KV. What other neuroprotectants are produced by NT-201 RPE cells in the Neurotech device?

- Lowy Medical Research Institute and International MacTel Project Annual Meeting. New York City, New York.

POSTER PRESENTATIONS:

2011

- **Marra KV**, Graham B, Carouso S, Cox D. Implementation of a Peltier-based cooling device for localized deep cortical deactivation during in vivo object recognition testing. Am. Phys. Soc. 57, Q39.00003 (2011)
- Ye F, McMahon G, **Marra KV**, Kempa K, Naughton MJ. A novel nanoscale coaxial optical microscope by converging array of subwavelength waveguides. Am. Phys. Soc. 56, H32.00011 (2011)

2012

- **Marra KV**. Effects of brain cooling on behavior: Fabricating a novel brain-cooling device. BCTalks 2012 Invited Speaker.
- **Marra KV**, McMahon G, Rizal B, Kirkpatrick T, Naughton MJ. Implementing a photovoltaic characterization system for the JEOL Multibeam Focused Ion Beam system to test nanocoax solar cells. 1st place in Boston College Undergraduate Research Symposium 2012

2013

- Keodara A, Arroyo JG, Nadia Z, **Marra KV**. Epiciliary membranes as a cause of chronic hypotony. American Academy of Optometry Annual Meeting. San Diego, CA.
- **Marra KV**, Wagley S, Omar A, Kinoshita T, Kovacs K, Kuperwaser M, Arroyo JG. Functional and anatomic outcomes following endocyclophotocoagulation (ECP) surgery for neovascular glaucoma as compared to routine glaucoma care. The Association for Research in Vision and Ophthalmology Annual Meeting. Seattle, WA.
- Wagley S, Salhi R, **Marra KV**, Arroyo JG. Periodontal disease and age-related macular degeneration: results from the National Health and Nutrition Examination Survey III. The Association for Research in Vision and Ophthalmology Annual Meeting. Seattle, WA.

2014

- **Marra KV**, Kovacs K, Wagley S, Akella S, Teague GC, Johnson W, Lashkari K, and Arroyo JG. Angiogenic and Inflammatory Biomarkers Associated with Neovascular Glaucoma. New England Ophthalmology Society. Boston, MA.
- **Marra KV**, Kovacs K, Wagley S, Akella S, Teague GC, Johnson W, Lashkari K, and Arroyo JG. Angiogenic and Inflammatory Biomarkers Associated with Neovascular Glaucoma. Harvard's Annual Research Symposium. Boston, MA.
- **Marra KV**, Kovacs K, Wagley S, Akella S, Teague GC, Johnson W, Lashkari K, and Arroyo JG. Placental Growth Factor Levels Correlated with Retinal Ischemia Progression. The Association for Research in Vision and Ophthalmology Annual Meeting. Orlando, FL.
- Teague GC, Nandakumar N, Ma J, **Marra KV**, Arroyo JG, Baldwin ME, Johnson W, Lashkari K. Development of Biomarker Equations based on Multi-Dimensional Modeling of Cytokine Shifts in Retinal Diseases. The Association for Research in Vision and Ophthalmology Annual Meeting. Orlando, FL.

2015

- Yu G, Duguay J, **Marra KV**, Gautam S, Le Guern G, Arroyo JG. Ocular Coherence Tomographic Findings in Patients with Vitreomacular Traction Treated with Pneumatic Vitreolysis, Intravitreal Ocriplasmin, or Vitrectomy with Membrane Peeling. Harvard Medical School Department of Ophthalmology Poster Contest. Boston, MA
- **Marra KV**, Kwiatkowski MA, Yu G, Arroyo JG. Physical Activity and Age-Related Macular Degeneration: Results from the 2005-2006 National Health and Nutrition Examination Surveys. The Association for Research in Vision and Ophthalmology Annual Meeting. Denver, CO.
- Yu G, Duguay J, **Marra KV**, Gautam S, Guern GL, Arroyo JG. Ocular Coherence Tomographic Findings in Patients with Vitreomacular Traction Treated with Pneumatic Vitreolysis, Intravitreal Ocriplasmin, or Vitrectomy with Membrane Peeling. The Association for Research in Vision and Ophthalmology Annual Meeting. Denver, CO.
- Yu G, Duguay J, **Marra KV**, Gautam S, Guern GL, Arroyo JG. Ocular Coherence Tomographic Findings in Patients with Vitreomacular Traction Treated with Pneumatic Vitreolysis, Intravitreal Ocriplasmin, or Vitrectomy with Membrane Peeling. Massachusetts Eye and Ear Annual Ophthalmology Research Symposium. Boston, MA.

2016

- Yu G, Dai W, O'Loughlin L, Zhao L, Levi E, Bassiri A, Wagley S, **Marra KV**, Alsop DC, Arroyo JG. Magnetic Resonance Imaging of the Choroid in Patients with Age-Related Macular Degeneration. The Association for Research in Vision and Ophthalmology Annual Meeting. Seattle, WA.

2017

- **Honorable mention: Marra KV**, Murinello S, Bucher F, Aguilar E, Friedlander M. Characterization of the neuroinflammatory response in the oxygen-induced retinopathy model of ischemic retinopathy. UCSD MSTP Research Symposium. San Diego, CA.
- **Marra KV**, Murinello S, Bucher F, Aguilar E, Friedlander M. Characterization of the neuroinflammatory response in the oxygen-induced retinopathy model of ischemic retinopathy. The Association for Research in Vision and Ophthalmology Annual Meeting. Baltimore, MD.

2018

- **Marra KV**, Sakimoto S, Murinello S, Aguilar E, Bucher F, Friedlander M. Extracellular vesicles from endothelial colony forming cells as paracrine mediators of neurovasculotrophic repair of the retina. The Association for Research in Vision and Ophthalmology Annual Meeting. Honolulu, HI.
- Xaio S, Bucher F, We Y, Rokem A, Lee C, **Marra KV**, Fallon R, Diaz-Aguilar S, Aguilar E, Friedlander M, Lee A. Web based, fully automated, deep learning segmentation of oxygen induced retinopathy. The Association for Research in Vision and Ophthalmology Annual Meeting. Honolulu, HI.
- Bucher F, Aguilar E, **Marra KV**, Stahl A, Friedlander M. CxCl10 represents an important mediator in CNTF-induced improvement of outer retinal neovascularization. The Association for Research in Vision and Ophthalmology Annual Meeting. Honolulu, HI.

2019

- Ouchi, AO, Aguilar E, **Marra KV**, Qiang M, Guang Y, Lerner R, Friedlander MF. The role of Acid-sensing ion channel 1a in a mouse model of ischemic retinopathy. The Association for Research in Vision and Ophthalmology Annual Meeting. Vancouver, Canada.
- **Marra KV**, Aguilar E, Ouchi AO, Sakimoto S, Friedlander MF. Extracellular vesicles shed from endothelial colony forming cells (ECFCs) with high expression of CD44 are paracrine mediators of neurovasculotrophic retinal repair. UCSD MSTP Research Symposium. San Diego, CA.
- **Marra KV**, Aguilar E, Ouchi AO, Sakimoto S, Friedlander MF. Extracellular vesicles shed from endothelial colony forming cells (ECFCs) with high expression of CD44 are paracrine mediators of neurovasculotrophic retinal repair. UCSD Jacobs School of Engineering Research Expo. San Diego, CA.

2021

- **Marra KV**, Aguilar E, Ouchi AO, Wei G, Sakimoto S, Friedlander MF. Differentially expressed microRNAs within extracellular vesicles of a functionally active subpopulation of endothelial colony forming cells demonstrate neurovasculotrophic effects. Association for Research in Vision and Ophthalmology Annual Meeting. Virtual.
- **Marra KV**, Aguilar E, Ouchi AO, Wei G, Sakimoto S, Friedlander MF. Differentially expressed microRNAs within extracellular vesicles of a functionally active subpopulation of endothelial colony forming cells demonstrate neurovasculotrophic effects. UCSD Jacobs School of Engineering Research Expo. San Diego, CA.

BOOK CHAPTERS:

Rezende F, Jayasundera T, Lee T, **Marra KV**, Arroyo JG. Management of Complicated Vitreoretinal Disease. Medford: Springer Publishing Company, 2014.

- **Marra KV**, Arroyo JG. Endoscopic cyclophotocoagulation for prolific diabetic retinopathy and neovascular glaucoma.
- **Marra KV**, Arroyo JG. Endoscopy-assisted vitrectomy: Cornea opacities and anterior segment disfiguration
- **Marra KV**, Arroyo JG. Endoscopic approach towards hypotony from cyclitic membranes
- **Marra KV**, Arroyo JG. Endoscopic management of intraocular foreign bodies

THESIS ADVISED:

- Akella S, Trinkaus-Randall V, **Marra KV,** Arroyo JG. Epidemiological analysis of large databases to investigate risk factors for age-related macular degeneration. Master of Medical Sciences Thesis from Boston University School of Medicine

PERIODICALS:

- **Marra KV**. “Inducing local brain deactivation to study object recognition signal processing in the brain.” Ex Libris. Oct 2011:5. Print.

- **Marra KV**. Summer of Discovery: Nuclear Power Plant Feasibility Study in Thailand. Heights. April 2010:7. Print.

SOCIETIES:

- Association for Research in Vision and Ophthalmology

PUBLIC SERVICE:

Invited Reviewer, Translational Medicine
Invited External Reviewer, NEJM
Invited External Reviewer, Science
Invited External Reviewer, PNAS
Invited External Reviewer, Journal of Clinical Investigations
Invited External Reviewer, Journal of Clinical Investigations Insight
Invited External Reviewer, Cell Metabolism
Invited External Reviewer, Journal of Experimental Medicine
SARS-CoV-2 qPCR Screening, Volunteer Scientist
COVID-19 Vaccination, Volunteer

PROFESSIONAL DEVELOPMENT:

2014, 2015	Harvard's Vitreoretinal Fellows Wetlab & Seminar Series
2017	ARVO Educational Course: Stem cells and organoids as models of tissue differentiation and eye
2019	Scintillon's 29th Flow Cytometry Development Workshop: Cells, Sensors, and Systems

TEACHING EXPERIENCE:

2011-2012	Connors Family Learning Center Tutor: Calculus I/II, Multivariable Calculus, Linear Algebra, General Chemistry, and all Physics courses
2013-2014	Master's Thesis Advisor: Sudheer Akella, Boston University
2017-2018	UCSD Bioengineering Graduate Teaching Assistant: MDE 231B Fundamentals of Physiology and Anatomy II BENG230B Cell and Molecular Biology BENG230C Cardiovascular Physiology

ABSTRACT OF THE DISSERTATION

Extracellular vesicles from endothelial colony forming cells
in the repair of ischemic retinal disease

by

Kyle Marra

Doctor of Philosophy in Bioengineering

University of California San Diego, 2021

Professor Adam Engler, Chair
Professor Martin Friedlander, Co-Chair

Current treatments for ischemic retinopathies inhibit vascular leakage and proliferation in late-stage disease but do nothing to repair dysfunctional vasculature or alleviate the underlying causes of the ischemia/inflammation that drives pathological neovascularization. Stimulation of functional, physiologic vascular growth and stability is a promising alternative therapeutic approach that may be achieved by the use of endothelial progenitor cells called endothelial

colony forming cells (ECFCs). Chapter 1 of this dissertation describes the characterization of ECFCs in an historical context and details the mechanisms mediating their neurovasculotrophic effects in the retina as well as other tissues. ECFCs differentiate into endothelial cells and can directly integrate into host vasculature, replacing lost or damage endothelial cells *in vivo*; ECFCs can also achieve their therapeutic effect by paracrine action. Extracellular vesicles (EVs) shed from ECFCs (EVs^{ECFCs}) have been newly identified as one such paracrine mechanism. Loaded with diverse cargo including proteins, RNA, and lipids, EVs^{ECFCs} facilitate intercellular communication and, through multiple mechanisms, may provide a novel approach for the treatment of complex retinal disorders. EVs' role in retinal physiology and pathophysiology are discussed in Chapter 2, which outlines research using several animal disease models to investigate possible mechanisms of EV^{ECFCs}-based treatment for ischemic retinopathies.

Chapter 3 describes the laboratory research that forms the basis for my dissertation. This body of work exploits our lab's recent publication demonstrating that ECFCs are not a homogeneous group of cells. ECFCs with high expression of CD44 hyaluronan receptor ($CD44^{hi}$ ECFCs) demonstrate superior rescue effects in mouse models of ischemic retinopathy and retinal degeneration when compared to ECFCs with low CD44 expression ($CD44^{lo}$ ECFCs). This dissertation research demonstrated that the superior effect of $CD44^{hi}$ ECFCs was attributable, at least in part, to bioactive microRNA (miR) cargo in EVs released from $CD44^{hi}$ ECFCs (EVs^{hi}). EVs^{hi} recapitulated rescue effects of $CD44^{hi}$ ECFCs; EVs from $CD44^{lo}$ ECFCs (EVs^{lo}) did not. Using small RNA sequencing to compare intravesicular miR within EVs^{hi} to EVs^{lo} and subsequent *in vivo* functional validation, candidate miRs mediating the augmented therapeutic effect of EVs^{hi} were identified.

Freestanding chapters 4 and 5 are reprints of publications I have co-authored during my PhD.

Overall, this dissertation describes the utility of ECFCs and their EVs in treating complex retinal diseases and provides novel insight into the neurovasculotrophic mechanisms of EVs^{hi}, bringing this therapy closer to clinical translation.

Chapter 1

Evaluation of endothelial colony forming cells in the repair of ischemic and neurodegenerative retinal tissue

1.1 Introduction and scope

The use of stem and progenitor cells in the repair of ischemic/neurodegenerative retina holds great promise as an option for restoring visual function. Current therapeutic approaches to the treatment of ischemic/neurodegenerative retinal diseases include intravitreal injection of vascular endothelial growth factor (VEGF) antagonists that inhibit vascular leakage and proliferation, and panretinal laser photocoagulation that ablates peripheral retinal tissue to reduce metabolic demand to match blood supply to the remaining central retina. These strategies target manifestations of late-stage disease and do nothing to alleviate the underlying ischemia driving the abnormal angiogenic response. A promising alternative treatment strategy is the promotion of physiologic vascularization and vessel stability by stem/progenitor cells. In the growing population of diabetic patients with chronic retinal ischemia, vascular homeostasis is a dynamic process that may be influenced by contributions from various vasculogenic progenitor cells. This begets the important question: Which vasculogenic progenitor cells repair ischemic tissue by

stimulating local angiogenesis and/or promoting *de novo* vessel formation (a process known as vasculogenesis)?

As the one true endothelial progenitor cell known to date, endothelial colony forming cells (ECFCs) are an extremely promising source of cell therapy that may achieve this effect. ECFCs home to ischemic areas and differentiate into endothelial cells to form *de novo* vasculature, also secreting factors to promote physiological vascular growth in a variety of animal models of ischemic disease.[1] Overall, this chapter discusses the utility and mechanisms of ECFCs in the treatment of ischemic/neurodegenerative tissues, with a particular focus on retinal diseases. We begin with outlining the historical context leading to the discovery of ECFCs as one of two well-characterized subpopulations of circulating $CD34^+$ progenitor cells (the other population being myeloid angiogenic cells, or MACs) alongside phenotypic and functional differences between the two cell types. Literature debating the origin of ECFCs is covered, followed by an overview of the preclinical considerations of ECFC-based therapy. Studies across fields are synthesized to discuss the mechanisms employed by ECFCs in treating ischemic/neurodegenerative diseases. In addition to summarizing key elements, this chapter concludes discussing ongoing research to improve ECFC-based therapy.

1.2 The paradigm shift of circulating endothelial progenitor cells

Evidence for viable circulating endothelial cells (CECs) began accumulating in the 1960s when putative CECs were observed to seed on biomaterials implanted within the large arteries and veins in experimental animal systems.[2] Intraprosthetic Dacron hubs (a synthetic polyester fabric impermeable to transmural capillary ingrowth) were implanted into the aorta of pigs[2] as well as the descending aorta and inferior vena cava of dogs.[3] Circulating cells adhered to the hub and formed scattered islands of endothelium in a process termed “fallout endothelialization.” In

canines that received bone marrow transplantation concurrent with hub implantation, these scattered islands of fallout endothelialization consisted solely of donor marrow cells. Some of these cells were endothelial cells (ECs) expressing the CD34 antigen.[4] CD34 is a 105- to 120kDA transmembrane glycoprotein expressed on a variety of hematopoietic and nonhematopoietic cells and progenitors that plays a role in cell-to-cell adhesion, in hematopoietic cell proliferation, and in differentiation control.[5] In the same study, 0.004-0.01% of human bone marrow-derived $CD34^+$ cells plated *in vitro* were reported to give rise to endothelial colonies. Together, these data suggested that a subset of $CD34^+$ cells may be a precursor endothelial cell capable of migrating within the peripheral circulation to colonize endothelial flow surfaces. Furthermore, these cells may be harvested from peripheral blood and expanded to form stable cell lines *ex vivo*.

Although data in animal models provided clear evidence of CECs that can travel within the peripheral blood to seed implanted materials, some human grafts function for decades *in vivo* without developing endothelial intima.[6] To identify CECs in humans, one study observed the circulating blood-derived and antithrombogenic "pseudointima" that formed along the blood-membrane barrier of implanted first-generation "Heartmate I" left ventricular assist devices used to treat heart failure patients. Initial reports on the composition of this pseudointima described scattered islands of endothelial cells believed to be deposited by blood-born endothelial cells or endothelial precursors.[7] Along with fibroblasts, monocytes, and multinucleated cells,[7] these cells were imbedded within a collagenous covering produced by resident myofibroblasts.[8] Following digestion of the pseudointima by collagenase, flow cytometric analyses of the cell suspension revealed that approximately 88% of the mononuclear cells expressed CD45 antigen, which is present on all hematopoietic cells and absent on nonhematopoietic cells. Of this $CD45^+$ cell

population, about 4% of cells also expressed the primitive hematopoietic progenitor cell marker CD34. When digested neointimal cells were plated with cytokine stimulation *in vitro*, these $CD34^+/CD45^+$ cells expanded 25-fold within two weeks and expressed surface marker CD14 indicative of myeloid origin.[9] This population of CD34+/CD45+/CD14+ cells have since been classified not as endothelial progenitors but rather as myeloid angiogenic cells (MACs).

These studies provided evidence that specialized hematopoietic and nonhematopoietic cells in peripheral blood may adhere and colonize on textured biomaterials in humans, thus suggesting the existence of circulating endothelial progenitor cells. The stage was set for a paradigm shift in our understanding of human vascular growth. Prior to 1997, neovascularization was thought to be comprised of two paradigms: 'vasculogenesis' and 'angiogenesis.' Vasculogenesis is the embryonic process by which endothelial progenitors, or angioblasts, form *de novo* embryonic blood vessels. Angiogenesis is the postnatal process whereby new vasculature is formed by proliferation, migration, and remodeling exclusively by fully differentiated endothelial cells within pre-existing blood vessels.[10] Based on studies demonstrating the existence of circulating endothelial progenitor cells in humans, a third mechanism termed 'postnatal vasculogenesis,' whereby endothelial progenitor cells form *de novo* vasculature in adults was proposed. This vasculogenic mechanism received its first experimental support with a foundational paper by Asahara et al.[11] in 1997 where putative endothelial progenitor cells were first isolated.

Asahara's discovery of endothelial progenitor cells exploited findings from the current understanding of embryonic vasculogenesis, which initiates with the formation of a cluster of peripheral angioblasts surrounding a core of hematopoietic stem cells (HSCs) together called a 'blood island.'[12] In addition to their spatial correlation, both angioblasts and HSCs shared

distinguishing antigens CD34 and vascular endothelial growth factor receptor-2 (VEGFR-2, also referred to as KDR or in mice as Flk-1) that suggested the possibly of a common precursor. Embryos with knocked-out expression of VEGFR-2 developed defects in both hematopoietic and angioblastic cell lines, corroborating the existence of a bipotential precursor cell for these lineages.[13] Asahara searched for this common precursor cell type by using magnetic bead-conjugated antibodies for CD34 or VEGFR-2 to isolate cell populations from mononuclear cells (MNCs) in peripheral blood (PB). After culturing these MNCs for 24 hours on fibronectin plates with endothelial differentiation medium, non-adherent cells were removed and clusters of spindle-shaped cells resembling "blood island-like" clusters emerged in culture between 3-7 days. The immunophenotype of these cells were positive in the expression of endothelial surface cell markers CD31, VEGFR-2, and Tie-2 and also exhibited markers specific to hematopoietic cell lineage such as CD45. Plated $CD34^+$ cells from circulation expanded and differentiated into endothelial cells *in vitro*, and heterologous, homologous, and autologous cells incorporated into sites of active angiogenesis in mouse and rabbit models of unilateral hindlimb ischemia *in vivo*. In a single paper, Asahara et al. was the first to provide evidence that $CD34^+$ cells isolated from PB MNCs contain circulating endothelial progenitor cells that can be expanded *ex vivo,* differentiate into endothelial cells, and be transplanted *in vivo* to participate in postnatal vasculogenesis and rescue damaged vasculature. The proposal of these data that PB-derived endothelial progenitor cells may function in vascular homeostasis and ultimately aid in the treatment of vascular disease galvanized this area of research, with over 10,000 publications on the endothelial progenitor cells since their discovery.

1.3 Distinguishing progenitor cell populations

Asahara et al.[11] isolated a population of $CD34^+$ cells within MNCs from peripheral blood and seeded them on fibronectin-coated plates to observe the formation of adherent "blood island-like" clusters consisting of putative endothelial progenitor cells. In the fledgling days of EPC research, investigators interpreted the formation of cell clusters with 'blood island-like' morphology like those first observed by Asahara et al. as a quantitative measure of EPCs. An incorrect assumption was made that these different culture assays derived similar 'blood island-like' clusters of EPCs with similar functional attributes. Today, it is known that cells isolated using magnetic bead-assisted $CD34^+$ or VEGFR-2^+ pulldown are, in fact, a heterogeneous cell population. A variety of culture assays can derive 'blood island-like' clusters and this phenomenon led to the misappropriation of the term 'EPC' in the literature, erroneously describing multiple different cell types that were not actual EPCs. For years after the seminal paper by Asahara et al., differing cell culture techniques combined with a lack of concordance in the stem cell field led to the indiscriminate use of "endothelial progenitor cells (EPCs)" to describe a variety of tissue-resident and circulating cell types with vasculotrophic capacity. The details of these culture assays and their true resultant cell populations are illustrated in **Figure 1.1**.

Investigation of the origin, phenotype, and function of these cells over the years has led to the characterization of two distinct cell populations that each contribute to vascular repair via differing mechanisms: endothelial colony forming cells (ECFCs) and myeloid angiogenic cells (MACs). In brief, ECFCs are true endothelial progenitor cells capable of differentiating into mature endothelium and participate in postnatal vasculogenesis to form *de novo* vasculature. MACs are hematopoietic progenitor cells that provide vasculotrophic support via their secretion

Figure 1.1: **Culture assays and their resultant cell populations.** In Method 1, colony forming unit-Hill (CFU-Hill) cells are harvested from peripheral blood mononuclear cells (PB MNCs). PB MNCs are seeded on fibronectin-coated plates for 48 hours, then nonadherent cells are re-plated to begin forming colonies within 4-9 days. CFU-Hill cells have a morphology where spindle-shaped cells radiate outward from a central core of round cells. These cultures peak in growth between 2-3 weeks, do not form viable secondary cultures, and die by 4 weeks. In Method 2, Vasa et al. cultured low density PB MNCs for 4 days in endothelial growth factors and fetal calf serum (FCS) before removing nonadherent cells. This assay did not result in colony formation. A variety of overlapping names have been attributed to different cell types cultured using Methods 1 and 2 due to similarities in the timing of their appearance in cell culture as well as the immunophenotype and lineage of cells in these populations. In Method 3, PB MNCs are plated for 24 hours before nonadherent cells are removed. Daily media changes for 7 days followed by media changes every other day result in the derivation of endothelial colony forming cells (ECFCs). ECFCs display a cobblestone morphology and are able to participate in postnatal vasculogenesis through the *de novo* formation of blood vessels *in vivo*. Modified from Hirschi et al. Assessing identity, phenotype, and fate of endothelial progenitor cells. Arterioscler Thromb Vasc Biol. 2008;28:1584-1595.

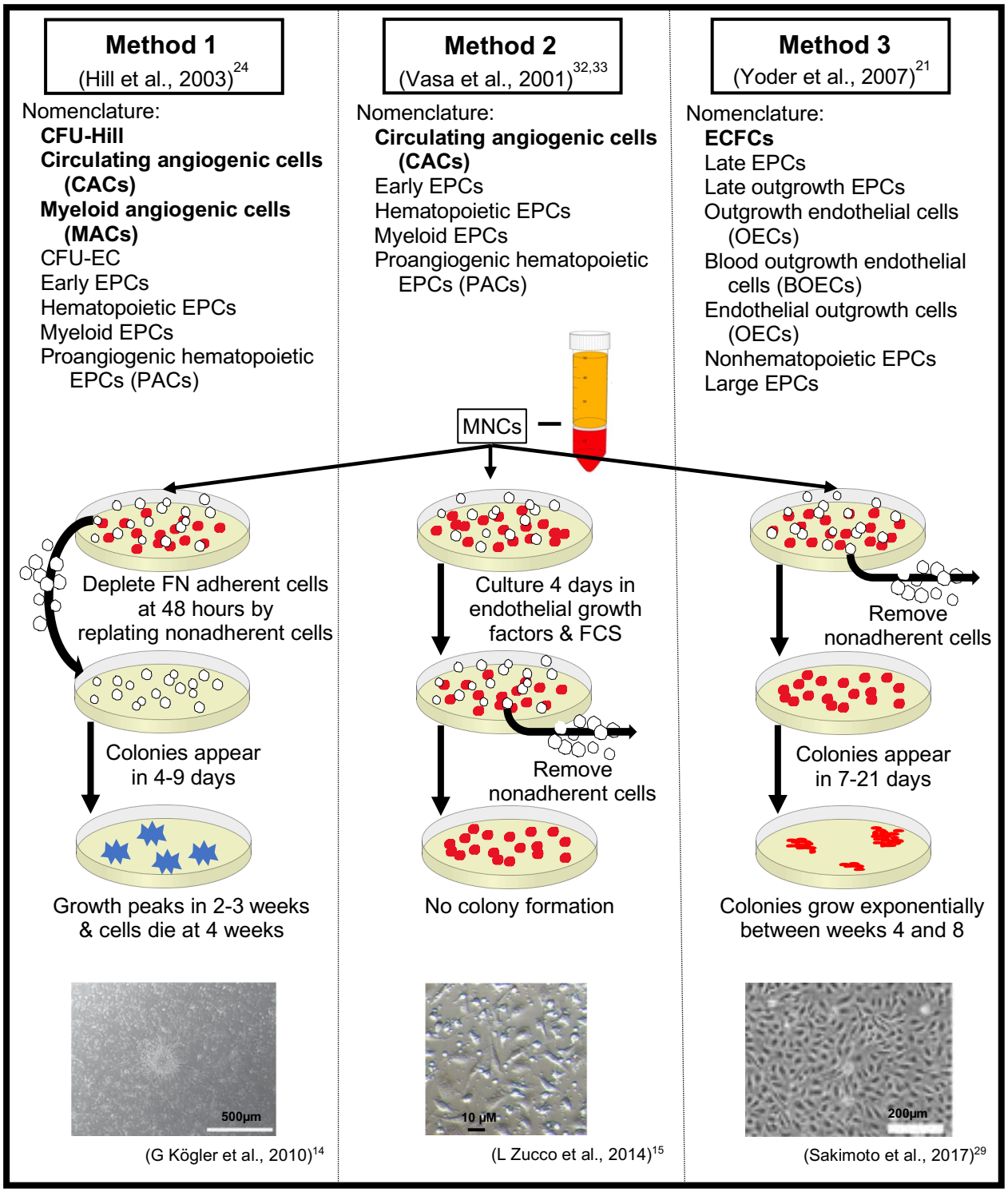
Method 1
(Hill et al., 2003)[24]
Nomenclature:
CFU-Hill
Circulating angiogenic cells (CACs)
Myeloid angiogenic cells (MACs)
CFU-EC
Early EPCs
Hematopoietic EPCs
Myeloid EPCs
Proangiogenic hematopoietic EPCs (PACs)
Method 2
(Vasa et al., 2001)[32,33]
Nomenclature:
Circulating angiogenic cells (CACs)
Early EPCs
Hematopoietic EPCs
Myeloid EPCs
Proangiogenic hematopoietic EPCs (PACs)
Method 3
(Yoder et al., 2007)[21]
Nomenclature:
ECFCs
Late EPCs
Late outgrowth EPCs
Outgrowth endothelial cells (OECs)
Blood outgrowth endothelial cells (BOECs)
Endothelial outgrowth cells (OECs)
Nonhematopoietic EPCs
Large EPCs
MNCs
Deplete FN adherent cells at 48 hours by replating nonadherent cells
Colonies appear in 4-9 days
Growth peaks in 2-3 weeks & cells die at 4 weeks
500µm
(G Kögler et al., 2010)[14]
Culture 4 days in endothelial growth factors & FCS
Remove nonadherent cells
No colony formation
10 µM
(L Zucco et al., 2014)[15]
Remove nonadherent cells
Colonies appear in 7-21 days
Colonies grow exponentially between weeks 4 and 8
200µm
(Sakimoto et al., 2017)[29]

of paracrine mediators. Herein lies a source of confusion that may make it difficult for those not aware of this historical context to understand the EPC literature. The indiscriminate classification of both ECFCs and MACs as "EPCs" in literature requires that readers understand the phenotype and function of ECFCs and MACs as well as the cell culture methodologies used to derive each cell type in order to know which of these distinct subpopulations of progenitor cells is being discussed. In agreement with a recently published paper by Medina et al.[16] establishing consensus among those working in the field, this text refrains from the indiscriminate use of the term "EPC" and elects to use precise nomenclature of ECFCs and MACs based on characterized cellular phenotypes and function described below. Readers are encouraged to consult this comprehensive characterization of MACs and ECFCs to discern exactly which tell type(s) are being described in literature.

1.3.1 Myeloid angiogenic cells: critical support cells

MACs are phenotypically myeloid progenitor cells with vasculotrophic functionality via paracrine action.[17,18] Emerging evidence characterizing their genetic signature indicates that MACs represent alternative M2 macrophages.[19] MACs can neither differentiate into endothelial cells nor incorporate into host vasculature. Instead, these cells exhibit their vasculotrophic effects by secreting chemoattractants and vascular trophic mediators that promote the homing, proliferation, and differentiation of local precursor cells. Specifically, the secretion of various cytokines such as hepatocyte growth factor (HGF), interleukin (IL)-8, G-CSF, and GM-CSF significantly induce endothelial tube formation *in vitro* and vascular repair *in vivo.*[20] MACs also contribute to angiogenesis through secretion of IL-8, triggering downstream transactivation of VEGFR-2 on mature endothelial cells, which in turn induces phosphorylation of extracellular signal-regulated kinase (ERK). MACs injected into the mouse oxygen-induced retinopathy

(OIR) model of ischemic retinopathy maintained their myeloid features, such as CD68 expression and amoeboid/spherical morphology, and rescued the pathological neovascularization (NV) and vaso-obliteration (VO) of the OIR phenotype.[19]

MACs are derived from the bone marrow and may be isolated from peripheral blood MNCs using well-defined isolation protocols for *in vitro* cell culture. Initial studies enriched MAC populations by using a popular assay called the colony forming unit (CFU)-Hill assay. In this culture methodology, MNCs are pre-plated on fibronectin-coated plates and cells that are nonadherent after 48 hours are re-plated onto new fibronectin-coated plates[21] (**Figure 1.1, Method 1**). The rationale behind replating nonadherent cells was to remove possible contamination of the culture with early-adhering mature endothelial cells in circulation. It is now understood that this fibronectin-enrichment step is not necessary, and more recent studies culture MACs within 5-7 days by directly seeding them on fibronectin-coated plates with endothelial growth medium-2 (EGM-2) supplemented with 10% FCS.[19] Colonies appear with 'blood island-like' morphology within days. These colonies of spindle-shaped cells radiating from a central core mimic numerous features of endothelial cells including their expression profile of surface proteins and angiogenic molecules as well as their endothelial nitric oxide (eNO) production. These clusters were named CFU-Hill cells and for several years CFU-Hill cells were incorrectly referred to as EPCs. Today, the cells are well-characterized and more accurately named MACs to designate their lineage and function. Their growth peaks between 2 and 3 weeks. Lacking the ability to form secondary colonies, MACs die by week 4.[22]

This assay became a commercially available culture kit and after several years, it was discovered that CFU-Hill cell colonies in truth contain no EPC progeny. The spindle-shaped

cells radiating from a central core are macrophages with characteristics (i.e., surface proteins, angiogenic molecule production, and eNO production) similar to endothelial cells. As cells of the monocyte/macrophage lineage, these cells ingest bacteria and lack functionality required to be deemed EPCs. Specifically, CFU-Hill cells fail to form blood vessels *de novo* when implanted within collagen gels *in vivo* and thus do not possess the ability to directly participate in postnatal vasculogenesis. Instead, CFU-Hill are of the hematopoietic lineage and consist of monocyte/macrophage fated cells. The CFU-Hill culture assay therefore is a quantitative measure of intercellular interaction between these hematopoietic cells and not a quantitative measure of EPCs. Prior to the studies published by Yoder and Ingram[21] that led to the identification of these cells as MACs, alternate names included CFU-ECs, early EPCs, hematopoietic EPCs, myeloid EPCs, proangiogenic hematopoietic EPCs, and circulating angiogenic cells.

Although cell culture methodology is certainly critical to harvesting a target cell population and for understanding which cell type is being discussed in literature, a more effective characterization of these progenitor subtypes based on their immunophenotype and function is summarized in **Figure 1.2**. No specific marker for MACs exists to date, but a combination of surface proteins is now accepted to define these cells. By flow cytometry, MACs share some markers with ECFCs such as CD31, CD144, von Willebrand factor, and VEGFR-2. In contrast to ECFCs, however, MACs are defined by positive expression of CD45 and CD14, and negative expression of CD146. MACs can be isolated from populations of CD34+ cells, but the expression level of CD34 decreases over time in culture.[23] MACs are not endothelial cells, but their contribution to angiogenesis is substantial. The frequency of MACs in circulation is inversely correlated to the risk for cardiovascular disease,[24] diabetes,[25] COPD,[26] and rheumatoid

		MACs	ECFCs
Immunophenotype			
Shared markers	CD31	+	+
	vWF	+	+
	VEGFR-2	+	+
	CD34	+/-	+/-
	CD105	+	+
	CD144	+	+
Different markers	CD146	-	+
	CD45	+	-
	CD14	+	-
	CD115	+	-
Function			
Clonal proliferative capacity		-	+
Viability to re-plating		-	+
De novo vessel formation *in vivo*		-	+
Home to ischemic sites *in vivo*		+	+
Phagocytose bacteria		+	-
Paracrine support of angiogenesis		+	+
Integration into host vasculature		-	+

Figure 1.2: Comparison of surface proteins and cell function between MACs and ECFCs. Both populations share markers including CD31, vWF, VEGFR-2, CD105, and CD144. CD34 is a common marker of human stem, progenitor, and vascular endothelial cells. While MACs and ECFCs can be isolated from CD34+ cell populations, the expression of CD34 decreases in both cell types over time in cell culture (as denoted by the +/-). Differences in cell surface proteins can be used to differentiate MACs and ECFCs. The MAC immunophenotype is positive for expression of CD14, CD45, and CD105 and negative for expression of CD146; in contrast, the ECFCs immunophenotype is negative for expression of CD14, CD45, and CD105 and positive for expression of CD146. Functional characteristics of these cells are also useful in distinguishing cell populations. Unlike MACs, ECFCs possess clonal proliferative capacity and are viable upon replating for expansion into stable populations *ex vivo*. Both MACS and ECFCs home to areas of ischemia where they support angiogenesis albeit by different mechanisms. MACs secrete supporting paracrine factors while ECFCs can integrate into host vasculature in addition to secreting paracrine mediators. As myeloid cells, MACs can also function to phagocytose bacteria.

arthritis[27] in humans, and MACs have demonstrated rescue effects in murine models of ischemic disease[19] by recruiting/stimulating ECFCs to promote neovascularization.[23]

1.3.2. Endothelial colony forming cells: true endothelial progenitors

The functional requirements to classify cells as "EPCs" are the exhibition of endothelial progenitor characteristics such as commitment to an endothelial fate, capacity to self-assemble into functional blood vessels *in vivo*, and the ability to fully integrate into host vasculature.[16] ECFCs are classified as "true" endothelial progenitor cells because circulating and tissue-resident ECFCs are the only cell type currently known to possess such *in vivo* vasculogenic capacity by differentiating into endothelial cells to form primitive capillary plexi without the presence of existing vasculature.[28]

ECFCs are derived using the culture assay of Yoder et al. and validated by a combination of surface markers identified by flow cytometry.[21] Briefly, MNCs from adult peripheral blood PB or UCB are plated on type 1 rat tail collagen-coated wells and nonadherent cells are aspirated after 24 hours, leaving adherent cells to be cultured in endothelial growth medium (**Figure 1.1, Method 3**). Xeno-free media and xeno-free attachment and detachment substrates have been developed by the Friedlander lab allow for culture of ECFCs using animal free materials, bringing allogeneic ECFC therapy closer to clinical translation.[29] Following daily media changes for 7 days, media changes every other day results in the formation of colonies with cobblestone morphology within 1-3 weeks. ECFCs can be passaged to form secondary colonies and grow exponentially between 4 and 8 weeks.[22]

Studies have aided in the characterization of the immunophenotype, functionality, and therapeutic mechanisms of ECFCs. By flow cytometry, there is no surface antigen to date that uniquely identifies ECFCs. The ECFC immunophenotype is characterized by expression of

CD31, CD105, CD144, CD146, von Willebrand factor, and VEGFR-2, but must be negative for hematopoietic markers including CD45, CD14, and CD115 as well as mesenchymal antigens including CD70, CD90, and α-smooth muscle actin (α-SMA). CD34 has also been characterized on ECFCs, but expression declines during *in vitro* expansion (**Figure 1.2**).[16]

In a series of publications,[21, 30] Yoder and Ingram redefined cells in the field of EPC research, concluding that: 1) there exists a unique population of high proliferative potential-ECFCs that demonstrate functional characteristics of true EPCs and 2) that ECFCs are clonogenically, immunophenotypically, and functionally distinct from MACs and other cells often inaccurately termed EPCs. Evidence suggests that ECFCs may not be a homogenous group of cells. A complete hierarchy of UCB- and PB-derived ECFCs has been demonstrated to exist on the basis of clonogenic and proliferative capacity, with some ECFCs displaying high proliferative potential (HPP).[30] Single HPP-ECFCs can be clonally expanded *in vitro* into greater than 2,000 cells in 14 days and may be re-plated to form secondary HPP-ECFC colonies of over 2,000 cells after 14 additional days. During *in vitro* expansion, a subpopulation of ECFCs cultured from peripheral blood MNCs lose expression of the stem and progenitor cell surface marker CD34. This occurrence may be partially explained by the observation that CD34 is downregulated in ECFCs exposed to particular serum supplements and growth factors. In comparison to $CD34^-$ ECFCs, ECFCs with positive expression of CD34 demonstrate improved capillary-like sprout formation, increased tip-cell gene expression, and decreased endothelial barrier function with loosened cell-cell interaction between PB-ECFCs.[31] Furthermore, ECFC populations that are high in their expression of CD44 ($CD44^{hi}$ ECFCs) demonstrate superior neurovasculotrophic effects in murine models of ischemic retinopathy and retinal neurodegeneration than ECFCs with low CD44 expression ($CD44^{lo}$ ECFCs).[29] Correlations

between phenotype and function of ECFCs merit continued efforts to better understand the heterogeneity of ECFCs in culture. These data suggest that there exists a spectrum of proliferative capacity and immunophenotype within ECFC cultures, giving rise to the idea of identifying the most active of ECFCs for use as therapy in treating ischemic disease.[29]

1.3.3 The misnomer of other "circulating angiogenic cells" as EPCs

In 2001, Vasa et al. described a protocol to isolate and culture 'blood island-like' clusters of cells that were named "circulating angiogenic cells (CACs)" and incorrectly defined these populations as EPCs. Colonies were formed by plating PB-derived low density MNCs on fibronectin- and gelatin- coated dishes with endothelial growth factor-supplemented media with fetal calf serum (**Figure 1.1, Method 2**).[32, 33] Nonadherent cells were removed after 4 days in culture, and adherent cells that were able to ingest acetylated low-density lipoprotein (Ac-LDL) or fluorescently labeled *Ulex eruopaeus agglutinin 1* plant lectin were used for cytochemical analysis. These cells were incorrectly believed to be EPCs since they expressed von Willebrand factor (vWF), vascular endothelial (VE)-cadherin, and VEGFR-2 on flow cytometry. However, subsequent studies that found that cells in these cultures had strikingly similar characteristics to macrophages including co-expression of CD45, CD11b, CD11c, CD13, CD68, endothelial nitrous oxide synthase (eNOS), and E-selectin, and took up India ink. Macrophages cultured in medium containing particular endothelial growth factors and fetal calf serum also expressed many of these surface proteins, which were previously believed to be specific to endothelial cells.[34-36] Culturing PB MNCs on fibronectin- and gelatin-coated plates had been a commonplace method used to enrich monocyte populations.[37] Furthermore, CACs lack the ability to form colonies.[28]

Together, these reports demonstrated that the culture conditions and growth factors used in these isolation techniques enrich monocytic cell populations and not EPCs.[28] In fact, it is now understood that CACs isolated in this fashion arose from *in vitro* conditions and do not exist *in vivo*.[16] Nevertheless, numerous studies have used this culture methodology[20, 38-47] and inaccurately deemed these populations as EPCs, CACs, and other misnomers listed in **Figure 1.1, Method 2**. This nomenclature is erroneous since such a population has never been identified to circulate *in vivo* from blood samples. Since these cultures produce a heterogeneous cell population that the most current literature suggests may arise a result of *in vitro* culture conditions that do not exist *in vivo*,[16] literature using this culture methodology have been excluded from the current discussion. Adding to this confusion, overlapping nomenclature was used to describe both CFU-Hill cells and cells cultured in this assay due to similarities in the timing of their early appearance in cell culture as well as the immunophenotype and lineage of cells in these populations.

1.4 The origin of ECFCs and other vascular progenitor cells

The origin of human ECFCs remains unresolved. An early study published by Lin et al. in 2000 provided the first evidence suggesting a bone-marrow origin for these circulating endothelial progenitor cells with a high capacity to differentiate into cells with a vascular endothelial phenotype.[48] Blood was drawn from 4 patients who had received a sex-mismatched bone marrow transplant. Analysis of donor or recipient Y-specific DNA in endothelial cell-enriched cultures grown from recipient blood revealed that 95% of cells from fresh blood contained the recipient genotype. The same blood samples were cultured *in vitro* and after 4 weeks, endothelial cells cultured demonstrated a gradual change from recipient to donor genotype. Using the culture methods of Yoder et al,[21] cells isolated from circulation with

recipient genotype expanded 17-fold while cells with the donor genotype expanded more than 1000-fold. These results suggested that circulating endothelial cells in fresh blood originate from the vessel walls and have limited proliferative capacity. In contrast, the cells responsible for the *ex vivo* cultures of endothelial cells from blood were claimed to be derived from transplantable marrow-derived cells.

This finding lead to the generation of an exciting hypothesis that bone marrow-derived angioblasts with high proliferative potential exist and may engraft to areas of vascular injury. However, definitive evidence of the existence of these rare angioblasts with robust proliferative potential has not yet been discovered. Proof of circulating angioblasts would require two groundbreaking discoveries: (1) the identification of a novel and specific marker unique to this cell and not expressed on mature endothelium, and (2) development of a single-cell culture assay capable of accurately detecting the starting clone and its specific progeny.[49] While existence of a bone marrow-derived angioblasts would be an exciting revolution in endothelial progenitor cell research, proof of this hypothesis has not been published. Without these data, a bone-marrow origin for ECFCs remains controversial, and more recent studies provide evidence suggesting that ECFCs do not originate from the bone-marrow.[50] In male patients previously transplanted with female bone marrow, ECFCs isolated from peripheral blood and venous wall exhibited an XY genotype. MACs derived from these patients displayed an XX genotype, which was consistent with their bone marrow origin.[51]

A growing body of literature has identified that ECFCs arise from various progenitor cell niches within the vascular wall of large vessels. The idea that ECFCs originating within the vascular wall contribute to postnatal vasculogenesis began with a publication by Alessandri et al. in 2001.[52] Aortic explants from human embryos embedded in collagen gels grew branching

capillary-like structures with luminal cells expressing markers CD31, CD34, vWF, and VEGFR-2 indicative of endothelial differentiation. These capillary-like structures of mature endothelial cells sprouted from immature $CD34^+/CD31^-$ endothelial-like cells in the outer regions of aortic rings, suggesting they developed into $CD31^+$ endothelial cells via vasculogenesis rather than angiogenesis. To demonstrate this, immature $CD34^+/CD31^-$ cells were isolated from aortas using the same magnetic bead-assisted $CD34^+$ cell derivation and expansion protocol employed by Asahara et al. to isolate vasculogenic $CD34^+$ cells from PB MNCs. The $CD34^+/CD31^-$ cell population differentiated into a more mature endothelial phenotype expressing CD31 and vWF after 1 week, and after 3 weeks these cells were seeded on Matrigel to form a net of capillary-like structures following 24 hours of incubation. These findings were the first report of *ex vivo* formation of human microvasculature by vasculogenesis in adults.

ECFCs have since been isolated from the vascular wall of human aorta,[53] pulmonary artery,[54] and saphenous vein,[55] as well as human lung tissue,[56] placenta,[57] white adipose tissue,[58] and human induced pluripotent stem cells (hiPSCs) sorted for Neuropilin 1 and CD31.[59] RNA sequencing demonstrated that ECFCs display a gene expression profile more closely resembling human coronary artery endothelial cells (HCAECs) and HUVECs than non-endothelial cell types, including the subcutaneous adipose tissue-derived stromal vascular fraction.[60] The transcriptomic profile of ECFCs is closer to that of microvascular ECs than macrovascular ECs.[61] Altogether, evidence points to the vascular wall of large arteries as an origin for ECFCs and ongoing research has elucidated where within the vessel wall ECFCs reside.

1.4.1 Tissue-resident ECFCs within the vascular wall of large arteries

A considerable body of research has demonstrated a significant role of tissue-resident progenitor cells in vascular growth. The term “vascular precursor cells” describes a general pool

of stem/progenitor cells that give rise to mature cell types composing the blood vessel walls, such as endothelial cells, smooth muscle cells (SMCs), and fibroblasts. Except for smooth muscle progenitor cells, which are stored and produced in the bone marrow, vascular precursor cells originate within the vascular wall. Embedded within the vascular wall, these tissue-resident vascular progenitor cells must cooperate with the ensemble of other vascular cells in the blood vessel wall to coordinate homeostasis, growth, and repair through the continuous release of paracrine signaling molecules.[62, 63] The first *in vivo* data showing that tissue-resident vascular progenitor cells play a major role in postnatal vasculogenesis was published in 2004 with the demonstration that depletion of bone marrow prior to femoral artery occlusion did not attenuate initial vascular growth in rats.[63] Tissue-resident progenitor cells therefore also participate in vascular repair. TIE2-GFP transgenic mice expressing green fluorescent protein (GFP) in endothelial cells received transplants of wire-injured carotid artery segments from wild-type mice. Flanking ECs were observed to migrate into the injured vascular segments, and no homing or implantation of circulating progenitor cells was evidenced.[62] Literature centers on two main functions of resident vascular progenitor cells: (1) as the origin of various cell types that form new blood vessels, and (2) as a source of inflammatory cells mediating local immune response.

Where within the vessel wall do these vascular precursors reside? Of particular relevance, where do ECFCs reside? Knowledge of the answers to these questions is likely incomplete, but here we describe the current understanding of the composition of these vascular progenitors in the vascular wall from the luminal side outward. The mature blood vessel wall consists of three concentric layers – the tunica intima, tunica media, and tunica adventitia. The tunica intima consists of a simple squamous ring of endothelium surrounded by connective tissue consisting of collagen, laminin, fibronectin, and other extracellular matrix molecules. Underneath lies a basal

layer of elastic tissue called the internal elastic lamina, which separates the tunica intima from the tunica media. The tunica media is comprised of smooth muscle cells, collagen, and elastic tissue. The outermost layer known as the tunica adventitia provides a limiting barrier consisting of collagenous and elastic fibers to protect the vessel from overexpansion.

The intima is the innermost layer of a vessel and is one home for ECFCs. Traditionally, all intimal ECs were believed to be terminally differentiated mature ECs that can proliferate and migrate to replace nearby damaged ECs via angiogenesis.[64] Paradoxically, human umbilical vein endothelial cells (HUVECs) and human aortic endothelial cells (HAECs), which have been considered fully differentiated and mature ECs that are often used as control cells in progenitor cell studies, can be passaged for at least 40 population doublings with growth kinetics similar to adult- and umbilical cord blood-derived vascular progenitor cells. Clarity to this apparent contradiction was provided by evidence of a complete hierarchy of ECFCs within both HUEVCs and HAECs derived from vessel walls. In this study, HUVECs or HAECs were compared to umbilical cord blood-derived ECFCs. Single cells from each population demonstrated an ability to proliferate into colonies, and this clonogenic potential was similar between all three cell sources. All expanded cells expressed EC surface markers CD31, CD141, CD105, CD146, CD144, vWF, and VEGFR-2. These data suggest that a subset of ECFCs exist within the population of endothelial cells in the vascular intima and give rise to the ability of endothelial cells from both veins and arteries (HUVECs and HAECs, respectively) to proliferate.[53]

Home to a variety of vascular precursor cell types, the tunica media of blood vessels consists of concentric structural collagen and elastic fibers as well as SMCs responsible for mediating contractility. Isolated from the tunica media of adult mice, a “side population” (SP) of cells that are lineage-negative (i.e., devoid of lymphocytes, macrophages, granulocytes,

erythrocytes, and red blood cells via magnetic bead-assisted negative selection) with surface characteristics c-kit$^{-/low}$Sca1^{+}CD34$^{-/low}$ are multipotent *in vitro*. When cultured with VEGF, SP cells differentiate into endothelial cells expressing CD31, VE-cadherin, and vWF; when cultured with TGF-β and platelet derived growth factor-BB (PDGF-BB), SP cells differentiate into SMCs expressing characteristic αSMA, calponin, and SM-MHC.[65] In addition to this evidence in mice, two distinct cell types with proliferative capacity have been identified between the media and adventitia in human thoracic aorta – one population of CD34^{+} cells and another composed of c-kit^{+} cells. Interestingly, both cell types expressed markers of mesenchymal stem cells (MSCs). With VEGF induction, these cells acquired an endothelial immunophenotype characterized by increased VEGFR-2 and vWF expression and an ability to form capillary-like structures in angiogenesis assays *in vitro*.[66] Together, these studies suggest that cross-talk between vessel-resident mesenchymal stromal cells may induce differentiation of mesenchymal stromal cells into endothelial cells to play a role in vascular healing and homeostasis.

Between the medial smooth muscle and adventitial blood vessels lies the 'vasculogenic zone.' First reported by Zengin et al., this zone is another source of tissue-resident vascular progenitor cells in adults and was found in vessels from a wide range of organs including urinary bladder, testis, prostate, kidney, lung, heart, liver, and brain.[67] Immunohistochemical and flow cytometric analysis of human internal thoracic artery (HITA) demonstrated that immature CD34^{+}/CD31^{-} cells occupy this vasculogenic zone. In a HITA ring assay, capillary-like outgrowths grew within a week. These sprouts consisted of CD34^{+} cells that migrated as immature CD34^{+}/CD31^{-} cells from the vasculogenic zone and developed activated endothelial cell marker carcinoembryonic antigen-related cell adhesion molecule 1 as well as mature endothelial surface markers VEGFR-2, Tie2, and VE-cadherin. This phenomenon indicated that

endothelial precursors within the vasculogenic zone have the capacity to differentiate into mature endothelial cells *ex vivo*. Also within the vasculogenic zone reside multipotent stem cells capable of differentiating into hematopoietic and local immune cells including macrophages.[68] In mice, immature $CD34^+/CD31^-$ endothelial cells residing in the vessel wall have progenitor-like functionality. A small population of c-kit-expressing ECs in the vascular endothelium of mice is capable of clonogenic expansion *in vivo* and *in vitro*.[69] Expressing the markers CD31, CD105, Sca1, CD117, and c-kit, these vascular endothelial stem cells comprised only 0.4% of nonhematopoietic $CD31^+/CD105^+$ vessel wall ECs but a single transplanted VESC can generate functional blood vessels that connect to host vasculature *in vivo*.

1.5 Preclinical considerations of ECFC-based therapeutics

Before entering clinics, an ECFC-based therapeutic must meet a variety of logistical, biological, and safety standards. Various preclinical studies have demonstrated ECFCs' ability to meet such requirements. Logistically, ideal cells should be easy to derive, propagate, and maintain since cell culture is characterized by intensive labor, time, and monetary costs. Derivation and differentiation protocols require standardization and optimization to achieve adequate cell numbers that could meet clinical demands. The protocol to obtain ECFCs from MNCs in umbilical cord or peripheral blood has been well documented.[70] ECFCs have high proliferative capacity *in vitro*, rapidly form colonies that display characteristic monolayer cobblestone-like morphology by day 6, demonstrate a well-defined cocktail of identifying surface markers, and double every 34 hours in the first 40 days.[16, 29, 71] In a mouse model of ischemic retinopathy (oxygen-induced retinopathy, OIR), delivery of low dose ($1x\ 10^3$) ECFCs is as effective as higher doses (1×10^5), a cell number 500-fold lower than that required to treat murine ischemic limb models.[72] These data demonstrate the feasibility of manufacturing

sufficient cell numbers for treatment of large sums of patients suffering from ischemic disease using blood from a single cord blood donor, an important implication for minimizing manufacturing costs.

Biologically, cultured cell therapies must demonstrate long-term *in vitro* expansion capacity with low immunogenicity, robust repeatable functionality *in vivo*, and genetic and karyotypic stability. Autologous cells are ideal, presenting the lowest risk of immune response and rejection. A stable *ex vivo* population of ECFCs can be derived from PB MNCs relatively quickly, meaning they may prove useful as an autologous therapy.[30] While this turnaround time for ECFC isolation and expansion may limit their utility as an autologous therapy for acute ischemic conditions like myocardial infarction, autologous ECFCs may represent a therapy for diseases with a wider therapeutic window such as retinopathy of prematurity or chronic ischemic/degenerative diseases like diabetic retinopathy. However, the number and angiogenic capacity of circulating vasculotrophic cells in PB may vary depending on disease state such as diabetes.[73]

Alternatively to PB-derived ECFC-based autologous therapies, umbilical cord blood (UCB)-derived ECFCs are a promising source allogeneic therapy. Banks of allogeneic cells from pooled umbilical cord blood of healthy patients is a viable cryotherapy modality. Allogeneic ECFCs derived from UCB exhibit a low pro-inflammatory and pro-thrombotic profile.[74] Nevertheless, the immunocompatibility of ECFCs can be optimized via the creation of cell banks where donor cells' human leukocyte antigens (HLA) haplotypes are characterized in detail to match population requirements. Such a model is currently employed for stem cell banking of human embryonic stem cells in China[75] and for human induced pluripotent stem cells in Japan.[76] The karyotype of ECFCs is considered relatively stable. However, chromosomal screening prior

to clinical use of cryopreserved cells may be required since chromosomal abnormalities, most often translocation/deletion defects on chromosome 14, have been reported.[71] In addition, the Friedlander lab has developed xeno-free media and xeno-free cell attachment substrate that allow for robust *ex vivo* expansion of ECFC lines using animal free products, bringing allogeneic ECFC cryotherapy one step closer to a clinical reality.[29] Additionally, UCB-derived ECFCs are non-controversial as they can be harvested painlessly from otherwise discarded tissue in great abundance and provide robust proliferative potential to facilitate blood vessel formation *in vivo*.[77] Furthermore, expansion of ECFCs from human term placenta is capable of producing the equivalent number of cells as obtained from 27 umbilical cord blood donors.[78]

One important consideration of ECFCs in culture is that *ex vivo* expansion of ECFCs leads to replicative senescence and an impaired vasoreparative function *in vivo* in 'late-passage cells,' which were operationally defined to be later than passage 6 for peripheral blood- and passage 12 for cord blood-derived ECFCs. This senescence is markedly delayed relative to other endothelial cell types, suggesting an ability for long-lasting effects with little risk of tumor growth. However, this phenomenon has a senescence-associated secretory phenotype (SASP) with cytokines IL6, IL1-alpha, IL1-beta, and IL8 as major regulators. This inflammatory component of ECFC senescence has implications in their clinical use because these cytokines may affect microenvironment conditions, cell engraftment and survival, and, ultimately, the clinical outcome. Depletion of IL8 by shRNA in late passage ECFCs delays their senescence, improves their proliferation rates, and restores their vasoreparative capacity in treating OIR mice, which indicates that modulation of the SASP may be used to optimize ECFC expansion and therapeutic benefit.[79] Early passage ECFCs do not display hallmarks of senescence; in fact, some

evidence supports a role of IL8 in the mitogenic effect of UCB-derived ECFCs in passages 4 through 8.[80]

Lastly, ECFCs have demonstrated a favorable safety profile in preclinical studies. The majority of ECFCs intravitreally injected into OIR mice exhibit a pyknotic nucleus suggestive of cell death after 24 hours, and by day 3 no human DNA was detectable by PCR analysis for human Alu sequences. No immune cell infiltration, tissue edema, tumor formation, and retinal detachment were detected 7 days after intravitreal ECFC-injection into OIR mice.[72] ECFCs were not tumorigenic and did not induce thrombosis or infarcts in 9 organs examined 7 months after systemic tail vein delivery in nonobese diabetic/severe combined immunodeficiency (NOD/SCID) mice.[81] ECFCs have been observed to home to sites of ischemia/angiogenesis, and intravitreal injections easily deliver localized and concentrated cell therapy to the retina. While intravitreal injections deliver cells directly to target tissues, systemic delivery may bypass the need for ECFCs to cross the internal limiting membrane (although intravitreally injected ECFCs have been shown to cross the ILM in murine disease models[72]) and may avoid some complications associated with intravitreal drug delivery including endophthalmitis, retinal detachment, elevated intraocular pressure, and ocular hemorrhage.[82] In the murine OIR model, systemic administration of ECFCs into the carotid artery promoted vascular repair only in the ipsilateral ischemic eye, and this homing mechanism to ischemic areas may lower risk of deleterious side effects from systemic delivery.[72] In mouse models of ischemic hindlimb, ECFC treatment demonstrated low immunogenicity; comparable numbers of immune cell infiltration were observed in UCB-derived ECFC-treated mice versus control mice, and these ECFCs persisted for at least 4 weeks following injection.[83] Both at steady-state and following stimulation with γ-interferon, immature ECFCs from UCB exhibit an HLA-ABC^{+} and HLA-DR^{-}

immunophenotypes similar to that of MSCs, which are often classified as non-immunogenic and thus commonly transplanted without stringent HLA-matching. UCB-derived ECFCs demonstrated a weaker pro-inflammatory and pro-thrombotic gene expression profile than adult PB-derived ECFCs. UCB-derived ECFCs exposed to allogeneic lymphocytes and monocytes induced fewer co-stimulatory molecules and pro-inflammatory cytokines than adult PB-derived ECFCs. Ultimately, a definitive assessment of ECFCs' safety profile must come from in-human clinical trials, which will dictate the level of immunosuppression or HLA-matching required for ECFC therapy since ECFCs express the HLA-ABC milieu at baseline and HLA-DR upon induction with γ-interferon.[74]

1.5.1 Bolus ECFC transplantation

Two routes of delivery have been utilized for *in vivo* studies of the use of ECFCs for tissue repair and regeneration: bolus injection of cells either systemically or directly into the target tissue, and implantation of biocompatible scaffolding embedded with cell therapy. Cells injected systemically as a bolus have induced tissue regeneration in numerous neovascularization-dependent animal models of peripheral ischemia,[84-88] vessel damage,[89] traumatic brain injury,[90, 91] stroke,[77, 92, 93] acute kidney injury,[94] acute myocardial infarction,[95-97] lung-related diseases,[98, 99] and diabetes-related or hyperoxia-induced ischemic retinopathy.[29, 71, 72, 100] Though effective in a wide variety of ischemic contexts, success of systemically applied therapeutic ECFCs suffered from low engraftment and limited survival time within target tissues. Bolus injection of ECFCs do home to areas of ischemic injury, but also accumulate within untargeted organs. Tail vein injected cells were present as single cells or lines of cells in nine organs: brain, gut, heart, kidney, liver, lung, ovaries/testis, spleen, and bone marrow. Three hours post-injection, the highest numbers of ECFCs were detected in the lungs by qPCR. Stained cells

in sectioned tissue were found predominantly in peribronchial areas and, more rarely, in the alveoli and bronchi. ECFCs lodged in lung tissue through interaction with E-selectin, P-selectin, and α_4 integrin on mouse vasculature; treatment of mice with antibodies to these proteins prior to ECFC injection resulted in fewer cells lodged in lungs. Pre-treatment of mice with anti-vascular cell adhesion molecule (VCAM) did not reduce lodging in mouse lung, bone marrow, or spleen, suggesting that α_4 integrin may bind other ligands in these tissues. Antibody inhibition resulted in only a partial reduction of lodged cells, so ECFCs likely lodged in lungs by mechanical forces as well.[81] Lodging of ECFCs in the lungs may be transient; in the murine model of ischemic hindlimb, ECFCs were only temporarily trapped in the lungs and homed to the ischemic area after 6 hours.[101] Between 24 and 96 hours after tail vein injection of radiolabeled ECFCs, approximately 70% of radioactivity localized to the spleen in liver.[102] ECFCs within these nine different organs expanded (6-fold in bone marrow and spleen, 3-fold in liver and ovaries/testis, and 1.5-2 fold in all other organs) over the 2-16 week time course after injection, indicating many organs provide a favorable environment for implantation and expansion of ECFCs. Older passage 15 ECFCs demonstrated equal expansion capacity *in vivo* in comparison to younger ECFCs.[81] On one hand, the widespread localization of ECFCs may be a caveat to systemic administration; on the other hand the *in vivo* survival and expandability together with the low toxicity of ECFCs may prove useful in delivering gene therapy.

Many studies injecting ECFCs systemically showed efficacy but were unable to provide a detailed mechanistic understanding of ECFCs' contribution to neovascularization. While understanding the systemic distribution of ECFCs is an important pre-clinical consideration for therapy, intravitreal injection of ECFCs directly targets retinal tissue maximizing the potential for cells to home to ischemic sites in need of vascular repair. Since cells are largely contained

within the vitreous, this targeted administration of bolus ECFCs reduced cells in systemic circulation and thus minimizes risk of deleterious off-site effects. In this contained system, the dosage of intravitreally cells injected can be titrated to accurately investigate the required cell number to achieve a desired therapeutic effect in retinal tissue. ECFCs can be intravitreally injected with small gauge needles to limit injection trauma although reflux of injected cells can confound accurate quantification of an injected dose. Since the average diameter of ECFCs in cell suspension ranges from 12-18 μm, ECFCs are not lysed when passed through 34G and 36G microneedles with internal diameters of 85 μm and 35 μm, respectively.

1.5.2 ECFC pre-vascularization of tissue-engineered scaffolds

ECFCs can pre-vascularize a variety of biocompatible tissue-engineered constructs for transplantation. Studies *in vivo* indicate that implantation of pre-vascularized tissue-engineered scaffolds may represent a highly effective and feasible therapeutic approach for harnessing the neovascularization and regeneration ability of ECFCs. There are several advantages of this approach: (1) alteration of the natural or synthetic scaffolding materials offers control of microenvironmental influences on vascularization; (2) addition of vasculotrophic mediators within the scaffold can improve tissue regeneration; and (3) co-implantation of multiple cell types may augment neovascularization and/or intercellular cross-talk to promote differentiation towards a tissue-specific cell fate. These advantages support utilizing biocompatible scaffoldings enriched in pro-angiogenic factors that are pre-vascularized with ECFCs in combination with other cell type(s) as a viable therapeutic strategy for tissue regeneration.

Seeding ECFCs in a variety of natural biomaterials including hyaluronic acid,[103-105] gelatin,[106, 107] alginate,[108] and collagen or fibrin hydrogels[109-111] promoted vasculogenesis *in vivo* upon implantation. Each natural biomaterial possesses individual properties that may be

disadvantageous for tissue engineering. Efforts to optimize scaffolding material by chemical modification or combination with peptides have sought to overcome these limitations and augment the *in vivo* pro-angiogenic potential of ECFC pre-vascularized constructs.[105-108] The most commonly used synthetic polymers include poly-L-lactide, poly(D,L-lactic-co-glycolic acid), biphasic calcium phosphate, β-tricalcium phosphate or polycaprolactone because they are inexpensive, FDA approved, and their mechanical properties can optimized to improve in vivo neovascularization.[112] Lacking cell adhesion peptides, synthetic materials are coated with natural biopolymers including fibrin,[113] fibronectin,[114] or RGD sequences[115] and can also be crosslinked with growth factors including VEGF,[116] HGF, angiopoietin (Ang)-1,[117] or bone morphogenetic protein-2[118] to enhance their proangiogenic effects on injected or infiltrating cells. Studies transplanting ECFCs and other cell types within scaffolds offer insight into mechanisms of combination therapy that rely on intercellular cross-talk and are covered in greater depth in a later section (1.7.4).

1.5.3 Limitations of ECFC-based therapy

Certain obstacles to translation must be addressed before ECFCs become a clinical reality. First, despite our growing understanding of the ECFC immunophenotype, there is still no known distinguishing marker for HPP-ECFCs. This highly anticipated finding would allow for prospective isolation of a homogenous population of ECFCs with the highest therapeutic potential. Instead, current ECFC culture techniques contain the entire ECFC hierarchy consisting of low proliferative potential-ECFCs, ECFC clusters, and even non-proliferative endothelial cells.[53] Second, UCB-ECFCs are a promising source of allogeneic cryotherapy but the manufacturing costs incurred with processing, freezing, and storage of banked haplotypes might be prohibitive. Third, autologous ECFCs present a combination of obstacles. ECFC isolation is

not currently plausible in the pediatric patient since these cells circulate in the blood stream at a concentration of 1 cell per 10^6-10^8 mononuclear cells.[53] If this obstacle were overcome, perhaps ECFCs may be an option for infantile ischemic retinopathies like retinopathy of prematurity, but the expense of banking a cell line with single-lineage differentiation capacity for (only potential) use in adulthood is once again problematic. In adolescents and adult patients, autologous ECFCs may be harvested from PB but are less clonogenic, proliferative, and angiogenic than UCB-ECFCs.[23] However, efforts to improve the proliferative capacity of PB-derived ECFCs are successful and ongoing.[98] Lastly, disease states alter the frequency and function of isolated ECFCs. In diseases like diabetes where these cells may pose a promising treatment strategy, ECFC functions may be impaired to such an extent that cells may not be a viable option to promote revascularization.[73]

1.6 Goals and mechanisms of ECFC-based therapy

Is the utility of ECFC-based cell therapy derived from the cells' ability to integrate into the host to replace lost or damaged endothelium? Or is the therapeutic benefit of ECFC-based cell therapy owed to their ability to support, protect, and promote growth of resident progenitor and mature endothelial cells via paracrine action?

Cell replacement strategies are currently under investigation for the treatment of various retinal diseases including macular degeneration, where atrophy of the retinal pigment epithelium is part of a chain of events leading to the loss of vision. Injections of embryonic stem cell-derived and induced pluripotent stem cells differentiated into RPE demonstrated biocompatibility and visual improvement for some patients in phase I and II clinical trials.[119] While these results support the concept of replacing damaged cells with stem cells, replacement cell strategy may be more difficult to apply to ischemic disease where an underlying ischemic drive affects numerous

cell types. Diabetic retinopathy, for instance, decreases function of the vascular endothelium, vascular pericytes, retinal pigment epithelium, and choriocapillaris while also exhibiting glial dysfunction, activated microglia, and neuronal damage.[120] Harnessing the ability of stem and progenitor cells to target multiple cell types with multiple mechanisms simultaneously via paracrine action is a promising alternative approach. Such strategies may extend the capacity of treatments beyond targeting vascular leakage in end-stage disease by promoting physiologic vascular growth and stability as well as neuroprotection.

There are significant considerations to cell-based therapy, including an unclear therapeutic window for treatment. Generally, both cell replacement and support strategies are reliant upon the existence of sufficient viable retinal cells. One concern is that transplantation of replacement cells at a time when vasculopathy and neurodegeneration are beyond rescue may limit the treatment's ability to restore or preserve vision. This is also true for support cells, which additionally rely on the viability of sufficient viable target cells in order to effectively achieve their trophic paracrine effects. Conversely, treatment too early may reduce the benefits of cell therapy. Without sufficient degeneration of host cells, early transplantation of replacement cells may not allow for engraftment and functionality of implanted cells. Use of support cells or paracrine mediators may circumvent this obstacle since early treatment would likely be effective even if encountering a limited population of damaged cells. Early diagnosis and intervention to prevent progression in conditions like diabetic retinopathy have the highest likelihood of success in such a complex disease.

Successful treatment of ischemic/degenerative retinopathy would be defined by restoring or minimizing vision loss in patients. To do so, cell therapy must address the underlying ischemic drive by providing trophic support to delay or rescue vascular/neural degeneration

and/or by replacing damaged vasculature and neurons. This section discusses the various mechanisms by which ECFCs exert such neurovasculotrophic effects. We begin with a discussion of literature detailing the therapeutic mechanisms of ECFCs in retinal animal models. Some reports demonstrate the role that integration of ECFCs plays in improving endothelial cell junctions and vascular integrity.[71] Others have not observed ECFCs to integrate into host retinal vasculature and attribute the efficacy of ECFCs to secreted factors like insulin-like binding protein (IGFBP) 2 and IGFBP3. While studies in retinal disease models are most clinically relevant to ischemic retinopathies, findings from across fields offer additional insights into the mechanisms of ECFC treatment. Transplanted ECFCs interact both directly[121] and indirectly[122] with the host's immune system. ECFCs also improve vascular defects by regulating components of extracellular matrix (ECM) remodeling[123] as well as stimulating the release of growth factors from endogenous cells.[83, 90-92, 96] Lastly, we discuss studies co-injecting ECFCs and other cell types as they shed light on the intercellular cross-talk that facilitates improved therapeutic outcomes in combination therapy.[124]

1.6.1 Therapeutic mechanisms of ECFCs in ischemic retinal disease

Within the eye, ECFCs have reproducibly demonstrated efficacy in reversing diabetes-related or hyperoxia-induced ischemic retinopathy.[29, 71, 72, 100] Earlier studies published by Medina et al. suggested that ECFCs integrate into retinal vasculature to rescue OIR mice.[71] In the Friedlander lab, intravitreally injected ECFCs were not observed within the retinal vasculature but, rather, remained in the vitreous and lens with some cells assuming perivascular positions in regions of ischemia, presumably mediating rescue of OIR retinas via paracrine action.[29] In a more recent publication by Medina and colleagues, ECFCs intravitreally injected into healthy mice were observed to reside in the vitreous and not integrate into host vasculature. Within 3

days of delivery these ECFCs underwent cell death and no human Alu sequences were detected in mouse retinas.[72] The mechanism of ECFC-mediated vascular repair in the retina is likely a combination of both direct cell replacement and paracrine effects. Though ECFC integration into retinal vasculature has been observed, engraftment occurs at low levels. Perhaps this results from limitations of experimental animal models used in these studies. After the peak of the neovascular phase of the OIR model on day 17, the pre-retinal neovascular tufts regress spontaneously and the vasculature is restored to normal physiological patterning by day 21.

The observation that ECFCs did not integrate into healthy mouse eyes may also be due to their immunocompetency. While retina disease models more amenable to ECFC engraftment may facilitate evaluation of the contribution of ECFC integration to their mechanism of action, evidence to this point has demonstrated potent therapeutic effects with minimal (if any) integration of ECFCs into host retinal vasculature. This suggests that harnessing the paracrine mechanisms of ECFCs may be a promising strategy for the treatment of ischemic retinopathies. Here, we review the publications to date that provide insight into putative mechanisms of ECFCs as cell replacement therapy followed by reports describing their paracrine effects in neurovasculotrophic retinal repair.

1.6.2 Integration of ECFCs

When co-cultured with human retinal microvascular endothelial cells (hRMECs) *in vitro*, ECFCs demonstrated an ability to integrate alongside hRMECs forming a confluent and homogenous monolayer after 2 days. The same effect was observed when ECFCs were co-cultured with human dermal microvascular endothelial cells (DMECs). Using immunohistochemistry, the confluent cell monolayer was observed to uniformly express proteins of adherens and tight junctions such as cadherin, ß-catenin, and zonula occludens (ZO)-1,

indicating intercellular junctions between ECFCs and DMECs characteristic of an endothelial barrier. A distinctive characteristic of endothelial cells is the ability to form 3D culture systems when plated on Matrigel basement membrane matrix. The *de novo* tube formation of ECFCs is this system was comparable to that of hRMECs. When co-cultured, ECFCs incorporated into tubes formed predominantly by hRMECs and this phenomenon persisted when ECFCs were plated at a lower ratio of 1:4.[71]

Upon injection of quantum dot labeled ECFCs into the murine OIR model of ischemic retinopathy, Medina et al. observed integration of single cells within the intraretinal vasculature to form mosaic vessels with host cells. Injected ECFCs preferentially homed to the central zone of ischemia and rescued the neovascularization and vaso-obliteration in OIR mice.[71] ECFCs that were derived from human induced pluripotent stem cells also rescue NV and VO in OIR mice and quantum dot-labeled cells were similarly seen to integrate into host vasculature.[59] The integration of ECFCs may be enhanced by co-transplantation with other agents. For instance, ECFCs that were intravitreally injected along with adeno-associated virus serotype 2 encoding a more stable, soluble, and potent formulation of angiopoietin 1 (AAV.COMP-Ang1) into mice with diabetic retinopathy exhibited a significantly higher degree of integration. Exposure of ECFCs to AAV.COMP-Ang1 in vitro increased cell migration and tubulogenesis. A vascular growth factor, Ang-1 is a therapeutic target for diabetic retinopathy as it is abnormally low in patients with diabetic retinopathy.[125] Ang-1 binds Tie-2 on endothelial cells to induce vessel quiescence and maturation. Ang-1 also inhibits vascular leakage by preventing VEGF-induced degradation of VE-cadherin, a transmembrane protein in the adherens junction between endothelial cells that enhances vascular integrity and lowers vascular permeability.[126, 127] Additional techniques to improve the therapeutic benefits of ECFCs is the subject of ongoing

research, but limited research to date has evaluated the impact of these methodologies on the efficacy of ECFCs in retinal diseases.

1.6.2 Paracrine action of ECFCs

Studies from the Friedlander lab reported that ECFCs intravitreally injected into OIR mice were not observed within host vasculature. Injected GFP+ ECFCs were observed to home to the vitreous or lens and assumed perivascular positions to secrete paracrine factors mediating the rescue response. Conditioned media (CM) of ECFCs recapitulated these rescue effects in OIR, further suggesting paracrine mechanism of action. To characterize and identify functionally active cells within the ECFC population, the Friedlander lab proposed to fractionate ECFCs into two populations: cells that are high in their surface marker expression of CD44 ($CD44^{hi}$) and those with low expression ($CD44^{lo}$).[29] The transmembrane glycoprotein CD44 is the canonical receptor for hyaluronic acid, which is abundant in the vitreous body, and also acts as a receptor for extracellular matrix proteins including collagen and osteopontin.[128, 129] CD44 can form co-receptor complexes with receptor tyrosine kinases to participate in cellular signaling, and cells with high CD44 expression display stem-like properties in normal and neoplastic tissue and home to specific tissue niches.[129-131] The Friedlander lab's hypothesis was based on the lab's earlier work demonstrating that injection of lineage-negative $CD44^{hi}$ hematopoietic stem cells migrated to avascular regions of the retina, differentiated into microglia, and rescued the OIR phenotype in a hypoxia-inducible factor 1-α (HIF-1α) dependent fashion.[132] Intravitreal injection of $CD44^{hi}$ ECFCs rescued both neovascularization and vaso-obliteration in the OIR model. $CD44^{lo}$ ECFCs had no effect, nor did ECFCs with knocked-down CD44 expression via lentiviral transduction of short hairpin RNA against CD44.[29]

Findings also indicated neurotrophic activity for $CD44^{hi}$ ECFCs. Thicknesses of the inner nuclear layer (INL) and inner plexiform layer (IPL) are reduced in OIR mice, and treatment with $CD44^{hi}$ ECFCs restored the INL and IPL to thicknesses comparable to normoxic mice. Electroretinography (ERG) measurements of retinal neural function demonstrated that $CD44^{hi}$ ECFCs improved the scotopic b wave (rod-driven) response in OIR mice, suggesting improved function of the inner retina. A more thorough characterization of the neuroprotective effects of $CD44^{hi}$ ECFCs was carried out in the retinal degeneration 10 (RD10, $Pde6b^{rd10/rd10}$) mouse model of neurodegeneration. In the RD10 mouse model, photoreceptor cell death begins concurrently with vascular atrophy in the retina's deep vascular plexus. The ONL degenerates chiefly by apoptosis resulting in progressively worsening neural function on ERG. Injection of $CD44^{hi}$ ECFCs into RD10 mice rescued both the vascular and neurodegenerative components of the model. Integrity of the deep vascular plexus was preserved following injection with $CD44^{hi}$ but not $CD44^{lo}$ ECFCs. $CD44^{hi}$ ECFCs were neuroprotective in RD10 mice, improving ONL thickness while also decreasing the density of apoptotic cells in the ONL. Both photopic (cone-driven) and scotopic (rod-driven) responses were increased following treatment with $CD44^{hi}$ ECFCs relative to $CD44^{lo}$ ECFC or vehicle controls.[29] Together, this work demonstrated the existence of a therapeutically active subset of ECFCs characterized by elevated CD44 expression that is responsible for the therapeutic benefit of ECFCs in murine models of ischemic retinopathy and neurodegeneration.

While the efficacy of ECFCs is linked to expression levels of CD44, the exact mechanistic role of this surface marker remains unclear. Evidence suggests CD44 may mediate the vasculotrophic and neurotrophic through its correlated expression with IGFBPs.[29] Knockdown of CD44 in ECFCs grown in 3D culture conditions downregulated several

proangiogenic factors including IGFBP2 and IGFBP3 when compared to control ECFCs. Media conditioned by cells with knocked-down expression of CD44 contained reduced levels of IGFBP2 and IGFBP3 compared to CM from control ECFCs. Significant reduction of these IGFBPs were detected in OIR eyes treated with CD44 knockdown versus control ECFCs. Intravitreal injection of human recombinant IGFBP2[29] or IGFBP3[29, 133, 134] alone rescued the OIR model. ECFC-CM rescued OIR, and depletion of these IGFBPs from CM attenuated this effect. Together, these data indicated a correlation between CD44 expression and the production of IGFBP2 and IGFBP3, which alone were effective in rescuing OIR, and demonstrated the involvement of IGFBP2 and IGFBP3 in the paracrine rescue mechanism of ECFCs in mouse models of ischemic retinopathy.

As the name implies, IGFBPs are classically known for their endocrine role as carriers for insulin-like growth factors (IGFs). Localizing in pericellular and intracellular compartments, IGFBPs possess both endocrine function as well as autocrine and paracrine functions to regulate cell migration, adhesion, apoptosis, survival[135] and the cell cycle.[136, 137] IGFBP3 is the most well-characterized of this protein family, responsible for carrying approximately 75% of serum IGF1 and IGF2. Similar to other members in the IGFBP family, IGFBP3 has effects independently of carrying IGF1. Human studies on the vitreous proteins of diabetics with varying degrees of neovascular eye disease demonstrated that ischemia is a potent stimulus for the local tissue production of IGFBP3.[138] Increased IGFBP3 expression as a result of hypoxia promoted angiogenesis in some systems but inhibited vascular growth in others, thus exhibiting a system-dependent effect on vasculature.[136, 137, 139, 140]

In the retina, evidence has suggested a multifaceted role for IGFBP3 as a protective agent for ischemic retinopathies, especially in the context of diabetes. IGFBP3 promoted the

endothelial maturation and function of heterogeneous CD34+ progenitor cell populations *in vitro*,[133] decreased apoptosis of retinal endothelial cells,[141] and restored normal insulin signaling in retinal endothelial cells of diabetic rats.[142] Following oxygen-induced vaso-obliteration, IGFBP3 knockout mice demonstrated a 31% increase in the area of vessel loss and 30% fewer CD34+ cells compared to IGFBP-expressing controls, suggesting that IGFBP3 may contribute to vessel repair via interactions with cells within the CD34+ population.[134] Exposure of the heterogeneous CD34+ cell population to IGFBP3 *in vitro* induced differentiation into mature endothelial cells and increased cell migration and capillary tube formation. Levels of IGFBP3 were undetectable in CD34+ cells. As a result, these immature CD34+ cells were sensitive to minor increases in endogenous tissue levels or exogenous administration of IGFBP3.[133] *In vitro*, IGFBP3 decreased apoptosis in retinal endothelial cells through activating IGFBP3 receptor in an hyperglycemic environment.[141] In streptozotocin (STZ)-induced diabetic rats, treatment with non-binding IGFBP3 (modified to not bind to IGF-1) restored normal insulin signaling and improved retinal neural function on ERG. Animals treated with non-binding IGFBP3 displayed significantly reduced TNFα, which typically suppresses insulin signal transduction. A reduction in TNFα was associated with decreased proapoptotic markers, restored insulin receptor phosphorylation, increased anti-apoptotic markers (including Akt and Bcl-xL), and reduced IRS-1, Ser307, and SOCS3. These data suggest that the upstream inhibition of TNFα by IGFBP3 diminish the glucose-dependent effects of TNFα on suppressing insulin signal transduction.[142]

Clinical studies demonstrate increased levels of IGFBP2 and IGFBP3 as well as the IGF ligands IGF-1 and IGF-2 in the vitreous in patients with neovascular eye diseases.[138] This elevation is believed to be caused by increased vascular leakage in disease. In addition to its clinical relevance in the disease progression and therapeutic potential for diabetic retinopathy,

IGFBP3 also bears significance in other ischemic retinal diseases such as retinopathy of prematurity (ROP). Low levels of IGFBP3 in the serum of premature infants born in the time period when ROP occurs (between postmenstrual weeks 30-35) are associated with increased risk of developing proliferative ROP.[143] Decreased levels of IGF1 in the serum of premature infants diminished vascular growth and increased risk of ROP. However, the IGF1:IGFBP3 ratio was similar between premature infants that develop proliferative ROP and those who do not, while acid labile subunit levels were similar between ROP and non-ROP infants.[134] These data suggest IGF1 and IGFBP3 are the important components of the IGF1 complex, which consists of IGF1, IGFBP3, and the acid labile subunit. Restoration of both IGF1 and IGFBP3 levels while keeping the IGF1/IGFBP3 ratio intact may be crucial towards preventing pathologic retinal neovascularization in ROP. An rhIGF1/rhIGFBP combination is currently available and may be a promising means of reducing ROP risk. The transplantation of IGFBP-secreting ECFCs or ECFCs engineered to overexpress IGFBPs remains an unexplored alternative therapeutic strategy.

In addition to demonstrating a role of IGFPBs in the function of $CD44^{hi}$ ECFCs, the Friedlander lab also demonstrated upregulation of 12 neurotrophin-related genes in the retinas of RD10 mice eight days after treatment with $CD44^{hi}$ ECFCs relative to retinas treated with $CD44^{lo}$ cells.[29] These data suggest indirect effects of ECFCs in mediating neuroprotection. The effect of these upregulated neurotrophic genes remains unclear, and the regulation of angiogenic factors in the retina following ECFC treatment remains unexplored but may benefit from the findings from studies in other ischemic systems detailed below.

1.7. Therapeutic mechanisms of ECFCs: studies across fields

While studies within the retina certainly offer the most relevant information on the path to developing ECFC-based therapeutic options for ischemic retinopathies, literature from across multiple fields provide additional mechanistic understanding of ECFC's contributions to neovasculature in ischemia. Generally, ECFCs have the following rescue effects: (1) modulating inflammatory cascades and immune cell infiltration, (2) regulating proteins that remodel the extracellular matrix, (3) stimulating endogenous cells to secrete trophic mediators, (4) recruiting and enhancing other vasculotrophic progenitor cells including MSCs and myeloid cells.

1.7.1 Immunomodulatory effects of ECFCs

ECFCs interact with immune cells and modulate the inflammatory response. Neutrophils present at the site of laser-induced vascular injury recruited ECFCs via the binding of P-selectin glycoprotein ligand-1 (PSGL-1) on ECFCs to L-selectin on neutrophils.[121] ECFCs were activated by this interaction with neutrophils *in vitro* and demonstrated improved proangiogenic properties, suggesting that cooperation between ECFCs and neutrophils can facilitate endothelial regeneration at sites of vascular injury. In a mouse model of cerebral aneurism, systemic transfusion of ECFCs exerted protection on degeneration of the vessel wall by regulating the inflammatory cascade, decreasing apoptosis in smooth muscle cells, and inhibiting infiltration of macrophages.[123]

Other reports attribute the immunomodulatory effects of ECFCs to their secretion of paracrine factors. In models of ischemia/reperfusion-induced acute kidney injury (AKI), integration of intravenously administered ECFCs within post-ischemic kidneys was not detected by confocal microscopy.[122] Support for an paracrine nature of ECFC activity was provided by the observation that ECFC conditioned media protected against AKI. Infusion of ECFC-CM

attenuated the I/R-induced mRNA upregulation of intercellular adhesion molecule-1 (ICAM-1) in whole kidneys and protein expression in the peritubular capillary bed, which decreases significantly in density following AKI. In the early post-ischemic period, there is increased expression of ICAM-1, which is an endothelial adhesion molecule that serves as a ligand for LFA-1 during leukocyte transmigration. Reduction of ICAM-1 by ECFC-CM suggests that secreted factors may influence ischemic endothelium to suppress activation, differentiation, and/or transmigration of immune cells. Support for this mechanism came from the demonstration that administration of ECFC-CM significantly reduced the number of cells expressing IL-17 as well as T-helper (Th)-17 cells in the post-ischemic kidney. Infiltration of Th-17 cells has been associated with exacerbation of AKI in rats[144] while deletion of the IL-17A gene protects against AKI induced by cisplatin.[145, 146] Together, these data suggest that protection against AKI by ECFCs may be achieved by a mechanism whereby secreted factors cause a reduction of ICAM-1, which in turn decreases the infiltration of deleterious Th-17 cells and subsequently their IL-17 secretion. A direct effect of secreted factors on leukocyte activation cannot be excluded. Nonetheless, these data provide proof of concept for ECFC-derived paracrine mediators to positively affect the immune response to ischemia. A characterization of the immunomodulatory effects of ECFCs and their paracrine mediators in the immune-privileged retina may similarly offer insight into their therapeutic mechanism.

1.7.2 Effects of ECFCs on the matrix metalloproteinases

ECFCs also mediate proteins that interact with components of the ECM to improve vascular dysfunction. ECFCs improved functional outcomes in a mouse model of cerebral aneurism by downregulating matrix metalloproteinases (MMPs) MMP-2 and MMP-9 and increased tissue inhibitor of metalloproteinase-1 (TIMP-1) expression in the aneurysmal wall.[123]

The level of VCAM-1, NF-κB, and eNOS was also decreased following treatment with ECFCs. ECFCs suppressed apoptosis of SMCs in the aneurismal wall and significantly downregulated inducible nitrous oxide synthase (iNOS) while increasing Bcl-2. Reversal of the dysregulation of MMP-2, MMP-9, TIMP-1, VCAM-1, NF-κB, eNOS, iNOS, and Bcl-2 by ECFCs in the context of improving aneurysmal vessels is of particular interest since microaneurysms in retinal vasculature are often the first clinical sign of diabetic nonproliferative eye disease. Many of these factors play a role in the pathogenesis of diabetic retinopathy.

MMPs are a family of 24 known zinc-dependent proteases that cleave and remodel the ECM as well as other substrates such as growth factors, signaling molecules, cell surface receptors, other proteinases, and intracellular targets. Together with their endogenous TIMP inhibitors, MMPs regulate the protease activity profile to play a major role in determining the intercellular proteome and thus cell activity. Also known as gelatinase A and gelatinase B, respectively, MMP-2 and MMP-9 are both gelatinases secreted in a latent pro-form that are activated upon their interaction with membrane bound proteins on the target cell surface. MMP-2 and MMP-9 function to cleave their substrates including type IV collagen, elastin, and denatured interstitial collagen to facilitate the migration of endothelial cells through the basement membrane.[147] Both MMP-2 and MMP-9 were detected in the plasma and retinas of patients with diabetes[148, 149] and demonstrated increased levels of activation in the vitreous of patients with proliferative diabetic retinopathy (PDR).[150] Elevated concentrations of MMP-9 were measured in the epiretinal neovascular membranes of patients with PDR.[151] Elevated plasma MMP-9 is associated with age-related macular degeneration and choroidal neovascularization,[152] and activated MMP-9 was reported to be involved in the development of vitreous hemorrhage in patients with PDR.[153] MMP-2 and MMP-9 have distinct contributions to the pathogenesis of

diabetic retinopathy, which presents the interesting possibility that downregulation of these MPPs by ECFCs may be relevant to their therapeutic mechanism.

Activation of MMP-2 induced apoptosis in retinal capillary cells, which are the cells that demonstrate the characteristic histopathology of diabetic retinopathy. The mechanism of MMP-2-induced apoptosis is not entirely clear but may include a role for MMP-2 in mitochondrial dysfunction. MMP-2 cleaves nuclear poly ADP ribose polymerase (PARP) to induce apoptosis via a pathway in the mitochondria that involves the mitochondrial release of apoptosis-inducing factor. MMP-2 also damaged the retina by inhibiting the gap junction protein connexin 43 and heat shock protein 60, which maintains mitochondrial integrity and chaperons proteins into the organelle.[154] In human diabetic retinopathy, accelerated retinal capillary cell apoptosis is similarly related to mitochondrial dysfunction and PARP activation, supporting a role of MMP-2 in capillary cell apoptosis in DR. Inhibition of MMP-2 improved mitochondrial superoxide release and membrane permeability, prevented cytochrome C leakage from mitochondria, and inhibited capillary cell apoptosis. Since accelerated apoptosis of retinal capillary cells precedes the classic clinically observable histopathological lesions of diabetic retinopathy,[155] proper regulation of MMP-2 may by a promising target in treating early diabetic retinopathy and further evaluation of the effect of ECFC-based therapy on MMP-2 in the retina is merited.

MMP-9 is associated with both of the hallmark pathologic features of diabetic retinopathy: vasculopathy and neuropathy. *In vitro*, MMP-9 production was increased in the immortalized human retinal pigment epithelial cell line ARPE-19 and bovine retinal microvessel endothelial cells (BRMVEs) after exposure to hyperglycemic conditions; both MMP-2 and MMP-9 increased permeability of BRMVEs and ARPE-19 by degrading occludin, a protein component of tight junctions.[156] Compared to wild type mice with STZ-induced diabetes, MMP-

9 knockout mice with diabetes demonstrated reversal of the diabetic phenotype with restored vascular permeability in the blood retinal barrier.[157] MMP-9 mediates angiogenesis through multiple mechanisms. MMP-9 cleaves the angiostatic factor tissue pathway inhibitor, which is a major physiologic inhibitor of components of the coagulation cascade and independently a potent inhibitor of angiogenesis.[158] Studies in humans with PDR found a significant correlation between vitreous fluid levels of MMP-9 and VEGF. In addition to stimulating the endogenous production of VEGF in RPE cells *in vitro*,[159] MMP-9's proteolytic activity on the ECM releases the matrix-embedded VEGF reservoir to stimulate the VEGF-driven angiogenic switch *in vivo*.[160, 161] Retinal neurodegeneration results in part from MMP-9-mediated destruction of CD133 (also known as prominin-1), a neuroprotective protein critical to photoreceptor cell function via its involvement in disk maturation of the outer segments of rod photoreceptors. Disease states of chronic inflammation like diabetes result in increased MMP-9 that causes loss of CD133 in rod outer segments and leads to retinal degeneration.[157]

A deleterious role for these MPPs has been demonstrated in mouse models of ischemic retinopathy. MMP-2 and MMP-9 were significantly elevated in the OIR model,[162] and genetic deletion of MMP-2 and MMP-9 in OIR mice resulted in a 75% and 44% reduction in pre-retinal NV.[163] Selective inhibition of each of these MMPs both rescued the OIR phenotype,[162] but the more robust decrease in NV of mice treated with an MMP-2 inhibitor suggested a dominant role in the angiogenic process.[163] In the laser-induced choroidal neovascularization (CNV) mouse model, a model of the exudative phase of macular degeneration, MMP-2 and MMP-9 synergistically promoted CNV. Injection of pharmacological inhibitors of MMP as well as the overexpression of MMP inhibitors TIMP-1 and TIMP-2 proved an effective strategy for reducing laser-induced CNV.[164] Downregulation of these MPPs by ECFCs in vascular microaneurysm

mouse models raises the exciting possibility that ECFCs may repair damaged retinal vasculature in mouse models of diabetic retinopathy, but the role of MPPs in ECFC-based therapy remains an area of ongoing research.

1.7.3 ECFC stimulation of endogenous growth factor release

The vasculotrophic and neurotrophic activities of ECFCs have also been attributed to indirect mechanisms where ECFC-secreted paracrine mediators induce endogenous production of angiogenic and neurotrophin-related factors. In rat models of myocardial infarction, intramyocardially delivered ECFCs upregulated the gene expression levels of angiogenic factors Ang-2, fibroblast growth factor (FGF)-2, IGF-1, and stromal derived factor (SDF)-1α in the ischemic peri-infarcted areas.[96] While some literature on ischemic hindlimb mouse models report integration of ECFCs,[101] others observed minimal integration and thus credited vascular rescue to ECFC-induced upregulation of endogenous mediators such as angiogenic factors VEGF and FGF as well as leukemia inhibiting factor (LIF), IL15, and IL18 in treated ischemic tissue.[83] IL15[165] and IL18[166] have been shown to induce anti-apoptotic signaling pathways in cells exposed to hypoxic conditions. In STZ-induced diabetic mice, treatment with LIF preserved retinal ganglion cells and thickness of the neural retina and restored the retinal vasculature to physiological vessel patterning.[167] In mouse models of stroke, VEGF and IGF-1 were upregulated in the ischemic cortex following treatment with ECFCs.[92] In mouse models of traumatic brain injury, VEGF and SDF-1 expression were increased in the region of injured brain for mice treated with ECFCs intravenously.[90] In a follow-up study, intracerebroventricular transplantation of ECFCs increased expression of angiopoietin-1.[91] Experiments aimed to evaluate the effect of ECFCs on endogenous release of angiogenic and neurotrophic factors within the retina are limited but encouraging, demonstrating the upregulation of neurotrophin-

related genes following transplantation of CD44^{hi} ECFCs in OIR mice.[29] Future studies investigating the secondary effects of these genes dysregulating ECFC transplantation in the retina may elucidate the indirect contribution of ECFCs to ischemic retinal tissue repair.

1.7.4 ECFCs in combination therapeutic applications

A greater understanding of both the paracrine and integration mechanisms by which ECFCs contribute to tissue repair has been provided by studies employing co-injection of ECFCs with other cell types. Most often, the additional cell source used in combination therapy is selected to function to provide pericyte-like structural and/or paracrine support. A wide variety of cell types including 10T1/2 cells (mouse embryonic fibroblasts),[168, 169] fibroblasts,[170] SMCs[171] and SMC progenitors,[172] adipose stromal cells,[173] and especially mesenchymal stem cells[101, 124, 174-180] have achieved this effect. In these studies, implantation of duel-cell therapy embedded in biocompatible scaffolding produced blood vessels that were organized with perivascular cells closely surrounding an ECFC-lined lumen, and injection of both cell types maximized vascularization.

Early studies subcutaneously implanting Matrigel-embedded ECFCs and human saphenous vein smooth muscle cells into immunodeficient mice demonstrated the *de novo* creation of human blood vessels that anastomosed with murine vasculature within 7 days.[171] Interactions along the Ang-1/Tie2 signaling axis of smooth muscle progenitors and ECFCs promoted ECFC survival and the formation of stable vascular networks.[172] When ECFCs were preincubated *in vitro* with 10T1/2 mouse embryonic fibroblast cells in collagen overnight before implantation into a cranial window, UCB-ECFCs but not PB-ECFCs formed rapid and robust blood vessel that were long-lasting.[168] The 10T1/2 cells functioned as perivascular-like cells that released paracrine factors to stabilize endothelial cells.[169, 181, 182] When these collagen constructs

were seeded with UCB-ECFCs, the derived endothelium displayed low vascular permeability and a flow rate comparable to neighboring brain capillaries.[168] Increased intraluminal rolling leukocytes were observed in UCB-ECFC vascular complexes exposed to IL1β-induced inflammatory stress, suggesting that endothelium generated by ECFCs from UCB undergoes physiological cytokine activation during systemic inflammation. However, these cell sources of perivascular support are not suitable for clinical translation. Harvesting SMCs from healthy vasculature of patients harbors serious morbidity, and murine-derived cell lines are not appropriate for use in humans. Additional groups repeated similar work to create vascular networks lined by ECFCs following co-implantation with human dermal fibroblasts[170, 183] or human adipose tissue[173] in Matrigel, but these methods require prevascularization of scaffolding that relies on an *in vitro* preincubation step.

Optimizing the vasculogenic potential of combination therapy with ECFCs relies on the identification of an ideal source of co-injected perivascular cells, which the literature currently suggests to be mesenchymal stem cells. MSCs possess several favorable qualities including ease of isolation with minimal donor morbidity risk, availability in large quantities, and low immunogenicity. MSCs can be isolated in a minimally invasive fashion from many human tissues like bone marrow, adult peripheral blood, umbilical cord blood, and adipose tissue.[175] When ECFCs and MSCs embedded in Matrigel were implanted subcutaneously in immunodeficient mice, a significantly more robust formation of long-lasting vascular beds was formed. Once an ECFC/MSC Matrigel construct transplanted in one mouse is vascularized, the now vascularized scaffolding could become re-perfused in a secondary mouse.[176] Furthermore, MSCs harvested from a variety of tissues including bone marrow, white adipose tissue, skeletal muscle, and myocardium all possess the ability to generate extensive networks of ECFC-lined

vasculature.[178] These capabilities extend the application of tissue-engineered ECFC/MSC constructs to larger grafts that are able treat a variety of ischemic conditions. For instance, the promotion of vasculogenesis by tissue-engineered constructs embedded with ECFCs has been demonstrate to enhance osteogenesis,[184] attenuate MSC-mediated intimal hyperplasia,[179] and accelerate ischemic muscle recovery[185] in animal models.

During this process of vasculogenesis, cross-talk between ECFCs and MSCs initiated the vasculogenic process of forming ECFC-composed luminal structures surrounded by mesenchymal cells. ECFCs provided early angiocrine support by secreting PDGF-BB to facilitate the regenerative capacity of co-transplanted MSCs, which preferentially express platelet derived growth factor receptor (PDGFR-β). The PDGFR-β^+ MSCs were highly dependent on ECFC stimulation with PDGF-BB to avoid apoptosis and preferentially resided in perivascular locations within the vascularized implant.[124] MSCs cultured *in vitro* were exposed to media conditioned by ECFCs and strongly increased their expression of angiogenic factors including Ang-1, basic FGF, VEGF, HGF, and SDF-1.[101] Conversely, secreted factors by MSCs support ECFCs. For instance, hypoxic ECFCs typically demonstrate reduced function *in vitro* and the majority undergo apoptosis fairly quickly *in vivo*. Secretion of HIF-1α from co-transplanted MSCs bypasses hypoxia-induced apoptosis of ECFCs and resulted in the formation of patent, perfused human vessels within mice.[186] Overall, cross-talk via paracrine signaling between ECFCs and MSCs is critical for the engraftment and long-term lineage-restricted differentiation and maturation of transplanted MSCs surrounding ECFC-composed vascular beds. Continued research into the cross-talk between ECFCs and MSCs may lead to an alternative therapeutic strategy of providing an ECFC-derived factor that either recruits host ECFCs or delivers angiocrine support to MSCs.

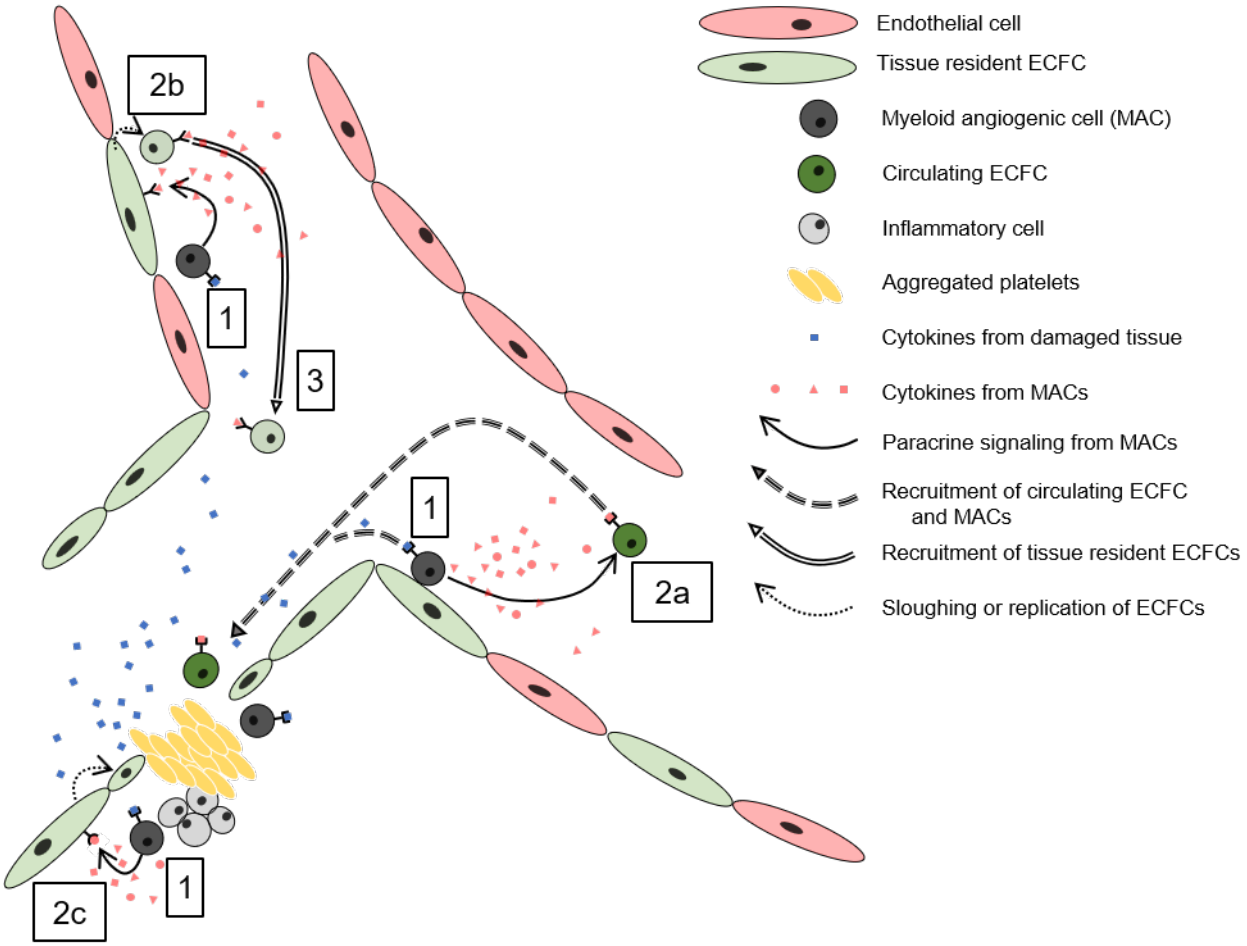

Schema 1.1: **ECFCs and MACs communicate for the *de novo* genesis of blood vessel walls at sites of injury or growth.** (1) Inflammatory cytokines secreted from damaged vasculature recruit myeloid angiogenic cells (MACs) in circulation. Once activated, MACs secrete paracrine factors that serve a variety of functions to contribute to neovascularization. The proposed functions of these bioactive mediators are (2a) to recruit ECFCs from circulation to the site of new vessel growth and activate ECFCs, (2b) to recruit ECFCs from the local vascular wall, or 2c) to activate adjacent ECFCs to replicate within the vascular wall. As the only cell known to participate in postnatal vasculogenesis, (3) ECFCs migrate to injury to recanalize the blood vessel lumen.

Co-implantation of ECFCs with MSCs also has immunomodulatory effects. The immunogenicity of ECFCs has been shown to reduce when cocultured with MSCs *in vitro*. In ECFC/MSC cultures stimulated with IFN-γ, HLA-DR was downregulated on both cells while HLA-ABC was downregulated on ECFCs. The typical induction of $CD4^+$ T cell proliferation by IFN-γ-stimulated ECFCs was suppressed when cells were cocultured with MSCs.[180] Co-transplantation of ECFCs/MSCs demonstrated reduced immunogenicity in long-term grafts,[180]

and recruited neutrophils, myeloid cells, macrophages, and monocytes quickly after implantation.[174] In turn, at sites of vascular injury, neutrophils recruited ECFCs via PSGL-1/L selectin and are critical to the regeneration of damaged vasculature in pathophysiologic conditions.[121]

Systemic antibody depletion of myeloid cells deleted the improved functional benefits of ECFC/MSC treatment, suggesting their efficacy is enhanced by a coordinated recruitment of host myeloid cells. Recruited myeloid cells to perivascular sites of vascular growth have been demonstrated to contribute to the formation of neo-vasculature via paracrine mechanisms of action.[174] MACs compose some of these myeloid cells that cooperate with ECFCs in postnatal vasculogenesis (**Schema 1.1**). First, MACs in circulation are attracted to the site of injury by signals from damaged tissue. Paracrine factors secreted by MACs function to recruit ECFCs from circulation and recruit and/or activate ECFCs from the local vascular wall. The relative contribution of recruited circulating versus tissue-resident precursor cells to new vessel formation is unclear. Guided by MACs, ECFCs migrated to the site of injury and replicate to recanalize the clot and restore integrity to the endothelial lining.[23]

1.8 Conclusions and future directions in ECFC research

Prior to 1997, vascular growth was believed to occur by two paradigms: vasculogenesis and angiogenesis. Vasculogenesis is an embryonic process whereby endothelial precursors known as angioblasts form *de novo* vasculature in the developing embryo. Angiogenesis is the postnatal process where fully differentiated endothelial cells within pre-existing vasculature undergo proliferating, migration, and remodeling to form new blood vessels. Studies investigating the endothelialization that occurred on implanted biomaterials led to the hypothesis that circulating endothelial progenitor cells in humans may form *de novo* vasculature in adults in

a third paradigm known as 'postnatal vasculogenesis.'[2] The first experimental evidence in support of vasculogenic mechanism was published in 1997 in a seminal paper by Asahara et al. demonstrating the first successful isolation of a population containing EPCs that can be expanded to form a stable population *ex vivo*, differentiate into endothelial cells, and transplanted *in vivo* to participate in postnatal vasculogenesis.[11] This notion that peripheral blood-derived endothelial progenitor cells may function in vascular homeostasis and possibly serve as a treatment strategy for vascular diseases galvanized the field of EPC research.

In this paper, Asahara applied magnetic bead-conjugated antibodies for CD34 or VEGF-2 to isolate cell populations from mononuclear cells in peripheral blood. These cells grew "blood island-like" clusters that resembled the blood-island clusters of angioblasts that surround a core of hematopoietic stem cells during embryonic vasculogenesis. For years, numerous other groups presented alternative cell culture methodologies that isolated $CD34^+$ cells capable of forming these blood island-like clusters and incorrectly interpreted these cells to be endothelial progenitor cells. Unfortunately, a variety of assays can produce colonies with blood island-like morphology, leading to wide-spread misappropriation of the term 'endothelial progenitor cells' to describe multiple cells types that were not true EPC. Characterization of the origin, phenotype, and function of these cells has led to the identification of two distinct cell populations that each contribute to vascular development and repair via differing mechanisms: endothelial colony forming cells and myeloid angiogenic cells.

The indiscriminate use of the term 'EPCs' and a host of overlapping misnomers to describe different cells with vascular trophic capacities requires a detailed understanding of the phenotype and function of MACs and ECFCs in order to comprehend the literature, especially early publications. Previously referred to as early EPCs, CFU-Hill cells, hematopoietic EPCs,

myeloid EPCs, or proangiogenic hematopoietic EPCs, MACs are not, in fact, endothelial progenitors but rather myeloid progenitor cells with a genetic signature indicative of alternative M2 macrophages.[19] MACs originate in the bone-marrow and can neither differentiate into endothelial cells nor integrate into vasculature. Rather, MACs provide trophic support to vasculature via paracrine action by secreting chemoattractants and vascular trophic mediators that promote homing, proliferation, and differentiation of local precursor cells.[19, 20] ECFCs are nonhematopoietic cells that exhibit the functional characteristics of true EPCs: (1) a defined endothelial cell phenotype, (2) a robust proliferative capacity, and (3) an ability to self-assemble to form *de novo* vasculature *in vivo*.[16] The origin of ECFCs remains unresolved. Some evidence suggested a bone marrow origin of ECFCs,[48] but this concept is still a matter of debate and requires definitive evidence of a bone-marrow derived angioblast with high proliferative potential.[49] Other reports denied a bone-marrow origin of ECFC[50, 51] and observed tissue-resident ECFCs within the vascular wall of various tissues and large vessels, [52-58, 60] particularly in the tunica intima[53] and in the so-called 'vasculogenic zone' between the medial smooth muscle and adventitial blood vessels.[67]

As true EPCs with robust proliferative potential and the capability of generating *de novo* blood vessels and supporting existing vasculature, ECFCs are a promising cell source in the treatment of ischemic, neurodegenerative, and angiogenesis-dependent diseases.[29, 71, 72, 77, 84-100] ECFCs can be harvested from UCB or placenta and cultured with xeno-free materials in numbers that may meet clinical demands.[29, 72, 78] The low inflammatory and thrombotic profile as well as the replicative senescence of late passage ECFCs suggests a favorable safety profile with low immunogenicity and tumorigenesis risk.[72, 74, 79-81, 83] ECFCs can be transplanted through bolus injection or within biocompatible scaffolds to optimize the regeneration ability of ECFCs.

Implantation of ECFCs within tissue-engineered scaffolds offer numerous advantages: (1) natural or synthetic scaffolding materials can be altered to control of microenvironmental influences on vascularization; (2) vasculotrophic mediators can be embedded within scaffolding to improve tissue regeneration; and (3) multiple cell types can be co-implanted with ECFCs in these constructs to augment neovascularization and/or intercellular cross-talk that promotes differentiation towards a tissue-specific cell fate.

Stem cell-based regenerative medicine strategies generally provide cell replacement and/or cell support. Cell replacement relies on the incorporation of transplanted stem/progenitor cells to act as replacement parts for injured or diseased tissue. Alternatively, stem/progenitor cells can act to provide trophic support via paracrine action. ECFC transplantation in various animal disease models has demonstrated that ECFCs function by both integration into host tissue and by paracrine action. Although ECFCs integrate within human retinal microvascular endothelial cells *in vitro*, ECFCs demonstrate limited (if any) engraftment within retinal tissue *in vivo* despite promoting potent rescue effects;[71] rather, a paracrine mechanism relying on the secretion of IGFBPs has been reported.[29] A population of ECFCs with high expression of CD44 has been identified as the bioactive subset capable of rescuing murine models ischemic retinopathy and neurodegeneration while cells with low CD44 expression have little effects.[29] ECFCs intravitreally injected into OIR mice along with adeno-associated virus serotype 2 encoding a stable, soluble, and potent formulation of Ang1 demonstrated a significantly higher degree of intgration. Ongoing research to improve the therapeutic capacity of ECFCs may focus on improving their ability to integrate and/or identifying ECFC-secreted factors that mediate their paracrine mechanisms of action.

Studies in animal models of diseases outside the retina have described additional therapeutic mechanisms of ECFCs that merit future investigation in retinal models of ischemia/neurogeneration. First, ECFC transplantation has immunomodulatory effects. In mouse models of laser-induced vascular injury, L-selectin expressed on neutrophils binds directly to PSGL-1 on ECFCs and increases their proangiogenic properties.[121] In murine models of cerebral aneurysm, ECFCs inhibit an inflammatory cascade as well as apoptosis in smooth muscles while also decreasing macrophage infiltration.[123] Paracrine-mediated immunomodulation by ECFCs was also identified in models of AKI, where ECFC CM protected against ischemic tissue damage by inhibiting infiltration of deleterious Th-17 cells and resultantly their IL-17 secretion.[122] Second, ECFCs also regulate expression of proteins including MMPs that interact with components of the ECM to improve vascular injury. ECFCs downregulate MMP-2 and MMP-9, which are increased and cause pathophysiology in various human retinal ischemic/neurodegenerative diseases[102, 133, 134, 136] as well as mouse models of ischemic/neurodegenerative retinopathy.[162-164] Third, transplanted ECFCs promote the secretion of endogenous angiogenic and neurotrophin-related growth factors that promote tissue regeneration. Future studies within the retina investigating the effects of these dysregulated genes would shed light on the indirect contributions of ECFCs to the repair of ischemic retinal tissue. Lastly, co-transplantation of ECFCs with other cell types augment their regenerative capacity and reveal mechanisms of intercellular cross-talk that mediate vascular growth. For example, MSCs are stimulated by ECFCs to avoid apoptosis and engraft in host tissue to assume pericyte-like locations and functions.[124] Meanwhile, ECFCs are stimilated by MSC secretion of HIF-1α to avoid hypoxia-induced apoptosis and form patent, perfused vessels.[186] MSCs also have immunomodulatory effects on ECFCs, reducing their immunogenicity by downregulating

their HLA complexes and increasing the recruitment of myeloid cells and MACs to promote the formation of neo-vasculature via paracrine mechanisms.[23, 174]

The use of ECFCs as a therapeutic option faces limitations. The heterogenous population of ECFCs contains cells with a range of proliferative capacity, and current culture techniques isolate the entire ECFC hierarchy including low proliferative potential-ECFCs, ECFC clusters, and even non-proliferative endothelial cells.[53] The immunophenotype of ECFCs is currently defined by a cocktail of surface markers, and no single distinguishing marker has identified ECFCs with high proliferative capacity. While ECFCs are a promising source of cryotherapy, the manufacturing costs associated with their development may be prohibitive. The concentration of ECFCs is extremely low in the pediatric population, limiting the possibility of autologous therapy for infantile and adolescent populations. Furthermore, ECFCs derived from adolescent and adult peripheral blood are less clonogenic, proliferative, and angiogenic than cord-blood derived ECFCs.[23] Finally, disease states like diabetes may reduce the frequency and impair the functionality of ECFCs, which may limit their utility as an autologous treatment modality.[73]

Ongoing efforts to improve efforts to improve the proliferative capacity of ECFCs are successful and ongoing.[98] An up-to-date and comprehensive review of studies developing strategies to improve the therapeutic potential of ECFCs is available elsewhere.[98] Generally, these strategies involve: (1) boosting ECFC expansion ex vivo, (2) priming dysfunctional ECFCs to rescue their angiogenic capacity, (3) priming healthy ECFCs to augment their angiogenic capacity, (4) injecting chemoattractants to stimulate homing of ECFCs into sites of neovessel formation, (5) epigenetic reprogramming of ECFCs, (6) genetic manipulation of proangiogenic signaling pathways in ECFCs, and (7) co-transplantation of ECFCs with other progenitor cells including MSCs and MACs. Evidence strongly suggests that ECFCs are a promising source for

tissue regeneration. Future efforts improving the restorative capacity of ECFCs and exploiting their multiple neurovasculotrophic mechanisms in retinal animal models are a promising approach towards the optimization of ECFC-based therapy for the treatment of complex retinopathies and may extend to the treatment of ischemic/neurodegenerative diseases in other organ systems as well.

Chapters 1 and 2 are currently being prepared for submission for publication of the material. Marra, KV; Friedlander, M. The dissertation author was the primary investigator and author of this material.

Chapter 2

Extracellular vesicles from endothelial colony forming cells as paracrine mediators of neurovasculotrophic repair

2.1 Introduction to extracellular vesicles

Extracellular vesicles are a promising and relatively new addition to the armamentarium of paracrine mediators of intracellular communication that exert their effects via the horizontal transfer of bioactive cargo including RNA, proteins, and lipids.[187] "Extracellular vesicles (EVs)" is a blanket term for three distinct types of vesicles shed from cells: exosomes (ranging from 40-120 nm in diameter), microvesicles (ranging from 50-1000 nm) and apoptotic bodies (ranging from 50-5000 nm). Each vesicle type exhibits unique mechanisms that regulate their biogenesis, surface characteristics, and intravesicular cargo (**Schema 2.1**).

The biogenesis of exosomes begins with inward budding of the plasma membrane to form early endosomes, which mature into multivesicular bodies (MVB) as they accumulate multiple phospholipid bilayer-bound intraluminal vesicles (ILVs). These ILVs are formed by inward budding of the of the MVB and, thus, contain cytosolic cargo as well as endosomal protein markers. MVB are either sent to the lysosome for degradation or fuse with the cell's plasma membrane to release ILVs into the extracellular space, at which point they are termed

Schema 2.1: **Biogenesis of exosomes and microvesicles.** External stimuli leading to increased extracellular adenosine triphosphate (ATP) opens the P2X7 receptor resulting in an influx of calcium ions into the cell. In microvesicle biogenesis, a cluster of surface proteins, tetraspanins, and cargo from the cytoplasm forms on a discrete portion of the plasma membrane. MV release is mediated by RAS-related protein 27 (RAB27), actin, the endosomal sorting complex required for transport (ESCRT), ADP ribosylation factor 6 (ARF6), soluble N-ethylmaleimide-sensitive protein receptor (SNARE) proteins, and phospholipase D2 (PLD2), which catalyzes the hydrolysis of phosphatidylcholine (PC) to produce phosphatidic acid (PA) and choline. MVs are shed by blebbing from the plasma membrane. Exosome biogenesis begins with endocytosis of the plasma membrane to form early endosomes. Exosomes are loaded with contents from endocytosis or from the trans-Golgi network. The formation of intraluminal vesicles (ILVs) through both ESCRT-dependent and ESCRT-independent mechanisms (not shown) matures the early endosome into a multivesicular body (MVB). MVBs fated for exosome biogenesis are transported by kinesin along microtubules with the aid of RAB proteins to the cellular periphery where SNARE proteins mediate fusion with the plasma membrane and release of ILVs, which are termed exosomes once in the extracellular space. Alternatively, MVBs destined for the degrative pathway are shuttled to the lysosome for digestion.

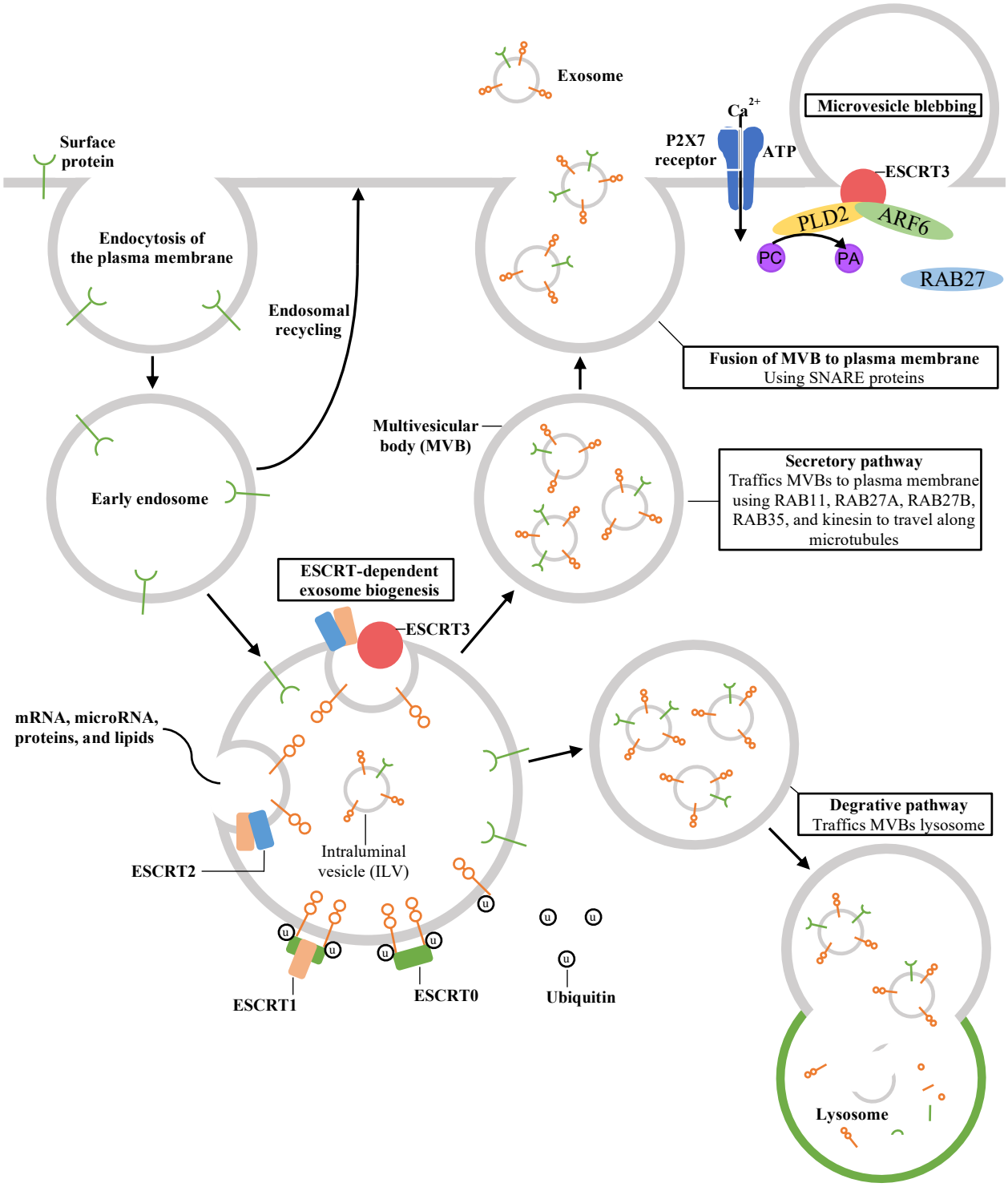
Exosome
Microvesicle blebbing
Ca 2+
P2X7 receptor
ATP
ESCRT3
PLD2
ARF6
PC
PA
RAB27
Surface protein
Endocytosis of the plasma membrane
Endosomal recycling
Fusion of MVB to plasma membrane
Using SNARE proteins
Multivesicular body (MVB)
Secretory pathway
Traffics MVBs to plasma membrane using RAB11, RAB27A, RAB27B, RAB35, and kinesin to travel along microtubules
Early endosome
ESCRT-dependent exosome biogenesis
ESCRT3
mRNA, microRNA, proteins, and lipids
Intraluminal vesicle (ILV)
ESCRT2
Degrative pathway
Traffics MVBs lysosome
ESCRT1
ESCRT0
Ubiquitin
Lysosome

exosomes. How the fate of MVBs is determined remains a subject of ongoing investigation. One mechanism of MVB and exosome formation has been characterized through the endosomal sorting complexes required for transport (ESCRT) pathway. The endosomal origin of exosomes results in their common surface expression of tetraspanins CD9, CD63, and CD81 as well as accessory proteins of the ESCRT pathway including Alix, TSG101, HSC70, and HSP90β. Microvesicles are formed by budding of the plasma membrane in a process that requires cytoskeleton components like actin and microtubules, molecular motors including kinesins and myosins, and fusion machinery like SNAREs and tethering factors, but details of their biogenesis as well as their specific surface markers remain poorly understood. Apoptotic bodies are shed from cells during programmed cell death. Apoptotic bodies are also released by membrane blebbing and are shed when cells are undergoing apoptosis.[188]

The biological function of exosomes and microvesicles has increased in significance over the past decade as they have become identified as a potent means of intercellular communication. In a wide range of physiological processes, exosome- and microvesicle-mediated messaging plays a variety of roles including the enhancement of coagulation, maturation of reticulocytes, promotion of angiogenesis, modulation of inflammation, facilitation of embryonic development, as well as the regulation of both innate and acquired immune responses. Within the nervous system, EVs can promote myelin formation, neuronal survival, neurite growth, and are an attractive therapeutic source for tissue repair.[189] While populations of exosomes and microparticles have demonstrated potential for therapeutic use in animal disease models like ischemic retinopathy,[190] apoptotic bodies have not so far been useful as a therapeutic option but, rather, function physiologically to aid in the removal of cell debris, regulation of antigen presentation, and modulation various immune cell responses.[191]

There are several advantages to using EVs as a tool for treating retinal disorders. As natural carriers of microRNA (miR), mRNA, protein, and lipids, EVs are potent mediators of intercellular communication via the horizontal transfer of this bioactive cargo. Delivery of intravesicular miR and mRNA into target cells modulates gene expression and promotes protein translation, respectively, while proteins and lipids delivered into target cells may have direct effects. EVs can therefore target multiple cell types and employ multiple mechanisms simultaneously, a promising multimodal therapeutic strategy for the treatment of complex disorders. Devoid of replicative machinery, EVs circumvent the risk of tumorigenesis associated with the transplantation of dividing/differentiating cells into the eye. Given that the rates of replication and death following cell injection are unknown, the actual dose of cell treatment following transplantation is unknown. The dose of EVs can be more closely estimated given that there is no possibility of replication following transplantation. Another advantage is that EVs are generally considered highly stable in long term storage at temperatures under -20˚C[192] and RNA quality within plasma EVs remains unchanged even after storage for 5 years at -20˚C.[193] Storage properties are specific to EVs from each cell source, and ECFC-derived EVs (EVs^{ECFCs}) were demonstrated to be stable in size at temperatures under -20˚C even after undergoing 10 freeze-thaw cycles.[194] Lastly, intact cell therapy including ECFC transplantation suffers from minimal engraftment into host tissue such as the retina.[29, 72] Transplantations of EVs^{ECFCs} were observed to accumulate within perivascular macrophages/microglia within areas of retinal ischemia.[190]

2.2 Selection of techniques for EV isolation

At this point in time in the relatively young field of extracellular vesicle research, standardization of techniques for vesicle isolation and characterization are still a work-in-progress.[195] Numerous techniques have emerged to isolate EVs from conditioned medium or

biofluids. These techniques employ the use of differential ultracentrifugation (UC), polymeric precipitation, immunoaffinity isolation (IA), microfluidic devices, ultrafiltration (UF), and size exclusion chromatography (SEC). Each technique results in an EV sample with differing levels of EV specificity, yield, 'purity' (i.e., macromolecule/vesicle aggregates and protein/liposome contamination), biological functionality, and overall quality. Furthermore, the techniques themselves require different amounts of sample volume, time, cost, expertise, and specialized equipment. Isolation techniques also differ in their scalability, which is a critical consideration in developing EV isolation protocols that can meet clinical demands. It is becoming common for a combination of techniques to be used in series to produce an EV sample that is appropriate for its downstream applications. An understanding of the pros and cons of each method is required prior to use of their resultant EV samples.

2.2.1 Differential ultracentrifugation and density gradients

Classically, extracellular vesicles have been isolated according to their buoyant density by differential ultracentrifugation of conditioned media or biofluids. Since high-speed spins may pellet dense particles and aggregate macromolecules/vesicles, techniques using differential UC begin with a low-speed spins of 300-500 *x g* for 5 minutes to remove small cell debris followed by a 15-20 minute spin of the supernatant at 1,500 - 2,000 x *g* to remove larger cellular debris. Vesicles in solution may be filtered through a 0.2 μm filter or subject to a 10,000 – 20,000 x *g* spin to isolate larger vesicles typically referred to as microvesicles. The final step is ultracentrifugation at speeds of 100,000 - 200,000 x *g* for 2 hours to pellet small vesicles typically referred to as exosomes. When using differential UC to isolate EVs, it is critical to monitor and record a variety of parameters that influence the outcome of this technique as centrifugal separation of EVs depends on the acceleration (*g* force) applied, the rotor type (fixed

angle versus swinging bucket), pelleting efficiency (rotor *k*-factor), sample viscosity, and spin time.[196] These parameters are often under-reported in literature, which may explain the lack of consistency in results. Differential UC does not lead to good size separation since sedimentation depends on the density of a vesicle (which is reliant upon the cargo within each vesicle) as well as the distance the vesicle needs to travel. Small vesicles near the bottom of the UC tube may pellet in the large vesicle pellet at low speeds, lowering EV yield. Large pellets near the top of the UC tube may pellet during the high-speed spin, resulting in contamination of the final EV samples with larger particles. High-speed spins also reduce EV sample purity by causing aggregation of EVs, pelleting of extravesicular macromolecules, lipoproteins, and other contaminants, and by lysing EVs to spill intravesicular contents.

To improve purity, the EV pellet can be resuspended in PBS and pelleted again, but this approach does not achieve absolute separation and risks highly reducing EV yield. Another approach towards improving the purity of EV samples derived using differential UC employs the concurrent use of top-loading or bottom-loading density gradient mediums. Samples are placed on top of top-loading density gradients prior to UC and separate EVs based on size and mass. Alternatively, bottom-loading density gradients are loaded below samples and separate EVs by allowing vesicles to float to the location where their density matches that of the medium, thus separating EVs based solely on density, which is classically between 1.1-1.19 g/mL. Protein and protein-RNA contaminants remain on the bottom of the tube. Sucrose gradients are commonly used, but are extremely viscous and hyperosmotic resulting in slow sedimentation rates (between 62 and 90hrs) and loss of water from within EVs, respectively.[195, 197] The issues presented by the hyperosmolar properties of sucrose can be overcome with a density gradient of iodixanol, also known as OptiPrep. which is an isosmotic solution. OptiPrep density gradient produce EVs with

well-preserved size and shape[198] and allows for the isolation of EVs from virions, apoptotic bodies, and HIV 1 particles.[199, 200] Although the use of OptiPrep results in increased EV purity, this technique is limited by its reliance on expensive equipment, complexity and time (up to two days), and its inability to scale to a capacity necessary for clinical demands.

2.2.2 Polymeric precipitation

Commercially available polymeric precipitation mixtures have been developed with the specific aim of isolating exosomes. The most popular reagent is poly-ethylene glycol (PEG), which is mixed with the conditioned medium or biofluid sample overnight and aggregates exosomes so they may be separated by low-speed centrifugation at 1500 *x g*.[201] There are also commercially available density gradient products including miRCURY Exosome Kits, ExoQuick, and Invitrogen Total Exosome Isolation Reagent, which reliably yield high quantities of quality exosomes. Advantages to this method lie in its simplicity, low cost, speed, and ability to process multiple samples simultaneously. However, samples obtained using polymeric precipitation are generally less pure in comparison to those obtained using differential UC. For instance, PEG-based exosome isolation also pellets non-exosomal proteins, immunoglobulins, lipoproteins, nucleoproteins, viral particles, immune complexes, and other contaminants.[200, 202] In addition, samples contain molecules of these biopolymers that interfere with downstream research applications including mass spectrometry, proteomic analysis, and RNA assays. These disadvantages present obstacles to use of polymeric precipitation mixtures in research settings. The advantages of polymeric precipitation technuqies (speed, easy of use, and scalability) make them an attractive method for rapid exosome extraction and analysis in a clinical setting, where, for instance, it may be used for biomarker detection for instance.[200, 201, 203, 204]

2.2.3 Immunoaffinity isolation

EVs of different subtypes express a surface protein profile that can be exploited in the process of immunoaffinity isolation,[204, 205] during which antibodies to surface proteins are used to positively select for target EV populations (immuno-enrichment) or to deplete target EV populations (immune-depletion or negative selection). Common immuno-capture antibodies include exosomal markers for tetraspanins CD9, CD63, and CD83 that typically coat magnetic beads,[202] gold-loaded ferric oxide nanocubes,[206] or other matrices[207] through covalent or high affinity interactions. Additional affinity methods rely on surface markers from parent cells including chondroitin sulfate peptidoglycan 4,[208] epithelial cellular adhesion molecule,[209] or exosome-binding molecules such as heat shock proteins[210] and heparin.[211] Following immunocapture, low speed centrifugation or magnetic pull-down is used to achieve physical separation and increase EV purity. The specificity of immunocapture provides several advantages to IA techniques. For instance, by using antibodies targeting exoplasmic features characteristic of exosomes' endosomal origin, IA can isolate highly specific exosome populations while excluding vesicles with cytosolic-outwards orientations like microvesicles. Highly specific antibodies in IA methods also yield highly pure vesicle populations. However, most commercially available antibodies for immunoprecipitation are non-specific. Furthermore, the integrity of vesicles is damaged when the antibodies used cannot be easily removed from the vesicles following immuno-precipitation.[212] Another limitation of IA is that selective antibodies also greatly decrease EV yield and may select for subsets of vesicles within a certain EV class.[204] In addition to reporting positively/negatively selected markers used for IA isolation of EVs, studies that rely on IA must also include isotype controls and report on the absence of contaminants. Altogether, IA capture is a very expensive isolation method requiring a large

sample volume and high quantities of antibody-conjugated beads to obtain small yields of EV samples, making this technique suitable for studies requiring small sample size, but not feasible for scaling to the demands of a clinically available therapeutic agent.

2.2.4 Microfluidic devices

Different microfluidic devices have also been developed to isolate EVs based on a variety of principals including membrane-based filtration, exosome trapping on nanowires, acoustic nanofiltration, nanoscale deterministic lateral displacement sorting, and viscoelastic flow sorting.[213] A large number of microfluidic devices rely on immunoaffinity capture to isolate EVs, particularly exosomes. A few of these chips include ExoChip with CD63 antibody-mediated capture,[214] gold electrolytes with CD9 antibody,[215] graphene oxide/polydopamine nanointerface with CD81 antibody,[216] and herringbone groove with CD9 antibody.[217] A comprehensive overview of the variety of microfluidic devices and their functionality and utility has been reported elsewhere.[213] As a high-throughput method, microfluidic devices have become increasingly attractive for use in EV isolation, detection, and analysis (i.e. lab-on-a-chip), resulting in a high degree of reproducibility, thus circumventing the need for multiple pieces of expensive EV characterization equipment.[200] Integrated microfluidic chips can simultaneously calculate exosome concentration, detect disease-specific exosome subpopulations, and quantify intravesicular proteins and mRNAs.[213] Additional advantages of microfluidic devices compared to other EV isolation methods include their significant reduction in required sample volume (as little as 10 μL[218]), reagents, and time as well as automation of multiple analyses. These advantages make microfluidic devices an attractive option for EV research as well as clinical applications like biomarker detection. Devices that use affinity-based isolation share many of the advantages and disadvantages of immunoaffinity-based methodologies as discussed above.

Although immunocapture microfluidic devices can isolate highly specific and pure samples of EV subpopulations, harvesting EVs based on surface proteins risks isolating subpopulations of vesicles rather than an entire EV class. Other disadvantages include the complexity and limited availability of devices as well as the tendency for samples to block microfluidic channels. These devices can analyze small volumes of sample, but this convenience acts as an obstacle to screening biofluid samples for scarce diagnostic biomarkers. Overall, the optimization of microfluidic devices for EV isolation and characterization in research as well as the clinic is expanding, but use of these devices are not yet standardized across the field.

2.2.5 Ultrafiltration

Another technique used to concentrate and/or isolate EVs from biofluids or conditioned medium employs passing sample through ultrafiltration membranes with pores of pre-determined sizes in decreasing order, typically 0.8, 0.45, 0.22, and 0.1 μm corresponding to retaining particles of diameters greater than 800, 450, 220, and 100 nm, respectively. First, large particles are removed as eluate following filtration of sample through large pore membranes of 0.8 and 0.45 μm in diameter to produce an exosome-enriched filtrate. This filtrate is then placed atop a membrane with pore sizes smaller than desired vesicles (0.22 and 0.1 μm) to pass small vesicles into the eluate and further enrich exosomes in the filtrate sample. Passage of sample through membranes may be achieved by applying pressure though use of centrifugation is most common, but deformation of EVs caused by application of pressure or centrifugal force to UF systems requires further research.[200, 203] UF requires no expensive laboratory equipment and is a faster and simpler protocol that isolates EVs with comparable morphology and higher yield relative to ultracentrifugation.[219] However, other reports describe disadvantages of UF including samples with suboptimal purity characterized by high protein contamination and suboptimal RNA yield

and quality (including microRNA).[220] Furthermore, EV samples harvested from urine contained low concentrations of EV proteins (such as aquaporin and nephrolysin) and high concentrations of non-EV contaminant proteins including albumin and α-1-antitrypsin.[221] There are several possible explanation for the high level of protein contamination in UF: (1) cutoff dimensions of UF systems are typically smaller than reported; (2) even low-affinity membranes bind EV proteins to create aggregates and clog pores;[200] and (3) protein molecules also block membrane pores as the sample is being concentrated.[222] Contaminating proteins significantly complicate downstream analyses of EV proteins. Repeated UF has been shown to improve the overall purity of EV samples but is inversely proportional to EV yield. A systematic analysis of multiple UF systems has demonstrated that 10kDA regenerated cellulose centrifugal filters from Amicon® are ideal for harvesting EVs, resulting in high EV recovery and undetectable levels of protein retention in the membrane. While systematic comparisons of filters have optimized UF protocols, a lack of standardized UF methodologies in published literature is a considerable obstacle to comparing results obtained across laboratories.[223]

2.2.6 Size exclusion chromatography

Size exclusion chromatography has recently emerged as an excellent single-step isolation protocol to quickly (approximately 20 minutes[224]) isolate EVs with high integrity and minimal protein contamination. In SEC, columns are first loaded with a porous gel filtration polymer that functions as a stationary phase. Biofluid or conditioned media is then loaded as a mobile phase onto these porous gel filtration polymers and as the sample flows through the column, large particles elute from the column first, then small vesicles, and soluble proteins elute last. Since large particles enter less pores within the stationary phase, they travel within the void space between polymers and have a shorter path-length to elution resulting in earlier elution relative to

smaller components in the sample. A number of commercially available gel polymers are available including crosslinked dextrans (Sephadex), agarose (Sepharose), polyacrylamide (Biogel P), or allyldextran (Sephacryl). Use of Sepharose CL-2B in the first popular paper that employed SEC for EV isolation popularized this particular gel polymer in the field,[225] however, a systematic study of polymers suggested that Sepharose 4B produces optimal resolution of EVs from contaminating proteins.[226] Comparative reports have demonstrated that SEC-based EV isolation protocols produce EV samples that are superior in purity, integrity, and functionality relative to those derived by differential UC, immunoaffinity capture, UF, and PEG-based procedures.[221, 224, 227-230] In contrast to differential UC-derived EV samples where spins of forces greater than 100,000 *x g* cause contaminating aggregation of EVs and macromolecules, gravity-mediated elution in SEC avoids this drawback.[231] Differential UC procedures alter the proteome, lipidome, and genome of vesicles and may render EVs ineffective at binding and uptake into target cells, thus reducing their ability to act as intercellular messengers.[232] Deformation of vesicles by contact and adherence to UF membranes may similarly affect vesicle function in ways that currently remain unknown.[222] PEG-based methods alter the exosomal proteome and co-precipitate proteins not associated with EVs.[228] SEC circumvents these disadvantages and has been recognized as a superior method of isolating EVs for functional and "-omics"-based downstream applications.[226, 230, 233-235] There are several disadvantages to SEC including its inability to differentiate between exosomes and microvesicles within their overlapping size range. While SEC can successfully isolate sufficient EVs from small volumes (0.5 µL – 2 mL) of biological samples like serum/plasma and saliva for downstream analyses,[236-239] the limited volume that can be loaded into an SEC column significant limits its stand-alone utility in isolating EVs from conditioned cell culture media, where vesicle concentration is relatively

dilute.[240] Results from a worldwide survey in 2016 demonstrated that 96% of respondents reported needing a starting volume >100 mL when isolating sufficient EVs from conditioned media.[241] Experiments using EVs derived from conditioned medium thus often use alternative methods to concentrate samples prior to isolating vesicles with SEC.

2.2.7 Combinatorial techniques

The EV isolation protocol employed in this dissertation utilizes serial UF, SEC, then repeated UF (UF-SEC-UF). Briefly, the UF-SEC-UF protocol begins by pooling media conditioned for 48 hours by cells seeded at a density of 2 X 10^6 cells/T75 flask. Pooled media is then spun at 300 x *g* for 5 min to remove cell debris and the supernatant is 0.22 μm vacuum-filtered prior to UF with 10kDa MWCO Amicon® filters to concentrate media to 1 mL by centrifugation at 4,000 x *g* in a swing-bucket rotor. This concentrated sample was subject to SEC using a 10 mL plastic syringe loaded with washed Sepharose CL-2B and packed with nylon stocking stopper. The 40 elution fractions of 0.5 mL were subject to a BCA protein assay to determine in which fraction detectible levels of protein began eluting. All prior fractions were pooled and again filtered with a 10kDa MWCO Amicon® filter to concentrate the final EV sample. Selection of this methodology draws from a comprehensive review of the literature demonstrating its superiority in isolating EVs for downstream functional and compositional studies, which were the primary aims of our research.[240, 242-244] Purity of EVs samples obtained with these techniques is optimized by use of an FBS- or serum-free culture medium and, relevant to the current study, a xeno-free medium for ECFCs was recently developed by the Friedlander lab.[29, 240] Lastly, adjusting the timing of the final UF step allows for control of the final vesicle concentration and thus treatment dosage for the current study's *in vivo* animal models and perhaps for future clinical applications.

2.3 EVs in retinal physiology and pathophysiology

Exchange of extracellular vesicles within the retina is critical to normal retinal functioning, and the specific roles of EVs from distinct cell types remains an area of ongoing investigation. Global inhibition of exosome secretion by daily injections of wild-type mice with the neutral sphingomyelinase inhibitor GW4869 caused marked reductions in retinal neural function. Small RNA sequencing comparing microRNA cargo in EVs from healthy versus degenerating mouse retinas suggests a physiological role of intravesicular miR in immune-modulation and phototransduction within the retina.[245] Proteomic analyses revealed that EVs from healthy adult neural retinas contain proteins integral to retinal function and homeostasis.[246] EVs are also essential to mediating intercellular communication during retinal development. Retinal progenitor cells release EVs containing developmental transcription factors, miR, and membrane proteins.[247] Small RNA sequencing of EVs harvested from retinal organoids generated by hiPSCs demonstrated that EV miR correlates with expression of hallmark features of native human retinal development.[248]

In contrast to their physiologic roles facilitating retinogenesis and maintaining proper intercellular communication to promote normal homeostasis in the healthy adult retina, EVs also contribute to the pathophysiology of many diseases. Plasma levels of EVs reflect the equilibrium between their shedding and uptake, and the general consensus is that plasma levels of endothelial cell-derived vesicles reflect the degree of injury to vascular or circulating cells. In various human vascular diseases such as diabetes,[249-251] cardiovascular disease,[252] hypertension,[253] and atherosclerosis,[254] increased numbers of endothelial EVs circulating in patient plasma have been reported. Increased EVs in the plasma of diabetic patients may be a surrogate biological marker of vascular dysfunction. The mechanisms that underpin the increased shedding of vesicles

remain unknown, but some evidence suggests that oxidative stress is one trigger for endothelial EV release in diabetics. In the plasma of patients with type 2 diabetes, increased levels of circulating endothelial-derived and platelet-derived EVs correlated with increased levels of anti-oxidized LDL antibodies, suggesting that shedding of EVs from endothelial cells may be influenced by oxidized LDL.[249] While it remains a matter of debate whether increased extracellular vesicles in diabetic patients are a cause or result of disease, the deleterious roles of these EVs on biological functions are becoming increasingly well-characterized.

Evidence suggests EVs from diabetic patients may be involved in the pathophysiology of disease progression via their promotion of coagulation, inflammation, endothelial dysfunction, and angiogenesis. EVs shed from a variety of cell types play numerous roles in vascular inflammation. Leukocyte-, erythrocyte-, hematopoietic cell-, and especially platelet-derived EVs contributed to the hypercoagulable state of diabetics by transferring their surface bound tissue factor to augment thrombus propagation *in vivo*.[255, 256] In diabetic patient plasma, levels of platelet-derived EVs were correlated with levels of monocyte-derived EVs and both independently correlated with disease progression from nonproliferative to proliferative diabetic retinopathy.[257, 258] Elevated platelet-derived EVs in the plasma of diabetic patients activated human endothelial cells *in vitro* by inducing their expression of adhesion molecules, cyclooxygenase-2, and the production of prostacyclin.[259] EVs from activated platelets delivered proinflammatory chemokines like CCL5 to endothelial cells to promote monocyte recruitment to endothelium.[260] Elevated levels of inflammatory cytokine CCL5 as well as angiogenic factor Ang-2 were measurable in the general pool of EVs harvested from the plasma of patients with uncontrolled diabetes, suggesting that EVs in diabetic patients play both an inflammatory and angiogenic role.[261]

Endothelial EVs are the vesicles in circulation that predominantly effect vascular function and angiogenesis. Endothelial-derived EVs are identified by positive expression of VE-cadherin (CD144) since this surface marker is exclusively expressed on endothelial cells. In the plasma of human patients with type 2 diabetes, elevated levels of VE-cadherin^{+} endothelial EVs correlated with *in vivo* functional measurements of endothelial dysfunction and were associated with increased risk for development of coronary artery disease, suggesting a role of endothelial EVs in the development of vascular complications.[250, 251] In patients with end-stage renal failure (where cardiovascular risk is chiefly dependent on endothelial dysfunction and arteriolar stiffness), only elevated levels of endothelial EVs correlated with markers of decreased renal function while EVs that were platelet-derived, erythrocyte-derived, or Annexin V positive did not. Exposure of rat aortic rings *in vitro* to endothelial EVs isolated from the plasma of end-stage renal failure patients resulted in reduced NO-mediated vasodilation in comparison to aortas exposed to healthy EVs.[262] Together, findings from these studies suggest that circulating endothelial EVs contribute to dysfunctional endothelium in vascular disease perhaps through impairment of the NO-mediated vasodilatory pathway.

In the vitreous of patients with PDR, platelet-derived EVs were increased and endothelial EVs were most abundant while photoreceptor and microglial EVs were comparable to healthy control samples.[263] PDR is associated with increased local shedding of endothelial EVs from endothelium of new vessels into the vitreous and increased leakage of platelet EVs into the vitreous through vasculature of compromised integrity. The entire population of vitreous EVs stimulated endothelial proliferation *in vitro* and angiogenesis in a murine *in vivo* Matrigel plug model, suggesting a proangiogenic effect of vitreous-resident EVs in diabetic eyes. Levels of platelet-derived EVs and endothelial EVs decreased to levels comparable to healthy controls

following treatment with panretinal laser photocoagulation or intravitreal injections of anti-VEGF therapy (Bevacizumab). In addition to suggesting that analysis of EVs within the plasma (or vitreous) of diabetic patients may prove to be a useful biomarker of retinal complications, these data further demonstrate a role of EVs in the pathogenesis of diabetes. A comprehensive discussion of the role of EVs in the pathophysiology, diagnosis, and treatment of diabetic retinopathy is available elsewhere.[264]

Endothelium in disease contexts undergoes cell injury, activation, dysfunction, and apoptosis leading to increased shedding of EVs. The surrounding microenvironment and activation state of endothelial cells and tissue-resident ECFCs affects the surface profile, intravesicular cargo, and thus the functional of EVs shed from host cells. Interactions between surface proteins on endothelial EVs and nearby target endothelial cells can promote intercellular signaling leading to apoptotic protection. For instance, EVs shed from starved human coronary artery endothelial cells inhibit campthotecin-induced apoptosis of nearby target endothelial cells, which is dependent on the activation of p38. Pretreatment of HCAECs with EVs from HCAECs ($EVs^{HCAECs)}$ reduced p38 by inducing MAPK phosphatase-1, which is regulated by annexin I expressed on EVs^{HCAECs} and acts to dephosphorylate/deactivate p38 to inhibit apoptosis.[265]

These *in vitro* studies demonstrated that EVs^{HCAECs} shed from starvation-induced apoptotic endothelial cells may confer protection from apoptosis to nearby endothelial cells.[265] In contrast, reports have suggested that EVs from healthy ECFCs provide superior therapeutic rescue to hypoxia/reperfusion injury than EVs^{ECFCs} under apoptotic stress.[266] *In vitro,* ECFCs that were subject to starvation stress (sECFCs) via culture with serum deprived (SD) media expressed lower levels of caspace 3 and higher levels of proangiogenic miRs compared ECFCs subject to apoptotic stress (aECFCs) via culture with SD media containing TNF-α. These expression

patterns corresponded to the levels on respective EVs shed from aECFCs and sECFCs. Hypoxia-reperfusion (H/R) injury to cultures of human brain microvascular endothelial cells (HBMECs) resulted in decreased viability, increased apoptosis and production of reactive oxygen species, and decreased nitrous oxide (NO) production and tube formation. While treatment with EVs from sECFCs demonstrated benefit in this H/R assay by decreasing reactive oxygen species production and apoptosis and increasing eNOS and NO production via the PI3K pathway, EVs from aECFCs demonstrated the opposite effects and worsened H/R injury. The benefits of EVs from sECFCs were attenuated when vesicles were treated with RNase suggesting a role for intravesicular RNA in mediating these effects. These data demonstrate the effects of cell microenvironment and cell type on EV-mediated intracellular communication. EVs^{ECFCs} undergoing apoptotic stress are disruptive to endothelial cells, which may have implications for the pathological response of blood vessels in the ischemic response. Transplants of EVs from healthy ECFCs may overcome this dysfunctional communication between endothelial cells during the ischemia-reperfusion injury, promoting physiological vascular growth that may be a promising therapeutic approach.

2.4 Introduction to ECFC-derived EVs

EVs^{ECFCs} exhibit a surface profile characteristic of ECFC origin,[267-270] activate an angiogenic program in endothelial cells via the horizontal transfer of RNA and promote ischemic tissue repair *in vivo*.[267, 271] In addition to stimulating angiogenic growth factor secretion and upregulating anti-apoptotic signaling, EVs^{ECFCs} trigger various signaling pathways in endothelial cells including the Erk1/Erk2 pathway and the PI3K/Akt survival pathway.[267, 270, 272]

EVs^{ECFCs} share several surface proteins of ECFCs including positive expression of ICAM-1, L-selectin, CD31, CD34, CD44, CD133, CD154, VEGFR-2, and the integrins α_4 and

β_1 (also known as CD29) and negative expression of integrins $\alpha_v\beta_3$ and α_6.[267, 268, 273] EVs^{ECFCs} also display tetraspanin surface markers of exosomes including CD9, CD63, and CD81 as well as Annexin V, but are negative in their expression of P-selectin, CD42b, CD14, and human leukocyte antigen class I and class II antigens.[268, 269, 273] Antibody blockade of α_4 or β_1 integrins, but not ICAM-1 or CD44, prevented uptake of EVs^{ECFCs} within human microvascular endothelial cells (HMECs) and HUVECs *in vitro*, suggesting the interaction of α_4 or β_1 integrins with endothelial cells may be required for their internalization of EVs^{ECFCs}. EVs^{ECFCs} promoted proliferation and migration in HMEC cultures and HUVEC cultures while also decreasing serum depravation-induced apoptosis. These anti-apoptotic effects were attenuated when EVs^{ECFCs} were pre-treated with anti-α_4 and/or anti-β_1 blocking antibodies, suggesting the necessity of α_4 or β_1 integrins for uptake of EVs^{ECFCs} into ECs.[267, 270] EVs^{ECFCs} stimulation of HMECs induced expression of $\alpha_v\beta_3$ and α_5 integrins but not of α_6 or β_1 integrins. EVs^{ECFCs}-induced tube formation was attenuated when HMECs were treated with antibody blockade of $\alpha_v\beta_3$ and α_5 integrins prior to stimulation with EVs^{ECFCs}, suggesting upregulation of $\alpha_v\beta_3$ and α_5 integrins in recipient endothelial cells is necessary for capillary-like tube formation.[267]

EVs from ECFCs activate an angiogenic program via the horizontal transfer bioactive RNA cargo into target endothelial cells.[267, 272] EVs^{ECFCs}-treatment of HMECs and HUVECs had proliferative and anti-apoptotic effects, but these were reduced when vesicles were pretreated with RNase, suggesting that these effects were mediated by the horizontal transfer of RNA cargo following EV uptake. In HMEC or HUVEC cultures on Matrigel treated with EVs^{ECFCs} at a dose of 10μg EV protein/5 X 10^4 cell/mL, a proangiogenic response characterized by the formation of capillary-like structures was observed. This dose equates to ~2.1 EVs per cell and emphasizes the potency of EVs^{ECFCs} in triggering an angiogenic response. This effect was also RNA-

mediated as capillary formation was minimal in cells incubated with EVs^{ECFCs} pretreated with RNase. Treatment of HMECs with EVs^{ECFCs} promoted angiogenesis and S-phase entry via regulation of the Erk1/Erk2 signaling pathway.[272] EVs^{ECFCs} treatment promoted Erk1/Erk2 phosphorylation (on both Thr202 and Tyr204 residues) and induced expression of upstream positive regulators of the Erk1/Erk2 pathway including FGF-2, IL-6, and IL-8 as well as downstream targets of this pathway including Id1, Cox-2, c-Myc, cyclin D1, and VEGFA. Blockade of the Erk1/Erk2 signaling pathway attenuated the observed proangiogenic effects of EVs^{ECFCs} on HMECs. EVs^{ECFCs} treatment also resulted in greater than 4-fold upregulation of eNOS, Ang-1, and E-selectin and greater than 1.5-fold upregulation of VEGFR-2, HIF-1α, CXCL16, and platelet-derived growth factor alpha; levels of MMP-9 and platelet-derived growth factor B were downregulated.[270, 272] Together, these data suggested that uptake of EVs^{ECFCs} in endothelial cells modulated the expression of various angiogenic genes and improved cell function in angiogenesis-related assays *in vitro* via the Erk1/Erk2 signaling pathway.

The proliferative and angiogenic effects of EVs^{ECFCs} on endothelial cells have also been attributed to the activation of the PI3K/Akt survival pathway, upregulation of eNOS, and upregulation of anti-apoptotic signaling also via their horizontal RNA transfer.[267] Phosphorylation of Akt in serum-starved HMECs was significantly increased following treatment with EVs^{ECFCs}; RNase pretreatment of EVs^{ECFCs} abrogated Akt phosphorylation. In cultures of EVs^{ECFCs}-treated HMECs, blockade of downstream signaling molecule PI3K by multiple inhibitors prevented the organization of HMECs into capillary-like structures. EVs^{ECFCs}-treatment upregulated eNOS expression (indicated by phosphorylation at ser1177) in HMECs and co-treatment with eNOS inhibitors prevented capillary formation. The anti-apoptotic effect of EV^{ECFCs}-treatment in serum-starved HMECs may be attributed to their upregulation of cellular

Bcl-xL expression. Activation of the PI3K/Akt signaling pathway and upregulation eNOS in HMECs by EVs^{ECFCs} was critical in the activation of the endothelial angiogenic pathway, and the possible regulation of these and other signaling pathways by candidate intravesicular miRs will be discussed in the following section. Functional effects seem to be specific to ECFC-derived EVs; EVs from MSCs failed to induce capillary-like formation in HMECs.[267]

EVs^{ECFCs} also augmented tissue vascularization *in vivo,* once again via their horizontal RNA transfer. Co-injection of EVs^{ECFCs} and HMEC-seeded Matrigel transplants in SCID mice stimulated HMEC formation of patent capillaries that anastomosed with murine vascular beds. This effect was not observed when EVs^{ECFCs} were pretreated with RNase prior to co-injection, implying RNA transfer is critical to HMEC vessel formation *in vivo*. These experimental results raise an exciting possibility in regenerative medicine: instead of transplanting intact cells (with their associated risks of immunogenicity and tumorigenesis), reprogramming tissue resident cells for ischemic repair may be achieved via transplantation of EVs^{ECFCs} and the horizontal transfer of their bioactive RNA cargo to regulate angiogenic pathways *in vivo*.[267]

2.5 Therapeutic mechanisms of ECFC-derived EVs: studies across fields

ECFC-derived EVs have demonstrated potent therapeutic activity in a wide range of ischemic animal models including ischemic retinopathy,[190] acute kidney injury,[94, 268, 271, 273, 274] hindlimb ischemia,[275] and diabetic wound healing,[272] as well as other angiogenesis-dependent animal models including traumatic brain injury (TBI),[276] re-endothelialization of vascular injury,[270] sepsis,[277] and osteogenesis.[278] Enriched in microRNAs targeting functional categories including vascular development, and endothelial cell migration, EVs^{ECFCs} regulate angiogenesis-related genes and wound healing in human retinal microvascular endothelial cells *in vitro* and

rescue vaso-obliteration in the OIR model *in vivo*.[190] The mechanism of transplanted EVs^{ECFCs} in models of AKI relied on intravesicular miR-126, miR-296, and miR-486-5p to promote ischemic tissue repair.[268, 273] In animal models of TBI, EVs^{ECFCs} promoted the formation of tight junction proteins to improve the blood-brain barrier and modulate enzymes involved in ECM remodeling.[276] Treatment of septic mice and models of acute lung injury with EVs^{ECFCs} demonstrated their role in vascular inflammation through miR-126-dependent mechanisms.[277, 279] The following section describes studies that shed light on mechanisms of EVs^{ECFCs} treatments, drawing insights on how these mechanisms may apply to the role of EVs^{ECFCs} in treating retinal ischemia. Overall, EVs^{ECFCs} are an effective treatment modality for a wide spectrum of diseases that rely on proper regulation of endothelial integrity and vascular homeostasis.

2.5.1 Ischemic retinopathy

One study to date has demonstrated the therapeutic effects of EVs^{ECFCs} in the murine OIR model of ischemic retinopathy.[190] Intravitreal injections of EVs^{ECFCs} rescued VO in the OIR model. On small RNA sequencing, EVs^{ECFCs} were enriched in specific miRs when compared to intact cells and 75% of all intravesicular miR reads targeted angiogenic functional categories including vascular development and endothelial cell migration. These data were supported by the demonstration that EVs were taken up by hRMECs *in vitro*, resulting in increased hRMEC migration and significantly altered expression of genes in functional categories of angiogenesis and endothelial cell migration. EVs stained with lipophilic dye CM-diI homed to areas of ischemia and associated with perivascular cells that stained positive for macrophage/microglia markers $F4/80^{+}$ and $Iba1^{+}$.

This study provided a foundational characterization of the intravesicular miR cargo enriched in EVs^{ECFCs}. However, this bioinformatic approach did not identify which intravesicular

miRs were bioactive, leaving potential miR-mediated mechanisms that facilitate the *in vivo* effects of EVs^{ECFCs} unexplored. Normalized miR counts in EVs^{ECFCs} were compared to host ECFCs to calculate fold-change, and more miRs were enriched in EVs^{ECFCs} relative to host cells than vice versa. The miR profile on small RNA sequencing was more similar between independent samples of EVs^{ECFCs} than between any sample of EVs^{ECFCs} and its corresponding ECFC population. Together these findings suggested a conserved subset of microRNAs destined for export may be preferentially loaded into EVs^{ECFCs}. Without comparison to an appropriate control population of EVs, however, it is difficult to identify bioactive miRs that may drive the rescue effects of EVs^{ECFCs} in OIR mice. Research identifying the functionally active population of EVs^{ECFCs} and the relationship between their cargo and therapeutic effects is detailed in the following chapter and may facilitate translation of EVs^{ECFCs}-based therapy into a clinical reality.

2.5.2 Acute kidney injury

In an ischemia-reperfusion model of AKI in mice, systemic application of EVs^{ECFCs} corrected plasma creatine, enhanced tubular cell proliferation, and prevented tubular necrosis and apoptosis.[273] Vesicles were localized in the peritubular capillaries and tubular cells *in vivo*, and vesicle uptake within hypoxic peritubular endothelial cells (TEnCs) and tubular epithelial cells (TEpCs) *in vitro* demonstrated a reliance on L-selectin. Treatment with EVs^{ECFCs} restored the expression of angiogenic and anti-apoptotic genes downregulated by hypoxia in TEnCs and inhibited hypoxia-induced apoptosis in TEpCs. These protective effects of vesicles *in vivo* and *in vitro* were attenuated following degradation of all RNA in vesicles by RNase, depletion of miRs in vesicles by Dicer knock-down in ECFCs, and depletion of miR-126 and miR-296 within vesicles via transfection of ECFCs with miR-antagomirs.[273] These data suggested ECFC-derived

EVs achieve their reno-protective effect by transferring intravesicular miRs, specifically miR-126 and miR-296, to reprogram hypoxic renal cells.

The vesicles analyzed in this report were a population consisting of both microparticles and exosomes, while follow-up studies used differential ultracentrifugation on these vesicle samples to produce a microparticle-enriched and an exosome-enriched sample and compared the efficacy of these two vesicle populations.[268] With a significant caveat being that the size-overlap of microparticles and exosomes makes the 'pure' separation of these two vesicle populations difficult to achieve via differential UC, this study suggested that the protective effects were conferred by transplantation of exosome-enriched but not by microparticle-enriched vesicle samples. Exosome-enriched samples contained miR-486-5p at levels 289-fold higher than microparticle-enriched samples and were found to horizontally transfer this miR to HUVECs *in vitro*. Within endothelial cells, miR-486-5p targeted phosphatase and tensin homolog (PTEN), which released its inhibition of signaling molecules in the Akt pathway thus enhancing Akt phosphorylation and inhibiting apoptosis.[271] These studies within the kidney highlight a potential role for the delivery of intravesicular miR-126, miR-296, and miR-486-5p in mediating ischemic tissue repair.

Literature investigating the role of miR-296 and miR-486-5p within the ischemic retina are limited. In premature infants diagnosed with ROP, plasma levels of miR-296-5p was upregulated 4.2-fold but this was not statistically significant and the clinical relevance of miR-296 to ROP development remains unclear.[280] However, miR-296 is a robust and early marker of hypoxia within the retina. In OIR mice, levels of miR-296 were significantly elevated at 12 hours after removal of mice from hyperoxia, during the onset of the ischemic drive.[281]

miR-296 has been classified as a pro-angiomiR capable of promoting angiogenesis through a positive feedback loop reliant on miR-296's translational suppression of its target hepatocyte growth factor-regulated tyrosine kinase substrate (HGS) mRNA within endothelial cells.[282] The HGS protein functions to regulate the levels of receptors for growth factors including PDGFR-β,[283] VEGFR-2,[284] and EGFR.[285, 286] Following the ligand-stimulation, ubiquitination, and internalization of these growth factor receptors, the ligand/receptor complexes are sorted to the lysosome for degradation in a process mediated by HGS. The down-regulation of HGS synthesis by miR-126 reduced degradation of growth factor receptors for PDGFR-β and VEGFR-2 in HBMECs *in vitro*.[282] Stimulation of HBMECs with VEGF, EFG, or conditioned media from U87 glioma cells (which have potent capacity for inducing angiogenesis[287]) increased miR-296 expression, suggesting a positive feedback loop whereby growth factor-stimulated release of miR-296 contributes to angiogenesis by increasing sensitivity of endothelial cells to these growth factors. These results were corroborated *in vitro* as downregulation of miR-126 in HBMECs attenuated their angiogenic capacity as characterized by decreased tube formation and migration in wound scratch assays. *In vivo*, systemic injection of miR-296 antagomirs inhibited angiogenesis of glioma xenographs in mice.[282]

2.5.3 Traumatic brain injury

Since the retina is an extension of the brain, findings from studies using various models of brain and CNS injury can also inform research on the mechanisms of ECFC-derived EVs as a therapeutic option for retinal disease. In mouse models of traumatic brain injury, delivery of intact ECFCs intravenously[90] or intracerebroventricularly[91] promoted angiogenesis and improved the integrity of blood-brain barrier via the upregulation of ZO-1 and claudin 5 proteins to strengthen tight junctions between endothelial cells. While ECFCs homed to the area of ischemic

injury in the brain and attenuated degradation of tight junctions to improve integrity of the blood-brain barrier, *in vitro* and *in vivo* evidence suggested that their mechanism of TBI repair may rely on EVs shed from transplanted cells.[276] EVs^{ECFCs} incorporated into primary rat brain microvascular endothelial cells (RBMECs) and improved their migration in scratch-wound assays *in vitro*. EV^{ECFCs} treatment attenuated the hypoxia-induced degradation of tight junction proteins ZO-1, occludin, and claudin 5 in RBMEC cultures, suggesting that vesicles can restore the blood-brain barrier. Hypoxic RBMECs increased PTEN expression, which was significantly reduced following treatment with EVs^{ECFCs}. This decreased PTEN expression resulted in increased activation of the Akt survival pathway (ascertained via observing phosphorylation at Thr308 and/or Ser473). *In vivo*, EVs^{ECFCs} transplanted into TBI models colocalized within murine endothelial cells and reduced brain edema as well as blood-brain barrier permeability following injury. PTEN expression was increased *in vivo* following TBI. Treatment with EVs^{ECFCs} reduced PTEN, which increased expression of phosphorylated Akt. Improvement of the blood-brain barrier via upregulation of ZO-1 and occludin but not claudin 5 was observed following treatment with EVs^{ECFCs}. Interestingly, the quick increase in MMP-9 that occurred following TBI was significantly reduced by treatment with EVs^{ECFCs} up to seven days following injury.[276] Intact ECFC transplantation in mouse models of cerebral aneurisms similarly attenuated elevated MMP-9 expression,[123] a mechanistic overlap between ECFC-based and EV^{ECFCs}-based transplantation that suggests the therapeutic effects of ECFCs may be attributable to EVs shed from host cells.

There is some evidence to suggest that hypoxia-induced elevation in MMP-9 expression in retinal and choroidal vascular cells may be attenuated by miR-126 in EVs^{ECFCs}. In the RF/6A cell line of retinal and choroidal vascular cells, hypoxia induced a time-dependent decrease in

miR-126 expression while resulting in increased expression of VEGF and MMP-9 proteins. Pre-treatment hypoxic RF/6A cells with miR-126-inhibitor exacerbated this increase in VEGF and MMP-9 protein; alternatively, miR-126-mimic attenuated VEGF and MMP-9 protein levels while significantly reducing the number of cells in S phase. These data suggested that hypoxia-induced downregulation of miR-126 in retinal choroidal cells *in vitro* results in augmented VEGF and MMP-9 protein expression as well as cell cycle suspension, which may be attenuated by addition of miR-126.[288] Perhaps sufficient delivery of miR-126 can be achieved by way of EVs^{ECFCs}, but additional research is necessary to validate this mechanism. While these data suggest a favorable effect of miR-126 on choroidal vascular cells, conclusions should be taken with some caution as RF/6A cells have recently been reported to lack key endothelial phenotypes.[288]

2.5.4 Sepsis

Sepsis models differ substantially from models of ischemic retinal disease. However, studies on models of sepsis shed light on additional mechanisms by which ECFC-derived EVs may improve vascular dysfunction, leukocyte trafficking, and cytokine-mediated inflammation, partially through their horizontal transfer of miR-126. In the cecal ligation and puncture model of sepsis in mice, systemically injected EVs^{ECFCs} prevented microvascular disfunction and improved outcome measurements of sepsis, at least in part, through the horizontal transfer of intravesicular miR-126 to target cells.[277] In septic mice, EV^{ECFCs}-treatment improved organ dysfunction in the liver, kidneys, and lungs and attenuated the sepsis-induced increase in plasma levels of pro-inflammatory cytokines (IL-6, IFNγ, and TNF-α) and anti-inflammatory cytokine IL-10 as well as the chemokine MCP-1. Addition of lipopolysaccharide (LPS) to cultures of HMECs *in vitro* increased their expression of VCAM-1 and high mobility group box-1

(HMGB1, also known as HMG-1). HMGB1 is a chemokine released from endotoxin-stimulated macrophages that mediates the pathophysiology and lethality of sepsis and a candidate therapeutic target for sepsis treatments.[289-291] LPS-induced increases VCAM-1 and HMGB1 were attenuated by co-treatment of HMECs with EVs^{ECFCs}. EVs from ECFCs transfected with inhibitors to miR-126-3p no longer suppressed levels of VCAM-1 in HUVECs while EVs from ECFCs transfected with inhibitors to miR-126-5p failed to suppress levels of HMGB1. EV^{ECFCs}-treatment suppressed sepsis-induced elevation of HMGB1 in the lungs, where EVs^{ECFCs} are known to accumulate, and EVs^{ECFCs} from cells depleted of both isoforms of miR-126 no longer improved animal survival.[277]

HMGB1 is a member of the high-mobility group chromosomal protein family, which is divided into three superfamilies HMGB, HMGN, and HMGA.[292] Located on chromosome 13q12, HMGB1 is a DNA-binding nuclear protein chiefly localized within the nucleus under physiologic conditions but when cells are stimulated, injured, or dying it is translocated extracellularly and becomes a danger-associated molecular pattern molecule inducing immune-inflammatory and angiogenic responses. Numerous studies suggest a role for HMGB1 in various ischemic/inflammatory ocular diseases such as uveitis, age-related macular degeneration, glaucoma, corneal disease, as well as diabetic retinopathy. In animal models of retinal ischemia and inflammation, HMGB1 is upregulated within retinal pigment epithelium, retinal endothelial cells, ganglion cells, Müller cells, astrocytes, and photoreceptors. The multiple mechanisms of activation and different roles of HMGB1 in a range of cell types is extensively reviewed elsewhere,[293] but evidence has demonstrated that elevated levels of HMGB1 drives diabetic retinopathy by amplifying both inflammation and angiogenesis. HMGB1 activates Toll-like receptors (TLRs) and receptors for advanced glycation end products (RAGE) to increase

production of proinflammatory mediators of the chronic inflammatory diabetic state. Interactions between HMGB1, TLRs (particularly TLR2 and TLR4), and RAGE trigger ERK1/2 signaling to activate NF-κB, which results in the upregulation of leukocyte adhesion molecules (including ICAM-1) as well as the production of inflammatory cytokines and mediators of angiogenesis from both endothelial and hematopoietic cells.[294] This pathway for pathological inflammation and angiogenesis is worsened by a positive feedback loop whereby NF-κB activation induces the expression of HMGB1 receptors, increasing sensitivity to this inflammatory and angiogenic cascade.[295]

HMGB1 is elevated in the vitreous humor of patients with proliferative diabetic retinopathy, and protein levels are significantly higher in the vitreous of PDR patients with active neovascularization in comparison to patients with inactive PDR.[296] Within fibrovascular epiretinal membranes harvested from PDR patients, *in situ* localization of HMGB1 and RAGE expression was present in vascular endothelial cells and stromal cells.[297] In addition to its inflammatory effects via targeting TL2/TLR4 and RAGE, HMGB1 effects a variety of other proinflammatory pathways that drive the pathogenesis of PDR. A significant upregulation of adhesion molecule ICAM-1 resulted *in vitro* upon HMGB1 treatment to human retinal microvascular endothelial cells and *in vivo* upon diabetes induction or intravitreal injection of HMGB1 in rats. In the vitreous of human patients with PDR, elevated HMGB1 levels were correlated with other adhesion molecules including soluble vascular adhesion protein-1 as well as markers of oxidative DNA damage.[298] HMGB1 has also been demonstrated to promote activation of signal transducer and activator transcription-3 (STAT-3) in the diabetic retina, particularly in retinal Müller cells. Upon phosphorylation, activated STAT-3 dimerizes and

translocates into the nucleus to promote the transcription of STAT-3-responsive genes including HIF-1α, ICAM-1, and VEGF that drive the progression of DR.[299]

Numerous studies have demonstrated that inhibition of HMGB1 signaling is a promising approach for the treatment of diabetic retinal complications.[300-302] In addition to protecting the mouse retina from injury induced by ischemia-reperfusion, inhibition of HMGB1 has been shown to reduce retinal insulin resistance in human primary retinal endothelial cells.[300, 303] In human retinal microvascular endothelial cells subject to hyperglycemia *in vitro*, HMGB1 inhibition with siRNA improved cell viability and attenuated high-glucose-induced oxidative stress and apoptosis. *In vivo*, silencing HMGB1 in diabetic rats improved retinal neural function on ERG.[301] Suppression of HMGB1 via the delivery of miR-126 within EVs^{ECFCs} may provide both vascular and neuronal protection in diabetic retinopathy. EVs isolated from human umbilical cord blood-derived MSCs suppressed the elevated HMGB1 signaling pathway and inflammation in high glucose-treated primary human retinal endothelial cells *in vitro*. EVs from MSCs transfected to overexpress miR-126 provided superior suppression of the HMGB1 axis and markers of inflammation, suggesting that delivery of miR-126 via EVs presents a promising strategy to attenuate hyperglycemia-induced injury to retinal endothelial cells.[304] Future studies on the effects of miR-126-5p within EVs^{ECFCs} on HMGB1 within animal models of ischemic retinopathy are necessary to investigate this possibility.

2.5.5 Acute lung injury

EVs^{ECFCs} also conferred protection through a miR-126-dependent mechanism in a murine LPS-induced acute lung injury model of acute respiratory distress syndrome, where disruption in the alveolar-capillary barrier leads to accumulation of proteinaceous edema and inflammatory cells in the alveolar space.[279] EV^{ECFCs} treatment protected from lung injury, reduced neutrophil

infiltration, and abrogated the LPS-induced increase in pro-inflammatory molecules including TNF-α, IL-6, IL-1b, IFN γ, macrophage inflammatory protein (MIP)-1, MIP-2, monokine induced by gamma interferon, and interferon gamma-induced protein-10 in bronchoalveolar lavage fluid. *In vitro,* human small airway epithelial cells (SAECs) transfected to overexpress either miR-126-3p or -5p increased expression of caludin1 and claudin 4 tight junction genes while occludin expression only increased with miR-126-3p expression. Overexpression of either miR-126 isoform in LPS-stimulated SAECs attenuated the increase in caludin1, claudin4, and occludin gene expression, suggesting miR-126 may also confer protection of epithelial tight junctions. While transfection with miR-126-3p decreased levels of its known target phosphoinositol-3 kinase regulatory subunit 2 in SAECs, transfecting of miR-126-5p decreased levels of its known target HMGB1 as well as VEGFA. Together these findings suggest that miR-126 improve the function of both endothelial and epithelial cells in models of ALI, providing evidence that EVs can target multiple cell types and enact multiple vasculotrophic mechanisms.

2.6 Neurovasculotrophic microRNA-126 in ECFC-derived EVs

As described above, an extensive body of work on the therapeutic mechanisms of ECFC-derived EVs describes a pivotal role for the horizontal transfer of miR by EVs^{ECFCs} into target cells, particularly miR-126.[273, 277, 279] The literature suggests that miR-126 is a master regulator of angiogenesis enriched in ECFC-derived EVs and is transferred horizontally by EVs^{ECFCs} to target cells to contribute to their therapeutic benefits *in vivo*. This section begins with an overview of miR processing followed by the genetic background of miR-126 and its gene Egfl7. Briefly discussed are pertinent signaling pathways to the role of miR-126 in embryologic vasculogenesis, followed by a more in-depth review of signaling pathways effected by miR-126 in angiogenesis and postnatal vasculogenesis. The mechanistic and functional effects of EV-

mediated horizontal transfer of miR-126 to active and senescent endothelium are reviewed, followed by a discussion of the role miR-126 plays in vascular inflammation. Altogether, the proangiogenic and neurotrophic properties of miR-126 suggest this microRNA may be a key component of EVs^{ECFCs} in the treatment of ischemic/neurodegenerative retinopathies.

After processing, mature microRNAs are small noncoding RNAs between 20-24 nucleotides that regulate target genes post-transcriptionally. The biogenesis of miRs begins in the nucleus with the transcription of a long primary transcript that is enzymatically processed by the nuclear enzyme Drosha into a shorter precursor species, which is subsequently exported out of the nuclear envelope via exportin-5, a Ran-GTP dependent nuclear export factor. The precursor miRNA in the cytoplasm is processed by the enzyme Dicer into its mature miR species that forms a complex with the RNA-induced silencing complex (RISC) and can then function to inhibit the expression of transcripts via binding to the complementary sequence within the 3'-UTR of target mRNA. Regulation of gene expression by miR takes place via one of two mechanisms. If miR exactly match the sequence on target mRNA, then the mRNA is degraded by Ago2-RISC; if the miR is similar but contains mismatches to target mRNA, then mRNA translation is blocked by Ago1-RISC.[305]

Human miR-126 is located at chromosome 9q34.3 within intron 9 of one of its target genes EGFL7, which encodes EGF-like domain-containing protein 7. Since they are located within a common transcript, miR-126 is expressed in parallel with EGFL7, which is expressed in three isoforms each with separate promotors. Both isoforms of miR-126 are expressed in zebrafish suggesting miR-126 is conserved in vertebrates; the murine Egfl7 gene encodes mmu-miR-126 at intron 7 suggesting that miR-126 is conserved in mammals. The 30kDa protein Efgl7 is expressed and secreted during development and governs lumen formation during

vasculogenesis. In adult mice, Egfl7 are increased in activated endothelial cells responding to vascular injury.[306] Egfl7 was highly expressed in ECFCs relative to other endothelial cell types (HUVECs and HMECs), and suppression of Egfl7 significantly increased proliferation, migration, and tube formation of ECFCs. Silencing Egfl7 in ECFCs transplanted within Matrigel into mouse models of hindlimb ischemia improved limb perfusion, suggesting that inhibition of Egfl7 improved the vasculogenic potential of ECFCs *in vivo*.[307] Both miR-126 and EGFL7 may collaborate in vascular homeostasis, but the functional relationship between these molecules during angiogenesis is unclear.

MicroRNA-126 is an endothelial-specific miR that plays a major regulatory role in physiological embryonic vasculogenesis, postnatal vasculogenesis, and angiogenesis. The roles of miR-126 in embryologic vasculogenesis is comprehensively reviewed elsewhere,[306] and so this review will cover the aspects of these mechanisms in embryogenesis that are relevant to the possible role of miR-126 in therapeutic strategies. The importance of miR-126 during normal vascular development has been demonstrated in a variety of knockdown animal models. Deletion of miR-126 in mice was embryonically lethal in a subset of animals, but surviving mice suffered from the effects of vascular leakage characterized by severe systemic edema, multifocal hemorrhages, and ruptured blood vessels. MicroRNA-126 knockdown of in zebrafish had no effect on gross morphology and patterning of vessels, but resulted in compromised endothelial tube formation and integrity with diffuse intracranial hemorrhaging.[308] Interestingly, absence of miR-126 resulted in significantly reduced retinal vascularization in post-natal day 2 mice.[309] During embryogenesis, miR-126 is upregulated in embryonic $CD31^+$ cells and plays a critical role in regulating angiogenic signaling and vascular integrity by suppressing inhibitors of VEGF signaling. In embryologic stem cell-derived $CD31^+$ endothelial cells, miR-126 plays a

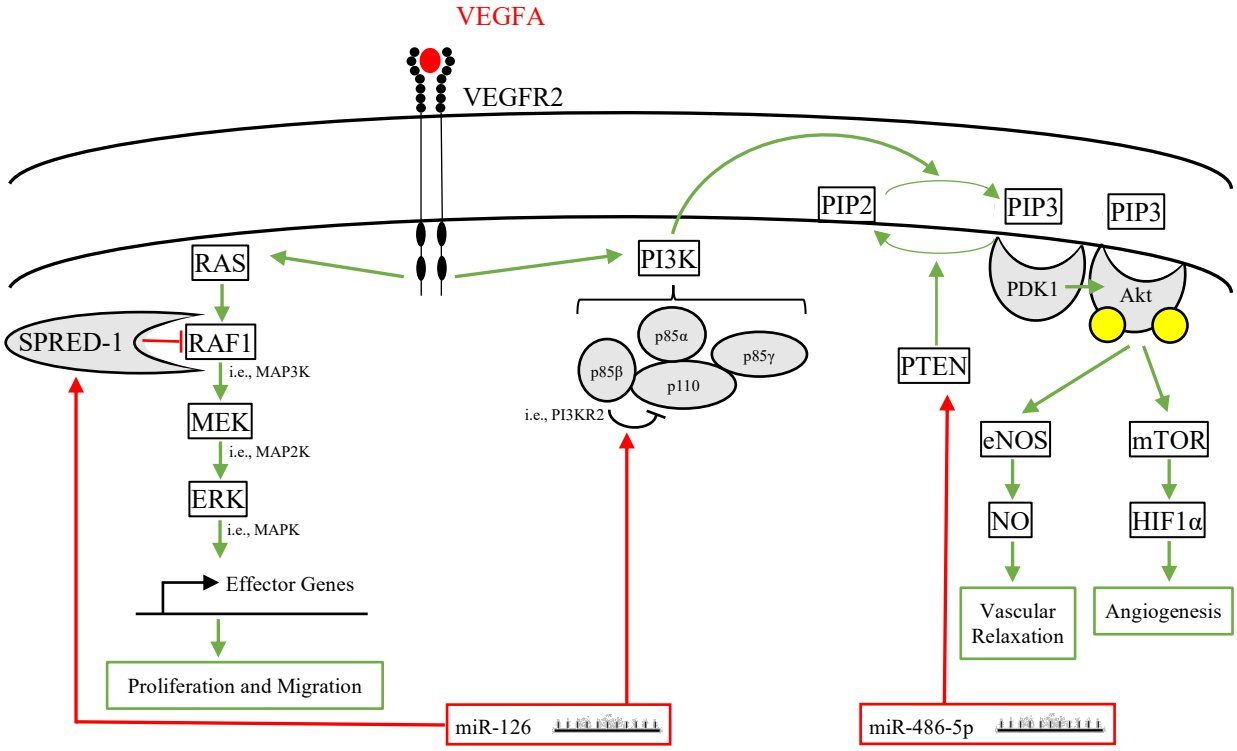

Schema 2.2: miR-126 and miR-486-5p promote vascular growth by suppressing upstream signaling molecules that inhibit angiogenic pathways. Green arrows represent positive regulation of the subsequent cellular process while red arrows represent negative regulation. Inhibited translation of SPRED-1 by miR-126 lifts the proteins suppression of RAS/RAF/MEK/ERK pathway to result in increased proliferation and cell migration. Inhibition of p85ß, also known as PI3KR2, lifts its inhibition of p110 resulting in the promotion of the PI3K/Akt pathway. Some findings indicate that miR-126 regulates upstream signaling molecules to upregulate HIF1α expression. Inhibition of the translation of PTEN by miR486-5p increases NO and HIF1α signaling within the PI3K/Akt pathway to result in vascular relaxation and angiogenesis, respectively.

proangiogenic role by inhibiting both Sprouty-related protein-1 (SPRED-1) and phosphoinositol-3 kinase regulatory subunit 2 (PIK3R2), which are negative regulators of signaling molecules in the PI3 kinase pathway (specifically PI3K) and of the MAP pathway (specifically RAF1), respectively.[308]

By targeting regulators of various signaling pathways as partially depicted in **Schema 2.2**, miR-126 promotes cell survival, proliferation, and motility while contributing to angiogenesis and postnatal vasculogenesis; here, we outline these signaling cascades and their modulation by miR-126. In response to extracellular signals such as VEGF, IGF-1, and FGF, the

Akt pathway (i.e., the PI3K/Akt pathway) is a critical signal transduction cascade that promotes cell survival and growth. Initiation of the Akt survival pathway begins with growth factor activation of a cell surface receptor that facilitates the phosphorylation/activation of the PI3K complex (comprised of three regulatory units p85α, p85β, and p85γ and one catalytic subunit p110), which acts as an upstream secondary messenger signaling molecule in the PI3K/Akt pathway for cell survival. Activated PI3K phosphorylates plasma membrane lipids to form the second messenger phosphatidylinositol (3,4,5)-trisphosphate (PIP_3) from phosphatidylinositol 4,5-bisphosphate (PIP_2). Through interaction with phosphoinositide docking sites, the serine/threonine kinases PDK1 and then Akt (i.e., Protein Kinase B) are recruited to the plasma membrane and fully activated. Activated Akt may phosphorylate a host of intracellular proteins to result in cell survival, growth, proliferation, migration, and angiogenesis. Akt contributes to angiogenesis by activating endothelial nitric oxide synthase that increases NO production to stimulate vasodilation and vascular remodeling. In addition, activated Akt activates mTOR to promote the transcription of HIF1-α transcription factors HIF-1 and HIF-2.[310]

Hypoxia-inducible factor-1, an oxygen-dependent transcriptional activator that regulates cell adaptation to hypoxic stress, is also regulated by miR-126.[16, 311] HIF-1 is a heterodimeric protein comprised of α and β subunits (i.e. HIF-1α and HIF-1β), and HIF-1α and its target genes have a demonstrated role in promoting neuroprotection within the hypoxic retina. HIF-1α is scarcely detectable in normoxic adult retinal tissue as the protein is readily ubiquitinylated for degradation. The proangiogenic molecular mechanisms of HIF-1α in hypoxic retina have been comprehensively reviewed elsewhere;[312] briefly, hypoxic stress upregulates expression of HIF-1α, which is translocated into the nucleus as a HIF-1α/β complex to stimulate downstream expression of target genes including but not limited to erythropoietin, VEGF, heme-oxygenase-1,

adrenomedullin, and glucose transporter-1 with neuroprotective effects on the CNS. In the context of retinal ischemia (such as DR, ROP, macular degeneration, glaucoma, and high-altitude retinopathy), however, elevated HIF-1α and VEGF levels are harmful to the retina.[313] A deeper understanding of the dysregulation of HIF-1α and methods that modulate expression of HIF-1α and its target genes warrant additional investigation as potential novel therapeutic approaches.

Interestingly, modulating levels of HIF-1α via extracellular vesicle-mediated horizontal transfer of miR-126 to senescent endothelium may be such a promising treatment strategy. Relative to early passage HUVECs, senescent HUVECs (i.e. cells with over 96 population doublings) exhibited decreased proliferation and migration in wound healing assays as well as decreased tube formation in angiogenesis assays.[311] Levels of HIF-1α mRNA and protein were decreased in senescent HUVECs in comparison to early passage HUVECs. Similarly, EVs from senescent HUVECs contained lower protein levels of HIF-1α than EVs shed from early passage HUVECs. HIF-1α protein was rapidly degraded in senescent HUVECs and in early passage HUVECs inhibition of HIF-1α impaired migration and tube formation. Thus, the loss of endothelial functions displayed by senescent endothelial cells were attributed to decrease of intracellular HIF-1α, suggesting that the lack of this protein in senescent endothelium is a key contributor to endothelial dysfunction in age-related vasculopathies. One possible conclusion from these findings is that HIF-1α-containing EVs shed from younger endothelial cells may function as an essential paracrine signaling method for maintaining vascular homeostasis and normal endothelial function. In contrast, the absence of HIF-1α in EVs shed from senescent ECs may result in the dysfunction of senescent endothelium.

Early passage HUVECs and their EVs contained appreciable levels of miR-126 while levels were low within quiescent HUVECs and were undetectable within their EVs. While inhibition of HIF-1α had no effect on levels of miR-126 within early passage HUVECs, inhibition of miR-126-3p, miR-126-5p, or both isoforms decreased concentrations of HIF-1α in early passage HUVECs and their EVs. These findings suggested that miR-126 is an upstream regulator of HIF-1α and miR-126 expression results in increased HIF-1α expression. Altogether, these data suggest that delivery of miR-126 to senescent endothelial cells may increase HIF-1α in targeted cells, thereby improving senescent endothelial function.[311] Since ECFC-derived EVs contain miR-126 and are taken up within HUVECs, perhaps one mechanism of the therapeutic efficacy of ECFCs and EVs^{ECFCs} is via vesicle-mediated transfer of miR-126 and its resultant restoration of HIF-1α levels to support the function of senescent endothelium.

miR-126 also suppresses various inhibitory upstream signaling molecules to promote the PI3K/Akt survival pathway. Regulation of the PI3K/Akt pathway is governed by a multitude of mechanisms, but the negative regulatory mechanisms by PIK3R2, PTEN, and SPRED-1 are most pertinent to our discussion as they are targets of miR-126 suppression (**See Schema 2.2**). It has been well-documented that miR-126 targets and inhibits several of these genes to lift their suppression of growth factor-mediated angiogenic signaling pathways. As one of the negative regulatory subunits of PI3K, PIK3R2 (also known as p85β) inhibits PI3K by stabilizing and inhibiting the catalytic subunit p110 by domain-specific interactions.[314] Expression of miR-126 in mature endothelial cells promoted the vascular remodeling and stabilizing effects of Ang-1 by potentiating the PI3K pathway via its direct inhibition of PIK3R2.[315]While VEGF is required for the formation of the initial vascular plexus, Ang-1 promotes maturation and stabilization in growing blood vessels. VEGF may pathologically increase vascular permeability and leakage

leading to tissue edema, but Ang-1 decreases vascular leakage by stabilizing existing vessels. PTEN suppresses the PI3K/Akt pathway by acting as a phosphatase to dephosphorylate PIP_3 back into PIP_2.[316] Lastly, SPRED-1 inhibits RAF1 within the growth factor-activated RAS/RAF/MEK/ERK pathway; vesicle-mediated delivery of miR-126 suppressed SPRED-1, lifting its inhibition of this pathway to enhance endothelial cell function.[317]

MicroRNA-126 also suppresses vascular inflammation. Endothelial cells at rest normally do not express adhesion molecules. During vascular inflammation, cytokines activate endothelial cells to induce expression of adhesion molecules such as VCAM-1, a surface protein that interacts with the $\alpha_4\beta_1$ integrin ligand very-late antigen 4 (VLA-4; CD49d/CD29) that is expressed on most leukocytes and activated neutrophils. MicroRNA-126 plays a role in attenuating vascular inflammation within ECs by suppressing translation of VCAM-1 protein to prevent leukocyte adherence to endothelial cells.[318] As part of pathophysiology of diabetic retinopathy, leukocyte adhesion to vascular endothelium leads to endothelial injury, breakdown of the blood-retina barrier, and capillary nonperfusion. In STZ-induced diabetic mice, hyperglycemia upregulated VCAM-1 expression on retinal vasculature.[319] In STZ-induced diabetic Long Evans rats with early diabetic retinopathy, antibody blockade of VLA-4 reduced vascular leakage and inflammatory cytokine production, suggesting that inhibition of the VCAM-1/VLA-4 interaction between endothelial cells and leukocytes may represent a promising clinical treatment strategy.[320] Furthermore in humans, elevated levels of soluble VCAM-1 are found in the serum of patients with type 2 diabetes with microvascular complications[321] as well as in the vitreous of patients with PDR.[322] Suppression of VCAM-1 by miR-126 and the subsequent decrease in leukocyte adherence to ECs could therefore have beneficial effects in

attenuating the chronic inflammation driving the pathology of ischemic retinopathies such as diabetic retinopathy.

The varied levels of miR-126 and their effects in different endothelial cell phenotypes is responsible for the regulation and heterogeneity of VCAM-1 protein expression on the surface of ECs during acute inflammation *in vivo*.[318] In multiple models of glomerulonephritis either via induction with anti-glomerular basement membrane, intravenous exposure to TNF-α, or induction of hemorrhaging shock, VCAM-1 mRNA expression was elevated in both arteriolar and glomerular endothelial cells while the protein expression of VCAM-1 was high in the arteriolar compartment cells but minimal in the glomerular compartment. These results implied that the heterogenous responsiveness of endothelial cells to acute inflammation was dependent on the microvascular phenotype and independent of the nature of the inflammatory stimulus. As the sequence of miR-126 is similar but not exactly complementary to a region within the 3'-UTR of VCAM-1,[323] these results also corroborate that miR-126 regulates VCAM-1 at the level of translation.[318] Levels of miR-126, Egfl7, and Ets1 (a transcription factor promoting the parallel expression of Egfl7 and intronic miR-126) were all high in glomerular ECs but low in arteriolar ECs. The higher VCAM-1 protein levels in glomerular ECs versus arteriolar EVs was attributable to the functional activity of elevated glomerular miR-126 suppressing translation of VCAM-1 mRNA in glomerular endothelial cells *in vitro*. Silencing miR-126 with antagomirs following TNF-α induction of acute renal inflammation *in vivo* resulted in increased VCAM-1 protein expression in endothelial cells throughout all compartments of the kidneys. Differing regulation of VCAM-1 protein expression by miR-126, thus, mediates the heterogeneity of the VCAM-1 surface profile across the range of renal microvascular endothelial cell phenotypes.

The role miR-126 plays in determining the microvascular heterogeneity of VCAM-1 protein expression, however, is not limited to renal ECs.[318] This study also examined the effects of TNF-α and antagomir-126 in the induction of VCAM-1 protein in the heart, lungs, and liver. Of these organs, only in the liver did VCAM-1 protein induction occur, indicating that the control of VCAM-1 protein expression by miR-126 in microvascular cells varies between the organ of origin. The role of miR-126 on vascular inflammation and VCAM-1 expression in ECs within the retina remain unexplored. Future studies aimed at elucidating the mechanism whereby miR-126-containing EVs^{ECFCs} rescue models of ischemic retinopathy may wish to investigate whether this intravesicular component may play a role in suppressing pathophysiologic vascular inflammation.

2.7 EC- and ECFC-derived EVs cross-talk with progenitor cells

Studies offer proof-of-concept evidence that EVs shed from endothelial cells may harbor cargo that function not only in the homeostasis of nearby endothelium[267] but also in the protection of endothelium in response to hypoxia in the context of arterial injury, perhaps through the recruitment of circulating progenitor cells.[46, 324-326] MicroRNA-126 was enriched in EVs harvested from starvation-induced apoptotic HUVECs and played a role in mediating vascular protection in a CXCL12-dependent manner.[327] MicroRNA-126 repressed the function of regulator of G protein signaling 16 (RG16), a heterotrimeric guanosine triphosphate-binding protein that inhibits the G protein-coupled receptor CXCR4. Since CXCR4 is the receptor for CXC chemokine CXCL12 (also known as SDF-1), lifting RG16 suppression of CXCR4 increased production of CXCL12, which is a chemokine known to counteract apoptosis and recruit circulating progenitor cells. In diet-induced atherosclerosis models in apolipoprotein-E deficient (*Apoe*$^{-/-}$) or LDL receptor deficient (*Ldlr*$^{-/-}$) mice, systemic downregulation of the

Cxcl12/Cxcr4 axis results in the significant expansion of bone marrow neutrophils and their recruitment to atherosclerotic lesions causing severe exacerbation of plaques.[326] By upregulating CXCL-12 production, delivery of miR-126 by EVs from apoptotic HUVECs conferred protection to atherosclerotic mouse models via the recruitment of murine Sca-1^{+}/Lin^{-} progenitor cells to areas of tissue injury. Together, these data provide evidence that miRs, particularly miR-126, delivered by endothelial cell-derived EVs may promote cross-talk and recruitment of progenitor cell types to promote tissue repair and homeostasis.

EVs^{ECFCs} may facilitate intercellular communication between other progenitor cells including MACs potentially via the transfer of miRs such as miR-126. The presence of miR-126 in ECFC-derived EVs makes it of importance to note studies that suggested miR-126 may promote the angiogenic properties of MACs. MACs are recruited by inflammatory chemokines to sites of vascular injury and promote angiogenesis via their secretion of angiogenic factors that may in turn promote tissue repair by circulating and tissue-resident ECFCs (**Schema 1.1**). By targeting PIK3R2 to lift its suppression of the PI3K/Akt pathway, miR-126 promoted the proliferation, migration, and differentiation of MACs. These effects were corroborated by *in vivo* findings demonstrating lower numbers of PB-derived MAC colonies correlated to lower placental levels of miR-126 from the blood of patients with preeclampsia versus a control group of healthy patients. Injection of miR mimics and antagomirs locally into the placenta of pregnant rats demonstrated that miR-126 increased vascular sprouting, microvascular density, and the weight of the placenta and fetus.[324] Together, these data suggest an essential role for miR-126 in angiogenic properties of MACs *in vitro* and possibly in placental vasculogenesis *in vivo*. A limitation of this study was an inability to exclude whether miR-126 effected other placental cell types *in vivo*. However, the placenta is a known niche of pools of hematopoietic stem cells.[328-330]

In *ex vivo* cultures of MACs isolated from the peripheral blood of patients with type II diabetes[46] as well as coronary artery disease,[325] miR-126 was downregulated relative to healthy control patients. MACs derived from diabetic blood exhibited decreased colony formation, migration, and proliferation with augmented apoptosis, but these functional deficits were attenuated with lentivirally-induced overexpression of miR-126. The target of miR-126 in MACs was SPRED-1 and miR treatment therefore upregulated the Ras pathway; treatment also resulted in increased signaling in the Akt survival pathway.[46] These data suggest that delivery of miR-126 to MACs, perhaps via ECFC-derived EVs, in diabetic patients may restore MAC cell function and thus improve their therapeutic efficacy but this approach requires corroborative data from retinal models of ischemia *in vivo*.

2.8 Conclusions and future directions

Extracellular vesicles shed from endothelial colony forming cells are strong candidates for the treatment of ischemic and neurodegenerative retinal disease. Similarly to cell-based therapies, delivery of diverse bioactive cargo by EVs can initiate multiple mechanisms within multiple cell types simultaneously. EVs, however, contain no replication machinery and transplantation carries little risk of tumorigenesis associated with transplantation of readily dividing intact stem/progenitor cells. Without the possibility of *in vivo* replication, dosing of EVs can be more precisely controlled. Their storage profile is EV-specific but is generally favorable to long-term storage at -20˚C with resistance to multiple freeze/thaw cycles. Research over the last decade has led to an increased understanding of EV biogenesis, content, and biological functions, and the therapeutic effects of EVs from ECFCs have been demonstrated across multiple animal disease models. [94, 190, 268, 270-278]

In these early days of EV research, there are currently no FDA approved EV-based treatments, posing numerous avenues for growth in the development of EVs^{ECFCs} as a therapeutic option. A range of EV isolation methodologies including differential ultracentrifugation, density gradients, polymeric precipitation, immunoaffinity isolation, microfluidic devices, ultrafiltration, and size exclusion chromatography have been developed for research applications, and selection of the proper EV isolation technique is critical in research settings where downstream applications may dictate a need to optimize particular characteristics like EV yield versus EV specificity or other parameters. However, a major challenge preventing the translation of EV-based therapeutics into clinics is the lack of a scalable manufacturing technique capable of producing clinical grade EVs^{ECFCs} in numbers that meet therapeutic demands. Ultrafiltration followed by size exclusion chromatography may represent a scalable technique to isolate EVs with preserved biophysical and functional characteristics,[242, 243] but additional work must be done to actualize this technique's capacity to scale. Once scaled isolation techniques are validated, considerable efforts to preserve EVs' formulation in storage and cold chain strategies must be achieved. EVs^{ECFCs} were able to maintain their surface characteristics, integrity, and biological function even after years in storage at -20˚C with multiple freeze/thaw cycles.[193, 194] While this is a testament to their capacity for prolonged storage, more rigorous evaluations of storage methods and their effects on EVs^{ECFCs} must be conducted to minimize the impact of storage conditions on vesicle integrity.

Intercellular communication through the exchange of extracellular vesicles is important to normal retinal function and development, and the roles of EVs from various cell types is the focus of ongoing research. In many vascular disease contexts such as diabetes,[249-251] cardiovascular disease,[252] hypertension,[253] and atherosclerosis,[254] increased levels of endothelial

EVs in patient plasma may reflect the degree of vascular injury. In the plasma of patients with type 2 diabetes, circulating endothelial-derived EVs are associated with increased oxidized LDLs and may be involved in the pathophysiology of disease progression through their promotion of coagulation, inflammation, endothelial dysfunction, and angiogenesis. Through an RNA-mediated mechanism, EVs from endothelium undergoing starvation stress inhibited apoptosis of nearby endothelium *in vitro* and benefited ischemic tissue by decreasing ROS production, apoptosis, and increasing eNOS and NO production via the PI3K pathway *in vivo*. EVs from endothelium undergoing apoptotic stress had the opposite effects and worsened ischemic injury.[266]

Transplants of EVs from ECFCs may be a promising therapeutic approach to treating ischemic disease by overcoming this dysfunctional communication, but a greater understanding of heterogeneous population of EVs^{ECFCs} and the relationship between their cargo and functional effects must be investigated. EVs^{ECFCs} horizontally transfer bioactive RNA cargo to activate an angiogenic program in target endothelial cells *in vitro*.[267] Multiple mechanisms of EVs^{ECFCs} have been described including the promotion of the Erk1/Erk2 survival pathway,[272] activation of the PI3K/Akt survival pathway, upregulation of eNOS, and upregulation of antiapoptotic signaling also via their horizontal RNA transfer.[267] EVs^{ECFCs} display potent rescue effects *in vivo* in ischemic animal models including ischemic retinopathy,[190] acute kidney injury,[94, 268, 271, 273, 274] hindlimb ischemia,[275] and diabetic wound healing,[272] as well as other animal models reliant on angiogenesis including traumatic brain injury,[276] re-endothelialization of vascular injury,[270] sepsis,[277] and osteogenesis.[278] Intravitreal injection of EVs^{ECFCs} rescued vaso-obliteration in the murine OIR model of ischemic retinopathy, and RNA sequencing found that 75% of intravesicular miR reads targeted angiogenic functional categories including vascular

development and cell migration.[190] Transplantation of EVs^{ECFCs} rescued animal models of AKI through mechanisms reliant on intravesicular miR-126, miR-296, and miR-486-5p.[268, 273] In animal models of TBI, EVs^{ECFCs} improve the blood-brain barrier by promoting the expression of tight junction proteins and enzymes of ECM remodeling.[276] Treatment of mouse models of sepsis and acute lung injury with EVs^{ECFCs} demonstrated a role in vascular inflammation through mechanisms dependent on intravesicular miR-126.[277, 279]

The literature suggests a role for intravesicular miR-126 in the therapeutic effects of EVs^{ECFCs}. [273, 277, 279] MicroRNA-126 is a well-documented master regulator of angiogenesis. In embryologic stem cell-derived $CD31^{+}$ endothelial cells as well as mature endothelial cells, miR-126 is pro-angiogenic through its inhibition of SPRED1 and PIK3R2, which are negative regulators of signaling molecules PI3K in the PI3 kinase pathway and RAF1 in the MAP pathway, respectively.[308] Early passage endothelial cells delivered extracellular vesicles enriched with microRNA-126 and HIF-1α to senescent endothelial cells to restore their function.[311] MicroRNA-126 also suppressed vascular inflammation by inhibiting translation of VCAM-1 protein to prevent leukocyte adherence to endothelial cells.[318] The different expression miR-126 expression in microvascular endothelial cells from different organs regulates the heterogeneity of VCAM-1 protein expression. However, the role of miR-126 on VCAM-1 expression and vascular inflammation in ECs within the retina remain unexplored. Inhibition of VCAM-1 protein expression by miR-126 may decrease leukocyte adherence to ECs in the retina to alleviate the chronic inflammation that drives ischemic retinopathies such as diabetic retinopathy, but experimental evidence of this proposal has not yet been provided.

In addition to mediating the homeostasis of nearby endothelium, EVs from ECFCs and endothelial cells also protect endothelium in response to hypoxia by the recruitment of

circulating progenitor cells.[46, 324-326] For instance, miR-126 in EVs from starved HUVECs suppressed RG16 to release its inhibition of CXCR4, which increased production the chemokine CXCL12 to counteract apoptosis and recruit murine Sca-1^{+}/Lin^{-} progenitor cells to areas of tissue injury *in vivo*.[327] MicroRNA-126 also promoted the angiogenic properties of MACs and restored functional deficits in MACs isolated from diabetic blood by upregulating the Akt survival pathway and suppressing SPRED-1 to upregulate the Ras pathway.[46, 324] These data suggest that delivery of miR-126, perhaps within EVs^{ECFCs}, may recruit progenitor cells and restore dysfunction caused by diabetes, but this mechanism has not yet been investigated within retinal tissue.

Overall, the molecular mechanisms that intravesicular miRs within EVs^{ECFCs} play in mediating retinal repair merit further investigation. Chapter 3 describes my dissertation research characterizing the rescue effects of two subpopulations of EVs^{ECFCs} (one effective and one ineffective population) in animal models of ischemic and neurodegenerative retinopathy. Comparison of their intravesicular small RNA content identified miR-503-5p as a critical mediator of the demonstrated neurovasculotrophic effects of the bioactive subpopulation of EVs. Future efforts may be directed to exploit these findings, as well as those within the extensive literature, to investigate the molecular mechanisms of miRs within EVs^{ECFCs} in retinal disease systems. Furthermore, the intravesicular protein and lipid profile of EVs^{ECFCs} and their effects in repairing damaged retinal tissue remains unexplored. Lastly, the surface profile of EVs^{ECFCs} and its effect on homing and uptake into target cells within the retina would aid our understanding of the *in vivo* mechanisms of this novel therapeutic agent. Ultimately, such studies would greatly improve our ability to optimize EV^{ECFCs}-based therapy for retinal disease.

Chapters 1 and 2 are currently being prepared for submission for publication of the material. Marra, KV; Friedlander, M. The dissertation author was the primary investigator and author of this material.

Chapter 3

Bioactive extracellular vesicles from a subset of endothelial progenitor cells rescue retinal ischemia and neurodegeneration

3.1 Abstract

Disruption of the neurovascular unit (NVU) underlies the pathophysiology of various CNS diseases.[120, 331, 332] One strategy to repair NVU dysfunction uses stem/progenitor cells to provide trophic support to the NVU's functionally coupled and interdependent vasculature and surrounding CNS parenchyma.[333] A subset of endothelial progenitor cells called endothelial colony forming cells (ECFCs) with high expression of the CD44 hyaluronan receptor ($CD44^{hi}$) achieve this effect. Relative to ECFCs with low CD44 expression ($CD44^{lo}$), $CD44^{hi}$ ECFCs provided superior neurovasculotrophic support via a paracrine mechanism.[29] Here, we identified that bioactive extracellular vesicles (EVs) from $CD44^{hi}$ ECFCs (EVs^{hi}) represent paracrine mediators that recapitulate the effects of intact cell therapy in murine models of ischemic/neurodegenerative retinopathy; vesicles from $CD44^{lo}$ ECFCs (EVs^{lo}) were ineffective. Small RNA sequencing comparing the microRNA (miR) cargo within EVs^{hi} and EVs^{lo} identified candidate miRs that contribute to these effects. EVs^{hi} may repair NVU dysfunction through

multiple mechanisms to stabilize hypoxic vasculature, promote vascular growth, and support neural cells.

3.2 Introduction

The NVU consists of neurons, perivascular astrocytes, microglia, pericytes, extracellular matrix, and vascular endothelial cells, together functioning to maintain the blood-brain/retinal barrier and local CNS homeostasis. Disruption of the NVU is central to the pathophysiology of various ischemic/neurodegenerative diseases of the CNS including ischemic stroke, Parkinson's, Alzheimer's, multiple sclerosis, amyotrophic lateral sclerosis, and diabetic retinopathy.[120, 331, 332] Ischemia promotes CNS remodeling, where neurovascular cross-talk between the neurons, glia, and microvascular cells of the NVU attempts to produce a microenvironment that favors tissue recovery. This remodeling is dependent on both neuronal outgrowth as well as capillary sprouting. Since multicellular cross-talk between local vascular networks and the neurons they supply in the NVU is critical to maintaining physiological function, one regenerative therapeutic strategy to repair the dysfunctional NVU focuses using progenitor and/or stem cells to provide support to the complex of vascular endothelial cells and surrounding CNS parenchyma that are functionally coupled and interdependent.[333]

Recent studies support the use of the endothelial progenitor cell known as ECFCs to achieve this effect. ECFCs home to areas of ischemia and exhibit potent rescue effects in a variety of animal models of ischemic/neurodegenerative CNS diseases including traumatic brain injury and ischemic stroke.[77, 90-92, 123, 334] As a readily accessible and visualized extension of the brain, the retina is an exceptional experimental system for modelling ischemic and neurogenerative CNS diseases for the preclinical development of novel treatment agents. Experiments in murine models of retinal ischemia/degeneration have provided proof-of-concept

evidence that vasculotrophic support by ECFCs (and other stem/progenitor cells) protects retinal neurons from undergoing apoptosis.[29, 59, 71, 72, 100, 335, 336] Several lines of evidence have suggested a predominantly paracrine therapeutic mechanism of ECFCs . For instance, while ECFCs have potent rescue effects in models of ischemic/neurodegenerative CNS diseases *in vivo*, low levels of engraftment have been observed within cerebral vasculature.[77, 90-92, 123, 334] ECFCs predominantly home to ischemic areas and assume perivascular positions within the retina,[29, 71, 72] and injection of ECFC-conditioned media (CM) in OIR mice recapitulated the rescue effects observed when using intact cell therapy.[29]

EVs from ECFCs are a promising new addition to the armamentarium of paracrine mediators of intracellular communication that confer therapeutic benefit via the horizontal transfer of bioactive cargo. EVs are a critical means of cell-to-cell communication within the NVU that act as bidirectional messengers both between the brain and periphery as well as within the brain.[337] EVs from ECFCs activate an angiogenic program in target endothelial cells and recruit and activate circulating and tissue-resident progenitor cells via their ability to horizontally transfer RNA.[267] The majority of intravesicular miR in EVs from ECFCs target angiogenic functional categories including vascular development and cell migration.[190]

ECFCs are not a functionally homogeneous cell population. $CD44^{hi}$ ECFCs rescue animal models of retinal ischemia (oxygen-induced retinopathy, OIR) and neurodegeneration ($Pde6b^{rd10/rd10}$ RD10 mice) via a paracrine mechanism; $CD44^{lo}$ ECFCs have little effect.[29] The current study exploited these findings to identify trophic miRs in EVs^{hi} shed from the bioactive subset of $CD44^{hi}$ ECFCs. First, we demonstrated that EVs^{hi} recapitulated the neurovasculotrophic rescue effects of intact cell transplantation in OIR and RD10 mice; EVs^{lo} had little effect. In OIR mice, EVs^{hi} homed to sites of ischemia and neovascularization and

incorporated within vasculature and perivascular microglia/macrophages. The rescue effect of EVs^{hi} was dependent on intravesicular miR as lentiviral miR knockdown attenuated the effects of $CD44^{hi}$ ECFCs and EVs^{hi} on OIR. Small RNA sequencing with RT-qPCR validation identified 7 candidate miRs upregulated in EVs^{hi} relative to EVs^{lo}. Of these, miR-23a-3p, miR-30a-5p, miR-216a-3p, and miR-503-5p independently rescued OIR mice. Individual knockdown of miR-23a-3p or miR-503-5p or combinatorial knockdown of all these miRs attenuated the effects of EVs^{hi}. Overall, EVs^{hi} rely upon intravesicular neurovasculotrophic miRs and target the NVU in ischemic/neurodegenerative diseases of the CNS to stabilize retinal vasculature to hypoxic damage, stimulate functional vascular growth, and provide trophic support to neurons.

3.3 Methods

3.3.1 Animals

OIR was induced on C57BL/6J mice (The Jackson Laboratory, JAX) as previously described.[29] Briefly, pups and their mothers were transferred from room air to an hyperoxic (75% O_2) chamber (Bio-Spherix) on postnatal day 7 (P7) for 5 days, during which the hyperoxic environment leads to vaso-obliteration (VO) of central retinal blood vessels. Pups were returned to room air and transferred to a surrogate mother on P12, and the resulting ischemia stimulates a neovascular (NV) phase characterized by the formation of preretinal neovascular tufts, which peak at P17. $Pde6b^{rd10/rd10}$ (RD10) mice (B6.CXB1-$Pde6b^{rd10}$/J) were purchased from JAX. C57BL/6J pups were used for vascular developmental models.

3.3.2 Cell preparation and culture

Human umbilical cord blood (UCB) was obtained following full-term gestation from healthy non-diabetic donors and was processed within 2 hours of delivery in all cultures. ECFCs were derived from 4 UCB donors and cultured as previously described.[29] In brief, UCB (40-60

mL) was diluted 1:2 in PBS with 20 μg/mL heparin (STEMCELL Technologies, 07980) and mononuclear cells were isolated using Lymphoprep (STEMCELL Technologies, 07851). After 3 PBS washes, mononuclear cells were resuspended in EC-Cult Xeno Free Media (XFM, STEMCELL Technologies, 0800) and seeded at a density of 50×10^6 cells/well onto 6-well plates coated with ACF cell attachment substrate (STEMCELL Technologies, 07130). After daily media changes for the first 7 days, medium was changed every other day. Passage 7 ECFCs were used for experiments. Human umbilical vein endothelial cells (HUVECs, Lonza, C2519A) were cultured using M200 medium (ThermoFisher, M200500) and passage 2 cells and their EVs were used in experiments in OIR mice.

3.3.3 ECFC immunophenotyping and sorting

The immunophenotype of ECFCs was determined by flow cytometry on 3 biological replicates of ECFCs using fluorescence-conjugated antibodies. ECFCs were sorted into $CD44^{hi/lo}$ populations as previously described.[29] Briefly, cells were detached (Animal Component-Free Cell Dissociation Kit, STEMCELL Technologies, 05426) and PBS washed. ECFCs were incubated for 20 minutes on ice with 20 μL of APC-conjugated primary murine monoclonal antibodies to human CD44 antibody (clone: G44-57, BD PharMingen, 559942) in 0.4 mL stain buffer (PBS [Dulbecco's, no Ca^{2+}, no Mg^{2+}, ThermoFisher, 14190250], 5% FBS, with 0.5mM EDTA), washed three times, and analyzed by FACSAria flow cytometer (BD) with FlowJo (TreeStar) software. Duplicate and dead cells were excluded from the sort using forward and side scatter to analyze their 2D profile. Fluorescence voltages were set using negative controls, and the same strategy for setting parameters and gating were applied to all samples. The same staining protocol was applied for all FACs analyses of ECFCs using antibodies and

concentrations listed in **Table S3.1**, and the same gating strategy was used for all cell sorting experiments.

3.3.4 EV isolation

EVs were isolated from ECFC CM as previously described with modifications.[242] Serum-free XFM (10 mL/T75 flask) was conditioned for 48 hours by sorted passage 7 $CD44^{hi/lo}$ ECFCs seeded at a density of 1.2×10^6 cells/T75 flask (ThermoFisher, 07-202-000). Pooled CM was removed of cell debris via centrifugation at 300 × *g* for 5 min (Beckman Coulter Alegra 6KR, ARIES™ Smart Balance Rotor) and supernatant was 0.22 μm vacuum-filtered (Corning, 430320). CM was loaded into an Amicon® Ultra-15 Centrifugal Filter Unit with an Ultracel-10 membrane (MWCO = 10 kDa; Merck Millipore, Billerica, MA, USA, UFC901024) for ultrafiltration (UF) to concentrate CM to1 mL via centrifugation at 4,000 *x g* (Beckman GS-6R, GH-3.8 swing bucket rotor). The concentrated sample was then subject to size exclusion chromatography (SEC) as previously described with some modifications.[225] For the SEC column, the tip of a 10 mL plastic syringe (Becton Dickinson, San Jose, CA, 309604) was packed with nylon stocking (20 denier, H&M, USA) and loaded with 10 mL Sepharose CL-2B (GE Healthcare; Uppsala, Sweden, 17014001) that was washed prior with elution buffer (PBS with 0.32% trisodium citrate, pH 7.4, 0.22 μm vacuum-filtered) three times. The column was run dry before UF-concentrated CM was loaded. Once the CM entered the stationary phase, 20 mL elution buffer was slowly added, and eluate was collected in approximately 40 sequential elution fractions (EF) of 0.5 mL each. Soluble protein of each EF was measured using a Pierce BCA protein assay (ThermoFisher, 23225) according to the manufacturer's instructions. Protein began eluting between fraction 8 and 12. All EFs prior to protein detection were pooled and concentrated to 250-500 μL using an Amicon® Ultra-4 Centrifugal Filter Unit with an

Ultracel-10 membrane (MWCO = 10 kDa; Merck Millipore UFC801024) by centrifugation at 4,000 × g to produce an EV-rich, soluble protein-poor sample (UF-SEC-UF sample). This sample was measured with nanoparticle tracking analysis (NTA) and aliquoted for experiments either fresh or after storage at -80ºC. EVs harvested using differential ultracentrifugation (UC) were isolated as previously described using a Beckman L-80 XP ultracentrifuge.[243] EV yield was calculated by multiplying the particle concentration on NTA by the final sample volume, divided by the number of T75 flasks from which CM was pooled. Experiments were performed with EVs from at least 4 biologically independent ECFC colonies derived from distinct UCB donors in OIR mice, and from 2 distinct UCB donors in RD10 mice. EVs from HUVECs were obtained from 2 independent UF-SEC-UF isolation protocols from a single population of expanded cells.

3.3.5 ECFC transfection

CD44 expression was knocked-down (KD) in ECFCs using green fluorescent protein (GFP) lentiviral-shRNA clones (CMV-Neo, clones TRCN0000308110 and TRCN0000296190, GenTarget Inc.) to CD44 (ECFCs-shCD44). DICER1 KD ECFCs (ECFCs-shDICER1) were generated using lentiviral-shRNA clones. Cell transfections were performed in accordance with the manufacturer's protocol with antibiotic selection with puromycin (sc-108071, Santa Cruz, 1µg/mL media for ECFCs-shCD44 and 5µg/mL media for ECFCs-shDICER1). Two separate lines of ECFCs-scrRNA were transfected with scramble RNA to serve as negative control cells in ECFCs-shCD44 experiments (GenTarget Inc.) or ECFCs-shDICER1 experiments (Santa Cruz, sc-108080). Knockdown of miR-7-5p, miR-23a-3p, miR-216a-3p, and miR-503-5p in ECFCs was achieved using miRCURY LNA miRNA Power Inhibitors with FAM labeling and the corresponding scramble miR (scrmiR) Negative Control A (YI04100814-DDB, YI04103406-

DDC, YI04104404-DDB, YI04100899-DDB, and YI00199006-DDB, respectively, Qiagen, 1 μM). Transfection efficiency was measured as the average percentage DAPI+/GFP+ cells in 5 sample confocal images of ECFCs-shCD44 or ECFCs-scrRNA fixed in 4% paraformaldehyde for 20 min. Knockdown efficiencies were measured on RT-qPCR.

3.3.6 EV characterization

Magnetic bead-assisted flow cytometry: Exo-Flow Capture Kits (Systems BioScience) were used in accordance with the manufacturer's protocol (**Table S3.1**) to confirm the presence of vesicles in all EV samples. Briefly, magnetic 9.1 μm streptavidin-coated beads were washed twice and incubated with 10 μL biotinylated CD9, CD63, CD81, or CD31 capture antibody for 2 hours at 4°C with gentle agitation every 30 min. Following 3 washes, beads were incubated with EV samples in a rotating rack at 4°C overnight for exosome capture. Beads were then washed twice before incubation with 10 μL of proprietary Exo-FITC antibodies for 2 hours on ice. After 3 additional washes, beads were suspended in wash buffer and analyzed by flow cytometry. A DynaMag™-2 (ThermoFisher, 12321D) stand was used to magnetically precipitate beads during wash steps. Nanoparticle tracking analysis: NTA was used on all EV samples to measure particle concentration. EV samples were diluted in DPBS (Dulbecco's no Ca^{2+}/Mg^{2+}, ThermoFisher, 14190) in a cuvette analyzed on the ViewSizer® 3000 (HORIBA Scientific, Irvine, CA). Upon illumination with blue (450 nm at 210 mW), green (520 nm at 12 mW), and red (635 nm at 8 mW) lasers, 50 videos (30 sec each, exposure: 15 ms) of Brownian motion of nanoparticles were recorded and analyzed by ViewSizer™ software to determine particle size distribution and concentration. Transmission electron microscopy (TEM): Negative stains of EV samples were imaged by a CM100FEI electron microscope at an 80kV accelerating voltage. First, a Formvar-carbon-coated grid was loaded with 8 μL of sample for 2 minutes to allow for adsorption. Excess

sample was removed from the grid using a clean filter paper. The coated side of grids were placed face down in a droplet of phosphotungstic acid for 2 minutes then samples were imaged. CM-diI staining: EVs^{hi} were incubated with CM-diI (ThermoFisher, C7001, 1μM) for 5 min at 37˚C, for 20 min on ice, and then were washed twice with PBS spins at 100,000 *x g* immediately prior to injection into OIR mice.

3.3.7 Intravitreal injections

Mice were injected intravitreally using a 33-gauge needle (Hamilton). All injections were 0.5 μL in volume. Intact $CD44^{hi}$ or $CD44^{lo}$ ECFCs and HUVEC controls were injected along with PBS vehicle controls. Exosome biogenesis and release from $CD44^{hi}$ ECFCs was pharmacologically inhibited by 1 hr incubation with the neutral sphingomyelinase inhibitor GW4869 (20μM) dissolved in DMSO (+GW4869) while control $CD44^{hi}$ ECFCs were incubated with an equal volume of DMSO (-GW4869). All cells were injected a concentration of 1×10^5 cells/μL in PBS vehicle. Following measurement of EV concentration using NTA, 1×10^5 EV particles/0.5 μL/eye were injected into OIR and RD10 mice. EVs from HUVECs served as an EV control. PBS served as a vehicle control. To ensure media components were not responsible for observed effects, non-conditioned media for ECFCs (XFM) and HUVECs (M200) was subject to the same UF-SEC-UF EV-isolation protocol and injected into OIR mice. EVs^{hi} sample was vesicle-depleted by 18 hours of ultracentrifugation at 120,000 *x g* and injected into OIR mice. ECFC-derived EVs isolated in a total of 9 UF-SEC-UF preps from media conditioned by each of 4 distinct biological UCB donors were tested in at least 3 litters of OIR mice. In RD10 mice, ECFC-derived EVs from 2 individual UCB donors promoted functional rescue of the neural retina on electroretinography. MicroRNA mimics of miR-7-5p, miR-23a-3p, miR-216a-3p, and miR-503-5p (ThermoFisher, mirVana mimics, MC11755, MC10644, MC24316,

MC10378, respectively) as well as scramble microRNA (ThermoFisher, mirVana mimic, Negative Control #1, 4464085) were intravitreally injected into OIR mice.

3.3.8 Immunofluorescence

To prepare retinal flat-mounts, enucleated eyes were fixed in 4% paraformaldehyde for 1 hour at 4ºC. The anterior capsule was removed to allow for dissection of the nuclei and cortex of the lens. The retina was separated from choroid and sclera, cleaned of remaining vitreous with fine brushes, and cut into four leaflets. Dissected retinas were incubated overnight in PBS with $Ca^{2+}Mg^{2+}$ with 10µg of fluorescently-labeled Isolectin *Griffonia simplicifolia*-IB4 (GS-IB4, ThermoFisher, I21412). For retinal cryosections, eyes fixed for 4 hours were punctured at the limbus with small forceps and incubated in 30% sucrose overnight prior to freezing in OCT media-filled molds for sectioning. For antibody staining, retinas were rehydrated with PBS prior to overnight incubation with gentle rocking at 4ºC in block buffer (PBS with 10% fetal calf serum, 10% serum matching the host species of the primary antibody, and 0.3% [v/v)] Triton X-100 [Sigma, T8787]). Primary antibodies used in this study are listed in **Table S3.1**. Following 5 washes in PBS for 10 min each, retinas were incubated with corresponding fluorescently labeled Alexa secondary antibodies (ThermoFisher) in block buffer with 0.1% (v/v) Triton X-100 overnight in 4ºC with gentle rocking. Nuclei were stained with Hoechst 33342 (ThermoFisher, 62249) or DAPI (ThermoFisher, 62248). In each staining protocol, retinas were washed 4 times in PBS for 10 min before mounting with SlowFade™ Gold Antifade Mountant medium (ThermoFisher, S36937). TUNEL staining was performed using an In-Situ Cell Death Detection Kit (Roche Diagnostics, 11684795910) according to the manufacturer's instructions.

3.3.9 Confocal microscopy and quantification

Retinas were imaged using a Zeiss 710 confocal laser-scanning microscope with ZEN 2010 software (Zeiss). Quantification of the percentage retina covered by NV and VO in OIR mice was quantified with our published deep learning algorithm.[338] In cases where quantification using this algorithm disagreed with expert's inspection of the images, reported measurements were quantified using manual quantification methods as previously described.[132] Briefly, the lasso tool in Photoshop CS6 (Adobe) was used to outline and record total retinal area and the VO was measured by tracing the central avascular retina; the magnetic lasso tool was used to highlight NV. VO was quantified manually for experiments injecting OIR mice on P7 for quantification on P10, P12, and P14. Vascular coverage in developmental models was quantified as the traced area of vascular coverage divided by the total retinal area traced using the lasso tool in Photoshop. For quantification of retinal thicknesses in OIR eyes, the inner nuclear layer (INL), inner plexiform layer (IPL), and outer nuclear layer (ONL) were measured in stitched 20x magnification images of retinal cross-sections and the averaged thickness at preselected distances from the optic nerve were reported. For quantification of vascular plexi in RD10 mice, 8 z-stack images (4 central and 4 peripheral) at 20x magnification (326 x 326 μm fields of view) were taken of each retina of P21, P25, P32, P40, and P60 mice. The images in focus on the deep and intermediate vascular plexi were selected for quantification at each location from the z-stack. For each eye, the total vessel area and length quantified using AngioTool Software[339] (US National Institutes of Health [NIH], Bethesda, MD) were reported as the averages from these 8 images per retina. The number of branch points was manually quantified in ImageJ (NIH). To quantify retinal thickness and density of TUNEL-positive cells in the ONL, a series of 20x magnification images of retinal cross-sections were acquired. To measure the density of

apoptotic cells, the number of apoptotic TUNEL+/DAPI+ cells was divided by the ONL area as calculated in ImageJ as previously described.[29] ONL thickness was measured at selected distances from the optic nerve using ImageJ as previously described.[340] Per eye, quantification of the percentage retinal area covered by cone photoreceptors was performed on 4 representative 20x images measured 500 μm from the optic nerve of red/green opsin-stained retinal flat-mounts. The percentage area of opsin positive pixels was obtained via threshold selection of gray-scaled images in ImageJ and results were normalized to those from normoxic retinas.

3.3.10 Ganzfeld electroretinography

Electroretinography (ERG) was performed as previously described.[29] Mice were dark-adapted overnight. Anesthesia was administered via intraperitoneal injection of 20 mg/mL ketamine and 2 mg/mL xylazine at a dose of 5 μL/g body weight. Following pupil dilation with 2.5% phenylephrine and 1% tropicamide, full-field ERGs using silver needle electrodes as reference (forehead) and ground (tail) were measured from the corneal surface using active contact lens electrodes (Mayo). Conditions were controlled via a Ganzfeld dome using Espion E2 computer software (Diagnosys). Dark-adapted (scotopic) recordings were made of rod responses to a series of white light flashes of increasing intensities (25 and 50 cd×s/m^2 reported). Light-adapted (photopic) conditions were induced by a 30 cd/m^2 background luminescence for 5 min and measurements were made on cone responses to a single flash (intensity 25 cd×s/m^2) as well as to 1-Hz flicker stimuli. For all ERG measurements, responses were filtered at 0.3-500 Hz and averaged signals were reported. To circumvent the observation that ERG measurements can vary significantly between litters of untreated RD10 mice (data not shown) and the possible bias imposed by eye dominance, treatment groups were randomized within each litter and both eyes were injected with the same treatment per mouse. ERG experiments investigating the effect of

EVs from sorted CD44$^{hi/lo}$ ECFCs were conducted separately from ERG experiments injecting EVs from ECFCs-shCD44 versus EVs from ECFCs-scrRNA.

3.3.11 Small RNA sequencing

Exosomal RNA extraction: RNA was extracted from EVs^{hi} and EVs^{lo} using the Plasma/Serum Circulating and Exosomal RNA Purification Mini Kit (Norgen BioTek, # 51000) as previously described.[341] Samples were incubated for 10 min at 60˚C with 100 µL warmed PS Solution A and 900 µL warmed PS Solution B (containing 2-Mercaptoethanol). After adding 1.5 mL of 100% ethanol, samples were centrifuged for 30 sec at 100 x *g*. The pellet was resuspended in 750 µL PS Solution C and incubated again for 10 min at 60˚C. After adding 750 µL of 100% ethanol, this solution was loaded onto the filter column and centrifuged for 1 min at 16,000 x *g*. Following 3 wash spins for 1 min at 16,000 x *g* using 400 µL Wash Solution, the column was centrifuged again to dry the membrane. The column was loaded with 30 µL water and a slow spin for 2 mins at 300 x *g* followed by a fast spin for 3 min at 16,000 x *g* eluted the RNA.
Library preparation and small RNA sequencing: Libraries for small RNA sequencing were constructed using the NEBNext Small RNA Library Prep Set for Illumina as previously described.[341] Reactions were conducted at 1/5th the suggested volume and adaptors at 1/6th the provided concentration with 18 PCR cycles. Libraries were prepared from 1.2 µL of RNA for each sample. A Zymo DNA Clean & Concentrator Kit (Zymo Research, D4013) was used to clean library product. Libraries were pooled based on PicoGreen measurements of concentration and the proportion of desired PCR product and adaptor dimers were observed using a Fragment Analyzer high sensitivity DNA array (Advanced Analytical). Pooled libraries were size selected to remove adapter dimers using the Pippin Prep HT instrument with the lower limit of size selection set to 125 and the upper limit set to 150. Size selected libraries were sequenced on a

MiSeq instrument for initial analyses and quality control before samples were sequenced on an Illumina HiSeq 4000 as 50 cycle single end reads. Analysis of small RNA sequencing data: All-pass filtered miRs with >10 reads in any one sample in each group were included for analyses. Qlucore Omics Explorer was used to for Principal Component Analysis, Hierarchical Clustering, and data visualization. Differential expression analysis was also performed by the Qlucore Omics Explorer using the "Two Group" comparison tool.

3.3.12 RT-qPCR

To measure ECFC transduction efficiency, total RNA was isolated from cells using the RNeasy Micro Kit (Qiagen, 74004) and reverse transcribed using the High-Capacity RNA-to-cDNA Kit (ThermoFisher, 4388950). The CFX96 Touch Real-Time PCR Detection System (Bio-Rad) was used to perform RT-qPCR using Taqman Gene Expression Assays or Taqman MicroRNA Assays for measurements of lentiviral transduction efficiency. Validation of small RNA sequencing data was achieved using TaqMan Advanced MicroRNA Assays targeting differentially expressed miRs according to the manufacturer's instructions. All materials used for RT-qPCR are listed in **Table S3.2**. The housekeeping genes used for normalization of RT-qPCR data was beta-actin for DICER1 KD cells, GAPDH for CD44 KD cells, and snU6 for all miR KD cells.

Analyses were performed as previously described with modifications.[342] Normalization of extracellular miR datasets has proved to be challenging. Standard approaches to normalization like using spike-in synthetic oligonucleotides, housekeeping small RNAs, or bioinformatic techniques often applied in cellular long RNA-seq datasets have not been successful. Studies of miRs within cells and tissues even advocate for use of sample-set-specific normalizers,[343] and the challenge of normalization in exosomal RNA datasets is commonly accepted.[344] For pairs of

endogenous miRs, the expression of each miR can serve as an endogenous control for the others, resulting in more reproducible features than the measured abundance of each individual miR.[342] This paired normalization approach was first described in Prince et al. and results in the formation of ratios of individual miR abundance.[345] For our RT-qPCR validation of sequencing data, this technique was implemented to form ratios of each miR upregulated in EVs^{hi} to each miR downregulated in EVs^{hi} on small RNA sequencing to assess whether these expression trends can be validated.

3.3.13 Statistics

PRISM (version 6, GraphPad Software) software was used for all statistical analysis. For experiments containing two groups, an unpaired, two-tailed Student's *t*-test was used. 1-way ANOVA with ad hoc Tukey analysis was used for multiple comparisons. For nonparametric data, a Kruskal-Wallis test with Dunn's multiple comparison test was performed. Statistical significance was determined with $P<0.05$.

3.3.14 Study approval

Experimental procedures using animals were approved by The Scripps Research Institute Animal Care and Use Committee. Experiments were performed in accordance with the NIH Guide for the Care and Use of Laboratory Animals (National Academies Press, 2011). In accordance with the Declaration of Helsinki, adult donors of umbilical cord blood provided informed consent prior to sample collection. Protocols were approved by The Institutional Review Board at The Scripps Research Institute and Scripps Memorial Hospital, La Jolla.

3.4 Results

3.4.1 Culture, immunophenotype, sorting, and transfection of ECFCs

Cultured human umbilical cord blood derived ECFCs exhibited their characteristic cobblestone morphology (**Figure 3.1A**). An ECFC immunophenotype was confirmed via flow cytometric analysis demonstrating positive expression of CD13, CD31, CD105, VEGFR-2, and HLA-ABC. ECFCs were negative in their expression of hematopoietic markers CD14 and CD45, mesenchymal marker CD90, and HLA-DR as previously reported (**Figure 3.1B**).[29] ECFCs were sorted into $CD44^{hi}$ and $CD44^{lo}$ populations (**Figure 3.1C**). ECFCs-shCD44 and control ECFCs-scrRNA were transfected with an efficiency of 90.1% and 93.1%, respectively, as measured using confocal microscopy (**Figure S3.1**). CD44 KD was also validated on flow cytometry (**Figure 3.1D**). RT-qPCR analysis demonstrated a CD44 KD efficiency of 40.3% in ECFCs-shCD44 relative to ECFCs-scrRNA. ECFCs-shDICER1 and another line of ECFCs-scrRNA served as control cells for *in vivo* experiments. KD efficiency of ECFCs-shDICER1 was 63.8% on RT-qPCR.

3.4.2 Isolation and characterization of EVs

An EV isolation protocol was implemented to optimize yield and purity of EVs harvested from CM.[242] Serial ultrafiltration, size exclusion chromatography, then repeat ultrafiltration was a robust and repeatable method for producing large quantities of soluble protein-poor EV-enriched samples. Early SEC elution fractions contained undetectable levels of soluble protein in a BCA protein assay (**Figure 3.2A**) and contained EVs expressing exosomal marker CD63 (**Figure S3.2**) on magnetic bead-assisted flow cytometry. These early protein-poor, EV-rich elution fractions were concentrated by UF and samples obtained by UF-SEC-UF isolated

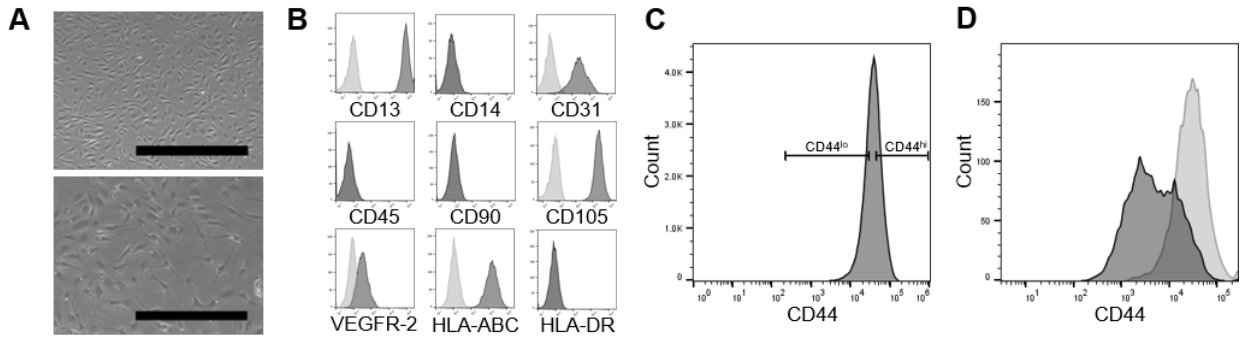

Figure 3.1: **ECFC characterization and CD44 sorting and knockdown**. (**A**) Representative images of confluent ECFC colonies taken at 5x (top) and 10x (bottom) magnification. Scale bar: 500 µm (top); scale bar: 200 µm (bottom). (**B**) Immunophenotypic characterization of ECFCs. Representative flow cytometry histograms of ECFCs demonstrated positive expression of CD13, CD31, CD105, and HLA-ABC and negative expression of hematopoietic markers CD14 and CD45, mesenchymal stem cell marker CD90, as well as HLA-DR (right-shifted, black-filled curves in comparison to grey-filled curves representing the appropriate isotype controls; n=3 replicates). (**C**) Representative gating strategy to sort $CD44^{hi}$ and $CD44^{lo}$ ECFCs using FACS. (**D**) Flow cytometric analysis of CD44 in ECFCs-shCD44 (black-filled curves) and ECFCs-scrRNA (grey-filled curves) following lentiviral-mediated transfection of ECFCs with shCD44.

significantly higher yields of EVs than samples isolated by differential ultracentrifugation (**Figure 3.2B**). On TEM, EVs isolated from CM via differential UC demonstrated the characteristic vesicle size and morphology but contained appreciable amounts of macromolecule and vesicle aggregates. Characteristic EV size/morphology was also observed in EV samples isolated using UF-SEC-UF, but vesicle/macromolecule aggregates were not observed on TEM (**Figure 3.2C**). NTA measured EVs within the appropriate size distribution (**Figure S3.3A**).

No differences were observed between the immunophenotypes of EVs^{hi} versus EVs^{lo} on magnetic bead-assisted flow cytometry as well as single particle flow cytometry. Using magnetic bead-assisted flow cytometry, both EVs^{hi} and EVs^{lo} expressed exosomal tetraspanins CD9, CD63, and CD81 and endothelial marker CD31 (**Figure 3.2D**). On single particle FACs analysis, a population of EVs^{hi} and EVs^{lo} demonstrated positive expression of tetraspanin markers CD9 and CD63 with a smaller population of CD81 positive EVs but were negative in their expression of tetraspanins CD82 and CD151 (data not shown). EVs expressed integrins α_5, α_6, β_1, and β_3 but

did not express integrin α_4 and adhesion molecule ICAM-1 on single particle FACs. (**Figure S3.3B**)

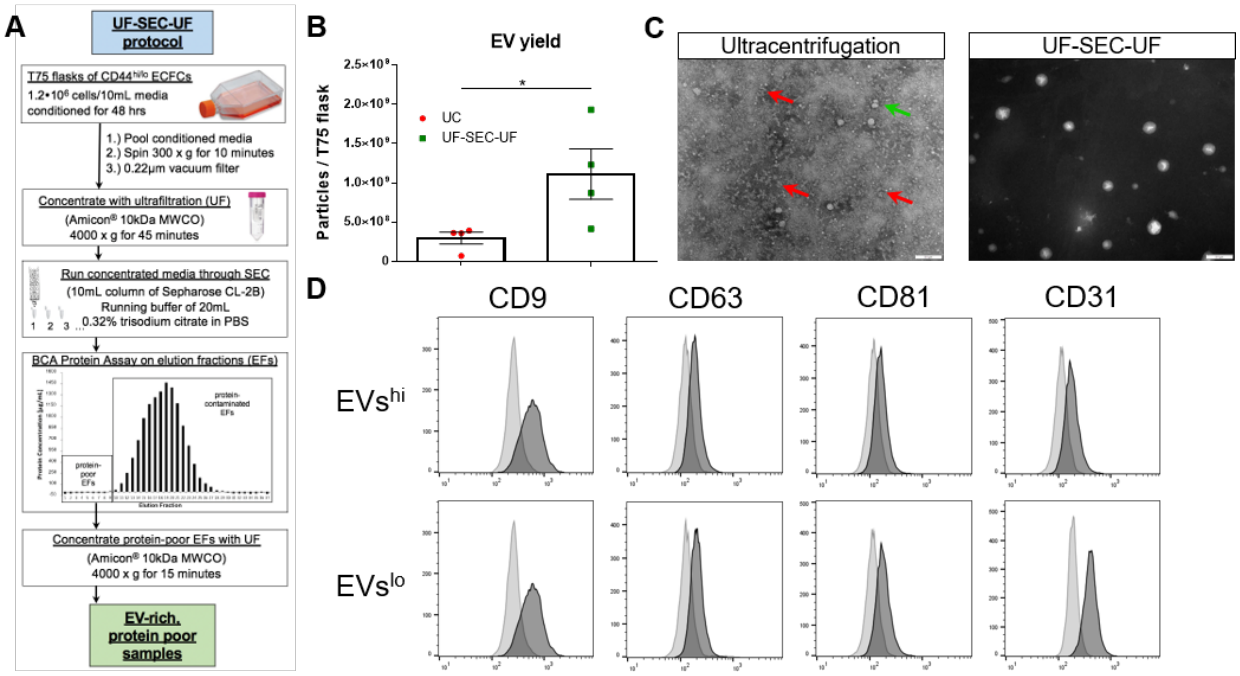

Figure 3.2: **EV isolation protocol, yield, morphology, and immunophenotype.** (**A**) Schematic of UF-SEC-UF protocol. (**B**) UF-SEC-UF obtained a significantly higher EV yield than differential UC. *P<0.05, two-tailed Student's *t*-test; n=4. Error bars represent SEM. (**C**) TEM of EV samples isolated via differential UC (left) or UF-SEC-UF (right). Differential UC samples demonstrated aggregation of macromolecules (red arrows) and EVs (green arrow). UF-SEC-UF produces EV samples devoid of contaminating aggregates. Scale bars: 0.2 µm. (**D**) Representative magnetic bead-assisted flow cytometry histograms of EVs^{hi} and EVs^{lo}. Both populations positively expressed tetraspanins CD9, CD63, and CD81, as well as endothelial marker CD31 (right-shifted, black filled curves compared to gray-filled curves of negative control samples; n=3 replicates).

3.4.3 EVs^{hi} rescued the OIR model of ischemic retinopathy

Intravitreal injections of $CD44^{hi}$ ECFCs on P12 more effectively rescued the NV and VO on P17 in OIR mice than $CD44^{lo}$ ECFCs or PBS control, as previously reported.[29] Injections of HUVEC control cells also failed to rescue OIR (**Figures 3.3A-B**). EVs^{hi} rescued NV and VO in OIR mice while EVs^{lo} or PBS vehicle did not. HUVEC EVs also did not recue OIR mice, suggesting these rescue effects were endothelial progenitor cell-specific. To control for components of cell culture media that may remain in EV samples isolated using the UF-SEC-UF

isolation protocol, non-conditioned ECFC media (XFM UF-SEC-UF) and vesicle-depleted HUVEC media (M200 UF-SEC-UF) were subjected to the same UF-SEC-UF isolation protocol and injected into OIR but had no effect. EVs^{hi} sample depleted of vesicles by ultracentrifugation at 120,000 *x g* for 18 hours failed to rescue OIR (**Figures 3.3C-D**), suggesting rescue effects were attributable to vesicles within the EVs^{hi} sample. $CD44^{hi}$ ECFCs treated with neutral sphingomyelinase inhibitor GW4869, the most widely used pharmacological agent to block exosome biogenesis and release, no longer rescued OIR mice (**Figure 3.3E**).[346-348]

The capacity to which CD44 expression on ECFCs correlates with therapeutic neurovascular benefit was investigated using a line of ECFCs with knocked down CD44 expression via lentiviral transfection with shRNA. OIR mice were injected on P12 with intact cells or EVs from ECFCs-shCD44 or ECFCs-scrRNA. ECFCs-shCD44 failed to reduce NV and trended towards increased VO on P17 in comparison to treatment with ECFCs-scrRNA, which rescued OIR mice (**Figure 3.3F**). EVs were isolated from media conditioned by both cell types. ECFCs-shCD44 EVs failed to rescue NV in OIR when compared to eyes treated with ECFCs-scrRNA EVs (**Figure 3.3G**).

EVs from 4 out of 4 cord blood donors successfully rescued OIR, suggesting that this therapy may be efficiently derived from any healthy donor or banks of pooled UCB. While most EVs were prepared fresh before injection, samples frozen at -80ºC for as long as 1 year retained therapeutic function in OIR, corroborating studies suggesting that the integrity and functionality of ECFC-derived EVs are stable in long-term storage with multiple freeze thaw cycles.[193, 194] A dose-response experiment injecting EVs^{hi} with serial 10-fold dilutions from an initial dose of 1.25×10^6 particles/0.5 μL/eye was performed to determine treatment potency. EVs^{hi}

Figure 3.3: **ECFCs with high CD44 expression and their shed EVs rescued OIR.** (**A-B**) Rescue of OIR mice by intravitreally injected cells. (**A**) Representative images of GS-IB4 lectin-stained flat-mounted P17 retinas treated at P12 with $CD44^{hi}$ (left) or $CD44^{lo}$ (right) ECFCs quantified for NV (in red) and VO (in yellow). Insets in **A** depict the original unquantified images. Scale bars: 1 mm. (**B**) Quantification of OIR retinas showed treatment with $CD44^{hi}$ ECFCs significantly reduced NV (left) and VO (right). Mice were also treated with $CD44^{lo}$ ECFCs and HUVEC controls. *P<0.05, 1-way ANOVA with Tukey analysis; n=7 retinas for $CD44^{hi}$ ECFCs, n=7 retinas for $CD44^{lo}$ ECFC, n=5 retinas for HUVECs. (**C-D**) Rescue of OIR mice by intravitreally injected EVs. (**C**) Representative images of GS-IB4 lectin-stained flat-mounted retinas treated on P12 with EVs^{hi} (left) or EVs^{lo} (right) quantified on P17 for NV (in red) and VO (in yellow). Inserts in **C** depict the original unquantified images. Scale bars: 1 mm. (**D**) Quantification of OIR retinas demonstrated treatment with EVs^{hi} significantly rescued NV (left) and VO (right). Mice also received treatment with EVs^{lo} and HUVEC EV controls. Additional controls included non-conditioned ECFC and HUVEC media subject to the UF-SEC-UF protocol (XFM UF-SEC-UF and M200 UF-SEC-UF, respectively) as well as EVs^{hi} sample depleted of vesicles via overnight UC (EVs^{hi} depleted) *P<0.05, **P<0.01, ***P<0.001, ****P<0.0001, 1-way ANOVA with Tukey analysis; n=100 retinas for EVs^{hi}, n=102 retinas for EVs^{lo}, n=10 retinas for HUVEC EVs, n=11 retinas for XFM UF-SEC-UF, n=5 retinas for M200 UF-SEC-UF, n=6 retinas for EVs^{hi} depleted. (**E**) Pharmacologic exosome inhibition via treatment with GW4869 attenuated the effects of $CD44^{hi}$ ECFCs on OIR mice. GW4869 (20μM) dissolved in DMSO was added to the media of sorted $CD44^{hi}$ ECFCs (+GW4869, n=12 retinas) or an equivalent volume of DMSO was added to media sorted $CD44^{hi}$ ECFCs (-GW4869, n=12 retinas) for 1 hr prior to intravitreal injection of washed cells on P12. *P<0.05, ****P<0.0001, two-tailed Student's *t*-test. (**F-G**) CD44 knockdown ECFCs and their EVs have reduced rescue effects in the OIR model. Quantification of NV and VO in OIR mice injected with (**F**) ECFCs-scrRNA (n=10 retinas) versus ECFCs-shCD44 (n=11 retinas) and (**G**) EVs from ECFCs-scrRNA (n=10 retinas) versus EVs from ECFCs-shCD44 (n=11 retinas). *P<0.05, **P<0.01, two-tailed Student's *t*-test. (**H**) Dose-response curve for OIR mice injected P12 with EVs^{hi}. Mice were treated with a starting dose of 1.25×10^{6} particles/0.5 μL/eye and serial 10-fold dilutions. *P<0.05, **P<0.01, Kruskal-Wallis test with Dunn's multiple comparison test; n=6-9 eyes per group. Error bars in all figures represent SEM.

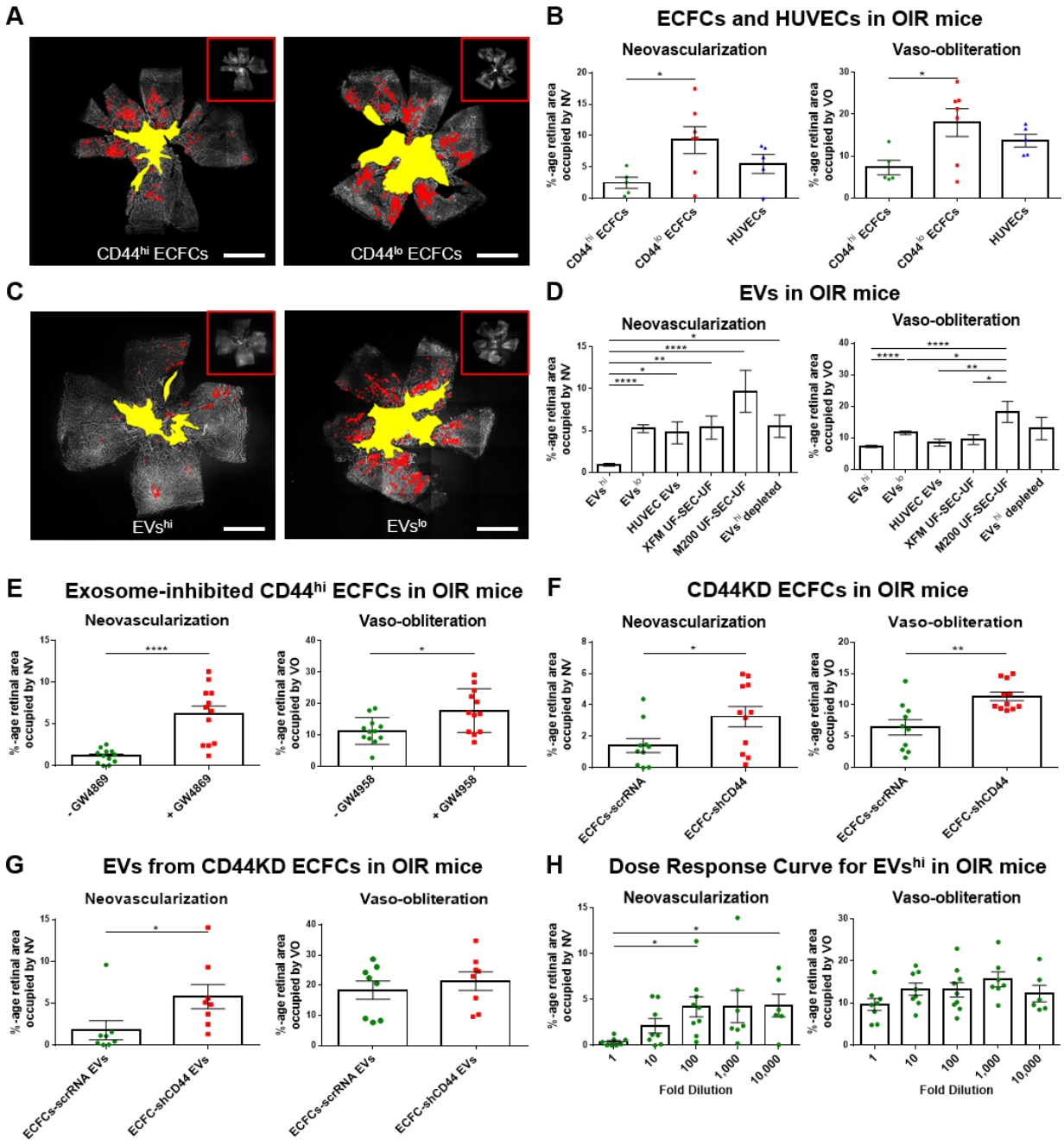
A
CD44hi ECFCs
CD44lo ECFCs
B
ECFCs and HUVECs in OIR mice
Neovascularization
Vaso-obliteration
%-age retinal area occupied by NV
%-age retinal area occupied by VO
CD44hi ECFCs
CD44lo ECFCs
HUVECs
C
EVshi
EVslo
D
EVs in OIR mice
Neovascularization
Vaso-obliteration
EVshi
EVslo
HUVEC EVs
XFM UF-SEC-UF
M200 UF-SEC-UF
EVshi depleted
E
Exosome-inhibited CD44hi ECFCs in OIR mice
Neovascularization
Vaso-obliteration
- GW4869
+ GW4869
- GW4958
+ GW4958
F
CD44KD ECFCs in OIR mice
Neovascularization
Vaso-obliteration
ECFCs-scrRNA
ECFC-shCD44
G
EVs from CD44KD ECFCs in OIR mice
Neovascularization
Vaso-obliteration
ECFCs-scrRNA EVs
ECFC-shCD44 EVs
H
Dose Response Curve for EVshi in OIR mice
Neovascularization
Vaso-obliteration
Fold Dilution
1
10
100
1,000
10,000

demonstrated a dose-dependent rescue effect on NV and VO, and these effects were significantly reduced once samples were diluted 100-fold (**Figure 3.3H**).

The experiments described thus far were performed with P12 injections immediately upon return from hyperoxia to room air, at the onset of the ischemic drive. To investigate the impact of treatment timing on efficacy, EVs^{hi} were injected into OIR mice either immediately before entering hyperoxia on P7 or two days after pups return to normoxia on P14. Injection with EVs^{hi} on P7 rescued the OIR phenotype as compared to injections with EVs^{lo} (**Figure S3.4A**). EVs^{hi} failed to rescue the OIR phenotype when injected on P14 (**Figure S3.4B)**. The successful rescue of OIR following P7 injections informed our hypothesis that P7 injections of EVs^{hi} promoted physiological angiogenesis in the context of vaso-obliteration. Injections were performed at P7 and retinas were evaluated at time points within (P10 and P12) and near the end (P14) of the vaso-obliterative phase of OIR. Decreased VO following EVs^{hi} suggested that EVs^{hi} promoted vascular growth during the vaso-obliterative phase of OIR (**Figure S3.5A**).

Retinal vascularization is typically completed at birth in humans, but the retina of infants born prematurely may be incompletely vascularized and, thus, carries increased risk of suffering from retinopathy of pre-maturity (ROP).[349] The murine OIR model is a well-established model that mimics the hallmark features of human ROP – initial vaso-obliteration and subsequent neovascularization – as well as other complications including vascular leakage.[350] Following the observation that EVs^{hi} rescue the OIR phenotype, we investigated the effects of EVs^{hi}-treatment on normal vascular development. These experiments may aid in our understanding of whether EVs^{hi} can prevent pathological neovascularization while allowing normal vascularization in premature infants at risk of ROP. Newborn mice are a useful developmental model of retinal vasculature since the vascularization of the murine retina occurs postnatally. After birth,

vasculature begins developing around the optic nerve head in mice and extends radially until reaching the peripheral retina at P21.[335] Wild-type pups were treated on P2 with EVs^{hi}, EVs^{lo}, PBS vehicle, or were untreated. Mice were sacrificed on P5 and the percent retinal coverage with vasculature was quantified. No effect on retinal coverage with vasculature was observed following treatment with EVs^{hi} or EVs^{lo}, suggesting EV treatment does not disturb normal retinal vascular development (**Figure S3.5B-C**).

While OIR mice classically model retinal ischemic vasculopathy, neuroprotective effects of EVs^{hi} on the inner retina were also observed. Following P12 injections of EVs^{hi}, the thickness of the INL and IPL on P30 was restored to 92% and 93% of INL and IPL thickness in normoxic mice, respectively, and were significantly improved relative to EVs^{lo} (**Figure S3.6A**). In agreement with published studies, the ONL thickness was not significantly affected in OIR mice.[29] To assess treatment effects on retinal neural function, ERG was performed on P30 eyes following P12 injection with EVs^{hi} versus PBS vehicle. Following injection of EVs^{hi}, the scotopic B wave amplitude was unchanged, the photopic B wave was significantly improved, and the flicker response trended towards improvement, but this was not statistically significant (**Figure S3.6B**). These data demonstrated that EVs^{hi} recapitulated the previously published effects of CD44^{hi} ECFCs on improving the INL and IPL thickness as well as retinal function in OIR mice.[29] The neuroprotective effects of EVs^{hi} were thoroughly evaluated in RD10 mice with retinal neurodegeneration, exhibited by severe thinning of the neural retina, predominantly via apoptosis in the ONL, as well as compromised retinal function on ERG.

3.4.4 EVs^{hi} homed to areas of retinal ischemia and associated with perivascular microglia and macrophages in OIR mice

EVs^{hi} stained with lipophilic dye CM-DiI were intravitreally injected into OIR mice on P12. Retinas were harvested at 2, 4, 6, and 12 hours after injection as well as on P13, P14, P15, and P17. Immunohistochemistry of retinal flat-mounts harvested as early as 2 hours after injection and as late as P17 showed that CM-diI labeled EVs^{hi} were observed within preretinal neovascular tufts (**Figure 3.4A**) and superficial macrophages/microglia (**Figure 3.4B**). These data were supported by immunohistochemistry of retinal cross-sections demonstrating the colocalization of CM-diI labeled EVs^{hi} with perivascular Iba1^{+} macrophages/microglia in the retinal ganglion cell layer, the INL, and the ONL (**Figure 3.4C-E**).

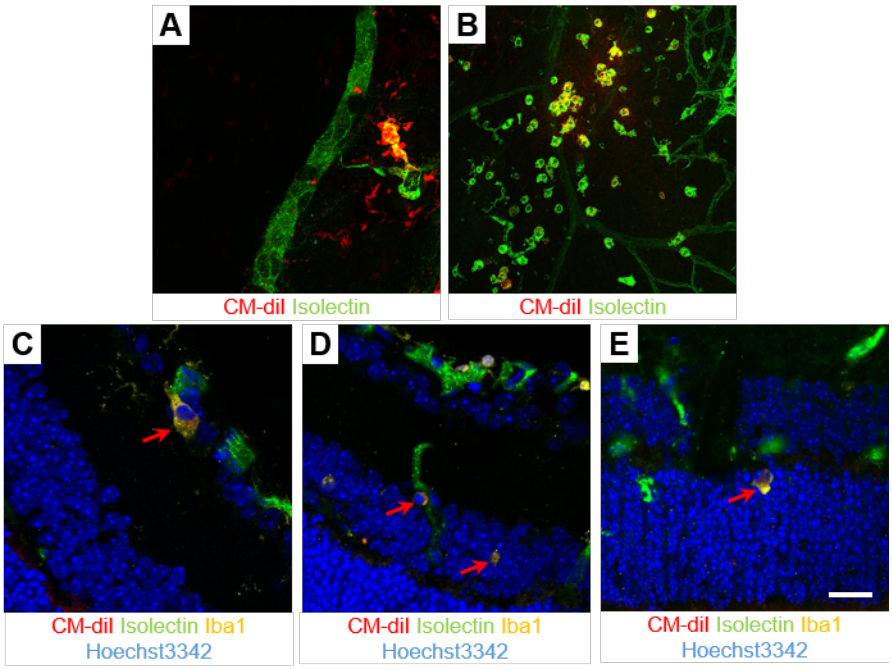

Figure 3.4: **EVs^{hi} homed to areas of retinal ischemia and associated with perivascular macrophages/microglia in OIR mice.** CM-diI labeled EVs^{hi} (red) were intravitreally injected into OIR on P12 and localized with immunohistochemistry. (**A and B**) Flat mounts of retinas harvested on P17 showed colocalization of EVs^{hi} with neovascularization in **A** and macrophages/microglia in ischemic regions in **B**. (**C-E**) Cross sections of retinas harvested on P15 demonstrated accumulation of CM-diI labeled EVs^{hi} (red) within perivascular Iba1+ microglia/macrophages (yellow) with Hochest3342 nuclear staining (blue) located in the retinal ganglion cell layer in **C**, the inner nuclear layer in **D**, and the outer nuclear layer in **E**. Red arrows indicate colocalization of EVs^{hi} and microglia. Scale bar: 20 µm.

3.4.5 EVs^{hi} demonstrated neurovasculotrophic effects in RD10 mice with inherited retinal degeneration

The neurovasculotrophic effects of EVs^{hi} were rigorously evaluated in RD10 mice, a model of inherited retinal degeneration that exhibits both vascular and neural defects. The RD10 model contains a missense mutation in the catalytic PDE6 ß subunit typically responsible for hydrolyzing cyclic GMP in photoreceptors' response to light. As a result, photoreceptor cell death begins concurrently with atrophy of the deep vascular plexus on P21. Between P20 and P25, cells in the outer nuclear layer die primarily by apoptosis, resulting in an ONL that quickly degenerates to 3 to 5 cell layers thick. By P45, the ONL is one cell layer thick.[336, 351, 352] RD10 mice were treated on P14 and quantified outcome measurements in this model were the degeneration of the deep and intermediate vascular plexus, apoptosis and layer thickness of the ONL, neural function on ERG, and immunohistochemical analysis of photoreceptor cell density.

Z-stack images of retinal flat-mounts stained with GS-IB4 were used to investigate the effects of EVs^{hi} on the delay of vascular atrophy in RD10 mice. Vessels in the deep vascular plexus demonstrated increased branching points, total area, and total length at multiple time points (P21, P25, P32, P40, and P60) following P14 injection with EVs^{hi} in comparison to eyes treated with EVs^{lo}, PBS, or untreated controls (**Figure 3.5A-B**). Atrophy of the intermediate plexus at these time points was also attenuated following treatment with EVs^{hi} (**Figure 3.5C**).

To evaluate neuroprotection, thickness and apoptosis in the ONL as well as neural function on ERG were investigated following P14 treatment of RD10 mice. ONL thickness at P21 (**Figure S3.7A**) and at P28 (**Figure 3.6A**) was more well preserved and apoptosis was reduced in the ONL of retinas treated with EVs^{hi}. Function of the neural retina was measured by full-field ERG, which assessed the integrity of photoreceptors as well as second- and third-order neurons in both dark-adapted (scotopic, rod-driven) and light-adapted (photopic, cone-driven)

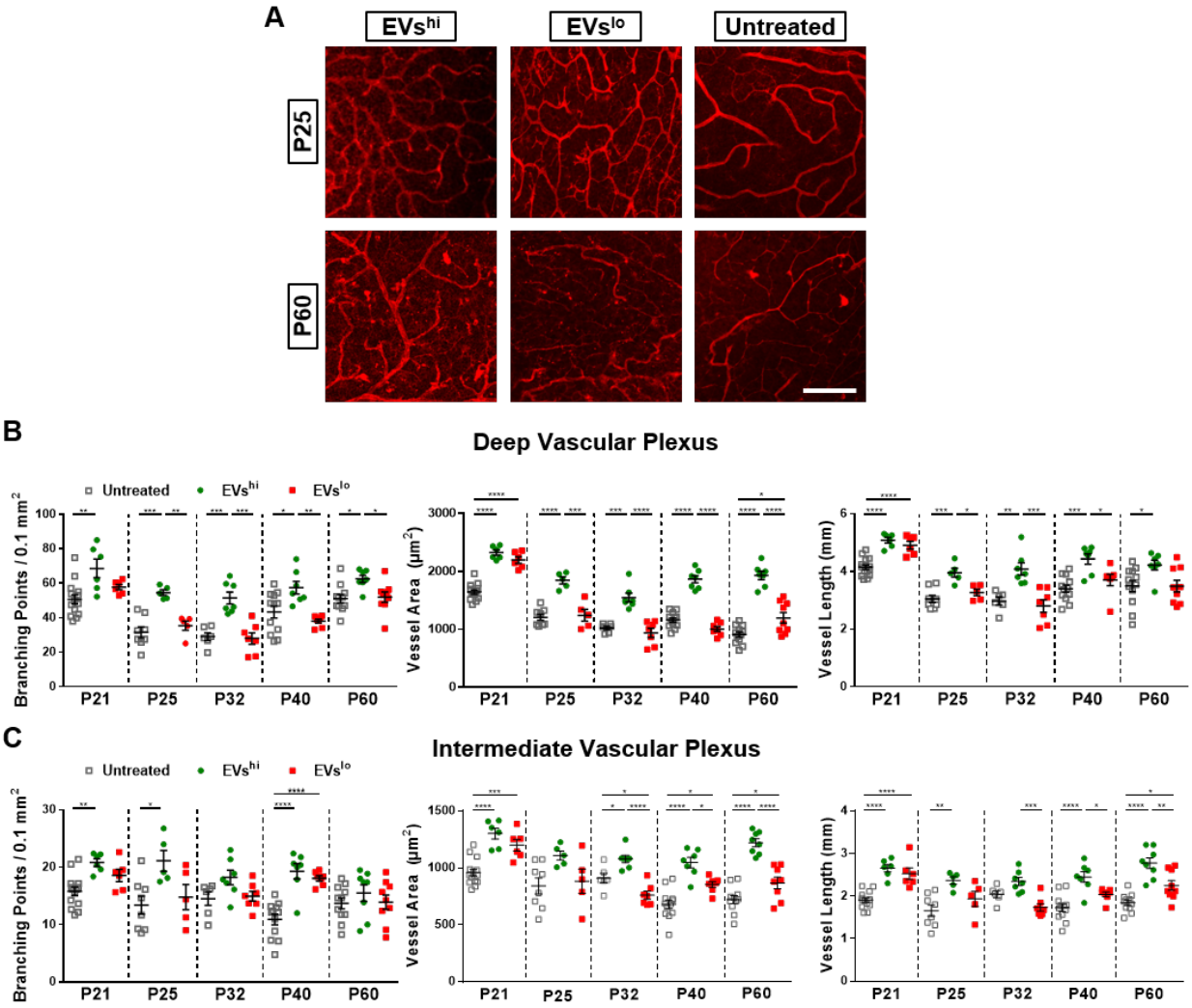

Figure 3.5: **EVs^{hi} provided vasculotrophic support to inherited retinal degeneration mice.** (**A**) Representative images of GS-IB4 lectin-stained flat-mounted P25 and P60 retinas focused on the deep vascular plexus of RD10 mice treated on P14 with EVs^{hi} or EVs^{lo} versus untreated mice. Scale bar: 100 µm. (**B-C**) Treatment of RD10 mice with EVs^{hi} delayed vascular atrophy. Quantification of the branching points (left), total vessel area (middle), and total vessel length (right) in the deep vascular plexus at P21, P25, P32, P40, and P60 demonstrated EVs^{hi} delayed atrophy of the deep vascular plexus in **B** and of the intermediate plexus in **C**. *P<0.05, **P<0.01, ***P<0.001, ****P<0.0001. 1-way ANOVA with Tukey analysis; n=5-9 retinas in EV groups, n=8-14 retinas in untreated groups. Error bars represent SEM.

conditions. On ERG, injections of EVs^{hi} significantly improved both scotopic and photopic signals at P42 compared to eyes injected with EVs^{lo}, PBS, or untreated controls (**Figure 3.6B**). In a second experiment, we assessed whether multiple treatments with EVs^{hi} may further augment retinal function on ERG. RD10 mice were injected once (at P14) or twice (at P14 and P21) and ERG responses were measured at P28. Single injection rescued the scotopic B wave,

photopic B wave, and flicker response of RD10 mice. Although repeated injection of EVs^{hi} significantly improved scotopic B wave and photopic B wave relative to PBS controls, decreased ERG recordings were measured in all groups injected twice when compared ERGs of mice treated with single injection (**Figure S3.7B-D**). These data suggested that repeated injections may have deleterious effects, which has also been observed in humans.[82, 353] EVs from ECFCs-shCD44 and ECFCs-scrRNA were injected into RD10 mice on P14 and ERG recordings were measured on P28. Treatment with EVs from ECFCs-scrRNA significantly increased scotopic B wave amplitude and trended towards improved photopic B wave amplitude and flicker response, but the latter effect did not reach statistical significance (**Figure S3.8**). These findings further supported a correlation between CD44 expression on ECFCs and the neuroprotective effects of shed EVs.

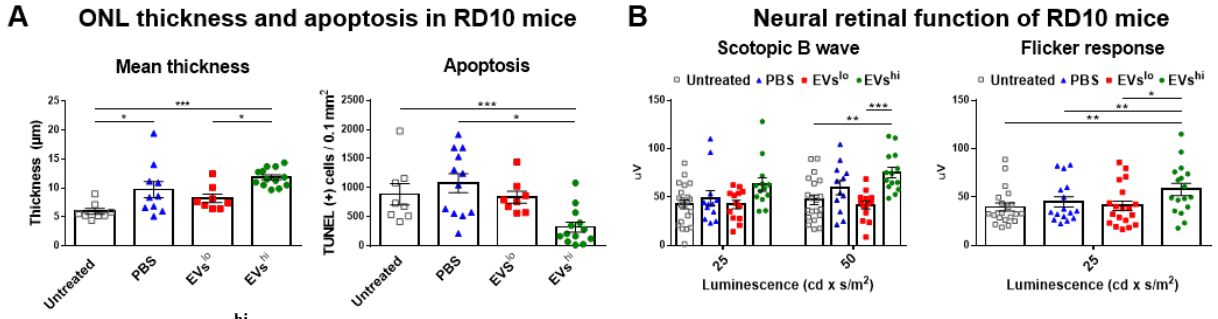

Figure 3.6: **EVs^{hi} provided neurotrophic support to inherited retinal degeneration mice.** (**A**) Immunohistochemistry of retinal cross sections harvested on P28 from RD10 mice treated P14 demonstrated a neuroprotective role of EVs^{hi}. Quantification of the ONL thickness (left) and density of apoptosis in the ONL via TUNEL staining (right). *P<0.05, ***P<0.01, 1-way ANOVA with Tukey analysis; n=13 retinas for EVs^{hi}, n=9 retinas for EVs^{lo}, n=10 retinas for PBS, n=8 retinas for untreated. (**B**) EVs^{hi} promoted functional rescue of neural retina in RD10 mice. ERG measurements on P42 showed pronounced and lasting improvement in both dark adapted (rod-driven scotopic B wave, left) and light-adapted (cone-driven flicker response, right) retinal function following P14 treatment with EVs^{hi}. *P<0.05, **P<0.01, ***P<0.001, 1-way ANOVA with Tukey analysis; n=12-14 retinas for EVs^{hi}, n=12-14 retinas for EVs^{lo}, n=12 retinas for PBS, n=20-22 retinas for untreated. Error bars in all figures represent SEM.

Retinal cross-sections stained to assess for rod- and cone-specific markers qualitatively suggested increased photoreceptor density in eyes treated with EVs^{hi}. (**Figure S3.9A-B**). Relative to untreated or EVs^{lo}-treated RD10 retinas, flat-mounts of P28 retinas stained for red/green opsin treated on P14 with EVs^{hi} exhibited significantly higher cone photoreceptor

density, which measured 75.3% of that observed in normoxic BL6 mice retinas (**Figure S3.9C-D**).

3.4.6 DICER1 knockdown reduced rescue effects of EVs^{hi} in OIR mice

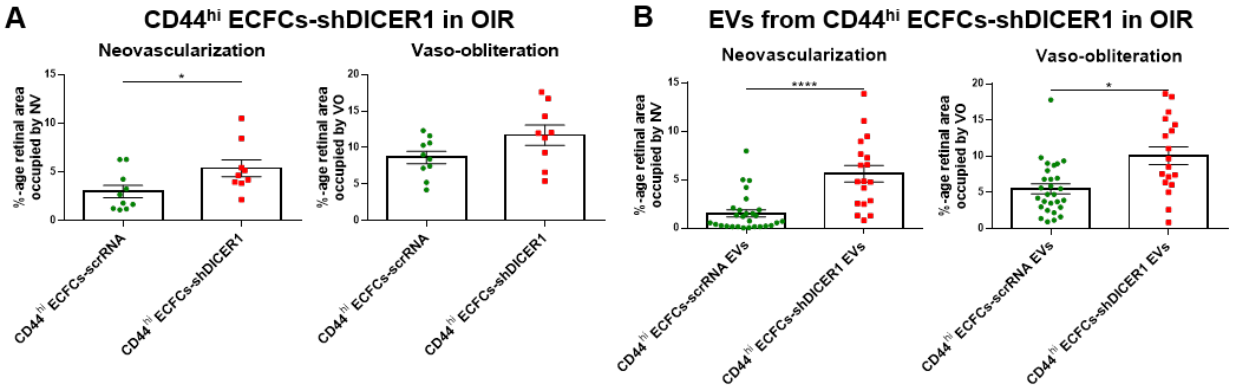

Figure 3.7: **DICER1 knockdown attenuated rescue effects of CD44^{hi} ECFCs and their EVs in OIR mice.** (**A-B**) Quantification of NV and VO in OIR mice injected with DICER1 knockdown CD44^{hi} ECFCs and their EVs. Injection of CD44^{hi} ECFCs transfected with shDICER1 (CD44^{hi} ECFCs-shDICER1) failed to rescue NV and EVs from CD44^{hi} ECFCs (CD44^{hi} ECFCs-shDICER1 EVs) failed to rescue both NV and VO relative to mice treated with respective scrRNA transfected cell (CD44^{hi} ECFCs-scrRNA) or EV (CD44^{hi} ECFCs-scrRNA EVs) controls. Quantification of NV (left) and VO (right) in OIR mice treated with intact cells are shown in **A** and quantification of EV-treated mice are shown in **B**. *P<0.05, ****P<0.0001, two-tailed Student's *t*-test; n=10 retinas for CD44^{hi} ECFCs-scrRNA, n=9 retinas for CD44^{hi} ECFCs-shDICER1, n=28 retinas for CD44^{hi} ECFCs-scrRNA EVs, n=18 retinas for CD44^{hi} ECFCs-DICER1 EVs.

Small RNA sequencing of EVs from the general population of ECFCs has previously demonstrated that 75% of all miR reads targeted functional categories including vascular development and endothelial cell migration.[190] EVs from ECFCs were taken up by endothelial cells *in vitro* and promoted an angiogenic program through the horizontal transfer of miR.[267] Based on these published findings, we hypothesized that the superior therapeutic effects of EVs^{hi} relative to EVs^{lo} may, at least in part, be attributable to neurovasculotrophic miRs within EVs^{hi}. First, ECFCs-shDICER1 and ECFCs-scrRNA were sorted in CD44^{hi} populations and these cells or their EVs were intravitreally injected in separate experiments into the eyes of OIR mice. In comparison to eyes treated with CD44^{hi} ECFCs-scrRNA, eyes intravitreally injected with CD44^{hi} ECFCs-shDICER1 failed to rescue NV and VO in the OIR model (**Figure 3.7A**). Injection of

CD44^{hi} ECFCs-shDICER1 EVs more drastically failed to rescue these parameters in OIR mice compared to eyes treated with CD44^{hi} ECFCs-scrRNA EVs (**Figure 3.7B**).

3.4.7 Small RNA sequencing identified candidate microRNAs with EVs^{hi}

To distinguish which candidate miRs may mediate rescue by EVs^{hi}, comparative small RNA sequencing between EVs^{hi} and EVs^{lo} was employed to identify differentially expressed miRs in EVs^{hi}. ECFCs were sorted into CD44$^{hi/lo}$ populations and EVs^{hi} (n=2) and EVs^{lo} (n=3) were isolated from CM and sent for small RNA sequencing. After filtering sequencing data to require >10 reads in one sample for each group, EVs^{hi} and EVs^{lo} on average contained similar numbers of unique miRs (EVs^{hi}=243.5 miRs, EVs^{lo}=235 miRs, P=0.19, two-tailed Student's *t*-test). Principal component analysis (**Figure S3.10A**) and hierarchical clustering (**Figure S3.10B**) revealed that EVs^{hi} and EVs^{lo} samples clustered more closely within each group than between groups. A total of 41 miRs were upregulated and 43 miRs were downregulated in EVs^{hi} compared to EVs^{lo} when thresholding with $p<0.05$ and Bonferroni correction (**Figure 3.10C**). To identify miRs possibly responsible for the therapeutic effects of EVs^{hi}, we elected to further investigate differentially expressed microRNAs thresholding with $q<0.05$, which helps circumvent the false positive rate inherent in thresholding large numbers of parameters with $p<0.05$ and Bonferroni correction. A heat map of differentially expressed miRs with $q<0.05$ are displayed in **Figure 3.8A**. A total of 9 miRs (miR-7-5p, miR-23a-3p, miR-30a-5p, miR-100-5p, miR-181b-5p, miR-221-3p, miR-216a-3p, miR-381-3p, and miR-503-5p) were upregulated and 10 miRs were downregulated (miR-409-3p, miR-30d-5p, miR-191-5p, miR-26a-5p, miR-584-5p, miR-26b-5p, miR-671-3p, miR-335-5p, miR-486-5p, miR-128-3p) in EVs^{hi} compared to EVs^{lo} (**Table 3.1**). All upregulated miRs validated well on RT-qPCR except miR-30a-5p and miR-381-3p (**Table S3.3**).

Table 3.1: **Differentially expressed microRNA between EVs^{hi} and EVs^{lo} on small RNA**

MicroRNA	MicroRNA Loci	EVs^{hi} - Normalized mean counts	EVs^{lo} - Normalized mean counts	Fold change (EVs^{hi}/EVs^{lo})	Bonferroni p value	q value
MicroRNAs differentially expressed in EVs^{hi}						
miR-503-5p	chrX:134546371	258.83	78.02	3.32	3.22E-04	7.65E-04
miR-23a-3p	chr19:013836595	6845.49	2775.63	2.47	1.22E-04	4.63E-04
miR-221-3p	chrX:045746180	14958.35	7380.74	2.03	1.72E-04	5.45E-04
miR-100-5p	chr11:122152275	100201.01	52513.74	1.91	3.29E-05	3.12E-04
miR-30a-5p	chr06:071403595	3234.32	1818.55	1.78	6.22E-04	1.18E-03
miR-7-5p	chr15:088611856 chr19:4770700 chr09:83969812	3289.77	1860.59	1.77	9.51E-05	4.63E-04
miR-216a-3p	chr02:055988981	522.53	308.84	1.69	2.20E-03	2.61E-03
miR-181b-5p	chr01:198858925 chr09:124693725	2064.35	1349.09	1.53	2.55E-03	2.84E-03
miR-381-3p	chr14:101045968	1234.65	826.82	1.49	8.57E-04	1.36E-03
MicroRNAs differentially expressed in EVs^{lo}						
miR-26b-5p	chr02:218402657	5138.14	7125.52	0.72	6.81E-06	1.29E-04
miR-409-3p	chr14:101065346	2114.88	3263.29	0.65	1.73E-03	2.19E-03
miR-191-5p	chr03:049020672	5230.83	8207.58	0.64	3.26E-03	3.36E-03
miR-26a-5p	chr12:057824658 chr03:37969413	83953.92	142182.89	0.59	1.32E-03	1.94E-03
miR-486-5p	chr08:041660484 chr08:41660444	2488.25	4561.96	0.55	4.27E-04	9.02E-04
miR-30d-5p	chr08:134804919	7837.81	14999.90	0.52	7.12E-04	1.23E-03
miR-584-5p	chr05:149062373	820.50	1607.73	0.51	1.20E-04	4.63E-04
miR-128-3p	chr03:035744527	3468.97	8575.92	0.40	3.36E-03	3.36E-03
miR-335-3p	chr07:130496162	181.15	485.10	0.37	1.45E-03	1.97E-03
miR-671-3p	chr07:151238488	62.38	214.41	0.29	2.30E-04	6.24E-04

MicroRNAs differentially upregulated within EVs^{hi} on small RNA sequencing were functionally validated in the OIR model. OIR mice were treated with miR mimics to evaluate whether miRs differentially upregulated in EVs^{hi} innately offered vasculotrophic rescue. Compared to eyes injected with negative control scramble miR, six miRs differentially upregulated in EVs^{hi} (miR-7-5p, miR-23a-3p, miR-30a-5p, miR-216a-3p, miR-381-3p, miR-503-5p) significantly reduced NV and 3 of those miRs (miR-30a-5p, miR-216a-3p, miR-503-5p) also reduced VO (**Figure 3.8B**). Altogether, miR-7-5p, miR-23a-3p, miR-216a-3p, and miR-503-5p were identified as "candidate miRs" since they were differentially expressed on small RNA

sequencing, validated on RT-qPCR, and demonstrated functional rescue effects in OIR. To evaluate the effect of combinatorial miR treatment in OIR, all candidate miR mimics as well as the two most neurovasculotrophic miR mimics in OIR (miR-216a-3p, and miR-503-5p) were injected into the model at various concentrations. Combinatorial injection of Injection of all candidate miR mimics as well as combinatorial miR-216a-3p and miR-503-5p injections rescued OIR mice in a dose-dependent manner (**Figure 3.8C**).

3.4.8 Knockdown of candidate miRs attenuated EVs^{hi} function *in vivo*

To obviate the contribution of these four 'candidate miRs' to the efficacy of EVs^{hi}, EVs from CD44^{hi} ECFCs transfected with antisense oligonucleotides to reduce expression of these miRs were injected into OIR mice along with another negative control line of EVs from ECFCs transfected to KD expression of scrmiR. KD efficiency was 62.9% for miR-7-5p KD ECFCs, 9.0% for miR-23a-3p KD ECFCs, 25.3% for miR-216a-3p KD ECFCs, and 48.3% for miR-503-5p KD ECFCs on RT-qPCR. Another cell line was generated with knocked down expression of both miR-216a-3p and miR-503-5p at KD efficiencies of 11.7% and 19.1%, respectively. A final cell line was generated with knocked down expression of all candidate miRs with a KD efficiency of 33.7% for miR-7-5p, 35.9% for miR-23a-3p, 44.3% for miR-216a-3p, and 34.9% for miR-503-5p.

EVs were isolated from sorted CD44^{hi} ECFCs with miR KD and injected into OIR mice. Relative to mice treated with EVs from CD44^{hi} ECFCs transfected with scrmiR controls, OIR mice treated with EVs from miR-7-5p KD CD44^{hi} ECFCs and miR-216a-3p KD CD44^{hi} ECFCs demonstrated slightly reduced rescue effects that were not statistically significant. Mice treated with EVs from miR-23a-3p KD CD44^{hi} ECFCs demonstrated significantly reduced rescue of VO while EVs from miR-503-3p KD CD44^{hi} ECFCs no longer rescued both NV and VO. Relative to

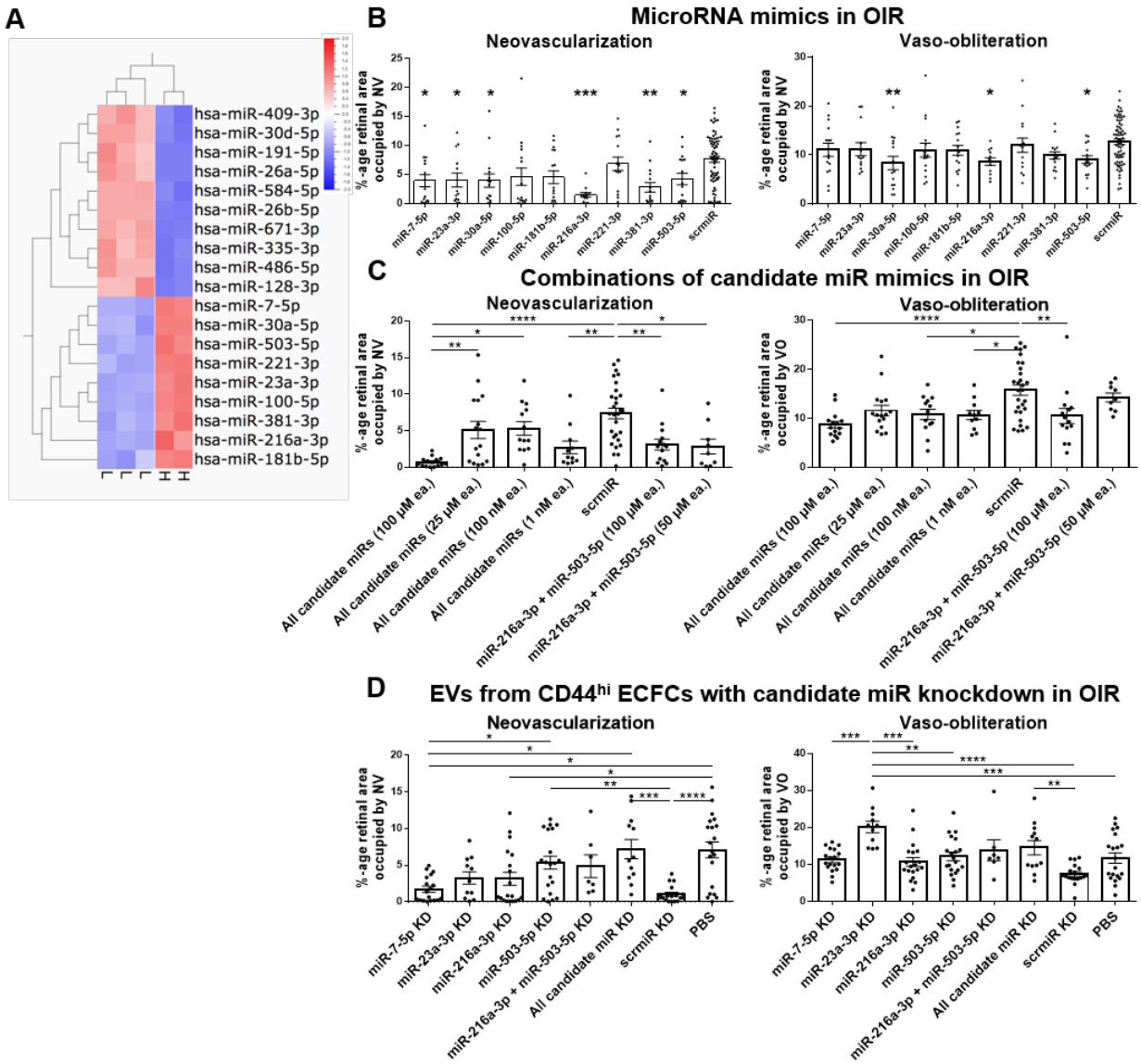

Figure 3.8: **Differentially expressed miRs were neurovasculotrophic and contributed to the *in vivo* rescue effects of EVs^{hi}.** (**A**) Heatmap of differentially expressed miRs on small RNA sequencing. (**B**) Injection of particular miR mimics upregulated in EVs^{hi} in **A** rescued NV and/or VO compared to scrmiR. n=12-16 retinas for miR mimics, n=72 retinas for scrmiR. n=12-16 retinas for miR mimics, n=72 retinas for scrmiR. (**C**) Combinatorial injection of miR mimics rescued OIR mice dose-dependently. 'Candidate miRs' were defined to be miR-7-5p, miR-23a-3p, miR-216a-3p, and miR-503-5p because these miRs were upregulated on small RNA sequencing in **A**, validated on RT-qPCR, and functional in rescuing OIR mice in **B.** Combination injection of the two most effective miR mimics (miR-216a-3p and miR-503-5p) and, separately, all 'candidate miR' mimics rescued OIR. n=9-14 retinas for miR-216a-3p and miR-503-5p, n=11-16 retinas for all candidate miRs, n=24 retinas for scrmiR. (**d**) EVs from CD44^{hi} ECFCs with KD expression of individual or combinatorial miRs no longer rescued OIR mice. Multiple cell lines of ECFCs were generated with KD expression of both miR-216a-3p and miR-503-5p, all candidate miRs together, and each candidate miR individually. EVs from CD44^{hi} ECFCs with KD expression of miR-23a-3p or miR-503-5p individually, or KD expression of all candidate miRs failed to rescue OIR mice. n=11-20 retinas for individual miR KD, n=7 retinas for miR-216a-3p and miR-503-5p KD, n=12 retinas for all candidate miR KD, n=18 retinas for scrmiR KD EVs, n=20 retinas for PBS. *P<0.05, **P<0.01, ***P<0.001, ****P<0.001, 1-way ANOVA with Tukey analysis for all statistics and error bars represent SEM.

EVs from scrmiR transfected CD44^{hi} ECFCs, EVs from CD44^{hi} ECFCs with KD of both miR-216a-3p and miR-503-5p trended towards reduced rescue, but these effects were not statistically significant. EVs from CD44^{hi} ECFCs with KD of all candidate miRs failed to rescue both NV and VO (**Figure 3.8D**).

3.5 Discussion

An extension of the CNS, the neurosensory retina exhibits extreme metabolic demands that are met by a highly organized vascular architecture consisting of three vascular plexi and the choriocapillaris that are sandwiched between multiple layers of neurons interspersed with various glial cell types. Endothelial and glial cells secrete factors that play critical roles in regulating retinal homeostasis and maintaining a neurovascular stem cell niche characterized by the potential for self-renewal and repair.[333] Trophic neurovascular cross-talk between vascular endothelial cells and other cells of the NVU lends merit to the concept of harnessing endothelial cells and their progenitors to rescue surrounding neurons under stress due to hypoxia or genetically encoded cell-specific mutations causing neurodegeneration. As true endothelial progenitor cells, ECFCs function to both stabilize atrophying retinal vasculature under hypoxic stress and protect retinal neurons from undergoing apoptosis and, thus, serve as a promising cell source of therapy for ischemic/neurodegenerative CNS diseases.[29, 335] In models of ischemic and neurodegenerative retinopathy, CD44^{hi} ECFCs are the functionally active cell subpopulation with trophic effects on neurovasculature in OIR and RD10 mice; these effects are likely achieved via a paracrine mechanism of action.[29]

In this study, we hypothesized that extracellular vesicles shed by CD44^{hi} ECFCs, as shuttles of neurovasculotrophic miRs, represent paracrine mediators responsible, at least in part, for the therapeutic effects of this bioactive CD44^{hi} ECFC population. We present multiple lines

of evidence in support of this hypothesis. First, we demonstrated that EVs^{hi} are the bioactive subset of EVs from ECFCs that provide potent neurovascular rescue effects in retinal models of ischemia and neurodegeneration. EVs^{hi} rescued vasculopathic and neurodegenerative diseases of the CNS by attenuating pathological neovascularization, promoting physiologic vascular growth, and rescuing neural cell loss in OIR and RD10 mice. When exosome shedding was pharmacologically inhibited by GW4869, $CD44^{hi}$ ECFCs no longer rescued the OIR model. Second, our data corroborated previous reports demonstrating that EVs from ECFCs assume perivascular positions and co-localize within macrophages and microglia.[190] We observed that EVs^{hi} also accumulated within neovascular tufts in the OIR model. Third, we demonstrated that neurovasculotrophic miRs differentially expressed within EVs^{hi} are required for their trophic effects. When miR expression was knocked down in $CD44^{hi}$ ECFCs via lentiviral transfection with shDICER1, cells no longer rescued NV in OIR mice; EVs from $CD44^{hi}$ ECFCs-shDICER1 failed to rescue both NV and VO. Small RNA sequencing and RT-qPCR validation identified dysregulated miRs between EVs^{hi} to EVs^{lo}. The bioactivity of upregulated miRs in EVs^{hi} was tested by injecting miR mimics into OIR mice. Four 'candidate' intravesicular miRs (miR-7-5p, miR-23a-3p, miR-216a-3p, and miR-503-5p) were upregulated in EVs^{hi} on small RNA sequencing, validated on RT-qPCR, and neurovasculotrophic in the OIR model. When the expression of miR-23a-3p or miR-503-5p was knocked down in $CD44^{hi}$ ECFCs, EVs from these cells failed to rescue the OIR phenotype. Similarly, EVs from ECFCs with combinatorial KD of all candidate miR mimics failed to rescue OIR mice. Together, these data suggest that EVs^{hi} represent a promising therapeutic agent for the treatment of ischemic and neurodegenerative retinopathies through a mechanism partially dependent on intravesicular miR composition.

ECFC-derived EVs have demonstrated potent therapeutic activity in a wide range of angiogenesis-dependent animal disease models including diabetic wound healing,[272] re-endothelialization of vascular injury,[270] traumatic brain injury,[276] and osteogenesis.[278] In addition, a mechanistic role for intravesicular miR has been demonstrated in ECFC EV-mediated repair of ischemic animal models of acute kidney injury[94, 268, 271, 273, 274] and hindlimb ischemia[275] as well as sepsis.[277] *In vitro*, EVs from the general population of ECFCs facilitated their proliferative and anti-apoptotic effects on human microvascular endothelial cells via miR-dependent mechanisms that upregulated eNOS,[267] promoted the activation of both the Erk1/Erk2[272] and the PI3K/Akt[267] signaling pathways, and suppressed sepsis-induced expression of high mobility group box 1 and vascular cell adhesion molecule 1.[277] In the ischemia/reperfusion model of acute kidney injury, the reno-protective effect of EVs from ECFCs on the ischemic kidney is attenuated when EVs are depleted of miR-126, miR-296, or miR-486-5p.[271, 273] Transplanted ECFC-derived exosomes horizontally transferred miR-486-5p (which targets PTEN to lift its inhibition of secondary messengers within the Akt survival pathway) into the proximal tubules, glomeruli, and endothelial cells through a homing mechanism that requires the interaction of exosomal CXC4 with SDF-1α expressed by endothelial cells.[274] Depletion of miR-126 from ECFC-derived EVs attenuated their rescue effects in murine models of sepsis,[277] and global miR knockdown abrogated their rescue effects in murine models of hindlimb ischemia.[275] In the only study to date investigating ECFC-derived EVs in retinal ischemia, EVs from the general population of ECFCs were found to be highly enriched in miRs that target functional categories including vascular development and endothelial migration, and uptake of these EVs within human retinal microvascular cells *in vitro* regulated their expression of angiogenesis-related genes and promoted wound healing.[190]

In the current study, we add to this growing literature by demonstrating that EVs^{hi} are the bioactive subset of vesicles that can rescue models of CNS ischemia and neurodegeneration through a mechanism dependent on intravesicular miR-23a-3p, miR-503-5p, and a combination of differentially expressed neurovasculotrophic miRs to confer the full extent of their therapeutic effects. In various models of ischemic and/or traumatic brain injury, miR-23a-3p decreased oxidative stress, neuron apoptosis, and neural inflammation to improve both vascular and neuronal outcomes.[354, 355] The role of miR-503 as an anti-angiogenic agent is consistent *in vitro* and *in vivo* across literature.[356] In a variety of cancer models, miR-503 inhibited tumor angiogenesis by downregulating vascular growth factors, particularly VEGF-A.[357-359] In glioma cells, miR-503 suppressed tumor angiogenesis by directly targeting and downregulating VEGF-A as well as by targeting leucine-rich repeats and immunoglobulin-like domains protein 2 (LRIG2).[357] LRIG2 positively regulates the endothelial growth factor receptor (EFGR)/VEGFA pathway, and downregulating LRIG2 inhibited angiogenesis in glioma by decreasing expression of VEGF-A and EGFR.[357, 360] In colon cancer models, overexpression of miR-503-5p inhibited tumorigenesis, lymphangiogenesis, and angiogenesis by directly targeting VEGF-A while stimulating the AKT signaling pathways.[358] In models hepatocellular carcinomas, miR-503 reduced tumor angiogenesis *in vitro* and *in vivo* by directly downregulating both VEGF-A and fibroblast growth factor-β (FGF-2), another highly potent angiogenic factor. Interestingly, hypoxia-induced expression of HIF1α decreased endogenous miR-503 expression in tumor cells leading to increased expression of FGF-2 and VEGF-A, making miR-503 a promising therapeutic target for regulating angiogenesis in response to hypoxia.[359] VEGF-A is overexpressed in a variety of ischemic/neurodegenerative diseases of the CNS and modulation of

this factor via therapeutic agents that restore miR-503-5p, such as transplantation of EVs^{hi}, is a promising treatment strategy.[361]

Since no FDA-approved EV-based therapeutics are currently clinically available, practical considerations in the therapeutic development of EVs remain under consideration. An EV isolation protocol capable of isolating 'pure' samples with a low soluble protein:EV ratio must be scalable to meet clinical demands. Comparative reports have demonstrated that SEC-based EV isolation protocols produce EV samples that are superior in purity, integrity, and functionality relative to the majority of other methods.[221, 224, 227-230] The UF-SEC-UF protocol significantly improved the yield and bioactivity of EVs while effectively isolating pure EVs samples suitable for use in downstream applications,[225, 242, 243] and the final concentration of the EV sample can be controlled by the last UF step. Our observation that EVs^{hi} from any healthy UCB donors rescued OIR mice supports the concept that EVs^{hi}-based therapy may be efficiently derived from any healthy donor or banks of pooled UCB. EVs^{hi} also demonstrated a favorable storage profile. While most EVs were prepared fresh before injection, samples frozen at -80ºC for as long as 1 year retained therapeutic function in OIR. EVs^{hi}-treatment prior to vaso-obliteration and at the onset of the ischemic drive effectively rescued OIR mice while injection of EVs^{hi} during neovascularization was ineffective. Ultimately, treatment timing must be determined by human clinical trials. EVs^{hi} demonstrated a favorable safety profile; treatment promoted physiologic vascular growth during the vaso-obliterative phase of OIR but did not affect developing vasculature of newborn pups.

In conclusion, this study demonstrated that the bioactive subset of $CD44^{hi}$ ECFCs shed therapeutic EVs^{hi} loaded with miRs that, at least in part, mediate their neurovasculotrophic effects in ischemia and neurodegeneration in brain tissue. Taken together, these results suggest

that EVs^{hi} loaded with trophic miRs are a promising novel therapeutic agent for the treatment of ischemic and neurodegenerative diseases of the CNS.

3.6 Supplementary materials

Table S3.1: Reagents for flow cytometry and immunohistochemical staining.

Reagent	Company	Host species	Catalog No.	Dilution Factor
Flow cytometry on ECFCs				
CD44 conjugated to APC	BD PharMingen	Mouse	559942	5 µL / test (1 x 10*6 cells in 100 µL buffer)
CD13 conjugated to APC	BioLegend	Mouse	301705	5 µL / test (1 x 10*6 cells in 100 µL buffer)
CD14 conjugated to FITC	BD PharMingen	Mouse	557153	5 µL / test (1 x 10*6 cells in 100 µL buffer)
CD31 conjugated to FITC	BD PharMingen	Mouse	560984	5 µL / test (1 x 10*6 cells in 100 µL buffer)
CD45 conjugated to FITC	BD PharMingen	Mouse	560976	5 µL / test (1 x 10*6 cells in 100 µL buffer)
CD90 conjugated to PE	BD PharMingen	Mouse	561970	5 µL / test (1 x 10*6 cells in 100 µL buffer)
CD105 conjugated to APC	BD PharMingen	Mouse	562408	5 µL / test (1 x 10*6 cells in 100 µL buffer)
VEGFR-2 conjugated to PE	R & D Systems	Mouse	FAB357P	5 µL / test (1 x 10*6 cells in 100 µL buffer)
HLA-A,B,C conjugated to PE	BioLegend	Mouse	311405	5 µL / test (1 x 10*6 cells in 100 µL buffer)
HLA-DR conjugated to APC	BioLegend	Mouse	307609	5 µL / test (1 x 10*6 cells in 100 µL buffer)
Flow cytometry on EVs				
CD9-Exo-Flow Capture Kit	SBI		EXOFLOW100A-1	10 µL capture antibody / 100 µL beads / 10 µL detection antibody / test
CD31-Exo-Flow Capture Kit	SBI		EXOFLOW200A-1	10 µL capture antibody / 100 µL beads / 10 µL detection antibody / test
CD63-Exo-Flow Capture Kit	SBI		EXOFLOW300A-1	10 µL capture antibody / 100 µL beads / 10 µL detection antibody / test
CD81-Exo-Flow Capture Kit	SBI		EXOFLOW400A-1	10 µL capture antibody / 100 µL beads / 10 µL detection antibody / test
Immunohistochemistry				
PECAM-1	BD PharMingen	Rat	553370	1:200
MAP2	Sigma	Mouse	M4403	1:1000
Arrestin	EMD Millipore	Rabbit	AB15282	1:200
Rhodopsin	EMD Millipore	Mouse	MABN15	1:1000
Opsin (Red/Green)	EMD Millipore	Rabbit	AB5405	1:200
Isolectin GS IB-4	ThermoFisher	N/A	I21413	1:200
Iba1	Wako	Rabbit	019-19741	1:200

Table S3.2: Reagents for RT-qPCR.

Product Line	Target	Company	Assay ID
Transduction efficiency measurements			
TaqMan Gene Expression Assay	CD44	ThermoFisher	Hs00229023_m1
TaqMan Gene Expression Assay	DICER1	ThermoFisher	Hs01075862_m1
TaqMan Gene Expression Assay	GAPDH	ThermoFisher	Hs02758991_g1s
TaqMan MicroRNA Assay	hsa-miR-7-5p	ThermoFisher	005723_mat
TaqMan MicroRNA Assay	hsa-miR-216a-3p	ThermoFisher	475580_mat
TaqMan MicroRNA Assay	hsa-miR-503-5p	ThermoFisher	001048
TaqMan MicroRNA Assay	U6 snRNA	ThermoFisher	001973
RT-qPCR validation of small RNA sequencing results			
TaqMan Advanced miRNA Assay	hsa-miR-7-5p	ThermoFisher	483061_mir
TaqMan Advanced miRNA Assay	hsa-miR-23a-3p	ThermoFisher	478532_mir
Taqman Advanced miRNA Assay	hsa-miR-26a-5p	ThermoFisher	477995_mir
Taqman Advanced miRNA Assay	has-miR-26b-5p	ThermoFisher	478418_mir
TaqMan Advanced miRNA Assay	hsa-miR-30a-5p	ThermoFisher	479448_mir
Taqman Advanced miRNA Assay	hsa-miR-30d-5p	ThermoFisher	478606_mir
TaqMan Advanced miRNA Assay	hsa-miR-100-5p	ThermoFisher	478224_mir
Taqman Advanced miRNA Assay	hsa-miR-128-3p	ThermoFisher	477892_mir
TaqMan Advanced miRNA Assay	hsa-miR-181b-5p	ThermoFisher	478583_mir
Taqman Advanced miRNA Assay	hsa-miR-191-5p	ThermoFisher	477952_mir
TaqMan Advanced miRNA Assay	hsa-miR-216a-3p	ThermoFisher	478770_mir
TaqMan Advanced miRNA Assay	hsa-miR-221-3p	ThermoFisher	477981_mir
Taqman Advanced miRNA Assay	hsa-miR-335-3p	ThermoFisher	478033_mir
TaqMan Advanced miRNA Assay	has-miR-381-3p	ThermoFisher	477816_mir
Taqman Advanced miRNA Assay	hsa-miR-409-3p	ThermoFisher	478084_mir
Taqman Advanced miRNA Assay	hsa-miR-486-5p	ThermoFisher	478128_mir
TaqMan Advanced miRNA Assay	hsa-miR-503-5p	ThermoFisher	478143_mir
Taqman Advanced miRNA Assay	hsa-miR-584-5p	ThermoFisher	478167_mir
Taqman Advanced miRNA Assay	has-miR-671-3p	ThermoFisher	478194_mir

Table S3.3: RT-qPCR validation of differentially expressed miRs on RNA sequencing.

		miRs upregulated in EVs^{hi}								
		miR-7-5p	miR-30a-5p	miR-503-5p	miR-221-3p	miR-23a-3p	miR-100-5p	miR-381-3p	miR-216a-3p	miR-181b-5p
miRs downregulated in EVs^{hi}	miR-409-3p	0.80	-7.70	5.08	-0.86	1.92	5.40	-5.24	12.37	2.14
	miR-30d-5p	7.49	-0.75	11.87	5.92	8.42	12.19	2.10	18.87	8.93
	miR-191-5p	6.38	-1.92	10.67	4.72	7.68	10.99	0.15	18.13	7.73
	miR-26a-5p	5.11	-3.13	9.67	3.66	6.66	9.82	-0.69	18.62	6.65
	miR-584-5p	1.34	-6.05	5.83	-0.12	3.01	6.15	-4.52	13.46	2.89
	miR-26b-5p	4.47	-4.12	8.74	2.79	5.68	9.06	-1.72	16.13	5.80
	miR-671-3p	23.44	-6.81	22.82	10.32	15.31	17.50	-15.19	37.88	13.89
	miR-335-3p	4.63	-4.21	9.34	3.08	10.10	9.00	-4.10	25.10	6.20
	miR-486-5p	3.50	-4.64	8.03	2.10	5.40	8.33	-0.90	15.85	5.08
	miR-128-3p	8.83	1.03	13.17	7.23	10.29	13.49	2.73	20.73	10.33

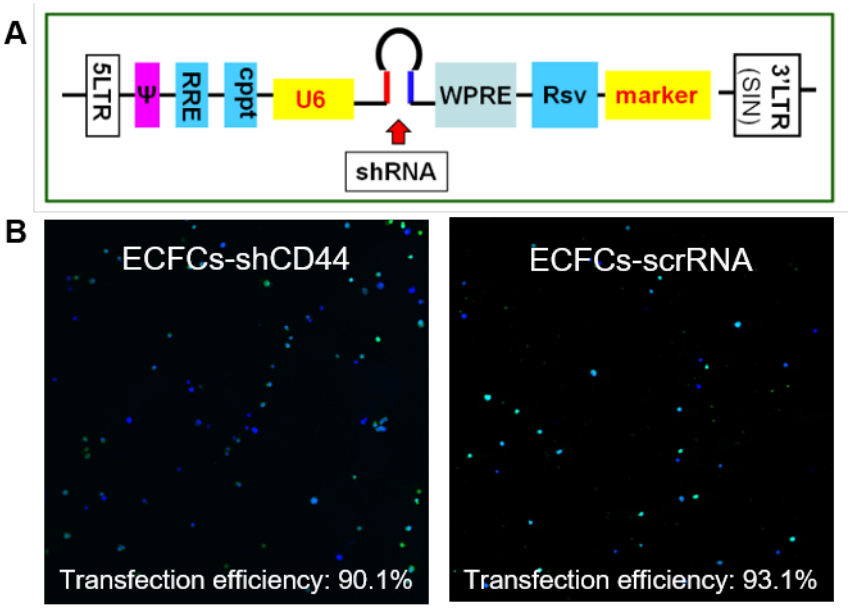

Figure S3.1: **Transfection efficiency of CD44 knockdown in ECFCs.** (**A**) Scheme of the lentiviral construct for CD44 KD. (**B**) Representative confocal images used to calculate transfection efficiency of ECFCs-shCD44 and ECFCs-scrRNA.

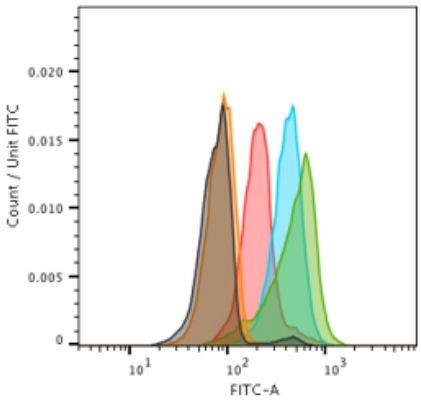

Figure S3.2: **Cytometric confirmation of exosomes in protein-poor early SEC EFs.** CD63-conjugated 9.1 µm diameter magnetic beads were incubated with SEC EFs 5 (orange), 10 (green), 15 (blue) and 19 (red) or PBS as negative control (black). After addition of exosome-targeting FITC detection antibodies, beads were analyzed by flow cytometry to provide bioluminescent confirmation that CD63+ exosomes began eluting between protein-poor EFs 5 and 10 and continued eluting in subsequent protein-contaminated fractions.

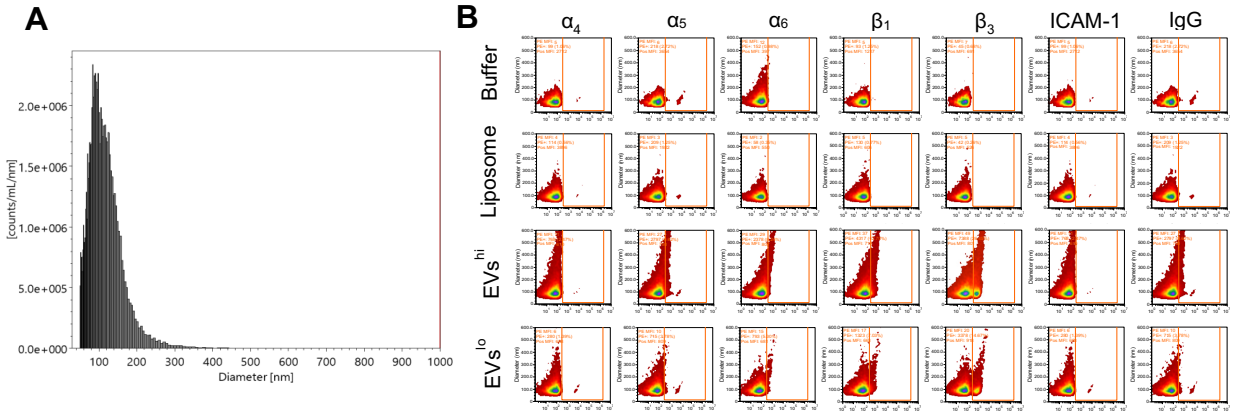

Figure S3.3: **Characterization of size distribution and immunophenotype of EVs^{hi} and EVs^{lo}.** (**A**) Representative nanoparticle tracking analysis measurement of EV sample. (**B**) Single particle flow analysis of EV immunophenotype. Both EVs^{hi} and EVs^{lo} positively expressed integrins α_5, α_6, β_1, and β_3 but negatively expressed of integrin α_4 and adhesion molecule ICAM-1.

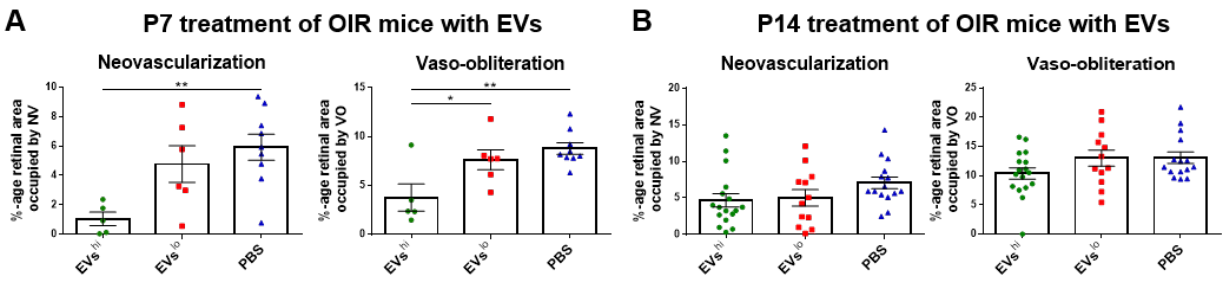

Figure S3.4: **Pretreatment of OIR mice with EVs^{hi} rescued the model while treatment during the neovascular phase fails.** (**A-B**) Quantification of NV (left) and VO (right) in mice treated with EVs^{hi}, EVs^{lo}, or PBS on P7 prior to incubation hyperoxia in **A** and at P14 two days into the neovascular phase of the OIR model in **B**. *P<0.05, **P<0.01, 1-way ANOVA with Tukey analysis; P7 injections: n=5 for EVs^{hi} n=6 for EVs^{lo}, n=9 for PBS; P14 injections: n=17 for EVs^{hi} n=12 for EVs^{lo}, n=15 for PBS. Error bars represent SEM.

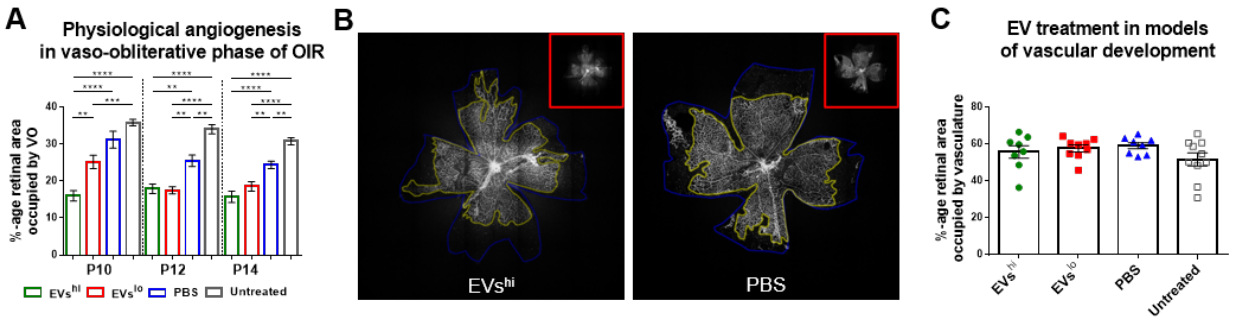

Figure S3.5: **EVs^{hi} promoted vascular growth during the vaso-obliterative phase of the OIR model and had no effect in models of vascular development.** (**A**) Quantification of VO in retinal flat-mounts of OIR mice during the vaso-obliterative phase following P7 injection with EVs^{hi}, EVs^{lo}, PBS, or untreated controls. **P<0.01, ***P<0.001, ****P<0.0001, 1-way ANOVA with Tukey analysis; n=11-13 retinas for EVs^{hi}, n=14-15 retinas for EVs^{lo}, n=13-16 retinas for PBS, n=16-21 retinas for untreated. (**B-C**) EV treatment does not affect vascular development. (**B**) Representative images of GS-IB4 lectin-stained retinal flat-mounts at P5 following P2 injection of wild type pups with EVs^{hi}, EVs^{lo}, PBS, or untreated controls. (**C**) Quantification of the percentage retinal area covered by vasculature showed no differences between treatment groups. 1-way ANOVA; n=8 retinas for EVs^{hi}, n=9 retinas for EVs^{lo}, n=8 retinas for PBS, n=10 retinas for untreated mice. Error bars represent SEM.

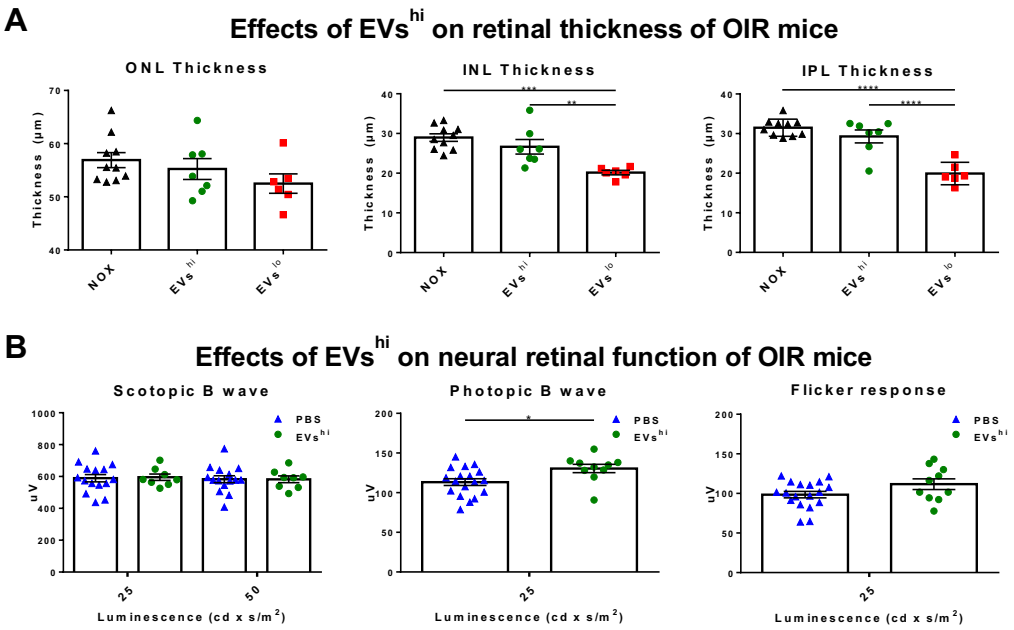

Figure S3.6: **EVs^{hi} were neuroprotective in the OIR model.** (**A**) Quantification of retinal thickness of the outer nuclear layer (ONL), inner nuclear layer (INL), and inner plexiform layer (IPL) at P30 following P12 treatment with EVs^{hi} versus EVs^{lo} as compared to normoxic (NOX) mice. Thicknesses were measured on retinal cross-sections and EVs^{hi} restored neural layer thickness comparable to that of normoxic mice. **P<0.01, ***P<0.001, ****P<0.0001, 1-way ANOVA with Tukey analysis; n=7 retinas for EVs^{hi}, n=6 retinas for EVs^{lo}, and n=10 retinas for normoxic mice. (**B**) ERG recordings of neural retinal function measured on P30 following P12 treatment of OIR mice with EVs^{hi} versus PBS vehicle. *P<0.05, two-tailed Student's *t* test; n=8-10 retinas for EVs^{hi}, n=15-18 retinas for PBS. Error bars represent SEM.

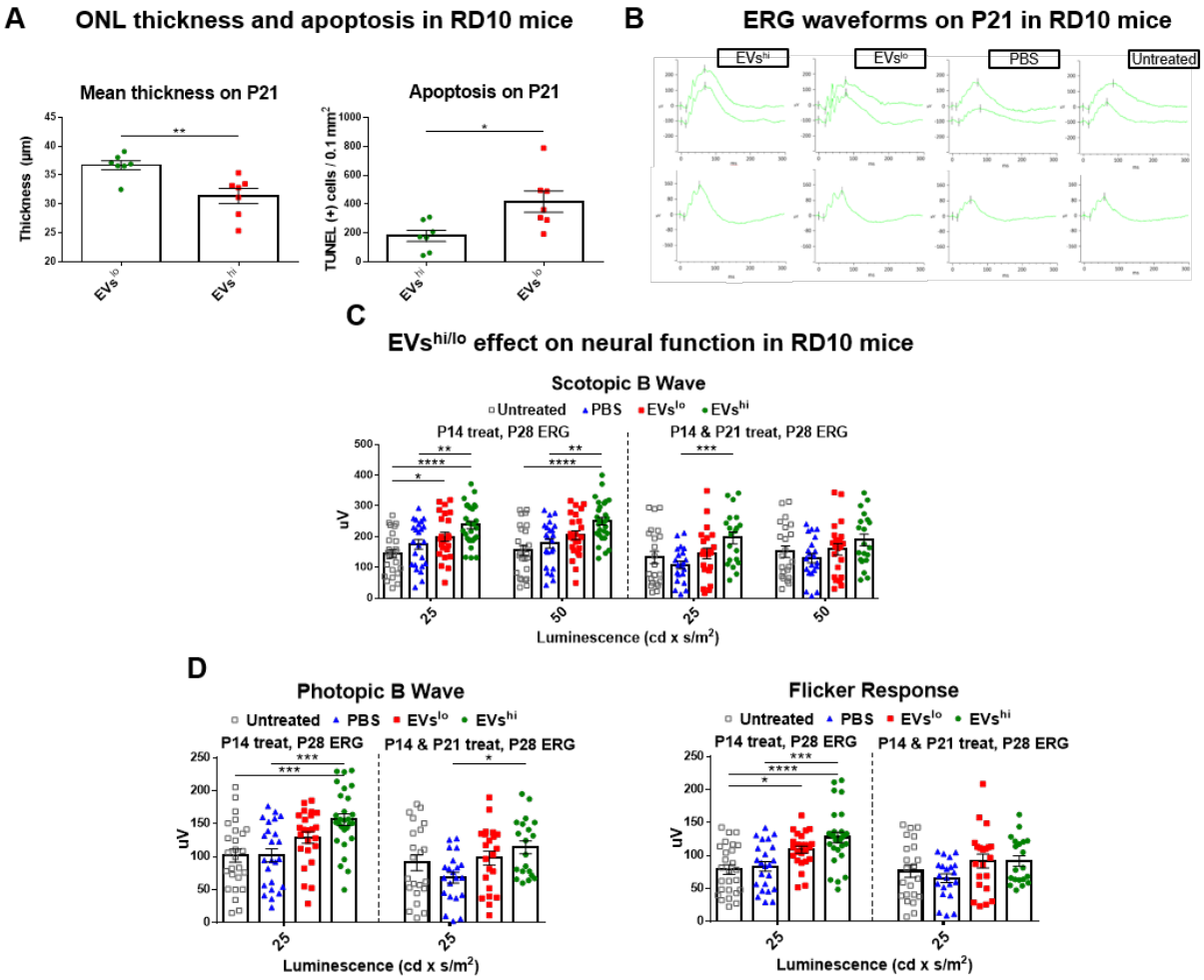

Figure S3.7: **EVs^{hi} ECFCs provided early neurotrophic support to inherited retinal degeneration mice.** (**A**) Quantification of outer nuclear layer (ONL) thickness (left) and TUNEL staining (right) on immunohistochemistry of cross-sections from RD10 retinas treated P14 with EVs^{hi} or EVs^{lo} and harvested on P21. *P<0.05, **P<0.01, Two-tailed Student's *t* test; n=7 retinas for both groups. (**B**) Representative waveforms of the mean ERG readings on P28 of RD10 mice treated on P14 with EVs^{hi}, EVs^{lo}, PBS, or untreated. (**C-D**) Repeated injections are deleterious to retinal function of RD10 mice. ERG recordings of mice treated once (on P14, left of dotted line) versus twice (on P14 and P21, right of dotted line) demonstrated that repeated injections decreased retinal function in dark-adapted (scotopic) responses in **C** and light-adapted (photopic and flicker) responses in **D** across all groups. *P<0.05, **P<0.01, ***P<0.001, ****P<0.0001, 1-way ANOVA with Tukey analysis; for experiments treating mice once at P14: n=28 retinas for EVs^{hi}, n=24 retinas for EVs^{lo}, n=23-24 retinas for PBS, n=25-26 retinas for untreated; for experiments treating mice twice at P14 and at P21: n=20 retinas for EVs^{hi}, n=21-22 retinas for EVs^{lo}, n=21 retinas for PBS, n=22 retinas for untreated. Error bars represent SEM.

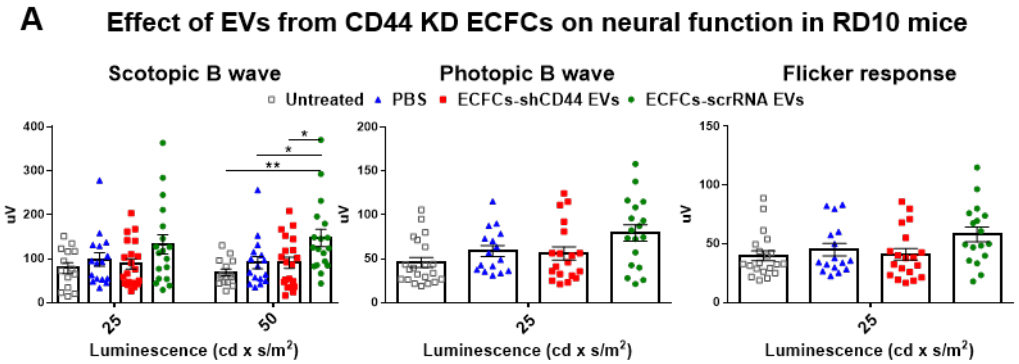

Figure S3.8: **EVs from ECFCs with CD44 knockdown did not preserve neural retinal function in inherited retinal degeneration mice.** EVs isolated from ECFCs transfected with shRNA to CD44 (ECFCs-shCD44 EVs) and from control ECFCs transfected with scramble RNA (ECFCs-scrRNA EVs) were injected into RD10 mice on P14 along with PBS and untreated controls for ERG measurements on P28. ECFCs-shCD44 EVs failed to rescue rod-driven dark-adapted responses (scotopic B wave), which were significantly improved by treatment with ECFCs-scrRNA EVs. *P<0.05, **P<0.01, 1-way ANOVA with Tukey analysis; n=18 retinas for ECFCs-scrRNA EVs, n=20 retinas for ECFCs-shCD44 EVs, n=16 retinas for PBS, n=14 retinas for untreated. Error bars represent SEM.

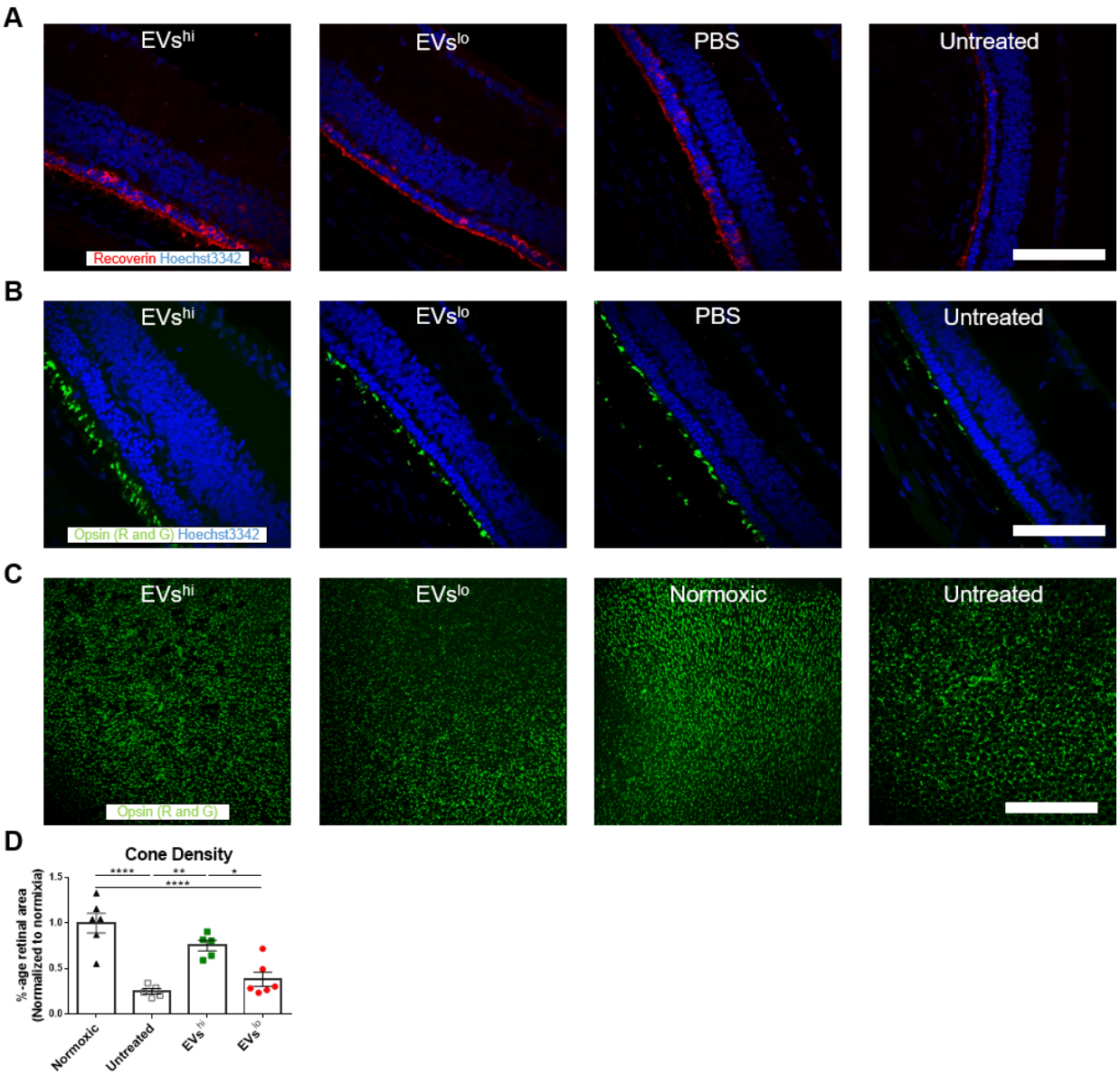

Figure S3.9: EVs^{hi} increased photoreceptor density in inherited retinal degeneration mice. (**A-B**) Immunohistochemistry for cone- and rod-specific markers on RD10 retinas treated P14 and harvested P28 demonstrate photoreceptor preservation by EVs^{hi}. Retinal cross-sections were stained for recoverin (in red) in **A** and for opsin red/green (in green) in **B** with Hoechst3342 nuclear staining (in blue). (**C**) Representative images of opsin red/green stained retinal flat-mounts. (**D**) Quantification of cone photoreceptor density. *P<0.05, **P<0.01, ****P<0.0001. 1-way ANOVA with Tukey analysis; n=6 eyes for each group. Scale bars: 50 μm.

Figure S3.10: Preliminary analyses of small RNA sequencing. (**A**) Principal component analysis of small RNA sequencing data of microRNAs (miRs) within EVs^{hi} samples (circles within triangles) and EVs^{lo} samples (circles). Samples clustered more closely within each group than between the two groups. (**B**) Unsupervised hierarchical clustering (HCL) of miRs reads from small RNA sequencing of EVs^{hi} and EVs^{lo}. Rows represent unique miRs, columns represent individual EVs^{hi} samples (H) or EVs^{lo} samples (L), and the HCL analysis separately clustered H and L samples. (**C**) Differential expression analysis thresholding for $p<0.05$ with Bonferroni correction factor showing 41 miRs upregulated and 43 miRs downregulated in EVs^{hi} as compared to EVs^{lo}.

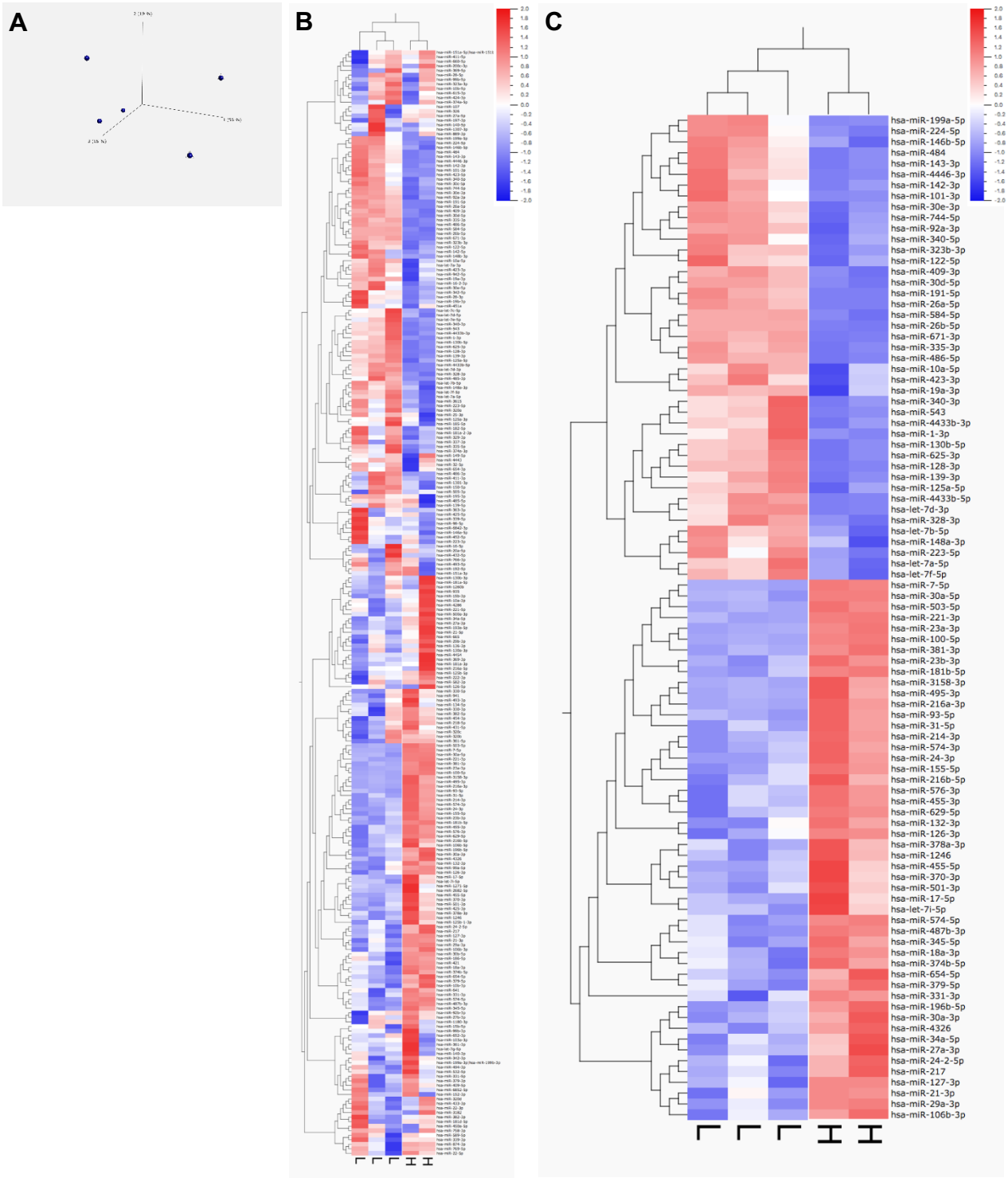
A
B
C
hsa-miR-199a-5p
hsa-miR-224-5p
hsa-miR-146b-5p
hsa-miR-484
hsa-miR-143-3p
hsa-miR-4446-3p
hsa-miR-142-3p
hsa-miR-101-3p
hsa-miR-30e-3p
hsa-miR-744-5p
hsa-miR-92a-3p
hsa-miR-340-5p
hsa-miR-323b-3p
hsa-miR-122-5p
hsa-miR-409-3p
hsa-miR-30d-5p
hsa-miR-191-5p
hsa-miR-26a-5p
hsa-miR-584-5p
hsa-miR-26b-5p
hsa-miR-671-3p
hsa-miR-335-3p
hsa-miR-486-5p
hsa-miR-10a-5p
hsa-miR-423-3p
hsa-miR-19a-3p
hsa-miR-340-3p
hsa-miR-543
hsa-miR-4433b-3p
hsa-miR-1-3p
hsa-miR-130b-5p
hsa-miR-625-3p
hsa-miR-128-3p
hsa-miR-139-3p
hsa-miR-125a-5p
hsa-miR-4433b-5p
hsa-let-7d-3p
hsa-miR-328-3p
hsa-let-7b-5p
hsa-miR-148a-3p
hsa-miR-223-5p
hsa-let-7a-5p
hsa-let-7f-5p
hsa-miR-7-5p
hsa-miR-30a-5p
hsa-miR-503-5p
hsa-miR-221-3p
hsa-miR-23a-3p
hsa-miR-100-5p
hsa-miR-381-3p
hsa-miR-23b-3p
hsa-miR-181b-5p
hsa-miR-3158-3p
hsa-miR-495-3p
hsa-miR-216a-3p
hsa-miR-93-5p
hsa-miR-31-5p
hsa-miR-214-3p
hsa-miR-574-3p
hsa-miR-24-3p
hsa-miR-155-5p
hsa-miR-216b-5p
hsa-miR-576-3p
hsa-miR-455-3p
hsa-miR-629-5p
hsa-miR-132-3p
hsa-miR-126-3p
hsa-miR-378a-3p
hsa-miR-1246
hsa-miR-455-5p
hsa-miR-370-3p
hsa-miR-501-3p
hsa-miR-17-5p
hsa-let-7i-5p
hsa-miR-574-5p
hsa-miR-487b-3p
hsa-miR-345-5p
hsa-miR-18a-3p
hsa-miR-374b-5p
hsa-miR-654-5p
hsa-miR-379-5p
hsa-miR-331-3p
hsa-miR-196b-5p
hsa-miR-30a-3p
hsa-miR-4326
hsa-miR-34a-5p
hsa-miR-27a-3p
hsa-miR-24-2-5p
hsa-miR-217
hsa-miR-127-3p
hsa-miR-21-3p
hsa-miR-29a-3p
hsa-miR-106b-3p

Chapter 3, in part, has been submitted for publication of the material as it may appear in Nature Medicine, 2021, Marra, KV; Aguilar, E; Usui-Ouchi A; Wei, G; Ideguchi, A; Sakimoto, S; Friedlander, MF. "Bioactive extracellular vesicles from a subset of endothelial progenitor cells rescue retinal ischemia and neurodegeneration." The dissertation author was the primary investigator and author of this material.

Chapter 4

Reprint: Fully automated, deep learning segmentation of oxygen-induced retinopathy images

JCI insight

TECHNICAL ADVANCE

Fully automated, deep learning segmentation of oxygen-induced retinopathy images

Sa Xiao,[1] Felicitas Bucher,[2,3] Yue Wu,[1] Ariel Rokem,[4] Cecilia S. Lee,[1] Kyle V. Marra,[2,5] Regis Fallon,[6] Sophia Diaz-Aguilar,[2] Edith Aguilar,[2] Martin Friedlander,[2,6] and Aaron Y. Lee[1,4,7]

[1]Department of Ophthalmology, University of Washington, Seattle, Washington, USA. [2]Department of Molecular Medicine, The Scripps Research Institute, La Jolla, California, USA. [3]Eye Center, Faculty of Medicine, University of Freiburg, Freiburg, Germany. [4]eScience Institute, University of Washington, Seattle, Washington, USA. [5]Department of Bioengineering, University of California, San Diego, San Diego, California, USA. [6]Lowy Medical Research Institute, La Jolla, California, USA. [7]Department of Ophthalmology, Puget Sound Veteran Affairs, Seattle, Washington, USA.

Oxygen-induced retinopathy (OIR) is a widely used model to study ischemia-driven neovascularization (NV) in the retina and to serve in proof-of-concept studies in evaluating antiangiogenic drugs for ocular, as well as nonocular, diseases. The primary parameters that are analyzed in this mouse model include the percentage of retina with vaso-obliteration (VO) and NV areas. However, quantification of these two key variables comes with a great challenge due to the requirement of human experts to read the images. Human readers are costly, time-consuming, and subject to bias. Using recent advances in machine learning and computer vision, we trained deep learning neural networks using over a thousand segmentations to fully automate segmentation in OIR images. While determining the percentage area of VO, our algorithm achieved a similar range of correlation coefficients to that of expert inter-human correlation coefficients. In addition, our algorithm achieved a higher range of correlation coefficients compared with inter-expert correlation coefficients for quantification of the percentage area of neovascular tufts. In summary, we have created an open-source, fully automated pipeline for the quantification of key values of OIR images using deep learning neural networks.

Introduction

Over the past 30 years, advances in our understanding of basic mechanisms of normal and abnormal angiogenesis have had a significant effect on the fields of cancer, cardiovascular, and ophthalmology research. Novel therapeutics, such as antivascular endothelial growth factor agents that target neovessel formation, play an important role in cancer therapy (1) and have revolutionized the therapeutic approach for neovascular retinal diseases, such as age-related macular degeneration and diabetic retinopathy (2). Due to its unique anatomical properties, the eye represents an ideal model system to study basic mechanisms in angiogenic diseases and to test novel antiangiogenic therapeutics (3).

The mouse model of oxygen-induced retinopathy (OIR) is one of the most commonly used rodent models to study ischemia-driven abnormal neovessel formation and retinal vasoproliferative disease (4). In this model, young pups at P7 exposed to an atmosphere containing 75% oxygen, which induces regression of the central capillary system, resulting in a centralized area of vaso-obliteration (VO). When pups are then transferred to room air on P12, this area of VO becomes hypoxic and triggers neovascularization (NV), resulting in the growth of abnormal vessels toward the vitreous (5). At P17, VO and NV areas represent primary readout parameters in this model.

High variability due to a volatile vascular phenotype and a subjective manual quantification method of assessing VO and NV represent the greatest challenges in this model. Controlling for body weight gain in pups and comparison to control-treated groups greatly improve reproducibility of OIR results (6). However, existing quantification protocols used to determine VO and NV areas still remain an important source for variability of OIR data within and between research groups (5, 7, 8). VO and NV quantification require expert knowledge, are prone to bias in the case of unmasked quantifiers,

Conflict of interest: A.Y. Lee received a hardware donation from NVIDIA Corporation.

Submitted: September 19, 2017
Accepted: November 15, 2017
Published: December 21, 2017

Reference information:
JCI Insight. 2017;2(24): e97585. https://doi.org/10.1172/jci.insight.97585.

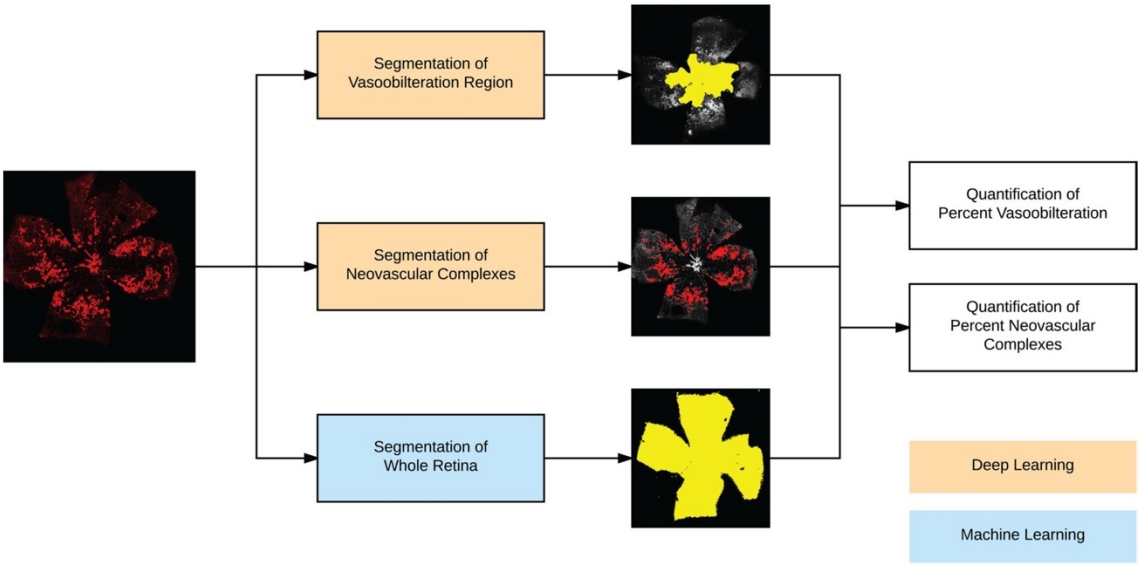

Figure 1. Overview of the fully automated analysis pipeline for oxygen-induced retinopathy images. The input image is fed through 3 separate fully automated methods: Segmentation of the vaso-obliteration region using deep learning, segmentation of the neovascular complexes using deep learning, and segmentation of the whole retina. These are combined to calculate quantitative ratios of the percentage of vaso-obliteration and percentage of neovascular complexes.

and remain heavily time-consuming. Automating this process will further improve the reproducibility of OIR experiments within and among labs working with this model. Prior attempts have led to partial automation of the segmentation tasks but still required several manual, subjective steps (8–10). Full automation will ensure common standards for the detection of VO and NV, eliminate the risk for user-dependent bias, and accelerate the quantification process, freeing valuable staff resources.

Using deep learning, the goal of our study was to create and validate a fully automated algorithm to segment the VO and NV regions on OIR images. Machine learning is the general field of training predictive models on large data sets with computers. The predictive models can be built implicitly or explicitly with hand-crafted features that best extract signal from noise in the data. Deep learning is a subfield of machine learning in which feature construction is automated and learned implicitly through a purely data-driven approach using many layers of neural networks.

The development of deeper neural networks has been facilitated by the advent of graphics-processing units suited for efficient evaluation of convolution as well as new neural network architectures. Recently, deep learning has revolutionized computer vision tasks, such as classification, object detection, and semantic segmentation (11–14), and is increasingly used in ophthalmic image-processing applications (15–18).

Here, we present an end-to-end solution using deep learning to automatically quantify VO and NV as primary readout parameters of the OIR retinal image.

Results

An overview of the fully automated pipeline is provided in Figure 1. As a standard machine learning practice, over a thousand images were used to develop and train the deep learning model and were divided into three sets: training, validation, and test (19). There were 682, 171, and 214 images in each set, respectively, for the two deep learning models (Figure 2).

For training the segmentation of the VO region, the model was trained with 14,000 iterations of batch sizes of 32. The learning curve of the training iterations and the validation set are shown in Supplemental Figure 1 (supplemental material available online with this article; https://doi.org/10.1172/jci.insight.97585DS1). For the test set, the model achieved a median Dice coefficient of 0.870, with a standard deviation of 0.135. Examples of model outputs are shown in Figure 3. A separate test set of

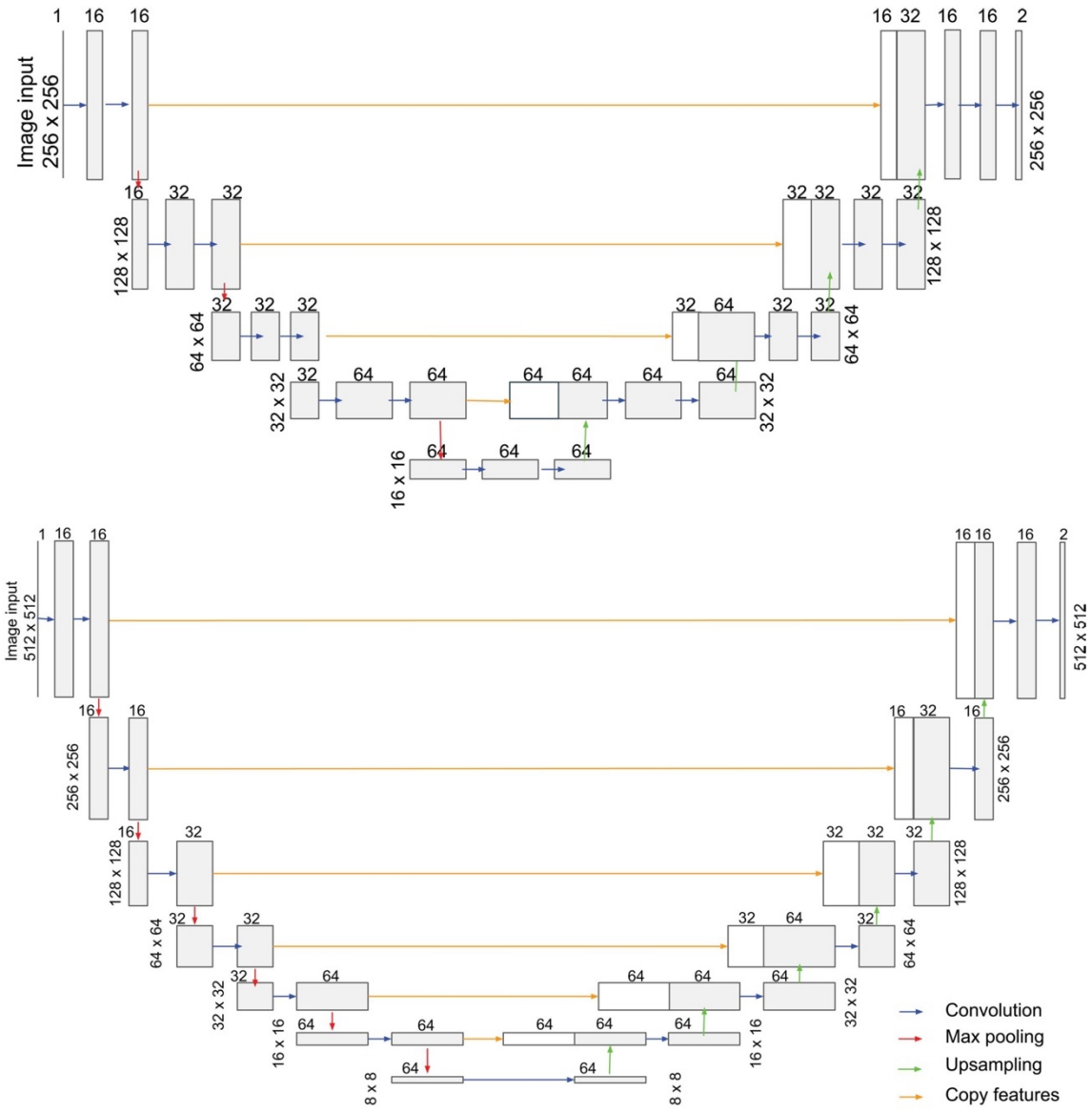

Figure 2. Deep learning model architectures used for vaso-obliteration and neovascular segmentation. The U-net architecture for vaso-obliteration (VO) segmentation (top) and neovascularization (NV) segmentation (bottom). For each convolutional layer, the filter size is 3 and the stride is 1. The number of filters is labeled on top of its corresponding layer. ReLU was used as the activation function. The receptive fields were 140 × 140 and 318 × 318 for VO and NV segmentation, respectively.

37 images was segmented by 4 human experts as well as the final trained deep learning model. Each human expert was set as the gold standard, and the other 3 human experts as well the deep learning model were compared with the gold standard (Figure 4).

For the training of the neovascular complexes, the model was trained with 60,000 iterations of batch sizes of 8. The learning curve of the training iterations and the validation set are shown in Supplemental Figure 2. The model achieved a median Dice coefficient of 0.750, with a standard deviation of 0.156, for the test set. Examples of model outputs are shown in Figure 5. Similar to the inter-rater reliability results

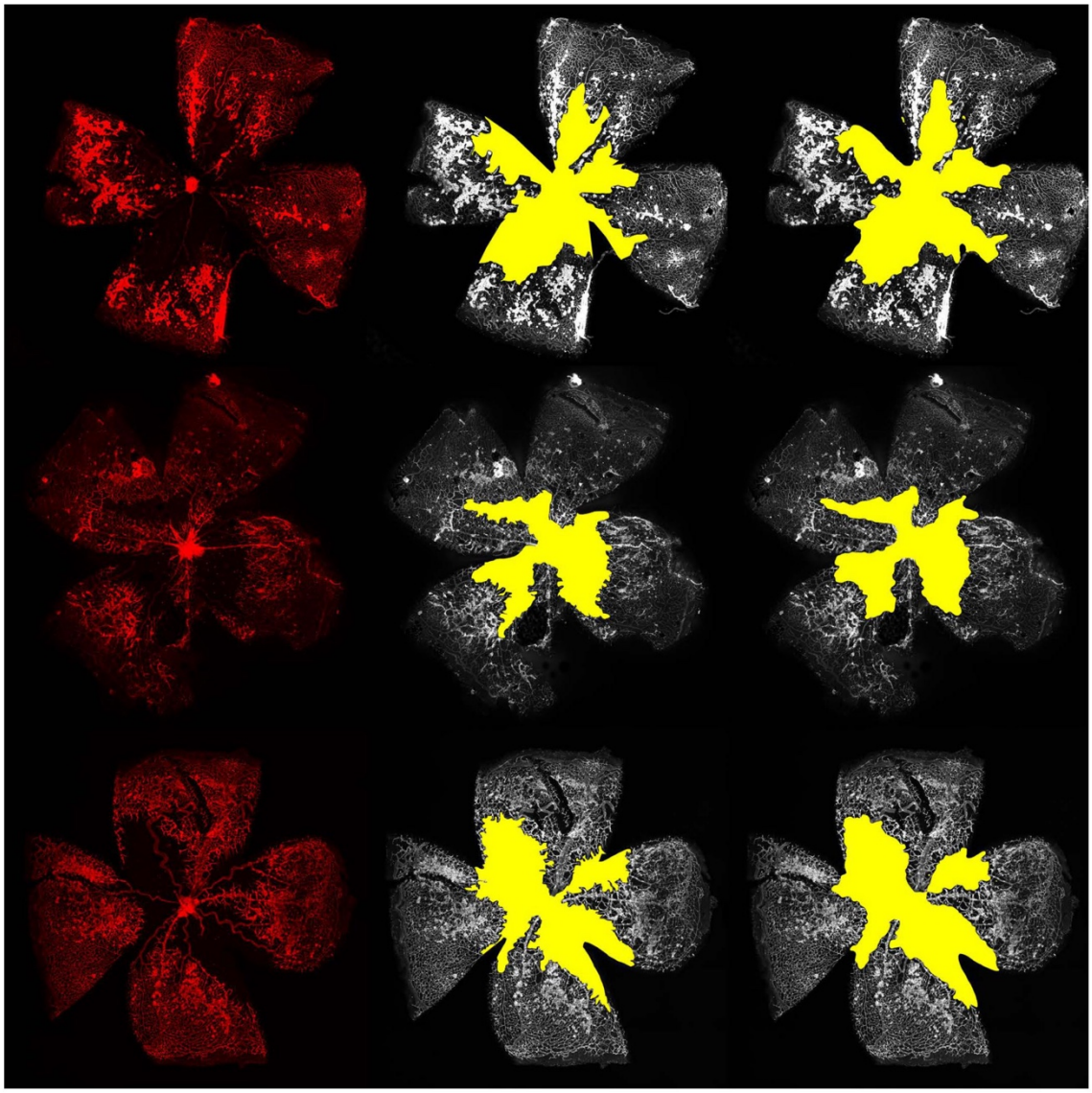

Figure 3. Example segmentations of vaso-obliteration region. The left column shows the original image, the middle column shows expert segmentations, and the right column shows deep learning segmentation.

for VOR, the trained deep learning model was able to achieve similar median Dice coefficients as human experts for a separate set of 37 images (Figure 6).

In order to fully automate the segmentation of the total retina, the k-means clustering algorithm was able to segment and identify the total retina. For the 37 retina images segmented by humans, the algorithm achieved a median Dice coefficient of 0.960, with a standard deviation of 0.013. Examples of algorithm outputs are shown in Figure 7. The median Dice coefficients between the automated segmentations were similar to the median Dice coefficients among the human experts (Figure 8).

For the 37 images that served as an independent test set, the deep learning–based algorithm generated two percentages: VO relative to the total retina and NV complexes relative to the total retina. Tables 1 and 2

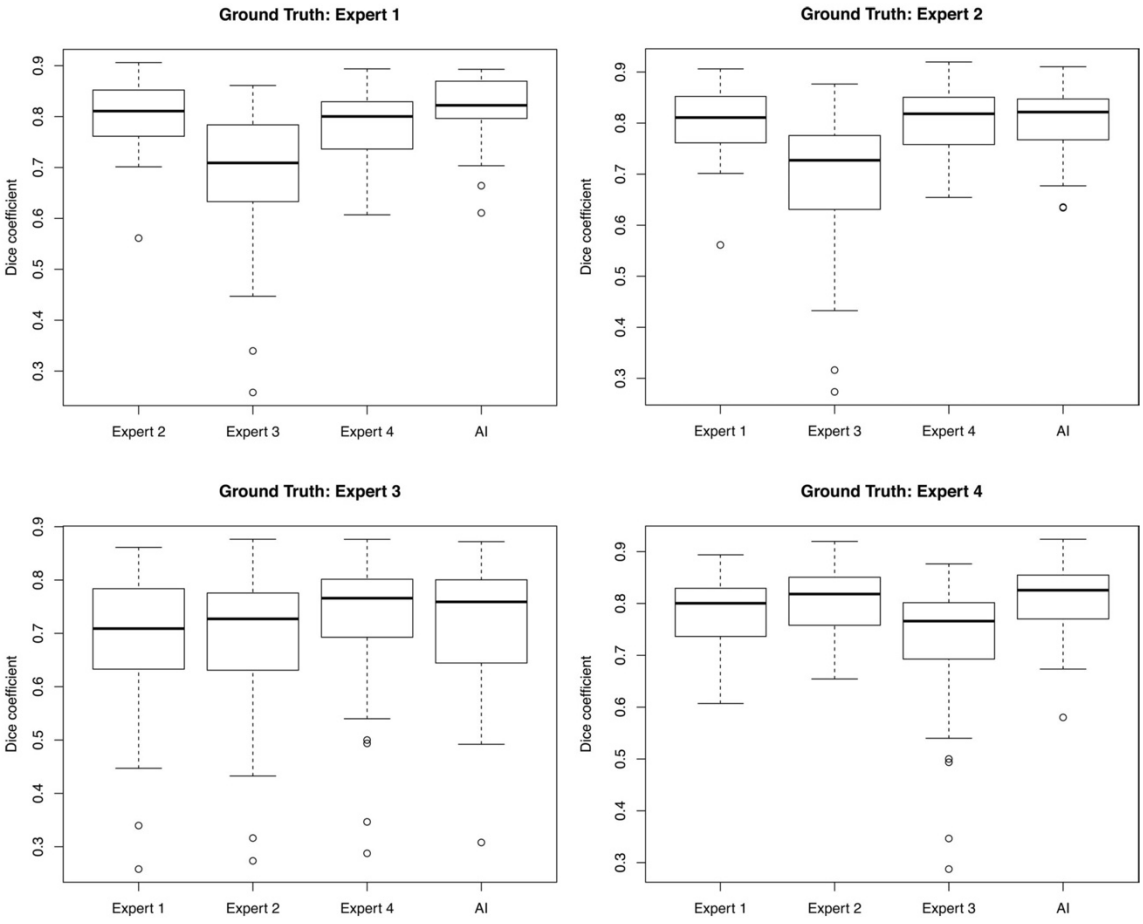

Figure 4. Inter-rater reliability with 4 human expert segmentations compared with deep learning for vaso-obliteration region. Inter-rater reliability with 37 images segmented by 4 human experts and the deep learning model for vaso-obliteration segmentation. Each set of box plots represents a different human expert set as ground truth compared against the other 3 human experts and the deep learning model using Dice coefficients. The middle bar represents the median, the box represents the interquartile range, and the whiskers extend to the most extreme data point, which is no more than 1.5 times the interquartile range from the box.

show the linear correlation between each pairwise comparison of human experts and the deep learning algorithm for the VO and NV percentages, respectively.

The code for this project has been published online as a free, public, open-source repository (https://github.com/uw-biomedical-ml/oir/tree/bf75f9346064f1425b8b9408ab792b1531a86c64). This repository contains setup instructions, the trained model architectures, the trained weights of all the models, software code for running the fully automated pipeline, and generation of formatted results. Users will be able to download this repository to further train the models if they wish. In addition, we have created an online web application located at http://oirseg.org where users may upload images that need to be processed and download the resulting segmentations and quantification results, without the need to setup any software locally.

Discussion

In this study, we have created a fully automated tool for the quantification of OIR images using a deep learning approach. The mouse model of OIR represents one of the most commonly used in vivo models to study basic mechanisms in ocular angiogenesis and test potential antiangiogenic therapeutics. In this model, reproducibility of experimental results can represent a major challenge due to high variability in

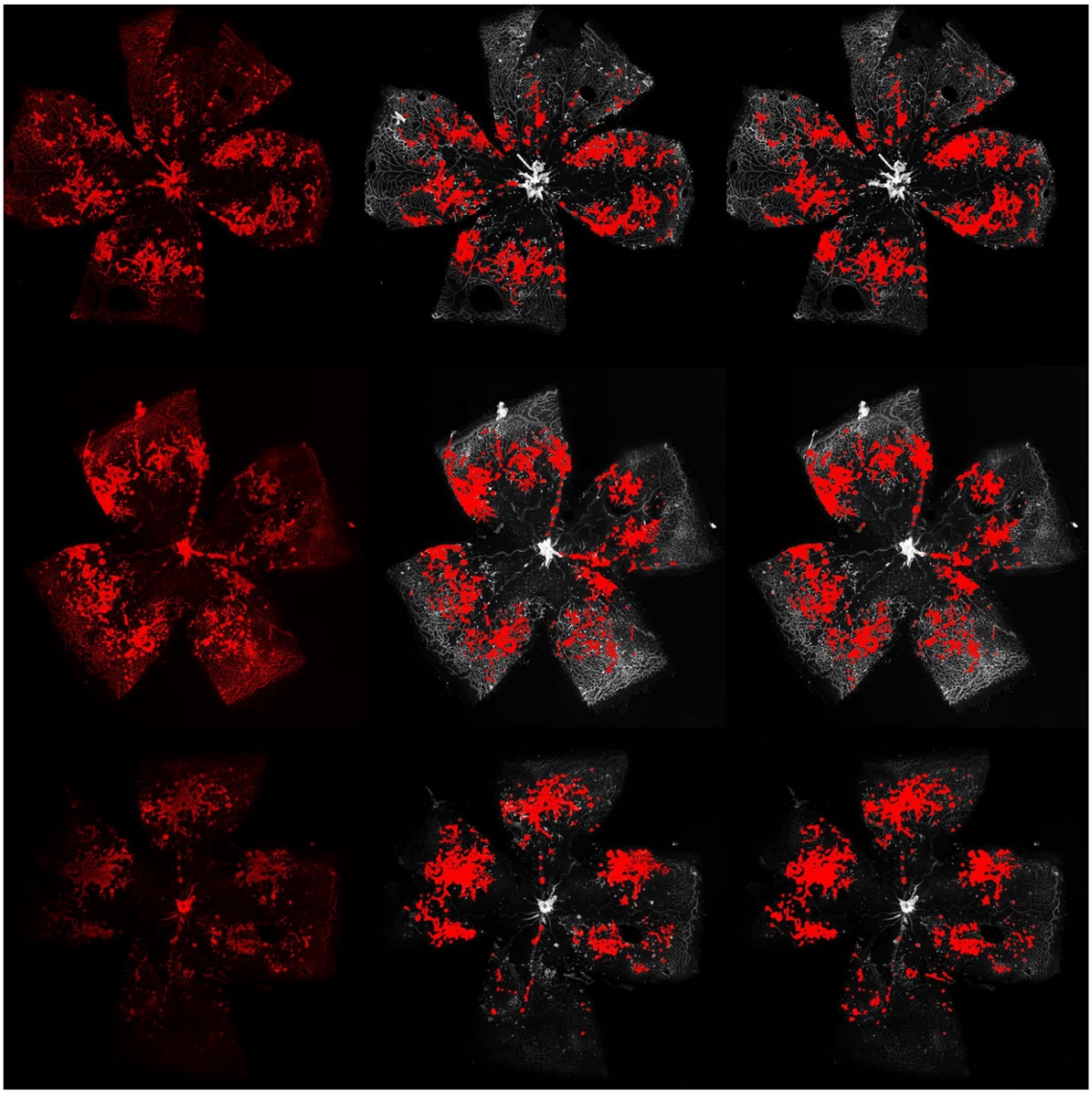

Figure 5. Example segmentations of neovascular tufts. The left column shows the original image, the middle column shows expert segmentations, and the right column shows deep learning segmentation.

the vascular phenotype. In addition, manual analysis of the model's readout parameters, area of VO and NV, is a time-consuming process, requiring expert knowledge and thus significant costs. While monitoring of confounders such as body weight can minimize the variability of the vascular phenotype, only fully automated quantification tools can eliminate potential grader bias.

Our fully automated deep learning approach identified and segmented the areas of VO and NV in the OIR images with high correlation to 4 separate expert human graders. After training with 682 images, the model achieved a mean Dice coefficient that is similar to inter-rater Dice coefficients when comparing those of human experts for the segmentation of VO area and NV regions. In addition, machine learning was used to identify the area of total retina in a fully automated fashion. We noted that with VO segmentation, the deep

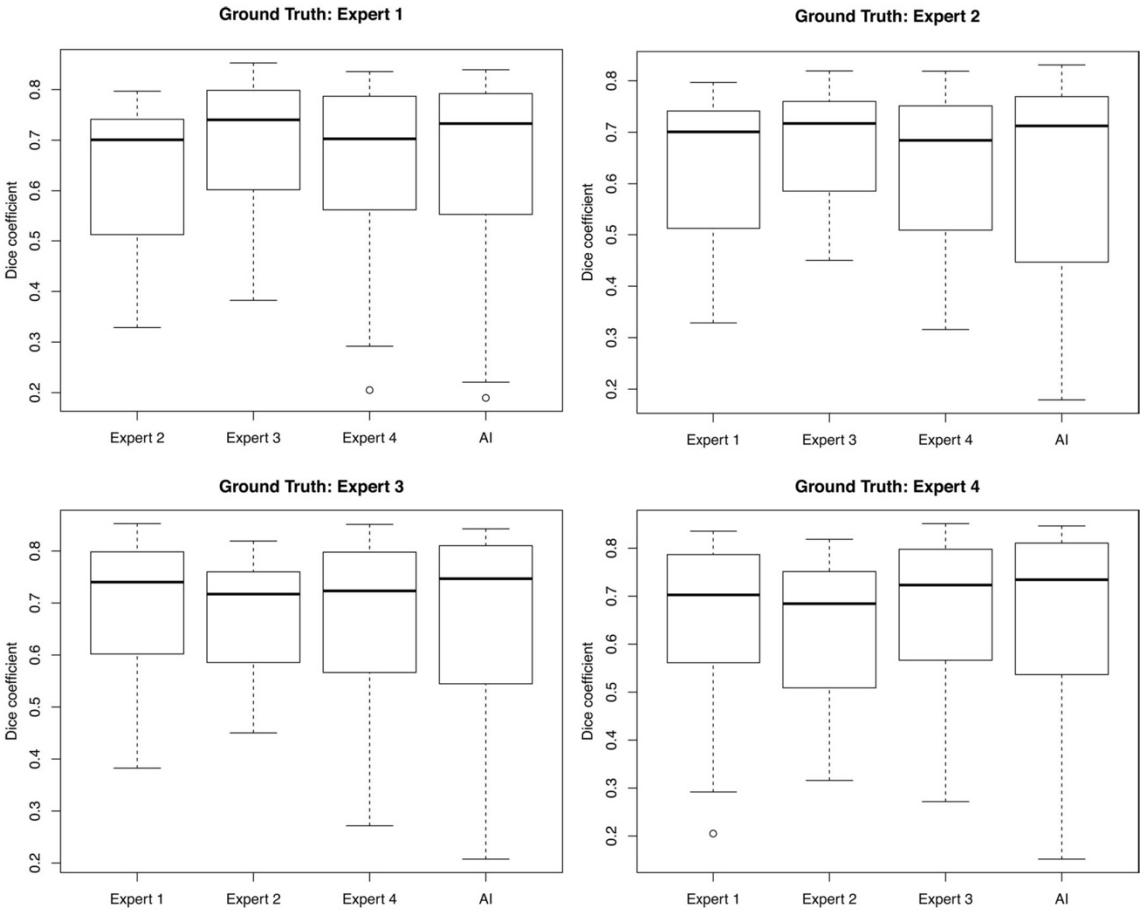

Figure 6. Inter-rater reliability with 4 human expert segmentations compared with deep learning for neovascular tufts. Inter-rater reliability with 37 images segmented by 4 human experts and the deep learning model for neovascular segmentation. Each set of box plots represents a different human expert set as ground truth compared against the other 3 human experts and the deep learning model using Dice coefficients. The middle bar represents the median, the box represents the interquartile range, and the whiskers extend to the most extreme data point, which is no more than 1.5 times the interquartile range from the box.

learning model generated smoother contours compared with expert graders (Figure 3). These differences did not translate to a difference in Dice coefficients or to a difference between the correlation of percent VO area. Our algorithm achieved a similar range of correlation coefficients (range 0.878–0.951) to expert inter-human correlation coefficients (range: 0.889–0.951) for quantification of the percentage area of VO. On inspection, deep learning appeared to generate segmentations that look very similar to human segmentations for neovascular complexes (Figure 5), and machine learning generated much more precise segmentations of the total retina and was able to ignore artifacts of the flat-mount preparation (Figure 7). Our algorithm achieved a higher range of correlation coefficients (range: 0.943–0.987) compared with inter-expert correlation coefficients (range: 0.925–0.972) for quantification of the percentage area of neovascular complexes. Because the contrast was varied during training of the models, the resulting algorithm is resistant to varying levels of contrast inherent in the OIR images (Figure 5, bottom row).

Prior attempts to automate this process have resulted in solutions that were partially automated but still required subjective manual input. Doelemeyer et al. described a computer-aided system in which the user traced the whole retina before the quantification of the VO region could be segmented, but the system could not quantify the neovascular regions (9, 10). Stahl et al. achieved automated segmentation of the neovascular regions

Table 1. Correlation coefficients of the percentage of total retina with VO regions for each pairwise comparison

	Expert 2	Expert 3	Expert 4	Deep learning
Expert 1	0.951	0.926	0.922	0.951
Expert 2		0.907	0.945	0.914
Expert 3			0.889	0.892
Expert 4				0.878

VO, vaso-obliteration.

but required manual segmentation of the VO region. Furthermore, automated quantification of the NV area required manual thresholding of the intensity in each quadrant of the whole-mount retina image, which may be subjectively biased (8). In contrast, we achieved a fully automated pipeline, which only takes the whole retina image as input and provides automated segmentation of the VO region, neovascular complexes, and whole retina. The algorithm also provides quantitative measures that can easily be incorporated into statistical analyses.

Key strengths of the study include the fully automated pipeline and the efficiency of the algorithm. The segmentation of VO and NV regions in each OIR image took less than few seconds, which makes the algorithm scalable to many hundreds or thousands of OIR images. In addition, the algorithm can run on a standard desktop computer without the need for specialized hardware.

Limitations of our study are that our models were trained on images of the mouse model of OIR generated from a single laboratory. Our models are currently not trained to segment images from the rat model of OIR. Furthermore, training on images generated from a single laboratory may also result in decreased generalizability, if there are systematic biases in which these images were graded. In that case, the algorithm may seem to perform poorly when compared with segmentations from a different laboratory. Future studies to collect segmentations from several key research groups to further train the model will be critical in improving the generalizability of the automated pipeline.

In general, automating the analysis of OIR images may not only improve the efficiency but also the overall quality of OIR results. All labs using this tool will automatically apply the same standards for the identification of VO and NV, thereby increasing the generalizability and reproducibility of study results. Future extensions of the tool may also include estimates of model accuracy of the deep learning segmentation and improved model accuracy as more images are used for training. This parameter would substantially depend on the original image quality and hence represent an important parameter to estimate the quality of flat-mount preparation and imaging.

The described pipeline may also open the door to simultaneously look at more readout parameters and detect more subtle changes in this model. For example, Fruttiger and colleagues suggested using vascular tortuosity as an early outcome measure in OIR (20). Other parameters affected by OIR include vascular density, diameter, and branching points, which together provide important insight into the health of the vascular bed (21). Currently, these parameters are not part of routine analyses because of the time and effort that would be required for their quantification. However, similar approaches to those performed in this study may provide a fully automated solution for an objective quantification of subtle vascular changes.

In summary, we present a fully automated analysis pipeline as a free and open-source analysis package for an objective quantification of the percentage area of VO and NV in OIR images. Our software

Table 2. Correlation coefficients of the percentage of total retina with NV regions for each pairwise comparison

	Expert 2	Expert 3	Expert 4	Deep learning
Expert 1	0.952	0.972	0.971	0.986
Expert 2		0.972	0.925	0.943
Expert 3			0.959	0.970
Expert 4				0.987

NV, neovascularization.

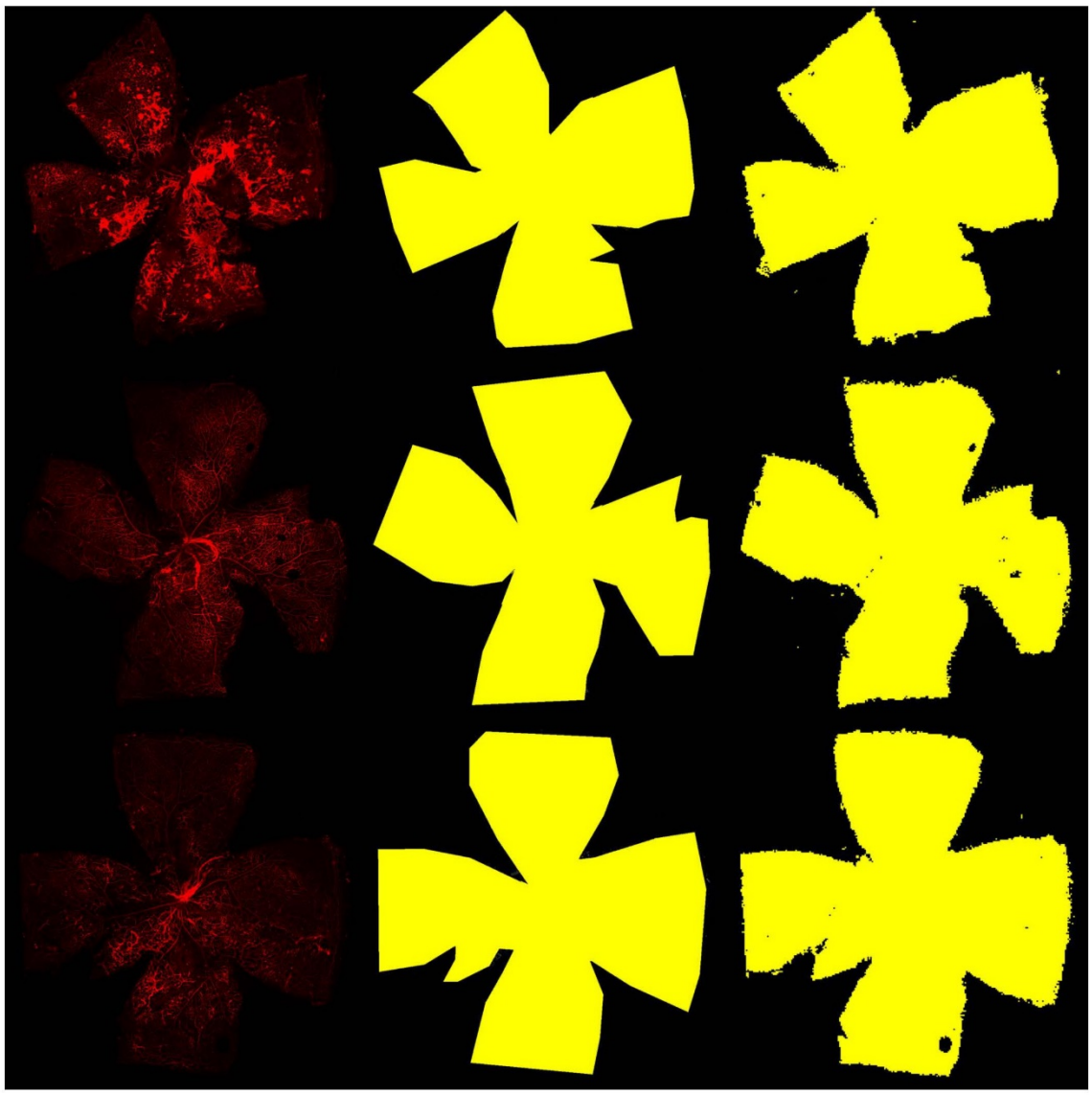

Figure 7. Examples of retina segmentation. The left column shows the input images, the middle column shows the human expert-labeled segmentations, and the right column shows the model prediction.

tool will allow OIR researchers to shift resources from the repetitive and time-consuming quantification process that requires expert training to more important tasks, such as data analysis and experimental planning. Future extensions of this tool could include a web-based segmentation system in which experts can provide corrected feedback for online iterative training of the deep learning models.

Methods

In this study, flat-mount images of C57BL/6, C57BL/ScSnJ, and transgenic mice (CB57/10ScSnD-md^{mdx}, B6Ros.Cg-Dmd$^{mdx\text{-}4Cv}$/J, B6.Cg-Dmd$^{mdx\text{-}3Cv}$/J, The Jackson Laboratory) subjected to the model of OIR were used. The OIR model was performed as previously described (4). In brief, pups (male and

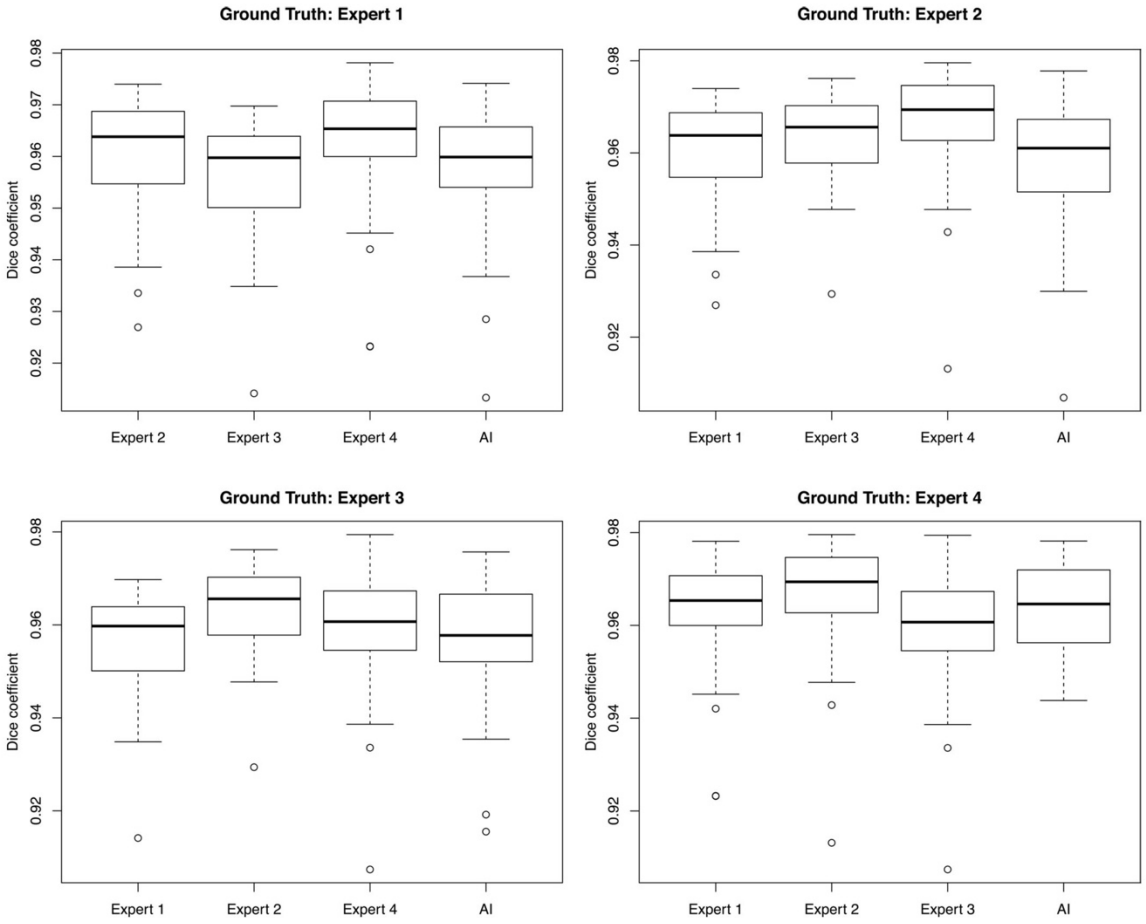

Figure 8. Inter-rater reliability with 4 human expert segmentations compared with deep learning for retina. Inter-rater reliability with 37 images segmented by 4 human experts and the deep learning model for total retinal area. Each set of box plots represents a different human expert set as ground truth compared against the other 3 human experts and the deep learning model using Dice coefficients. The middle bar represents the median, the box represents the interquartile range, and the whiskers extend to the most extreme data point, which is no more than 1.5 times the interquartile range from the box.

female) with their nursing mother were exposed to hyperoxia (75% oxygen) between P7 and P12 and then transferred to room air. Pups were weighed (6) and euthanized at OIR P17. Retinas were dissected, fixed in 4% paraformaldehyde on ice for 1 hour, stained with Isolectin B4 568 (I21412, Thermo Fisher Scientific), and flat-mounted. Flat-mount images were acquired with a confocal laser–scanning microscope (LSM710 Zeiss) using ×10 magnification and tile scanning (6 × 6 tiles) to capture whole flat-mount images. Manual quantification of the area of VO NV was performed according to an established protocol using Photoshop (Adobe) (5, 7).

The quantification of the percentage of the VO region and the percentage of the NV regions on the OIR images was broken down into 3 separate image analysis problems: the segmentation of the VO region, the segmentation of NV region, and identification of the total retinal area. We divided the images into 64%, 16%, and 20% for training, validation, and test sets, respectively.

In order to train the neural network within the confines of current GPU architectures, the original 3,000 × 3,000 images were downsampled to 256 × 256 for the training of the VO automated algorithm. The ground truth was created as a binary mask, with background set to false and the VO region set to true.

A modified version of the U-net architecture was utilized (Figure 2, top) (22, 23). The final output layer activation was set to a sigmoid function. Binary cross-entropy was used for the loss function during training and back-propagation. Batch normalization was applied after each convolutional layer (22). Adam, an adaptive learning optimizer, was set to an initial learning rate of 0.01 and was used for stochastic gradient descent (11).

To allow more generalizability of the trained model, online data augmentation was utilized during training by random rotation of 360 degrees and varying the contrast of the images by multiplying the images with a random value uniformly distributed between 0.7 and 1.3. Every 100 iterations, a random subset of the validation set was used to assess the model performance. At the end of training, the parameters of the model were frozen and the Dice coefficient was used to measure segmentation accuracy in the final held out test set.

Finer delineation was required for segmentation due to finer details found in neovascular complexes compared with VO regions; therefore the original 3,000 × 3,000 images were downsampled to 512 × 512. A modified version of the U-net architecture was utilized due to the different input size (Figure 2, bottom). All other hyperparameters were the same as the above described settings.

Segmentation of the whole retina was achieved as follows. Because the background brightness varies from image to image, there was no single threshold that could always identify the background from the retina region. Empirically, we found that pixels with intensity greater than 100 were always retina pixels. For the remaining pixels, we used k-means with k = 2 to cluster the pixels into background and retina regions based on log intensity alone.

Statistics. In order to validate the trained models, a test set of 37 images were manually segmented prospectively by 4 human experts. Each grader was set to the ground truth, and the other 3 graders as well as the deep learning output were compared with the ground truth by Dice coefficients for both the VO and NV regions. For each segmentation result, the percentage of VO and NV regions were calculated and a linear correlation coefficient was calculated for each pairwise comparison. All training and validation of images were performed using Torch7 and trained on one computer containing two NVIDIA Titan X Pascal GPU cards.

Study approval. C57BL/6 and transgenic mice used in these studies were treated in adherence with the National Institutes of Health *Guide for the Care and Use of Laboratory Animals* (National Academies Press, 2011). Animal studies were reviewed and approved by the Institutional Animal Care and Use Committee of The Scripps Research Institute.

Author contributions

SX and AYL designed the study. SX, YW, AR, and AYL created the deep learning model. FB, KVM, RF, SDA, and EA acquired the data. SX, YW, AR, CSL, MF, and AYL analyzed the data. SX, FB, CSL, and AYL wrote the manuscript. YW, AR, KM, RF, SDA, EA, and MF provided critical review and final approval of the manuscript.

Acknowledgments

We would like to acknowledge the NVIDIA Corporation for their generous donation of graphics cards for the development of artificial intelligence algorithms. This work was supported by grants from the National Eye Institute (K23EY024921 to CSL and R01 EY11254 to MF), the Lowy Medical Research Institute (to MF), the Gordon & Betty Moore Foundation (to AR), the Alfred P. Sloan Foundation (to AR), and the German Research Foundation (Bu 3135/1-1 to FB) as well as an unrestricted research grant from Research to Prevent Blindness (to CSL, AYL, SX, and YW). The contents of this manuscript do not represent the views of the US Department of Veterans Affairs or the US government.

Address correspondence to: Aaron Y. Lee, Department of Ophthalmology, University of Washington, Box 359608, 325 Ninth Avenue, Seattle, Washington 98104, USA. Phone: 206.543.7250; Email: leeay@uw.edu.

1. Jayson GC, Kerbel R, Ellis LM, Harris AL. Antiangiogenic therapy in oncology: current status and future directions. *Lancet*. 2016;388(10043):518–529.
2. Stahl A. *Anti-Angiogenic Therapy in Ophthalmology*. Cham, Switzerland: Springer International Publishing; 2016.
3. Stahl A, et al. The mouse retina as an angiogenesis model. *Invest Ophthalmol Vis Sci*. 2010;51(6):2813–2826.

4. Smith LE, et al. Oxygen-induced retinopathy in the mouse. *Invest Ophthalmol Vis Sci*. 1994;35(1):101–111.
5. Connor KM, et al. Quantification of oxygen-induced retinopathy in the mouse: a model of vessel loss, vessel regrowth and pathological angiogenesis. *Nat Protoc*. 2009;4(11):1565–1573.
6. Stahl A, et al. Postnatal weight gain modifies severity and functional outcome of oxygen-induced proliferative retinopathy. *Am J Pathol*. 2010;177(6):2715–2723.
7. Banin E, et al. T2-TrpRS inhibits preretinal neovascularization and enhances physiological vascular regrowth in OIR as assessed by a new method of quantification. *Invest Ophthalmol Vis Sci*. 2006;47(5):2125–2134.
8. Stahl A, et al. Computer-aided quantification of retinal neovascularization. *Angiogenesis*. 2009;12(3):297–301.
9. Chatenay-Rivauday C, et al. Validation of a novel automated system for the quantification of capillary non-perfusion areas in the retina of rats with oxygen-induced retinopathy (OIR). *Invest Ophthalmol Vis Sci*. 2003;44(13):2907–2907.
10. Doelemeyer A, et al. Automated objective quantification of vascular morphology in rodent oxygen-induced retinopathy. *Invest Ophthalmol Vis Sci*. 2003;44(13):3618–3618.
11. Kingma DP, Ba J. Adam: A Method for Stochastic Optimization. Cornell University Library. http://arxiv.org/abs/1412.6980. Published December 22, 2014. Updated January 20, 2017. Accessed December 6, 2017.
12. He K, Zhang X, Ren S, Sun J. Deep Residual Learning for Image Recognition. Cornell University Library. http://arxiv.org/abs/1512.03385. Published December 10, 2015. Accessed December 6, 2017.
13. Badrinarayanan V, Kendall A, Cipolla R. SegNet: A deep convolutional encoder-decoder architecture for image segmentation. *IEEE Trans Pattern Anal Mach Intell*. 2017;39(12):2481–2495.
14. Girshick R, Donahue J, Darrell T, Malik J. Rich Feature Hierarchies for Accurate Object Detection and Semantic Segmentation. Cornell University Library. https://arxiv.org/abs/1311.2524. Published November 11, 2013. Updated October 22, 2014. Accessed December 6, 2017.
15. Lee CS, Baughman DM, Lee AY. Deep learning is effective for classifying normal versus age-related macular degeneration OCT images. *Ophthalmology Retina*. 2017;1(4):322–327.
16. Prentašic P, et al. Segmentation of the foveal microvasculature using deep learning networks. *J Biomed Opt*. 2016;21(7):75008.
17. Abràmoff MD, et al. Improved automated detection of diabetic retinopathy on a publicly available dataset through integration of deep learning. *Invest Ophthalmol Vis Sci*. 2016;57(13):5200–5206.
18. Lee CS, Tyring AJ, Deruyter NP, Wu Y, Rokem A, Lee AY. Deep-learning based, automated segmentation of macular edema in optical coherence tomography. *Biomed Opt Express*. 2017;8(7):3440–3448.
19. Hastie T, Tibshirani R, Friedman J. *The Elements of Statistical Learning: Data Mining, Inference, and Prediction*. New York, NY: Springer New York Inc; 2001.
20. Scott A, Powner MB, Fruttiger M. Quantification of vascular tortuosity as an early outcome measure in oxygen induced retinopathy (OIR). *Exp Eye Res*. 2014;120:55–60.
21. Nakamura S, Imai S, Ogishima H, Tsuruma K, Shimazawa M, Hara H. Morphological and functional changes in the retina after chronic oxygen-induced retinopathy. *PLoS ONE*. 2012;7(2):e32167.
22. Ioffe S, Szegedy C. Batch Normalization: Accelerating Deep Network Training by Reducing Internal Covariate Shift. Cornell University Library. https://arxiv.org/abs/1502.03167. Published February 11, 2015. Updated March 2, 2015. Accessed December 6, 2017.
23. Ronneberger O, Fischer P, Brox T. U-Net: Convolutional Networks for Biomedical Image Segmentation. In: Navab N, Hornegger J, Wells W, Frangi A, eds. *Medical Image Computing and Computer-Assisted Intervention – MICCAI 2015*. Cham, Switzerland:Springer, Cham; 2015:234–241.

SUPPLEMENTARY FIGURES

Supplementary Figure 1: **Learning curves for segmentation of vaso-obliteration region.**

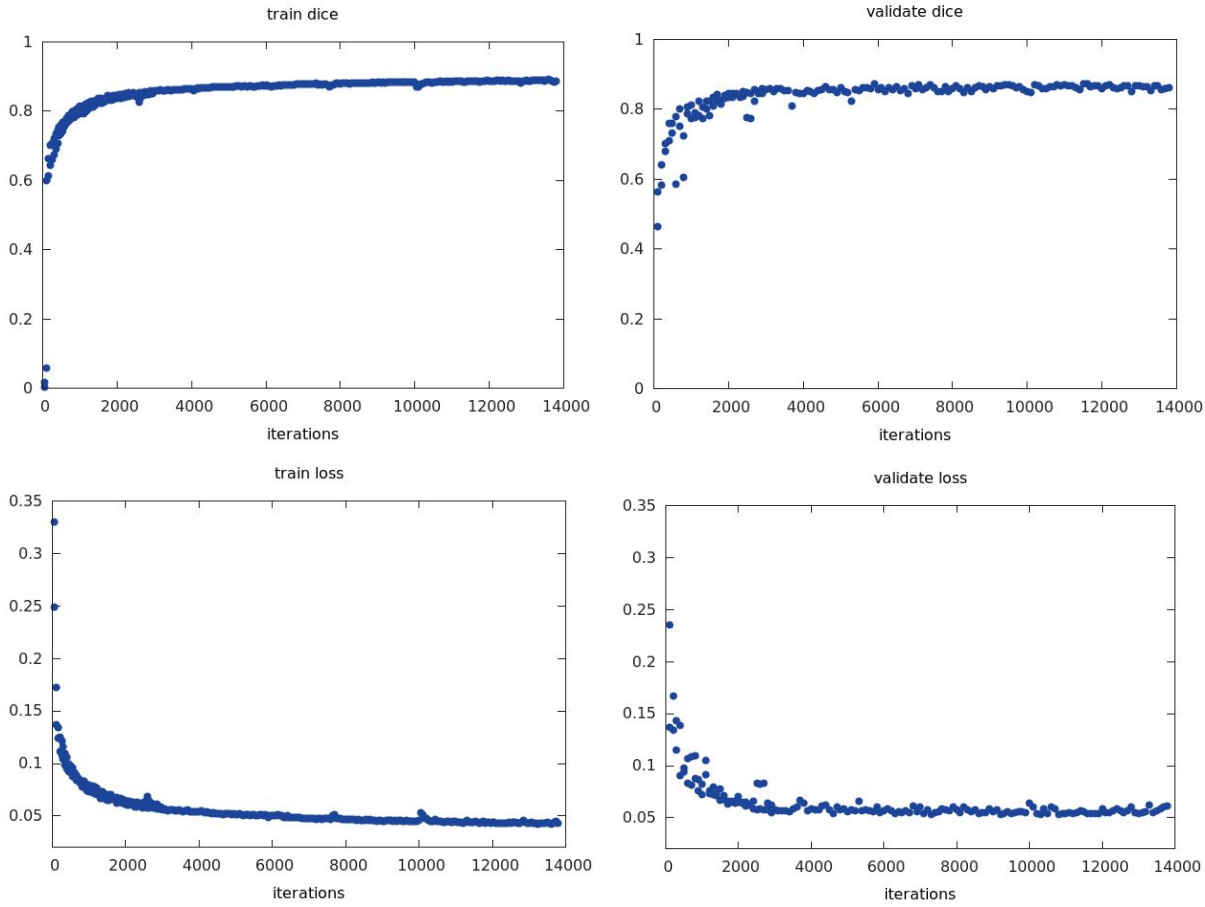

Upper left and upper right shows Dice coefficient of training set and validation sets, respectively. Lower left and lower right shows loss function by pixel-wise binary cross entropy of training and validation sets, respectively.

Supplementary Figure 2: Learning curves for segmentation of neovascular tufts.

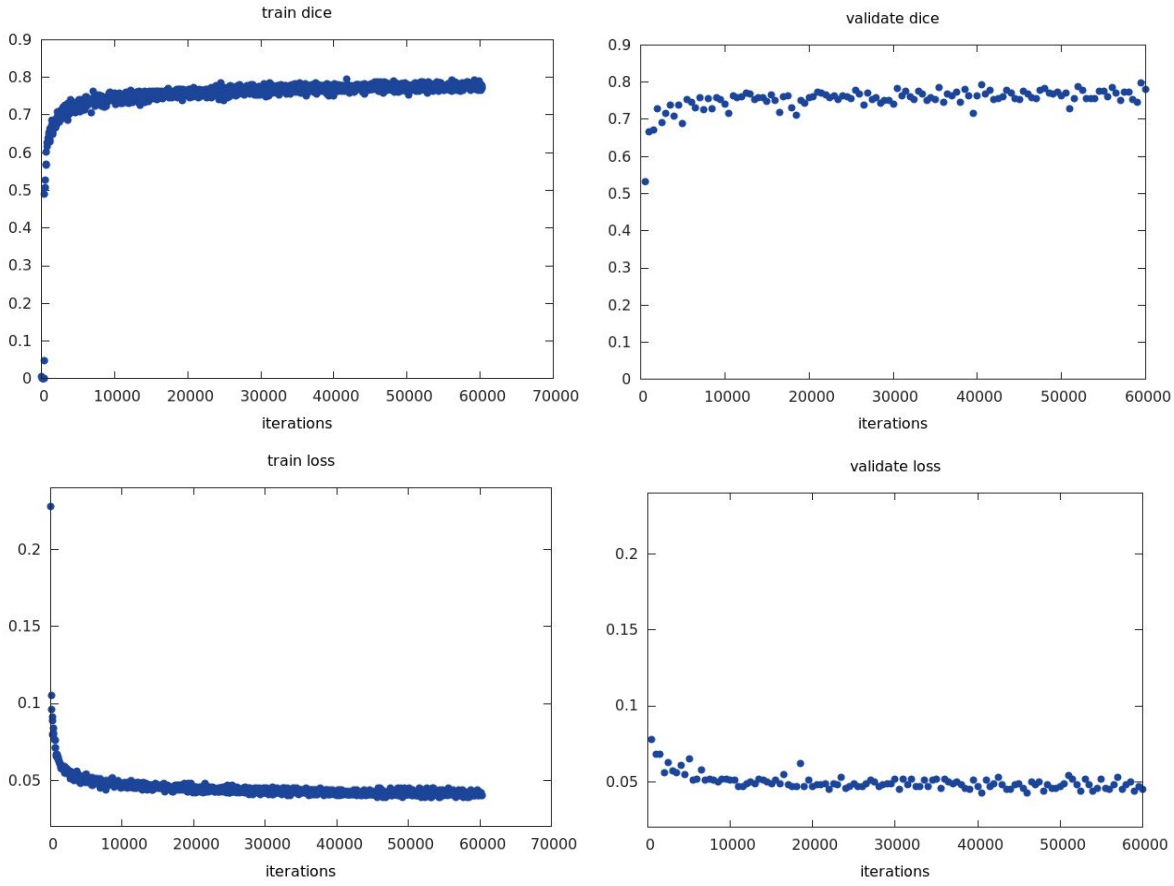

Upper left and upper right shows Dice coefficient of training set and validation sets, respectively. Lower left and lower right shows loss function by pixel-wise binary cross entropy of training and validation sets, respectively.

Chapter 4, in full, is a reprint of the materials as it appears in The Journal of Clinical Investigation Insight, 2017. Xiao, S; Bucher, F; Wu, Y; Rokem, A; Lee, CS; Marra, KV; Fallon, R; Diaz-Aguilar, S; Aguilar, E; Friedlander, M; Lee AY. The dissertation author was a co-investigator and co-author of this material.

Chapter 5

Reprint: Ciliary neurotrophic factor prevents development of outer retinal neovascularization through upregulation of CxCl10

CNTF Prevents Development of Outer Retinal Neovascularization Through Upregulation of CxCl10

Felicitas Bucher,[1,2] Edith Aguilar,[1] Kyle V. Marra,[1,3] Julian Rapp,[2] Jakob Arnold,[2] Sophia Diaz-Aguilar,[1,2] Clemens Lange,[2] Hansjürgen Agostini,[2] Günther Schlunck,[2] Andreas Stahl,[4] and Martin Friedlander[1,5]

[1]Department of Molecular Medicine, The Scripps Research Institute, La Jolla, California, United States
[2]Eye Center, Medical Center, Faculty of Medicine, University of Freiburg, Freiburg, Germany
[3]Department of Bioengineering, University of California, San Diego, San Diego, California, United States
[4]Department of Ophthalmology, University Medical Center Greifswald, Greifswald, Germany
[5]The Lowy Medical Research Institute, La Jolla, California, United States

Correspondence: Martin Friedlander, The Scripps Research Institute, 10550 N Torrey Pines Road, La Jolla, CA 92037, USA; friedlan@scripps.edu.

Received: March 28, 2020
Accepted: June 25, 2020
Published: August 11, 2020

Citation: Bucher F, Aguilar E, Marra KV, et al. CNTF prevents development of outer retinal neovascularization through upregulation of CxCl10. *Invest Ophthalmol Vis Sci.* 2020;61(10):20. https://doi.org/10.1167/iovs.61.10.20

Purpose. Ciliary neurotrophic factor (CNTF) is a well-characterized neurotrophic factor currently in clinical trials for the treatment of macular telangiectasia type II. Our previous work showed that CNTF-induced STAT3 signaling is a potent inhibitor of pathologic preretinal neovascular tuft formation in the mouse model of oxygen-induced retinopathy. In this study, we investigated the effect of CNTF on outer retinal and choroidal angiogenesis and the mechanisms that underpin the observed decrease in outer retinal neovascularization following CNTF treatment.

Methods. In the *Vldlr*$^{-/-}$ and laser-CNV mouse models, mice received a one-time injection (on postnatal day [P] 12 in the *Vldlr*$^{-/-}$ model and 1 day after laser in the Choroidal Neovascularization (CNV) model) of recombinant CNTF or CxCl10, and the extent of neovascular lesions was assessed 6 days posttreatment. STAT3 downstream targets affected by CNTF treatment were identified using quantitative PCR analysis. A proteome array was used to compare media conditioned by CNTF-treated and control-treated primary Müller cells to screen for CNTF-induced changes in secreted angiogenic factors.

Results. Intravitreal treatment with recombinant CNTF led to significant reduction in neovascularization in the *Vldlr*$^{-/-}$ and laser-CNV mouse models. Treatment effect in the *Vldlr*$^{-/-}$ was long-lasting but time sensitive, requiring intravitreal treatment before P19. Mechanistic workup in vitro as well as in vivo confirmed significant activation of the STAT3-signaling pathway in Müller cells in response to CNTF treatment and upregulation of CxCl10. Intravitreal injections of recombinant CxCl10 significantly reduced outer retinal neovascularization in vivo in both the *Vldlr*$^{-/-}$ and laser-CNV mouse models.

Conclusions. CNTF treatment indirectly affects outer retinal and choroidal neovascularization by inducing CxCl10 secretion from retinal Müller cells.

Keywords: CNTF, STAT3, angiogenesis, *Vldlr*$^{-/-}$, Müller cells

Age-related macular degeneration (AMD) and diabetic retinopathy (DR) represent common causes of vision loss in the Western world.[1] Anti-VEGF therapy has revolutionized therapeutic options and visual outcomes of patients with vasoproliferative retinopathy.[2] However, some patients with AMD and DR do not benefit from anti-VEGF therapy, and less common vasoproliferative retinopathies such as macular telangiectasia type I or II (MacTel) are not responsive to anti-VEGF therapy, suggesting that underlying mechanisms of neovascularization in these diseases are not completely understood.[3–5] Further research is necessary to either uncover disease-specific mechanisms, as was recently published for MacTel type II,[6] or to identify other common disease- and VEGF-independent angiomodulatory signaling pathways.

The contributions of the neurovascular unit and chronic inflammation to disease development have repeatedly been stressed.[7–9] Neuroprotective as well as inflammation-modulating therapeutic approaches have shown some success in animal models of proliferative retinopathies and small clinical case series but have not yet been successfully translated into clinical routine.[10,11] Ciliary neurotrophic factor (CNTF) is one of the best-studied neurotrophic agents.[12] As a member of the interleukin 6 cytokine family, CNTF is a strong activator of the JAK/STAT3 signaling pathway that plays a crucial role in the mediation of

Investigative Ophthalmology & Visual Science

inflammatory responses. CNTF binds to CNTF–receptor α (CNTF-Rα), which in turn recruits leukemia inhibiting factor receptor β (LifRβ) and glycoprotein 130 (gp130) as receptor subunits with intracellular signaling domains.[13–15] Formation of this heterotrimeric receptor complex then leads to activation of the JAK/STAT3 signaling pathway and STAT3-dependent gene expression. While LifRβ and gp130 are receptor components expressed on a wide variety of cell types, CNTF-Rα is selectively expressed on distinct cell types, including neuroglial cells in the central nervous system.[16,17]

Multiple preclinical studies provided strong support for the use of CNTF in the treatment of neurodegenerative diseases such as retinitis pigmentosa (RP) or glaucoma.[18–21] Encapsulated cell therapy (ECT) devices load cells into a biocompatible polymer capsule to allow continuous release of therapeutic agents into the vitreous upon implantation within the eye. Implantation of ECT using cells transfected to overexpress CNTF showed promise in reducing photoreceptor loss in mouse models of Retinitis pigmentosa (RP).[22] However, the clinical trial for use of this therapy in the treatment of RP did not meet its primary endpoint.[23] Clinical trial phase II data for the treatment of MacTel type II provided strong evidence that a CNTF-releasing device slows down disease progression.[23,24] Despite the advanced stage of clinical testing, the mechanism of CNTF action in the retina remains elusive.

Preclinical data in the retina have shown that retinal ganglion as well as photoreceptor cells express CNTF-Rα in the retina. Müller cells are also known to respond to CNTF treatment.[25] Rhee et al.[26] showed that CNTF-associated signaling in both photoreceptor and Müller cells is necessary to observe a neuroprotective effect in RP models. In a previous study, we showed that CNTF possessed a strong angiomodulatory effect reducing preretinal neovascularization (NV) in the mouse model of oxygen-induced retinopathy (OIR).[27] This effect could be partially attributed to a direct angiostatic effect of CNTF on vascular endothelial cells in the presence of soluble CNTF-Rα. In the current study, we aimed to elucidate whether the observed angiomodulatory effects of CNTF in OIR were model specific or whether CNTF exhibits a generalized angiostatic effect. The therapeutic effects of CNTF were analyzed in the murine *Vldlr*$^{-/-}$ model of intraretinal neovascularization as well as the laser-CNV model of choroidal NV. In this study, we demonstrated that CNTF strongly improved the vascular phenotype of various in vivo angiogenesis models and investigated indirect mechanisms that contribute to CNTF's angiomodulatory effects. Using gene expression assays of CNTF-treated retinas in vivo and Müller cells in vitro, we identified important CNTF-induced STAT3 downstream targets with an angiomodulatory effect.

Material and Methods

Animal Models

All animal work adhered to the National Institutes of Health (NIH) Guide for the Care and Use of Laboratory Animals. All animal protocols were approved by the Scripps Research Institute IACUC (08-0045-4).

Vldlr$^{-/-}$mice: B6;129S7-*Vldlr*^{tm1Her}/J were purchased from The Jackson Laboratory, Bar Harbor, Maine, US. Mice received intravitreal injections of recombinant protein at different concentrations and time points as specified in the figure legends. To allow for within-animal control, contralateral eyes were used for treatment and control (PBS/0.1% BSA) groups. Recombinant proteins used rat recombinant CNTF (CNTF, #557-NT-050; R&D Systems, Wiesbaden-Nordenstadt, Germany) and recombinant murine CxCl10 (500 ng, #250-16; Peprotech, Hamburg, Germany). Intravitreal injections were performed using a sharp 33-gauge Hamilton needle. Eyes were harvested and prepared for further analysis at time points specified. Retinas were stained with Isolectin GS-B4 (#I21412; ThermoFisher Scientific, Waltham, MA, USA) according to the protocol specified on page 7, inversely flatmounted, and imaged using a confocal laser-scanning microscope (LSM 700 or 710; Zeiss, Oberkochen, Germany). The number of tufts was determined by manual selection of tufts on immunofluorescent images of the inverted flatmounts using the Cell Counter plugin provided by ImageJ (NIH, Bethesda, MD, USA).

The laser-CNV model was performed as previously described.[28] Adult C57BL/6 mice at the age of 6 to 8 weeks received three laser burns per eye using a green Argon laser after anesthesia and pupil dilation. The presence of an air bubble was interpreted as a sign of successful of laser impact. C57BL/6 mice received intravitreal injection of recombinant protein 1 day after laser treatment. Mice received treatment in both eyes (CNTF, mrCxCl10, or PBS/0.1% BSA). Eyes were harvested for choroidal flatmounts 7 days after laser. CNV lesion size was measured by quantification of the CNV area.

For retinal development, C57BL/6 mice were treated with intravitreal injections of CNTF (500 ng) or PBS/0.1% BSA (control) at postnatal day (P) 7. Eyes were harvested 5 days after treatment and prepared for retinal whole mounts. The number of vessel junctions and total vessel length were determined using the AngioTool Software.[29]

Cell Culture

Mouse primary Müller cell cultures were isolated according to a previously published protocol.[30] In brief, retinas from P11 mouse pups were harvested and dissociated using the Papain Dissociation system (#LK003150; Worthington Biochemical Corporation, Lakewood, NJ, USA). Primary Müller cells were expanded in growth medium containing recombinant human endothelial growth factor (100 ng/mL, #PHG0311; Thermo Fisher Scientific), Neurobasal-A medium (#10888022; Thermo Fisher Scientific), N2 Supplement (#17502048; Thermo Fisher Scientific), 10% FBS Superior (#S0615; Merck, Biochrome, Berlin, Germany), L-Glutamine (2 mM, #25030081; Thermo Fisher Scientific), and Pen/Strep (#15140122; Thermo Fisher Scientific) and then transferred to differentiation media containing Neurobasal-A medium (#10888022; Thermo Fisher Scientific), 1% FBS Superior (#S0615; Merck, Biochrome), N2 Supplement (#17502048; Thermo Fisher Scientific), L-Glutamine (2 mM, #25030081; Thermo Fisher Scientific), Pen/Strep (#15140122; Thermo Fisher Scientific), and B27 Supplement (50×, #17504044; Thermo Fisher Scientific) for 7 days. Müller cells at passage P2 were used for immunohistochemistry as well as stimulation experiments. To generate Müller cell-conditioned media, passage P2 primary Müller cells were stimulated with 100 ng/mL CNTF or PBS control for 10 minutes. Cells were washed by PBS, and then fresh differentiation media were added and conditioned for 96 hours after stimulation for use in experiment. Human umbilical vein endothelial cells (HUVECs, #2519A; Lonza,

Basel, Switzerland) were cultured in endothelial growth medium 2 (EGM, #CC-3162; Lonza) and used up to passage P6.

Endothelial Proliferation and Spheroid Sprouting Assays

Cell proliferation was measured using an 3-(4,5-Dimethylthiazol-2-yl)-2,5-diphenyltetrazoliumbromid (MTT) assay according to previously published protocols.[31] In brief, following overnight incubation of HUVECs seeded into a 96-well plate, cells were starved for 24 hours in endothelial basal medium with 4% FBS (EBM, #CC-3121; Lonza, Basel, Switzerland) before stimulation for 72 hours with the following recombinant proteins: recombinant human vascular endothelial growth factor 165b (20 ng/mL, #3045-VE; R&D Systems, Minneapolis, MN, USA), recombinant human fibroblast growth factor–basic (bFGF, 50 ng/mL, #100-18B; Peprotech, Hamburg, Germany), and recombinant human CxCl10 (rhCxCl10, 625 nM, #200-12; Peprotech).

The endothelial spheroid sprouting assay was also performed according to well-established techniques.[32,33] Endothelial spheroids were formed in a hanging drop consisting of 500 HUVECs resuspended in EGM with 10% FBS and 0.25% carboxy-methylcellulose (#M0512; Sigma-Aldrich, Darmstadt, Germany). Spheroids were harvested the following day and 30 spheroids were poured into a 0.5-mL collagen I (1.5 mg/mL final concentration, #354236; Corning, Wiesbaden, Germany) in 24-well plates. Spheroid-containing gel solidified at 37°C for 30 minutes and was then stimulated with 100 µL EBM containing recombinant proteins: VEGF (25 ng/mL, #3045-VE; R&D Systems), bFGF (50 ng/mL, #100-18B; Peprotech), and CxCl10 (537.5 ng/mL, #200-12; Peprotech). Images of single spheroids were taken using an inverted light microscope (Zeiss Axio Vert). Total sprout length was determined by using a self-programmed ImageJ macro where sprouts have to be manually labeled using the "straight-line" tool.

Immunohistochemistry

Eyes were harvested and prepared for immunohistochemical analysis as previously described.[34] In brief, for retinal and choroidal flatmount preparations, eyes were fixed in 4% paraformaldehyde for 40 to 60 minutes on ice and incubated overnight with Isolectin GS-IB4 1:200 (# I21412; Thermo Fisher Scientific). For retinal cross sections, whole eyes were harvested 6 hours after intravitreal treatment, fixed in 2% PFA for 1 hour, and then incubated for 24 hours in 20% sucrose. Sections were fixed with 100% ethanol for 10 minutes followed by permeabilization with 0.3% Triton for 30 minutes and then blocked with 10% BSA for 1 hour. Primary Müller cells were fixed for 5 minutes in 100% methanol at –20°C and permeabilized using 0.3% Triton for 20 minutes. Cells were incubated overnight at 4°C with following primary antibodies: pSTAT3 rabbit mAb (#9145; Cell Signaling Technology, Danvers, MA, USA), chicken anti-mouse Gfap Ab (#ab4674; Abcam, Cambridge, UK), rabbit anti-Kir4.1 (KCNJ10) antibody (#APC-035; Alomone Labs, Jerusalem, Israel), rabbit anti-glutaminsynthetase Ab (#ab73593; Abcam), rabbit anti-mouse CRALBP Ab (#MA1-813; Thermo Fisher Scientific). The following secondary antibodies were used: chicken anti-rabbit 568 (#A-21441; Thermo Fisher Scientific) and goat anti-chicken 488 (#A-32931; Thermo Fisher Scientific).

Table. qPCR Primers

Target	Forward Primer 5' → 3'	Reverse Primer 3' → 5'
mbActin	GGC TGT ATT CCC CTC CAT CG	CCA GTT GGT AAC AAT GCC ATGT
mCebpd	CGACTTCAGCGCCTACA TTGA	GAAGAGGTCGGCGAAG AGTT
mCxCl10	CCAAGTGCTGCCGTCA TTTTC	GGCTCGCAGGGATGAT TTCAA
mSocs3	AGCTGGTGGTGAACG CCGTG	GCGTGCTTCGGGGGT CACTC
mVEGF164	GCCAGCACATAGAGAGA ATGAGC	CAAGGCTCACAGTGATT TTCTGG
mCNTF-Rα	TGTCTACACGCAGAAA CACAG	CCCAGACGCTCATACT GCAC
mLIF-R	TACGTCGGCAGACTCG ATATT	TGGGCGTATCTCTCTC TCCTT
mgp130	CCGTGTGGTTACATCTA CCCT	CGTGGTTCTGTTGATGAC AGTG

Western Blot, Protein Array, and ELISA

For all protein assays, single retinas were lysed in T-Per Buffer (#78519; Thermo Fisher Scientific) containing Phosphatase and Proteinase Inhibitor (#78430 and #78427; Thermo Fisher Scientific). Gel electrophoresis was run under denaturing conditions. Proteins were transferred to a nitrocellulose membrane, blocked with 5% skim milk for 1 hour, and incubated overnight at 4°C with the following antibodies: pSTAT3 rabbit mAb (#9145; Cell Signaling Technology), STAT3 (79D7) rabbit mAb (#4904; Cell Signaling), and anti-bActin Ab (#A1978; Sigma, St. Louis, MO, USA).

Müller cell-conditioned media were analyzed using the Mouse Angiogenesis Array Kit Proteome Profiler (#ARY015; R&D Systems). CxCl10 levels were determined using the mouse IP-10 ELISA Kit (CxCl10) (ab214563; Abcam).

Quantitative PCR, mRNA Array

mRNA was isolated according to the manufacturer's instructions using the miRNAeasy Kit (#217004; Qiagen, Hilden, Germany) and transcribed into cDNA using the High Capacity cDNA Reverse Transcription Kit (#4368814; Thermo Fisher Scientific). The following primers were used for quantitative PCR (qPCR) in the Table.

The RT^2 PCR Profiler PCR Array Mouse Il6/STAT3 signaling pathway (#PAMM-160Z; Qiagen) was used for mRNA array analysis.

Statistics

All graphs are presented as scatterplots. For in vivo experiments, graphs represent mean ± SEM. Statistical tests were applied as outlined in the figure legends. For qPCR analyses, graphs are plotted as mean ± 95% CI. Statistical tests were performed on delta Cycle Threshold (dCT) values to determine statistical significance.

For qPCR analysis, graphs plot mean ± CI. Statistical significance was determined using a two-tailed Student's *t*-test run on the dCT values. A P value <0.05 was considered statistically significant.

Results

Our previous studies have shown that CNTF has a potent effect in preventing the development of hypoxia-induced preretinal neovascularization.[27] It remains unclear whether this observed result represents a disease-specific effect of CNTF modulating the inner vascular plexus or if CNTF exerts a general antiangiogenic effect that also applies to the outer retina. To address this question, we tested recombinant rat CNTF in multiple angiogenesis models in the eye.

CNTF Prevents NV Development in the *Vldlr*$^{-/-}$ Model

In the *Vldlr*$^{-/-}$ model, a well-established model for retinal angiomatous proliferation, retinal neovascularization originates from the deep and intermediate vascular plexus and dives down to the choroid to form retinal-choroidal anastomoses most likely due to a metabolic defect.[35,36] When *Vldlr*$^{-/-}$ mice were treated with intravitreal injections of 500 ng CNTF at P12 before the onset of NV formation, the amount of NV at P18 is decreased by 60% in the CNTF-treated group compared to controls (Fig. 1A). However, treatment with lower concentrations of CNTF (5 ng) did not prevent intraretinal NV formation. Despite the short half-life of the recombinant protein, the treatment effect of CNTF injected at P12 was even more pronounced 22 days postinjection (P34), represented by a 75% decrease in NV in CNTF-treated eyes compared to controls (Fig. 1B). Delayed treatment with intravitreal CNTF at P19, a timepoint when NV are fully established, did not induce a decrease in intraretinal NV at P34.

CNTF Prevents CNV Development and Delays Formation of the Vascular Deep Plexus

In the laser-CNV model, retinal photocoagulation with an Argon laser induces choroidal neovascularization. Intravitreal injections of 500 ng CNTF 1 day postlaser significantly decreased CNV formation 7 days postlaser (Fig. 1C) while 5 ng CNTF again failed to provide a rescue effect. CNTF, therefore, strongly interferes with the development of pathologic neovascularization originating from the superficial[27] and deep retinal vascular plexus as well as the choroidal plexus in various retinal disease models. Given these data suggesting that CNTF has generalized antiangiogenic effects on vasculature throughout the retina, we hypothesized that CNTF also affects the retinal vascular development. To test this hypothesis, CNTF was injected intravitreally into wild-type mice at P7 and deep plexus formation was analyzed at P12. Figure 1D shows that injection of CNTF significantly delayed the formation of the deep vascular plexus at P12, confirming that CNTF affects angiogenesis during retinal development as well as in retinal disease.

CNTF Treatment Induces Long-Term Activation of the Jak/STAT3 Signaling Pathway in the *Vldlr*$^{-/-}$ Model

Considering the short half-life of CNTF when administered as recombinant protein,[27,37] the long-lasting effect of CNTF treatment on attenuating NV development in the *Vldlr*$^{-/-}$ model was unexpected. Since Jak/STAT3 signaling is strongly activated through CNTF, we hypothesized this signaling axis to play a role in mediating the long-lasting angiostatic effect of CNTF in vivo. In the *Vldlr*$^{-/-}$ model, intravitreal CNTF injections significantly increased levels of phosphorylated STAT3 (pSTAT3) in whole retinal lysates as soon as 6 hours after treatment in comparison to PBS/BSA-treated controls (Fig. 2A). Levels of STAT3 remained significantly elevated at 6 days after intravitreal injection of CNTF. The levels of pSTAT3 trended higher in CNTF-treated mice relative to controls at 6 days, but this comparison did not reach statistical significance as there was increased pSTAT3 expression in control-treated eyes. During retinal development, increased protein levels of pSTAT3 were detected at P32 but not P17 (Supplementary Fig. S1B), suggesting that there is no endogenous activation of the STAT3 signaling pathway before P18. On qPCR, expression levels of CNTF and STAT3 increased over time while the JAK inhibitor of STAT3, known as suppressor of cytokine signaling 3 (SOCS3), was downregulated (Supplementary Fig. S1A).

Next, we used a STAT3-target mRNA gene expression array to screen for important downstream genes regulated by CNTF treatments. Figure 2B shows all downstream genes that were upregulated more than twofold following CNTF treatment 24 hours and 6 days postinjection. Compared to the control-treated group, the most strongly upregulated genes in total retinal lysates 24 hours after CNTF injection included C-X-C motif chemokine ligand 10 (CxCl10), SOCS3, and CCAAT enhancer binding protein delta (Cebpd), a bZIP transcription factor involved in inflammatory responses.[38] CxCl10 remained one of the most strongly upregulated STAT3-target genes 6 days after CNTF treatment. qPCR analysis confirmed that CxCl10 and SOCS3 were both significantly upregulated over time while VEGF levels remained unaffected (Fig. 2C).

Müller Cells Respond to CNTF Treatment

To identify CNTF-responsive cells in CNTF-treated *Vldlr*$^{-/-}$ mice, we used pSTAT3 as an immunohistochemical marker in retinal cryosections. Figure 3A shows that pSTAT3 staining was detected in the superficial vascular plexus, as previously reported,[27] as well as the inner nuclear layer (INL), where Müller cells are located.[39] Next, we tested the effect of CNTF on Müller cells in vitro using primary murine Müller cell cultures. On immunohistochemistry, primary murine Müller cells were identified by positive glutamine synthetase, inward rectifying potassium channel 4.1 (Kir4.1), and *cis*-retinaldehyde binding protein (CRALBP) staining (Supplementary Fig. S2A). These cells expressed gp130, LifRβ, and CNTF-Rα at the mRNA level in vitro (Supplementary Fig. S2B). CNTF treatment strongly activated pSTAT3 signaling in primary Müller cell cultures (Fig. 3B). Similar to their expression levels in vivo, CxCl10 and SOCS3 were strongly upregulated in CNTF-treated Müller cells on qPCR, whereas VEGF164 levels were mildly altered (Fig. 3C). To further investigate the CNTF-induced changes in the Müller cell secretome, conditioned media from CNTF- and control-treated primary Müller cells were screened using the Mouse Angiogenesis Proteome Profiler (for a complete list of analytes contained on this array, please refer to Supplementary Table S1). As shown by the representative Proteome arrays in Figure 3D, the protein level of CxCl10 was higher in media conditioned by CNTF-treated Müller cells than control-treated cells. Quantitative analysis using ELISA confirmed that CxCl10 was significantly increased in CNTF-treated Müller cell-conditioned media. Taken together,

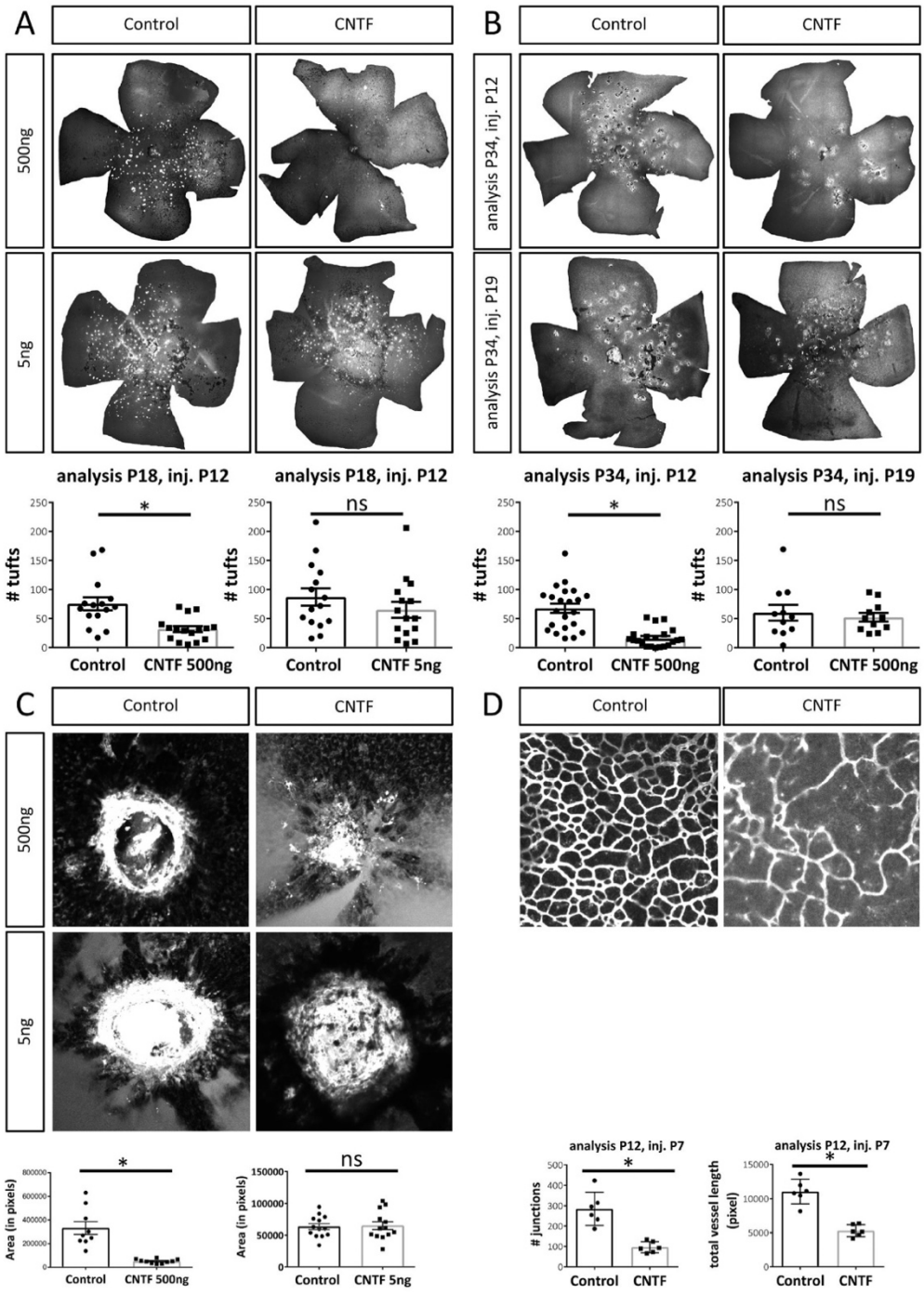

Figure 1. CNTF affects angiogenesis in the eye. (**A**) Representative flatmounts and quantification of NV tufts in *Vldlr*$^{-/-}$ mice at P18 following intravitreal treatment with 500 ng CNTF or 5 ng CNTF at P12. *n* (500 ng) = 16 mice, *n* (5 ng) = 15 mice, two-sided Student's *t*-test: *$P < 0.05$. (**B**) Representative flatmounts and quantification of intraretinal NV in *Vldlr*$^{-/-}$ mice at P34 following intravitreal injections of 500 ng CNTF at P12 or P19. *n* (P34 inj P12) = 21 mice, *n* (P34 inj P19) = 11 mice, two-sided Student's *t*-test: *$P < 0.05$. (**C**) Representative images and

quantified area of CNV lesions 7 days after laser injury following intravitreal injections of 500 ng or 5 ng CNTF 1 day after laser treatment. n (500 ng) = 10 retinas, n (5 ng) = 13 retinas, two-sided Student's t-test: $^*P < 0.05$. (**D**) Representative flatmounts and quantification of deep vascular plexus formation by the number of junctions at P12 following CNTF treatment (500 ng) at P7. $n = 6$ mice, two-sided Student's t-test: $^*P < 0.05$.

these data suggest that Müller cells increase secretion of CxCl10 in response to CNTF treatment.

CxCl10 Has an Angiostatic Effect in Vasoproliferative Disease Models of the Eye

CxCl10 is an interferon-inducible chemokine best known for its chemoattractant effect on T cells and leukocytes. CxCl10 has previously been shown to have angiostatic properties as well.[40,41] Based on our results showing that CNTF increases CxCl10 expression in retinal Müller cells, we hypothesized that Müller cell–secreted CxCl10 may be an important factor mediating the CNTF-induced angiostatic effect in retinal vasoproliferative disease models. In vitro, we confirmed that CxCl10 significantly inhibits endothelial cell proliferation and endothelial cell sprouting (Figs. 4A, 4B). This angiostatic effect was not limited to VEGF-induced sprouting but was also observed in bFGF-induced sprouting. In vivo, intravitreal injections of CxCl10 into *Vldlr*$^{-/-}$ mice at P12 led to a significant decrease in intraretinal NV at P18 (Fig. 4C). The angiostatic effect of CxCl10 was confirmed in the laser-CNV model where CxCl10-injected eyes demonstrated significantly smaller CNV lesions in comparison to control-treated eyes (Fig. 4D). These data show that CxCl10 has an angiostatic effect in the retina and support our hypothesis that CxCl10 is one of the factors mediating the CNTF-induced angiostatic effect in vasoproliferative retinal diseases.

Discussion

CNTF showed a significant treatment effect in multiple disease models of retinal angiogenesis (OIR, *Vldlr*$^{-/-}$ mice, laser-CNV) originating from different vascular layers and driven by distinct mechanisms. This observation suggests that the antiangiogenic properties of CNTF are attributable to a general effect rather than a disease-specific effect. To our knowledge, no other reports on CNTF's antiangiogenic properties outside the eye have been published, although Pasquin et al.[42] have recently shown that cardiotrophin-like cytokine factor 1, another CNTF-Rα ligand signaling through STAT3, also exerts a strong angiomodulatory effect in the OIR model. In comparison to our previously published observation that 5 ng CNTF significantly reduced preretinal NV in the OIR model, in our current study, higher CNTF concentrations were necessary to induce significant treatment effects in angiogenesis models of the outer retina and choroid.[27] This may be explained by the short half-life of the recombinant protein, which may lead to significantly lower CNTF concentrations in the outer retina compared to the vitreoretinal interface. Extensive dose-response experiments and determination of CNTF levels in the outer retina and choroid following intravitreal CNTF injections would be necessary to further address this hypothesis, although the variability of in vivo models may make the characterization of dose-response effects cumbersome.

In the *Vldlr*$^{-/-}$ model, CNTF showed a long-term treatment effect (Fig. 1B) that may be explained by its sustained activation of the Jak/STAT3 signaling pathway (Figs. 2A, 2B). The therapeutic success seems, however, to be time sensitive since significant reduction of NV was observed when CNTF was injected at P12 but not at P19 (Fig. 1B). Considering the fact that intraretinal NV in the *Vldlr*$^{-/-}$ model starts to develop around P14, CNTF prevented the development of NV but was not able to induce regression of preexisting NV. While retinal neovascular abnormalities spontaneously regress in the OIR and CNV model, the *Vldlr*$^{-/-}$ model is characterized by neovascular changes that persist over the long term.[35,43] Since the long-term effect of CNTF on the vascular phenotype was observed solely in the *Vldlr*$^{-/-}$ model in this study, our data cannot definitively conclude whether these prolonged effects are transferrable to other disease models of angiogenesis or are specific to the *Vldlr*$^{-/-}$ vasculopathy.

The short half-life of CNTF as recombinant protein has been well characterized,[37] whereas the long-lasting activation of that STAT3-signaling pathway in vivo is a novel observation. Rhee et al.[44] described a rapid decline in pSTAT3 levels in CNTF-treated dissociated P0 retinal cells after 90 minutes of treatment. The difference between these data and our results may lie in the difference between their ex vivo experimental setup on retinal tissue versus our in vivo design or the differences in time point of treatment (P0 versus P12), which greatly affects the status of retinal maturation.

In our previous work, we identified SOCS3 as a CNTF-induced endogenous inhibitor of cell proliferation in vascular endothelial cells.[27] Multiple studies have shown that Müller cells also respond to CNTF treatment with activation of the STAT3 signaling pathway, which corroborates our current findings in vivo as well as in vitro (Figs. 3A, 3B).[25,26,45] Immunohistochemical staining of pSTAT3 in retinal cryosections following CNTF treatment suggests that multiple retinal cell types, including Müller cells, respond to CNTF (Fig. 3A). While only a few bright nuclear pSTAT3 signals can be identified in the INL and ganglion cell layer (GCL), direct comparison of the control and CNTF-treated sample indicates a general shift in the pSTAT3 staining pattern from a nonspecific cytoplasmic labelling pattern in the control-treated sample to a more pronounced nuclear staining pattern in a variety of cell types within the INL and GCL in the CNTF-treated sample. We believe that this widespread pronounced nuclear label represents a positive response of multiple cell types to CNTF treatment. The difference between the clear increase in pSTAT3 signal in CNTF-treated samples in Western blot analysis and the moderate increase in nuclear pSTAT3 labeling in multiple cell types by immunohistochemistry may be explained by the technical challenges that come with immunohistochemical detection of phosphorylated proteins. These challenges include a different detection threshold when using immunohistochemistry as compared to Western blot analysis. In CNTF-treated samples, less pronounced nuclear pSTAT3 labels could be found throughout different layers of the INL, suggesting that multiple cell types in the INL respond to CNTF. Since the immunohistochemical images we have provided only allow for indirect identification of CNTF-responsive cells based on the nuclear localization in

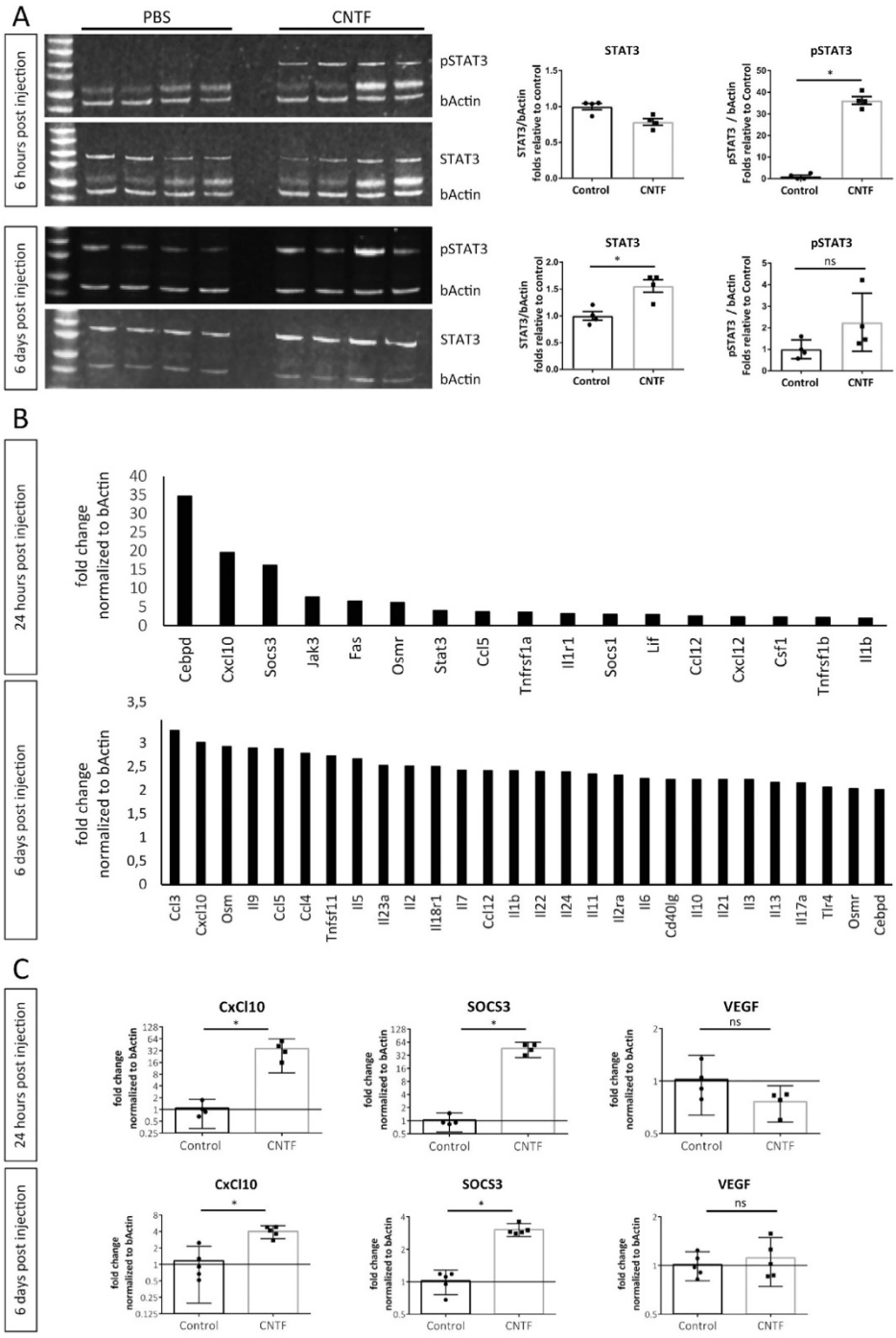

Figure 2. CNTF induces long-term activation of the Jak/STAT3 signaling pathway in *Vldlr*$^{-/-}$ mice. (**A**) pSTAT3, STAT3, and β-actin levels of retinal lysate 6 hours or 6 days after intravitreal injections with 500 ng CNTF or PBS/BSA vehicle control. Each column represents one biological replicate. $n = 4$ mice per group and time point. *$P < 0.05$, two-tailed Mann-Whitney test. (**B**) STAT3 targets upregulated more than twofold following 24 hours and 6 days after CNTF treatment identified using a STAT3 mRNA array on whole retinal lysates. $n = 3$ mice per group and per time point. (**C**) qPCR analysis of selected targets genes comparing expression levels between CNTF and control-treated eyes. $n = 4$–5 mice per group and per time point. Two-sided Student's *t*-test: *$P < 0.05$. All experiments were performed in the *Vldlr*$^{-/-}$ model.

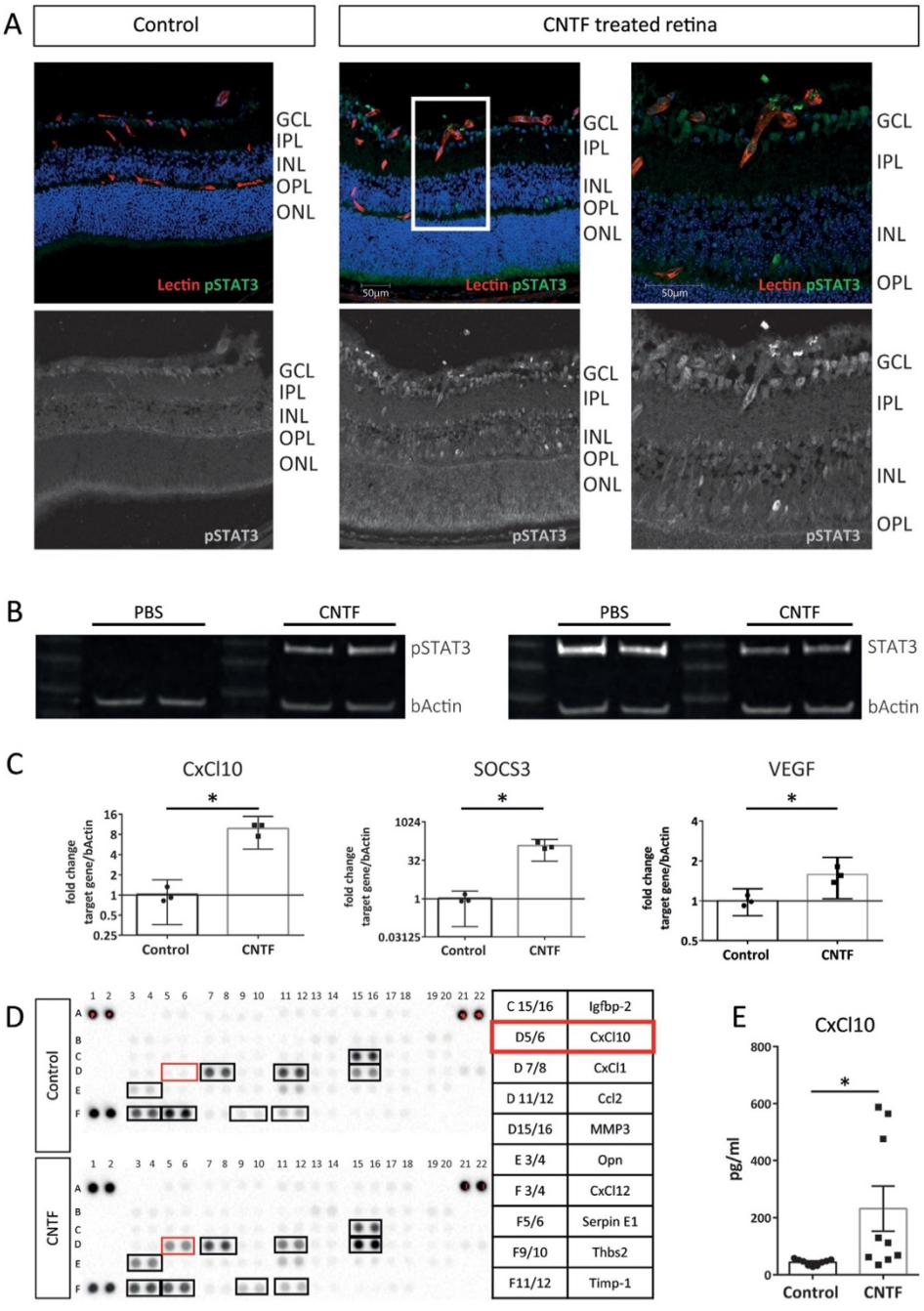

Figure 3. CNTF activates the JAK/STAT3 signaling pathway in Müller cells. (**A**) Immunohistochemical staining for pSTAT3 as a marker for STAT3 activation in retinal cryosections following CNTF treatment compared to untreated controls. (**B**) Western blot analysis for pSTAT3 levels in primary Müller cells 10 minutes after exposure to CNTF compared to untreated controls. (**C**) qPCR analysis shows gene expression of selected STAT3 target genes in primary Müller cells 1 hour post-CNTF treatment. Graphs show representative results of three independent experiments. Two-sided Student's *t*-test: $^*P < 0.05$. (**D**) Proteome profiler Mouse Angiogenesis Array comparing Müller cell–conditioned media of CNTF-treated Müller cells versus PBS control-treated cells. Opn, osteopontin; Thbs2, thrombospondin; $n = 1$ assay. (**E**) ELISA assay quantifying CxCl10 levels in Müller cell–conditioned media with and without CNTF treatment. $n = 9$ samples, two-sided Student's *t*-test: $^*P < 0.05$.

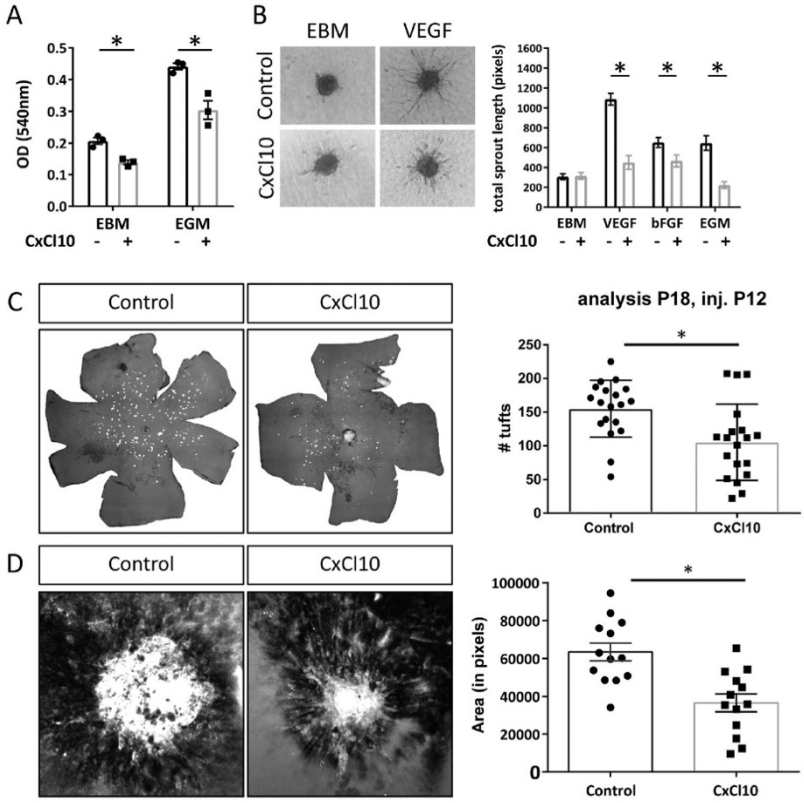

Figure 4. CxCl10 inhibits endothelial cell proliferation in vitro and in vivo. (**A**) MTT assay results of HUVECs after exposure to CxCl10 (537.5 ng/mL) under basal (EBM) and growth (EGM) stimulating conditions. $n = 3$ independent experiments, two-way ANOVA, $^*P < 0.05$. (**B**) Endothelial cell sprouting of HUVECs in response to CxCl10 (537.5 ng/mL) under diverse proangiogenic stimuli ($n = 14$–28 spheroids per group, two-way ANOVA, $^*P < 0.05$). (**D**) NV at P18 following intravitreal injection of CxCl10 (500 ng) in *Vldlr*$^{-/-}$ at P12. $n = 19$ mice, two-sided Student's *t*-test: $^*P < 0.05$. (**E**) CNV area 7 days postlaser following intravitreal injection of CxCl10 (500 ng) 1 day after laser treatment. $n = 13$ eyes, two-sided Student's *t*-test: $^*P < 0.05$.

the INL that correspond to the nuclear localization of Müller cells and horizontal cells, in vitro experiments were necessary to elucidate the role of Müller cells in CNTF's angiomodulatory effect in the retina (Figs. 3B–3E, Supplementary Fig. S2). In this study, we chose to focus on the interaction of Müller glia and endothelial cells in the context of CNTF treatment; further studies will be necessary to investigate the role of neuronal cells of the INL and GCL (including ganglion cells) that are likely to contribute to the overall angiomodulatory effect of CNTF on the retina based on the observed widespread pSTAT3 signal in retina cryosections.

To characterize the molecular mechanism by which Müller cells activated by CNTF act on vascular endothelial cells, we ran an mRNA array on CNTF-treated whole retina lysates and compared the results with the results of a semiquantitative proteome profiler array of Müller cell–conditioned media following CNTF treatment. CxCl10 was strongly upregulated in both assays. These data were consistent with a study by Xue et al.,[46] who identified CxCl10 as one of multiple genes upregulated in sorted Müller cells following intravitreal treatment with CNTF. Interestingly, results on VEGF levels following CNTF treatment were inconsistent between in vivo and in vitro settings showing unaltered VEGF levels in vivo (Fig. 2C) and a 1.5-fold increase in VEGF levels in vitro (Fig. 3C). Our in vivo data are consistent with findings from previous study results in the OIR model showing no increase in retinal VEGF following CNTF treatment.[27] The modest VEGF increase in Müller cells in response to CNTF treatment may not be detectable in vivo since VEGF levels are determined in whole retinal lysates, where Müller cells represent only a small fraction of the total cell population. Taken together, these data support that CxCl10 may be an important mediator of CNTF's indirect Müller cell–mediated angiostatic effect on vascular endothelial cells.

While our mRNA array yielded results consistent with STAT3 activation following CNTF treatment, this study was limited to identifying established STAT3 targets like CxCl10. Other techniques such as RNA-Seq analysis or liquid chromatography/mass spectrometry on Müller cell–conditioned media will be necessary to identify further CNTF-induced STAT3 targets.

CxCl10's angiostatic effect has been well established, but its role in the retina remains unclear.[40,47] Increased levels of CxCl10 were found in the aqueous humor of patients with age-related macular degeneration.[48] Nawaz et al.,[49] however, found an association between levels of CxCl10 and resolution of angiogenesis with induction of fibrosis in patients with diabetic retinopathy. Ha et al.[50] suggested a role of CxCl10 in retinal inflammation and oxidative stress in response to retinal ischemia. Gao et al.[51] postulated an angiostatic effect of CxCl10 in inflamed corneas. Our data show that CxCl10 is capable of inhibiting retinal as well as choroidal neovascularization (Figs. 4C, 4D). These data align with results from Fujimura et al.,[52] who showed that loss of the CxCl10 receptor CxCR3 leads to an increase in NV area in the laser-CNV model. Interestingly, the observed CxCl10 treatment effect in the *Vldlr*$^{-/-}$ model as well as the laser-CNV model was smaller than the CNTF-induced treatment effects (Fig. 1A). In the *Vldlr*$^{-/-}$ model, the number of tufts was reduced to 42% (normalized to the mean of the control group) in CNTF-treated eyes compared to 68% in CxCl10-treated eyes. Normalized to the mean CNV area of the control-treated group of the laser-CNV model, the mean CNV area was reduced 85% in the CNTF-treated group and reduced 32% in the CxCl10-treated group. This clearly supports the hypothesis that Müller cell–secreted CxCl10 is one of the multiple factors besides endothelial SOCS3 that mediate CNTF's angiostatic effect in retinal vasoproliferative disease.

Acknowledgments

The authors thank Marc Guder (Eye Centre, University of Freiburg) as well as Mauricio Rosenfeld (The Scripps Research Institute) for excellent technical support.

Supported by grants to MF from the National Eye Institute (R01 EY11254 and R24 EY022025) and the Lowy Medical Research Institute (MacTel). FB was supported by the German Research Foundation (Bu3135/1-1) and the Dr. Werner-Jackstädt-Nachwuchspreis of the German Retina Society. KVM was supported by the National Eye Institute (F30 EY029131-01) and the University of California, San Diego Medical Scientist Training Program (T32 GM007198-40).

Disclosure: **F. Bucher**, None; **E. Aguilar**, None; **K.V. Marra**, None; **J. Rapp**, None; **J. Arnold**, None; **S. Diaz-Aguilar**, None; **C. Lange**, None; **H. Agostini**, None; **G. Schlunck**, None; **A. Stahl**, None; **M. Friedlander**, None

References

1. Bourne RR, Stevens GA, White RA, et al. Causes of vision loss worldwide, 1990–2010: a systematic analysis. *Lancet Global Health*. 2013;1:e339–e349.
2. Cheung N, Wong IY, Wong TY. Ocular anti-VEGF therapy for diabetic retinopathy: overview of clinical efficacy and evolving applications. *Diabetes Care*. 2014;37:900–905.
3. Krebs I, Glittenberg C, Ansari-Shahrezaei S, Hagen S, Steiner I, Binder S. Non-responders to treatment with antagonists of vascular endothelial growth factor in age-related macular degeneration. *Br J Ophthalmol*. 2013;97:1443–1446.
4. Suzuki M, Nagai N, Izumi-Nagai K, et al. Predictive factors for non-response to intravitreal ranibizumab treatment in age-related macular degeneration. *Br J Ophthalmol*. 2014;98:1186–1191.
5. Chatziralli IP, Sharma PK, Sivaprasad S. Treatment modalities for idiopathic macular telangiectasia: an evidence-based systematic review of the literature. *Semin Ophthalmol*. 2017;32:384–394.
6. Gantner ML, Eade K, Wallace M, et al. Serine and lipid metabolism in macular disease and peripheral neuropathy. *N Engl J Med*. 2019;381:1422–1433.
7. Ambati J, Atkinson JP, Gelfand BD. Immunology of age-related macular degeneration. *Nat Rev Immunol*. 2013;13:438–451.
8. Tang J, Kern TS. Inflammation in diabetic retinopathy. *Prog Retinal Eye Res*. 2011;30:343–358.
9. Gardner TW, Davila JR. The neurovascular unit and the pathophysiologic basis of diabetic retinopathy. *Graefe Arch Clin Exp Ophthalmol*. 2017;255:1–6.
10. Pardue MT, Allen RS. Neuroprotective strategies for retinal disease. *Prog Retinal Eye Res*. 2018;65:50–76.
11. Rubsam A, Parikh S, Fort PE. Role of inflammation in diabetic retinopathy. *Int J Mol Sci*. 2018;19:942.
12. Wen R, Tao W, Li Y, Sieving PA. CNTF and retina. *Prog Retinal Eye Res*. 2012;31:136–151.
13. Stahl N, Yancopoulos GD. The tripartite CNTF receptor complex: activation and signaling involves components shared with other cytokines. *J Neurobiol*. 1994;25:1454–1466.
14. Stahl N, Boulton TG, Farruggella T, et al. Association and activation of Jak-Tyk kinases by CNTF-LIF-OSM-IL-6 beta receptor components. *Science*. 1994;263:92–95.
15. Elson GC, Lelievre E, Guillet C, et al. CLF associates with CLC to form a functional heteromeric ligand for the CNTF receptor complex. *Nat Neurosci*. 2000;3:867–872.
16. Ip NY, McClain J, Barrezueta NX, et al. The alpha component of the CNTF receptor is required for signaling and defines potential CNTF targets in the adult and during development. *Neuron*. 1993;10:89–102.
17. Davis S, Aldrich TH, Valenzuela DM, et al. The receptor for ciliary neurotrophic factor. *Science*. 1991;253:59–63.
18. LaVail MM, Unoki K, Yasumura D, Matthes MT, Yancopoulos GD, Steinberg RH. Multiple growth factors, cytokines, and neurotrophins rescue photoreceptors from the damaging effects of constant light. *Proc Natl Acad Sci USA*. 1992;89:11249–11253.
19. Pease ME, Zack DJ, Berlinicke C, et al. Effect of CNTF on retinal ganglion cell survival in experimental glaucoma. *Invest Ophthalmol Vis Sci*. 2009;50:2194–2200.
20. Lipinski DM, Barnard AR, Singh MS, et al. CNTF gene therapy confers lifelong neuroprotection in a mouse model of human retinitis pigmentosa. *Mol Therapy*. 2015;23:1308–1319.
21. Li Y, Tao W, Luo L, et al. CNTF induces regeneration of cone outer segments in a rat model of retinal degeneration. *PLoS One*. 2010;5:e9495.
22. Tao W, Wen R, Goddard MB, et al. Encapsulated cell-based delivery of CNTF reduces photoreceptor degeneration in animal models of retinitis pigmentosa. *Invest Ophthalmol Vis Sci*. 2002;43:3292–3298.
23. Birch DG, Weleber RG, Duncan JL, Jaffe GJ, Tao W. Randomized trial of ciliary neurotrophic factor delivered by encapsulated cell intraocular implants for retinitis pigmentosa. *Am J Ophthalmol*. 2013;156:283–292.e281.
24. Chew EY, Clemons TE, Jaffe GJ, et al. Effect of ciliary neurotrophic factor on retinal neurodegeneration in patients with macular telangiectasia type 2: a randomized clinical trial. *Ophthalmology*. 2019;126:540–549.
25. Wen R, Song Y, Kjellstrom S, et al. Regulation of rod phototransduction machinery by ciliary neurotrophic factor. *J Neurosci*. 2006;26:13523–13530.

26. Rhee KD, Nusinowitz S, Chao K, Yu F, Bok D, Yang XJ. CNTF-mediated protection of photoreceptors requires initial activation of the cytokine receptor gp130 in Muller glial cells. *Proc Natl Acad Sci USA*. 2013;110:E4520–E4529.
27. Bucher F, Walz JM, Buhler A, et al. CNTF attenuates vasoproliferative changes through upregulation of SOCS3 in a mouse-model of oxygen-induced retinopathy. *Invest Ophthalmol Vis Sci*. 2016;57:4017–4026.
28. Lambert V, Lecomte J, Hansen S, et al. Laser-induced choroidal neovascularization model to study age-related macular degeneration in mice. *Nat Protocols*. 2013;8:2197–2211.
29. Zudaire E, Gambardella L, Kurcz C, Vermeren S. A computational tool for quantitative analysis of vascular networks. *PLoS One*. 2011;6:e27385.
30. Ueki Y, Karl MO, Sudar S, et al. P53 is required for the developmental restriction in Muller glial proliferation in mouse retina. *Glia*. 2012;60:1579–1589.
31. Mosmann T. Rapid colorimetric assay for cellular growth and survival: application to proliferation and cytotoxicity assays. *J Immunol Methods*. 1983;65:55–63.
32. Korff T, Augustin HG. Tensional forces in fibrillar extracellular matrices control directional capillary sprouting. *J Cell Sci*. 1999;112(pt 19):3249–3258.
33. Buehler A, Sitaras N, Favret S, et al. Semaphorin 3F forms an anti-angiogenic barrier in outer retina. *FEBS Lett*. 2013;587:1650–1655.
34. Banin E, Dorrell MI, Aguilar E, et al. T2-TrpRS inhibits preretinal neovascularization and enhances physiological vascular regrowth in OIR as assessed by a new method of quantification. *Invest Ophthalmol Vis Sci*. 2006;47:2125–2134.
35. Dorrell MI, Aguilar E, Jacobson R, et al. Antioxidant or neurotrophic factor treatment preserves function in a mouse model of neovascularization-associated oxidative stress. *J Clin Invest*. 2009;119:611–623.
36. Joyal JS, Sun Y, Gantner ML, et al. Retinal lipid and glucose metabolism dictates angiogenesis through the lipid sensor Ffar1. *Nat Med*. 2016;22:439–445.
37. Dittrich F, Thoenen H, Sendtner M. Ciliary neurotrophic factor: pharmacokinetics and acute-phase response in rat. *Ann Neurol*. 1994;35:151–163.
38. Balamurugan K, Sterneck E. The many faces of C/EBPdelta and their relevance for inflammation and cancer. *Int J Biol Sci*. 2013;9:917–933.
39. Bringmann A, Pannicke T, Grosche J, et al. Muller cells in the healthy and diseased retina. *Prog Retinal Eye Res*. 2006;25:397–424.
40. Luster AD, Greenberg SM, Leder P. The IP-10 chemokine binds to a specific cell surface heparan sulfate site shared with platelet factor 4 and inhibits endothelial cell proliferation. *J Exp Med*. 1995;182:219–231.
41. Angiolillo AL, Sgadari C, Taub DD, et al. Human interferon-inducible protein 10 is a potent inhibitor of angiogenesis in vivo. *J Exp Med*. 1995;182:155–162.
42. Pasquin S, Chehboun S, Dejda A, et al. Effect of human very low-density lipoproteins on cardiotrophin-like cytokine factor 1 (CLCF1) activity. *Sci Rep*. 2018;8:3990.
43. Hu W, Jiang A, Liang J, et al. Expression of VLDLR in the retina and evolution of subretinal neovascularization in the knockout mouse model's retinal angiomatous proliferation. *Invest Ophthalmol Vis Sci*. 2008;49:407–415.
44. Rhee KD, Goureau O, Chen S, Yang X-J. Cytokine-induced activation of signal transducer and activator of transcription in photoreceptor precursors regulates rod differentiation in the developing mouse retina. *J Neurosci*. 2004;24:9779–9788.
45. Peterson WM, Wang Q, Tzekova R, Wiegand SJ. Ciliary neurotrophic factor and stress stimuli activate the Jak-STAT pathway in retinal neurons and glia. *J Neurosci*. 2000;20:4081–4090.
46. Xue W, Cojocaru RI, Dudley VJ, Brooks M, Swaroop A, Sarthy VP. Ciliary neurotrophic factor induces genes associated with inflammation and gliosis in the retina: a gene profiling study of flow-sorted, Muller cells. *PLoS One*. 2011;6:e20326.
47. Campanella GSV, Colvin RA, Luster AD. CXCL10 can inhibit endothelial cell proliferation independently of CXCR3. *PLoS One*. 2010;5:e12700.
48. Liu F, Ding X, Yang Y, et al. Aqueous humor cytokine profiling in patients with wet AMD. *Mol Vis*. 2016;22:352–361.
49. Nawaz MI, Van Raemdonck K, Mohammad G, et al. Autocrine CCL2, CXCL4, CXCL9 and CXCL10 signal in retinal endothelial cells and are enhanced in diabetic retinopathy. *Exp Eye Res*. 2013;109:67–76.
50. Ha Y, Liu H, Xu Z, et al. Endoplasmic reticulum stress-regulated CXCL10/CXCR3 pathway mediates inflammation and neuronal injury after retinal ischemia. *Invest Ophthalmol Vis Sci*. 2014;55:2178–2178.
51. Gao N, Liu X, Wu J, et al. CXCL10 suppression of hem- and lymph-angiogenesis in inflamed corneas through MMP13. *Angiogenesis*. 2017;20:505–518.
52. Fujimura S, Takahashi H, Yuda K, et al. Angiostatic effect of CXCR3 expressed on choroidal neovascularization. *Invest Ophthalmol Vis Sci*. 2012;53:1999–2006.

Figure S1

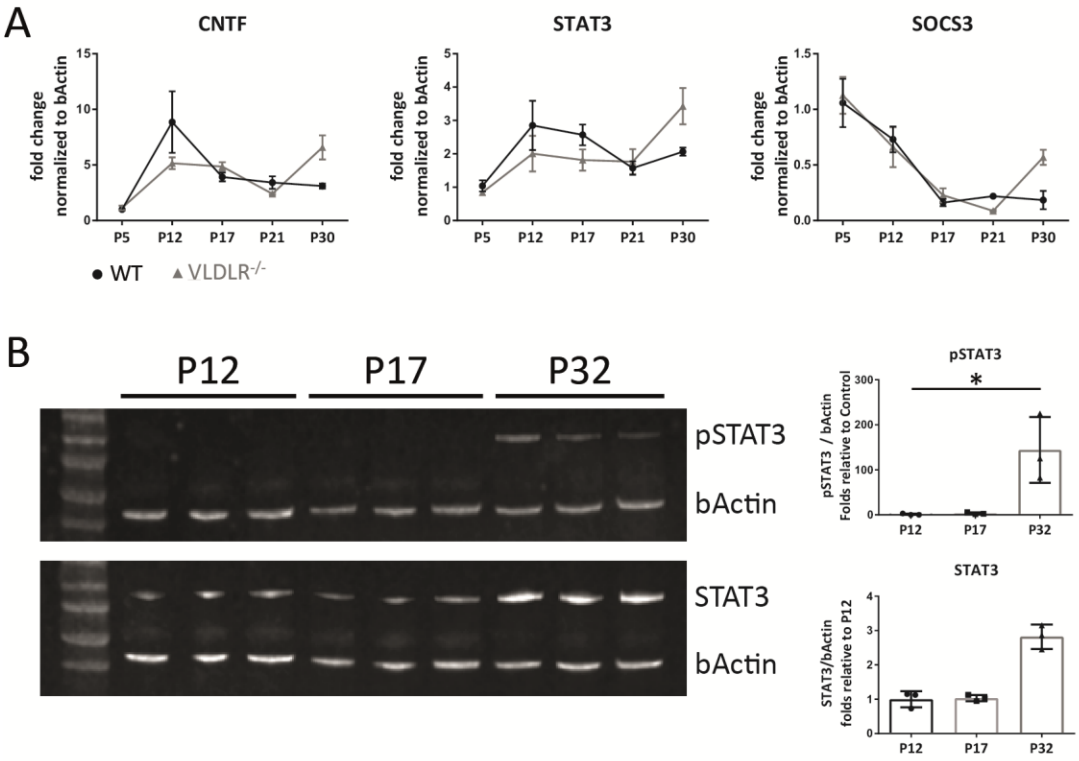

Supplemental Figure S1. Endogenous regulation of CNTF/STAT3 signaling during retinal maturation in the VLDLR -/- model. (A) mRNA expression levels of CNTF, STAT3, and SOCS3 at multiple time points during retinal development normalized to P5. N=4 mice per group and time-point. (B) Western blot analysis of STAT3 and pSTAT3 levels at P12, P17and P32. Each column represents a biological replicate. N = 3 mice per group and time-point. Kruskal-Wallis Test with Dunn's multiple comparisons test, * $p<0.05$.

Figure S2

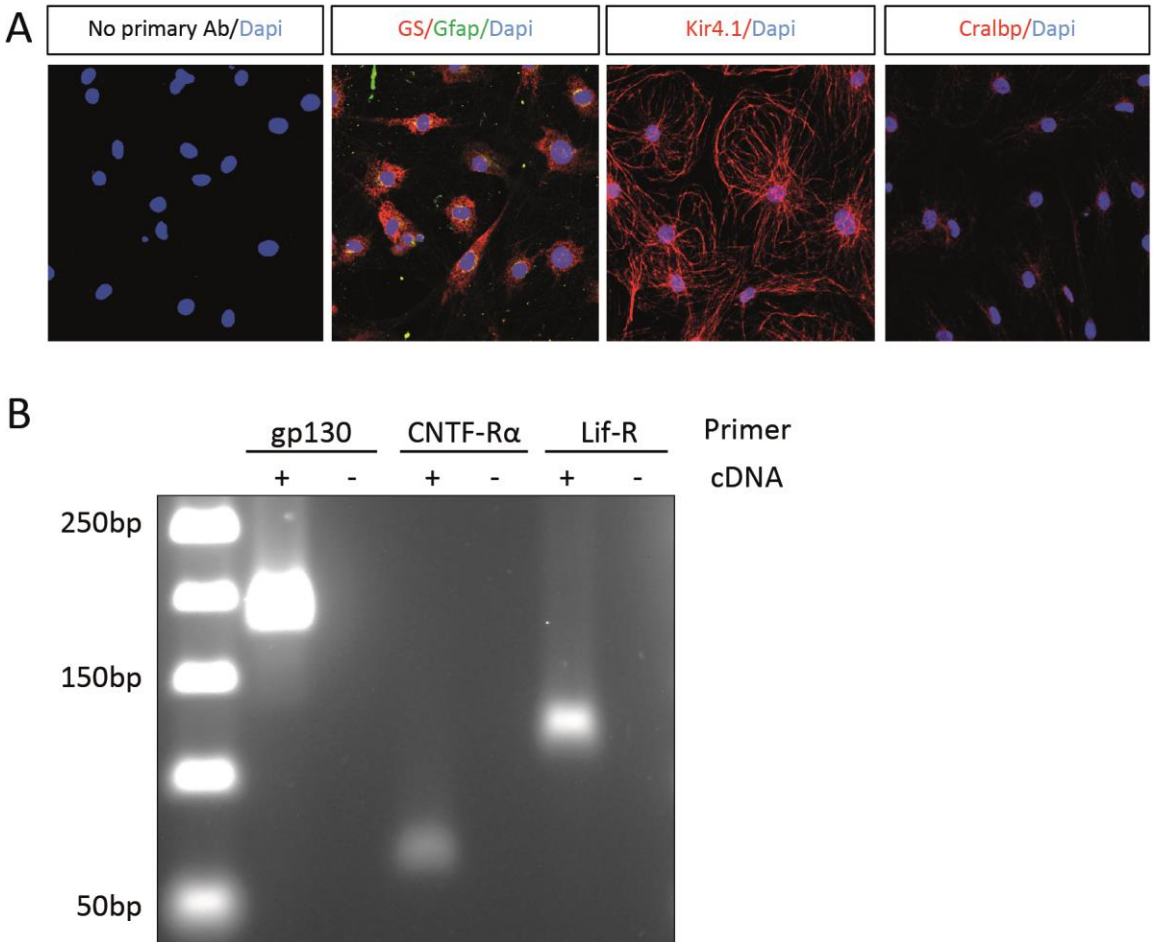

Supplemental Figure S2. Characterization of the primary Müller cell culture. (A) Representative immunohistochemical staining of primary Müller cells with Müller cell-specific markers Kir 4.1, GS, and Cralbp. (B) PCR analysis on primary murine Müller cell lysates for CNTF-Rα, gp130 and LifR expression.

Array Spot	Analyte	Abbreviation
A1/2	Reference Spots	
A5/6	ADAMTS1	METH1
A7/8	Amphiregulin	AR
A9/10	Angiogenin	ANG
A11/12	Angiopoietin-1	Ang-1
A13/14	Angiopoietin-3	Ang-3
A15/16	Coagulation Factor	Tissue Factor, TF
A17/18	CXCL16	-
A21/22	Reference Spots	
B3/4	Cyr61	CCN1,
B5/6	DLL4	-
B7/8	DPPIV	CD26
B9/10	EGF	-
B11/12	Endoglin	CD105
B13/14	Endostatin/Collagen XVIII	-
B15/16	Endothelin-1	ET-1
B17/18	FGF acidic	FGF-1, ECGF, HBGF-1
B19/20	FGF basic	FGF-2
C3/4	KGF	FGF-7
C5/6	Fractalkine	CX3CL1
C7/8	GM-CSF	-
C9/10	HB-EGF	-
C11/12	HGF	HepatopoietinA
C13/14	IGFBP-1	-
C15/16	IGFBP-2	-
C17/18	IGFBP-3	-
C19/20	IL-1α	IL-1F1
C21/22	IL-1β	IL-1F2
D3/4	IL-10	CSIF
D5/6	IP-10	CXCL10, CRG-2
D7/8	KC	CXCL1, CINC-1,GROa
D9/10	Leptin	OB
D11/12	MCP-1	CCL2/JE
D13/14	MIP-1α	CCL3
D15/16	MMP-3	-
D17/18	MMP-8	-
D19/20	MMP-9	-
D21/22	NOV	CCN3, IGFBP-9

Array Spot	Analyte	Abbreviation
E3/4	Osteopontin	OPN
E5/6	PD-ECGF	-
E7/8	PDGF-AA	-
E9/10	PDGF-AB/PDGF-BB	-
E11/12	Pentraxin-3	PTX-3,TSG-14
E13/14	Platelet Factor 4	CXCl4,PF4
E15/16	PlGF-2	-
E17/18	Prolactin	PRL
E19/20	Proliferin	-
E21/22	Reference	-
F3/3	SDF-1	CXCl12
F5/6	Serpin E1	PAI-1
F7/8	Serpin F1	PEDF
F8/10	Thrombospondin-2	TSP-2
F11/12	TIMP-1	-
F13/14	TIMP-4	-
F15/16	VEGF	VPF
F17/18	VEGF-B	VRF
F19/20	Negative	

Supplemental Table 1: Analyte Index of the Mouse Angiogenesis Proteome Profiler.

Chapter 5, in full, is a reprint of the materials as it appears in Investigative Ophthalmology & Visual Science, 2020. Bucher, F; Aguilar, E; Marra, KV; Rapp, J; Arnold, J; Diaz-Aguilar, S; Lange, C; Agostini, H; Schlunck, G; Stahl, A; Friedlander, M. The dissertation author was a co-investigator and co-author of this material. Work completed by the dissertation author contributed to generation of Figure 1 and Figure 4.

REFERENCES

1. Liao G, Zheng K, Shorr R, Allan DS. Human endothelial colony-forming cells in regenerative therapy: A systematic review of controlled preclinical animal studies. *Stem Cells Transl Med*. Nov 2020;9(11):1344-1352. doi:10.1002/sctm.20-0141

2. Stump MJ, G.; De Bakey, M.; Halpert, B. Endothelium grown from circulating blood on isolated intravascular dacron hub. *Am J Pathol*. 1963;43(3):361–367.

3. Shi QW, M.; Hayashida N.; Weehezak, A.; Clowes, A.; Sauvage, L. Proof of fallout endothelialization of impervious Dacron grafts in the aorta and inferior vena cava of the dog. *J Vasc Surg*. 1994;20:546-57. doi:10.1053/vs.1994.v20.57412

4. Shi QR, S.; Wu, M.; Wijelath, E.; Ishida, A.; Mohle, R.; Sauvage, L.; Moore, M.; Storb, R.; Hammond, W. Evidence for circulating bone marrow-derived endothelial cells. *Blood*. 1998;92(2):362-367.

5. Wood HB, May G, Healy L, Enver T, Morriss-Kay GM. CD34 expression patterns during early mouse development are related to modes of blood vessel formation and reveal additional sites of hematopoiesis. *Blood*. 1997;90(6):2300-2311. doi:10.1182/blood.V90.6.2300.2300_2300_2311

6. Zilla P, Bezuidenhout D, Human P. Prosthetic vascular grafts: wrong models, wrong questions and no healing. *Biomaterials*. Dec 2007;28(34):5009-27. doi:10.1016/j.biomaterials.2007.07.017

7. Frazier OB, R.; Eskin, S.; Duncan J. Immunochemical identification of human endothelial cells on the lining of a ventricular assist device. *Tex Heard Inst J*. 1993;20(2):78-82.

8. Salih VG, T.; Ciumbe, B.; Smith, S.; Dasse, K.; Frazier, O. The lining of textured surfaces in implantable left ventricular assist devices. An immunocytochemical and electronmicroscopic study. *Am J Cardiovasc Pathol*. 1993;4(4):317-25.

9. Rafii SO, M.; Seldomridge, A.; Ferris, B.; Asch, A.; Nachman, R.; Shapiro, F.; Rose, E.; Levin, H. Characterization of hematopoietic cells arising on the textured surface of left ventricular assist devices. *Ann Thorac Surg*. 1995;60:1627-32.

10. Folkman JS, Y. Angiogenesis. *J Biol Chem*. 1992;267(16):10931-10934.

11. Asahara TM, T.; Sullivan, A.; Silver, M,; Zee, R.; Li, T.; Witzenbichler, B.; Schatteman, G.; Isner, J. Isolation of putative progenitor endothelial cells for angiogenesis. *Science*. 1997;275:964-67.

12. Risau WF, I. Vasculogenesis. *Annu Rev Cell Dev Bioi*. 1995;11(73-91)

13. Shalaby FR, J.; Yamaguchi, T.; Gertsenst, M.; Wu, X.; Breitman, M.; Schuh, A. Failure of blood-island formation and vasculogenesis in Flk-1-deficient mice. *Nature*. 1995;376:62-66.

14. Kogler G, Critser P, Trapp T, Yoder M. Future of cord blood for non-oncology uses. *Bone Marrow Transplant*. Nov 2009;44(10):683-97. doi:10.1038/bmt.2009.287

15. Zucco L, Zhang Q, Kuliszewski MA, Kandic I, Faughnan ME, Stewart DJ, Kutryk MJ. Circulating angiogenic cell dysfunction in patients with hereditary hemorrhagic telangiectasia. *PLoS One*. 2014;9(2):e89927. doi:10.1371/journal.pone.0089927

16. Medina RJ, Barber CL, Sabatier F, Dignat-George F, Melero-Martin JM, Khosrotehrani K, Ohneda O, Randi AM, Chan JKY, Yamaguchi T, Van Hinsbergh VWM, Yoder MC, Stitt AW. Endothelial progenitors: a consensus statement on nomenclature. *Stem Cells Transl Med*. May 2017;6(5):1316-1320. doi:10.1002/sctm.16-0360

17. Pearson JD. Endothelial progenitor cells--an evolving story. *Microvasc Res*. May 2010;79(3):162-8. doi:10.1016/j.mvr.2009.12.004

18. Chambers SE, O'Neill CL, O'Doherty TM, Medina RJ, Stitt AW. The role of immune-related myeloid cells in angiogenesis. *Immunobiology*. Nov 2013;218(11):1370-5. doi:10.1016/j.imbio.2013.06.010

19. Medina RJ, O'Neill CL, O'Doherty TM, Knott H, Guduric-Fuchs J, Gardiner TA, Stitt AW. Myeloid angiogenic cells act as alternative M2 macrophages and modulate angiogenesis through interleukin-8. *Mol Med*. Sep-Oct 2011;17(9-10):1045-55. doi:10.2119/molmed.2011.00129

20. Mukai N, Akahori T, Komaki M, Li Q, Kanayasu-Toyoda T, Ishii-Watabe A, Kobayashi A, Yamaguchi T, Abe M, Amagasa T, Morita I. A comparison of the tube forming potentials of early and late endothelial progenitor cells. *Exp Cell Res*. Feb 1 2008;314(3):430-40. doi:10.1016/j.yexcr.2007.11.016

21. Yoder MC, Mead LE, Prater D, Krier TR, Mroueh KN, Li F, Krasich R, Temm CJ, Prchal JT, Ingram DA. Redefining endothelial progenitor cells via clonal analysis and hematopoietic stem/progenitor cell principals. *Blood*. Mar 1 2007;109(5):1801-9. doi:10.1182/blood-2006-08-043471

22. Hur J, Yoon CH, Kim HS, Choi JH, Kang HJ, Hwang KK, Oh BH, Lee MM, Park YB. Characterization of two types of endothelial progenitor cells and their different contributions to neovasculogenesis. *Arterioscler Thromb Vasc Biol*. Feb 2004;24(2):288-93. doi:10.1161/01.ATV.0000114236.77009.06

23. Banno K, Yoder MC. Tissue regeneration using endothelial colony-forming cells: promising cells for vascular repair. *Pediatr Res*. Jan 2018;83(1-2):283-290. doi:10.1038/pr.2017.231

24. Hill JZ, G.; Halcox, J; Schenke, W.; Waclawiw, M.; Quyyumi, A.; Finkel, T. Circulating endothelial progenitor cells, vascular function, and cardiovascular risk. *N Engl J Med*. 2003;348:593-600.

25. Loomans CJ, de Koning EJ, Staal FJ, Rookmaaker MB, Verseyden C, de Boer HC, Verhaar MC, Braam B, Rabelink TJ, van Zonneveld AJ. Endothelial progenitor cell dysfunction: a novel concept in the pathogenesis of vascular complications of type 1 diabetes. *Diabetes*. Jan 2004;53(1):195-9. doi:10.2337/diabetes.53.1.195

26. Palange P, Testa U, Huertas A, Calabro L, Antonucci R, Petrucci E, Pelosi E, Pasquini L, Satta A, Morici G, Vignola MA, Bonsignore MR. Circulating haemopoietic and endothelial progenitor cells are decreased in COPD. *Eur Respir J*. Mar 2006;27(3):529-41. doi:10.1183/09031936.06.00120604

27. Grisar J, Aletaha D, Steiner CW, Kapral T, Steiner S, Seidinger D, Weigel G, Schwarzinger I, Wolozcszuk W, Steiner G, Smolen JS. Depletion of endothelial progenitor cells in the peripheral blood of patients with rheumatoid arthritis. *Circulation*. Jan 18 2005;111(2):204-11. doi:10.1161/01.CIR.0000151875.21836.AE

28. Hirschi KK, Ingram DA, Yoder MC. Assessing identity, phenotype, and fate of endothelial progenitor cells. *Arterioscler Thromb Vasc Biol*. Sep 2008;28(9):1584-95. doi:10.1161/ATVBAHA.107.155960

29. Sakimoto S, Marchetti V, Aguilar E, Lee K, Usui Y, Murinello S, Bucher F, Trombley JK, Fallon R, Wagey R, Peters C, Scheppke EL, Westenskow PD, Friedlander M. CD44 expression in endothelial colony-forming cells regulates neurovascular trophic effect. *JCI Insight*. Jan 26 2017;2(2):e89906. doi:10.1172/jci.insight.89906

30. Ingram DA, Mead LE, Tanaka H, Meade V, Fenoglio A, Mortell K, Pollok K, Ferkowicz MJ, Gilley D, Yoder MC. Identification of a novel hierarchy of endothelial progenitor cells using human peripheral and umbilical cord blood. *Blood*. Nov 1 2004;104(9):2752-60. doi:10.1182/blood-2004-04-1396

31. Tasev D, Konijnenberg LS, Amado-Azevedo J, van Wijhe MH, Koolwijk P, van Hinsbergh VW. CD34 expression modulates tube-forming capacity and barrier properties of peripheral blood-derived endothelial colony-forming cells (ECFCs). *Angiogenesis*. Jul 2016;19(3):325-38. doi:10.1007/s10456-016-9506-9

32. Vasa MF, S.; Adler, K.; Aicher, A.; Martin, H.; Zeiher, A.; Dimmeler, S. Increase in circulating endothelial progenitor cells by statin therapy in patients with stable coronary artery disease. *Circulation*. 2001;103:2885-2890.

33. Vasa MF, S.; Aicher, A.; Adler, K.; Urbich, C.; Martin, M.; Zeiher, A.; Dimmeler, S. Number and migratory activity of circulating endothelial progenitor cells inversely correlate with risk factors for coronary artery disease. *Circ Res*. 2001;89(1):e1-e7.

34. Fernandez Pujol B, Lucibello FC, Gehling UM, Lindemann K, Weidner N, Zuzarte ML, Adamkiewicz J, Elsasser HP, Muller R, Havemann K. Endothelial-like cells derived from human CD14 positive monocytes. *Differentiation*. May 2000;65(5):287-300. doi:10.1046/j.1432-0436.2000.6550287.x

35. Schmeisser A, Garlichs CD, Zhang H, Eskafi S, Graffy C, Ludwig J, Strasser RH, Daniel WG. Monocytes coexpress endothelial and macrophagocytic lineage markers and form cord-like structures in Matrigel under angiogenic conditions. *Cardiovasc Res*. Feb 16 2001;49(3):671-80. doi:10.1016/s0008-6363(00)00270-4

36. Schmeisser AG, C; Daniel, WG.; Strasser RH. Phenotypic overlap between monocytes and vascular endothelial cells. *Adv Exp Med Biol*. 2003;522:59–74.

37. Hassan NF, Campbell DE, Douglas SD. Purification of human monocytes on gelatin-coated surfaces. *J Immunol Methods*. Dec 24 1986;95(2):273-6. doi:10.1016/0022-1759(86)90415-1

38. Yang Z, von Ballmoos MW, Faessler D, Voelzmann J, Ortmann J, Diehm N, Kalka-Moll W, Baumgartner I, Di Santo S, Kalka C. Paracrine factors secreted by endothelial progenitor cells prevent oxidative stress-induced apoptosis of mature endothelial cells. *Atherosclerosis*. Jul 2010;211(1):103-9. doi:10.1016/j.atherosclerosis.2010.02.022

39. Tepper OM, Galiano RD, Capla JM, Kalka C, Gagne PJ, Jacobowitz GR, Levine JP, Gurtner GC. Human endothelial progenitor cells from type II diabetics exhibit impaired proliferation, adhesion, and incorporation into vascular structures. *Circulation*. Nov 26 2002;106(22):2781-6. doi:10.1161/01.cir.0000039526.42991.93

40. He T, Joyner MJ, Katusic ZS. Aging decreases expression and activity of glutathione peroxidase-1 in human endothelial progenitor cells. *Microvasc Res*. Dec 2009;78(3):447-52. doi:10.1016/j.mvr.2009.08.009

41. Ii M, Takenaka H, Asai J, Ibusuki K, Mizukami Y, Maruyama K, Yoon YS, Wecker A, Luedemann C, Eaton E, Silver M, Thorne T, Losordo DW. Endothelial progenitor thrombospondin-1 mediates diabetes-induced delay in reendothelialization following arterial injury. *Circ Res*. Mar 17 2006;98(5):697-704. doi:10.1161/01.RES.0000209948.50943.ea

42. Urbich C, Heeschen C, Aicher A, Dernbach E, Zeiher AM, Dimmeler S. Relevance of monocytic features for neovascularization capacity of circulating endothelial progenitor cells. *Circulation*. Nov 18 2003;108(20):2511-6. doi:10.1161/01.CIR.0000096483.29777.50

43. Urbich C, Aicher A, Heeschen C, Dernbach E, Hofmann WK, Zeiher AM, Dimmeler S. Soluble factors released by endothelial progenitor cells promote migration of endothelial cells and cardiac resident progenitor cells. *J Mol Cell Cardiol*. Nov 2005;39(5):733-42. doi:10.1016/j.yjmcc.2005.07.003

44. Kalka C, Masuda H, Takahashi T, Kalka-Moll WM, Silver M, Kearney M, Li T, Isner JM, Asahara T. Transplantation of ex vivo expanded endothelial progenitor cells for therapeutic neovascularization. *Proc Natl Acad Sci U S A*. Mar 28 2000;97(7):3422-7. doi:10.1073/pnas.070046397

45. Ziebart T, Yoon CH, Trepels T, Wietelmann A, Braun T, Kiessling F, Stein S, Grez M, Ihling C, Muhly-Reinholz M, Carmona G, Urbich C, Zeiher AM, Dimmeler S. Sustained persistence of transplanted proangiogenic cells contributes to neovascularization and cardiac function after ischemia. *Circ Res*. Nov 21 2008;103(11):1327-34. doi:10.1161/CIRCRESAHA.108.180463

46. Meng S, Cao JT, Zhang B, Zhou Q, Shen CX, Wang CQ. Downregulation of microRNA-126 in endothelial progenitor cells from diabetes patients, impairs their functional properties, via target gene Spred-1. *J Mol Cell Cardiol*. Jul 2012;53(1):64-72. doi:10.1016/j.yjmcc.2012.04.003

47. Chavakis E, Aicher A, Heeschen C, Sasaki K, Kaiser R, El Makhfi N, Urbich C, Peters T, Scharffetter-Kochanek K, Zeiher AM, Chavakis T, Dimmeler S. Role of beta2-integrins for homing and neovascularization capacity of endothelial progenitor cells. *J Exp Med*. Jan 3 2005;201(1):63-72. doi:10.1084/jem.20041402

48. Lin YW, D.; Solovey, A.; Hebbel, R. Origins of circulating endothelial cells and endothelial outgrowth from blood. *J Clin Invest*. 2000;105:71–77.

49. Yoder MC. Is endothelium the origin of endothelial progenitor cells? *Arterioscler Thromb Vasc Biol*. Jun 2010;30(6):1094-103. doi:10.1161/ATVBAHA.109.191635

50. Tura O, Skinner EM, Barclay GR, Samuel K, Gallagher RC, Brittan M, Hadoke PW, Newby DE, Turner ML, Mills NL. Late outgrowth endothelial cells resemble mature endothelial cells and are not derived from bone marrow. *Stem Cells*. Feb 2013;31(2):338-48. doi:10.1002/stem.1280

51. Fujisawa T, Tura-Ceide O, Hunter A, Mitchell A, Vesey A, Medine C, Gallogly S, Hadoke PWF, Keith C, Sproul A, Roddie H, McQuaker G, Wilmut I, Mills NL, Brittan M. Endothelial progenitor cells do not originate from the bone marrow. *Circulation*. Oct 29 2019;140(18):1524-1526. doi:10.1161/CIRCULATIONAHA.119.042351

52. Alessandri GG, M.; Taccagni, G.; Colombo, A.; Nicosia, R.; Caruso, A.; Baronio, M.; Pagano, S.; Cova, L.; Parati, E. Human vasculogenesis ex vivo- embryonal aorta as a tool for isolation of endothelial cell progenitors. *Lab Investig*. 2001;81(6):875-85.

53. Ingram DA, Mead LE, Moore DB, Woodard W, Fenoglio A, Yoder MC. Vessel wall-derived endothelial cells rapidly proliferate because they contain a complete hierarchy of endothelial progenitor cells. *Blood*. Apr 1 2005;105(7):2783-6. doi:10.1182/blood-2004-08-3057

54. Duong HT, Comhair SA, Aldred MA, Mavrakis L, Savasky BM, Erzurum SC, Asosingh K. Pulmonary artery endothelium resident endothelial colony-forming cells in pulmonary arterial hypertension. *Pulm Circ*. Oct-Dec 2011;1(4):475-86. doi:10.4103/2045-8932.93547

55. Green L, Ofstein RH, Rapp B, Saadatzadeh MR, Bhavsar JR, Fajardo A, Dalsing MC, Ingram DA, Murphy MP. Adult venous endothelium is a niche for highly proliferative and vasculogenic endothelial colony-forming cells. *J Vasc Surg*. Dec 2017;66(6):1854-1863. doi:10.1016/j.jvs.2016.11.059

56. Alphonse RS, Vadivel A, Zhong S, McConaghy S, Ohls R, Yoder MC, Thebaud B. The isolation and culture of endothelial colony-forming cells from human and rat lungs. *Nat Protoc*. Nov 2015;10(11):1697-708. doi:10.1038/nprot.2015.107

57. Solomon I, O'Reilly M, Ionescu L, Alphonse RS, Rajabali S, Zhong S, Vadivel A, Shelley WC, Yoder MC, Thebaud B. Functional differences between placental micro- and macrovascular endothelial colony-forming cells. *Stem Cells Transl Med*. Mar 2016;5(3):291-300. doi:10.5966/sctm.2014-0162

58. Lin RZ, Moreno-Luna R, Munoz-Hernandez R, Li D, Jaminet SC, Greene AK, Melero-Martin JM. Human white adipose tissue vasculature contains endothelial colony-forming cells with robust in vivo vasculogenic potential. *Angiogenesis*. Oct 2013;16(4):735-44. doi:10.1007/s10456-013-9350-0

59. Prasain N, Lee MR, Vemula S, Meador JL, Yoshimoto M, Ferkowicz MJ, Fett A, Gupta M, Rapp BM, Saadatzadeh MR, Ginsberg M, Elemento O, Lee Y, Voytik-Harbin SL, Chung HM, Hong KS, Reid E, O'Neill CL, Medina RJ, Stitt AW, Murphy MP, Rafii S, Broxmeyer HE, Yoder MC. Differentiation of human pluripotent stem cells to cells similar to cord-blood endothelial colony-forming cells. *Nat Biotechnol*. Nov 2014;32(11):1151-1157. doi:10.1038/nbt.3048

60. Kutikhin AG, Tupikin AE, Matveeva VG, Shishkova DK, Antonova LV, Kabilov MR, Velikanova EA. Human peripheral blood-derived endothelial colony-forming cells are highly similar to mature vascular endothelial cells yet demonstrate a transitional transcriptomic signature. *Cells*. Apr 3 2020;9(4)doi:10.3390/cells9040876

61. Toshner M, Dunmore BJ, McKinney EF, Southwood M, Caruso P, Upton PD, Waters JP, Ormiston ML, Skepper JN, Nash G, Rana AA, Morrell NW. Transcript analysis reveals a specific HOX signature associated with positional identity of human endothelial cells. *PLoS One*. 2014;9(3):e91334. doi:10.1371/journal.pone.0091334

62. Hagensen MK, Raarup MK, Mortensen MB, Thim T, Nyengaard JR, Falk E, Bentzon JF. Circulating endothelial progenitor cells do not contribute to regeneration of endothelium after murine arterial injury. *Cardiovasc Res*. Feb 1 2012;93(2):223-31. doi:10.1093/cvr/cvr278

63. Khmelewski E, Becker A, Meinertz T, Ito WD. Tissue resident cells play a dominant role in arteriogenesis and concomitant macrophage accumulation. *Circ Res*. Sep 17 2004;95(6):E56-64. doi:10.1161/01.RES.0000143013.04985.E7

64. Ross RG, J.; Harker, L. Response to injury and ahterosclerosis. *Am J Pathol*. 1977 86(3):675–684.

65. Sainz J, Al Haj Zen A, Caligiuri G, Demerens C, Urbain D, Lemitre M, Lafont A. Isolation of "side population" progenitor cells from healthy arteries of adult mice. *Arterioscler Thromb Vasc Biol*. Feb 2006;26(2):281-6. doi:10.1161/01.ATV.0000197793.83391.91

66. Pasquinelli G, Tazzari PL, Vaselli C, Foroni L, Buzzi M, Storci G, Alviano F, Ricci F, Bonafe M, Orrico C, Bagnara GP, Stella A, Conte R. Thoracic aortas from multiorgan donors are suitable for obtaining resident angiogenic mesenchymal stromal cells. *Stem Cells*. Jul 2007;25(7):1627-34. doi:10.1634/stemcells.2006-0731

67. Zengin E, Chalajour F, Gehling UM, Ito WD, Treede H, Lauke H, Weil J, Reichenspurner H, Kilic N, Ergun S. Vascular wall resident progenitor cells: a source for postnatal vasculogenesis. *Development*. Apr 2006;133(8):1543-51. doi:10.1242/dev.02315

68. Torsney E, Xu Q. Resident vascular progenitor cells. *J Mol Cell Cardiol*. Feb 2011;50(2):304-11. doi:10.1016/j.yjmcc.2010.09.006

69. Fang S, Wei J, Pentinmikko N, Leinonen H, Salven P. Generation of functional blood vessels from a single c-kit+ adult vascular endothelial stem cell. *PLoS Biol*. 2012;10(10):e1001407. doi:10.1371/journal.pbio.1001407

70. Prasain N, Meador JL, Yoder MC. Phenotypic and functional characterization of endothelial colony forming cells derived from human umbilical cord blood. *J Vis Exp*. Apr 13 2012;(62)doi:10.3791/3872

71. Medina RON, C.; Humphreys, M.; Gardiner, T.; Stitt, A. Outgrowth endothelial cells: characterization and their potential for reversing ischemic retinopathy. *Investig Ophthalmol Vis Sci*. 2010;51(11):5906-5913. doi:10

72. Reid E, Guduric-Fuchs J, O'Neill CL, Allen LD, Chambers SEJ, Stitt AW, Medina RJ. Preclinical evaluation and optimization of a cell therapy using human cord blood-derived endothelial colony-forming cells for ischemic retinopathies. *Stem Cells Transl Med*. Jan 2018;7(1):59-67. doi:10.1002/sctm.17-0187

73. Tan K, Lessieur E, Cutler A, Nerone P, Vasanji A, Asosingh K, Erzurum S, Anand-Apte B. Impaired function of circulating CD34(+) CD45(-) cells in patients with proliferative diabetic retinopathy. *Exp Eye Res*. Aug 2010;91(2):229-37. doi:10.1016/j.exer.2010.05.012

74. Nuzzolo ER, Capodimonti S, Martini M, Iachininoto MG, Bianchi M, Cocomazzi A, Zini G, Leone G, Larocca LM, Teofili L. Adult and cord blood endothelial progenitor cells have

different gene expression profiles and immunogenic potential. *Blood Transfus*. Jan 2014;12 Suppl 1:s367-74. doi:10.2450/2013.0042-13

75. Lin G, Xie Y, Ouyang Q, Qian X, Xie P, Zhou X, Xiong B, Tan Y, Li W, Deng L, Zhou J, Zhou D, Du L, Cheng D, Liao Y, Gu Y, Zhang S, Liu T, Sun Y, Lu G. HLA-matching potential of an established human embryonic stem cell bank in China. *Cell Stem Cell*. Nov 6 2009;5(5):461-5. doi:10.1016/j.stem.2009.10.009

76. Okita KM, Y.; Sato, Y.; Okada, A.; Morizane, A; Okamoto, S.; Hong, H.; Nakagawa, M.; Tanabe, K.; Tezuka, K.; Shibata, T.; Kunisada, T.; Takahashi, M.; Takahashi, J.; Saji, H.; Yamanaka, S. A more efficient method to generate integration-free human iPS cells. *Nat Methods*. 2011;8(5):409-14.

77. Ding J, Zhao Z, Wang C, Wang CX, Li PC, Qian C, Teng GJ. Bioluminescence imaging of transplanted human endothelial colony-forming cells in an ischemic mouse model. *Brain Res*. Jul 1 2016;1642:209-218. doi:10.1016/j.brainres.2016.03.045

78. Patel J, Seppanen E, Chong MS, Yeo JS, Teo EY, Chan JK, Fisk NM, Khosrotehrani K. Prospective surface marker-based isolation and expansion of fetal endothelial colony-forming cells from human term placenta. *Stem Cells Transl Med*. Nov 2013;2(11):839-47. doi:10.5966/sctm.2013-0092

79. Medina RJ, O'Neill CL, O'Doherty TM, Chambers SE, Guduric-Fuchs J, Neisen J, Waugh DJ, Simpson DA, Stitt AW. Ex vivo expansion of human outgrowth endothelial cells leads to IL-8-mediated replicative senescence and impaired vasoreparative function. *Stem Cells*. Aug 2013;31(8):1657-68. doi:10.1002/stem.1414

80. He T, Peterson TE, Katusic ZS. Paracrine mitogenic effect of human endothelial progenitor cells: role of interleukin-8. *Am J Physiol Heart Circ Physiol*. Aug 2005;289(2):H968-72. doi:10.1152/ajpheart.01166.2004

81. Milbauer LC, Enenstein JA, Roney M, Solovey A, Bodempudi V, Nichols TC, Hebbel RP. Blood outgrowth endothelial cell migration and trapping in vivo: a window into gene therapy. *Transl Res*. Apr 2009;153(4):179-89. doi:10.1016/j.trsl.2008.12.009

82. Falavarjani KG, Nguyen QD. Adverse events and complications associated with intravitreal injection of anti-VEGF agents: a review of literature. *Eye (Lond)*. Jul 2013;27(7):787-94. doi:10.1038/eye.2013.107

83. Flex A, Biscetti F, Iachininoto MG, Nuzzolo ER, Orlando N, Capodimonti S, Angelini F, Valentini CG, Bianchi M, Larocca LM, Martini M, Teofili L. Human cord blood endothelial progenitors promote post-ischemic angiogenesis in immunocompetent mouse model. *Thromb Res*. May 2016;141:106-11. doi:10.1016/j.thromres.2016.03.012

84. Minami Y, Nakajima T, Ikutomi M, Morita T, Komuro I, Sata M, Sahara M. Angiogenic potential of early and late outgrowth endothelial progenitor cells is dependent on the time of emergence. *Int J Cardiol*. 2015;186:305-14. doi:10.1016/j.ijcard.2015.03.166

85. Goto K, Takemura G, Takahashi T, Okada H, Kanamori H, Kawamura I, Watanabe T, Morishita K, Tsujimoto A, Miyazaki N, Ushikoshi H, Kawasaki M, Mikami A, Kosai K, Minatoguchi S. Intravenous Administration of Endothelial Colony-Forming Cells Overexpressing Integrin beta1 Augments Angiogenesis in Ischemic Legs. *Stem Cells Transl Med*. Feb 2016;5(2):218-26. doi:10.5966/sctm.2015-0096

86. Mena HA, Zubiry PR, Dizier B, Schattner M, Boisson-Vidal C, Negrotto S. Acidic preconditioning of endothelial colony-forming cells (ECFC) promote vasculogenesis under proinflammatory and high glucose conditions in vitro and in vivo. *Stem Cell Res Ther*. May 2 2018;9(1):120. doi:10.1186/s13287-018-0872-7

87. Lee SH, Lee JH, Han YS, Ryu JM, Yoon YM, Han HJ. Hypoxia accelerates vascular repair of endothelial colony-forming cells on ischemic injury via STAT3-BCL3 axis. *Stem Cell Res Ther*. Jul 29 2015;6:139. doi:10.1186/s13287-015-0128-8

88. Kim BR, Jang IH, Shin SH, Kwon YW, Heo SC, Choi EJ, Lee JS, Kim JH. Therapeutic angiogenesis in a murine model of limb ischemia by recombinant periostin and its fasciclin I domain. *Biochim Biophys Acta*. Sep 2014;1842(9):1324-32. doi:10.1016/j.bbadis.2014.05.004

89. Suh W, Kim KL, Kim JM, Shin IS, Lee YS, Lee JY, Jang HS, Lee JS, Byun J, Choi JH, Jeon ES, Kim DK. Transplantation of endothelial progenitor cells accelerates dermal wound healing with increased recruitment of monocytes/macrophages and neovascularization. *Stem Cells*. Nov-Dec 2005;23(10):1571-8. doi:10.1634/stemcells.2004-0340

90. Zhang Y, Li Y, Wang S, Han Z, Huang X, Li S, Chen F, Niu R, Dong JF, Jiang R, Zhang J. Transplantation of expanded endothelial colony-forming cells improved outcomes of traumatic brain injury in a mouse model. *J Surg Res*. Nov 2013;185(1):441-9. doi:10.1016/j.jss.2013.05.073

91. Huang XT, Zhang YQ, Li SJ, Li SH, Tang Q, Wang ZT, Dong JF, Zhang JN. Intracerebroventricular transplantation of ex vivo expanded endothelial colony-forming cells restores blood-brain barrier integrity and promotes angiogenesis of mice with traumatic brain injury. *J Neurotrauma*. Dec 15 2013;30(24):2080-8. doi:10.1089/neu.2013.2996

92. Moubarik C, Guillet B, Youssef B, Codaccioni JL, Piercecchi MD, Sabatier F, Lionel P, Dou L, Foucault-Bertaud A, Velly L, Dignat-George F, Pisano P. Transplanted late outgrowth endothelial progenitor cells as cell therapy product for stroke. *Stem Cell Rev Rep*. Mar 2011;7(1):208-20. doi:10.1007/s12015-010-9157-y

93. Bayraktutan U. Endothelial progenitor cells: Potential novel therapeutics for ischaemic stroke. *Pharmacol Res*. Jun 2019;144:181-191. doi:10.1016/j.phrs.2019.04.017

94. Patschan D, Schwarze K, Tampe B, Zeisberg M, Patschan S, Muller GA. Endothelial Colony Forming Cells (ECFCs) in murine AKI - implications for future cell-based therapies. *BMC Nephrol*. Feb 6 2017;18(1):53. doi:10.1186/s12882-017-0471-3

95. Lee SH, Lee JH, Asahara T, Kim YS, Jeong HC, Ahn Y, Jung JS, Kwon SM. Genistein promotes endothelial colony-forming cell (ECFC) bioactivities and cardiac regeneration in myocardial infarction. *PLoS One*. 2014;9(5):e96155. doi:10.1371/journal.pone.0096155

96. Kim SW, Jin HL, Kang SM, Kim S, Yoo KJ, Jang Y, Kim HO, Yoon YS. Therapeutic effects of late outgrowth endothelial progenitor cells or mesenchymal stem cells derived from human umbilical cord blood on infarct repair. *Int J Cardiol*. Jan 15 2016;203:498-507. doi:10.1016/j.ijcard.2015.10.110

97. Brunt KR, Wu J, Chen Z, Poeckel D, Dercho RA, Melo LG, Funk CD, Ward CA, Li RK. Ex vivo Akt/HO-1 gene therapy to human endothelial progenitor cells enhances myocardial infarction recovery. *Cell Transplant*. 2012;21(7):1443-61. doi:10.3727/096368912X653002

98. Faris P, Negri S, Perna A, Rosti V, Guerra G, Moccia F. Therapeutic potential of endothelial colony-forming cells in ischemic disease: strategies to improve their regenerative efficacy. *Int J Mol Sci*. Oct 7 2020;21(19)doi:10.3390/ijms21197406

99. Alphonse RS, Vadivel A, Fung M, Shelley WC, Critser PJ, Ionescu L, O'Reilly M, Ohls RK, McConaghy S, Eaton F, Zhong S, Yoder M, Thebaud B. Existence, functional impairment, and lung repair potential of endothelial colony-forming cells in oxygen-induced arrested alveolar growth. *Circulation*. May 27 2014;129(21):2144-57. doi:10.1161/CIRCULATIONAHA.114.009124

100. Cahoon JM, Rai RR, Carroll LS, Uehara H, Zhang X, O'Neil CL, Medina RJ, Das SK, Muddana SK, Olson PR, Nielson S, Walker K, Flood MM, Messenger WB, Archer BJ, Barabas P, Krizaj D, Gibson CC, Li DY, Koh GY, Gao G, Stitt AW, Ambati BK. Intravitreal AAV2.COMP-Ang1 prevents neurovascular degeneration in a murine model of diabetic retinopathy. *Diabetes*. Dec 2015;64(12):4247-59. doi:10.2337/db14-1030

101. Schwarz TM, Leicht SF, Radic T, Rodriguez-Arabaolaza I, Hermann PC, Berger F, Saif J, Bocker W, Ellwart JW, Aicher A, Heeschen C. Vascular incorporation of endothelial colony-forming cells is essential for functional recovery of murine ischemic tissue following cell therapy. *Arterioscler Thromb Vasc Biol*. Feb 2012;32(2):e13-21. doi:10.1161/ATVBAHA.111.239822

102. Aicher A, Brenner W, Zuhayra M, Badorff C, Massoudi S, Assmus B, Eckey T, Henze E, Zeiher AM, Dimmeler S. Assessment of the tissue distribution of transplanted human endothelial progenitor cells by radioactive labeling. *Circulation*. Apr 29 2003;107(16):2134-9. doi:10.1161/01.CIR.0000062649.63838.C9

103. Hanjaya-Putra D, Shen YI, Wilson A, Fox-Talbot K, Khetan S, Burdick JA, Steenbergen C, Gerecht S. Integration and regression of implanted engineered human vascular networks

during deep wound healing. *Stem Cells Transl Med*. Apr 2013;2(4):297-306. doi:10.5966/sctm.2012-0111

104. Hanjaya-Putra D, Wong KT, Hirotsu K, Khetan S, Burdick JA, Gerecht S. Spatial control of cell-mediated degradation to regulate vasculogenesis and angiogenesis in hyaluronan hydrogels. *Biomaterials*. Sep 2012;33(26):6123-31. doi:10.1016/j.biomaterials.2012.05.027

105. Hanjaya-Putra D, Bose V, Shen YI, Yee J, Khetan S, Fox-Talbot K, Steenbergen C, Burdick JA, Gerecht S. Controlled activation of morphogenesis to generate a functional human microvasculature in a synthetic matrix. *Blood*. Jul 21 2011;118(3):804-15. doi:10.1182/blood-2010-12-327338

106. Chuang CH, Lin RZ, Tien HW, Chu YC, Li YC, Melero-Martin JM, Chen YC. Enzymatic regulation of functional vascular networks using gelatin hydrogels. *Acta Biomater*. Jun 2015;19:85-99. doi:10.1016/j.actbio.2015.02.024

107. Chen YC, Lin RZ, Qi H, Yang Y, Bae H, Melero-Martin JM, Khademhosseini A. Functional Human Vascular Network Generated in Photocrosslinkable Gelatin Methacrylate Hydrogels. *Adv Funct Mater*. May 23 2012;22(10):2027-2039. doi:10.1002/adfm.201101662

108. Silva EA, Kim ES, Kong HJ, Mooney DJ. Material-based deployment enhances efficacy of endothelial progenitor cells. *Proc Natl Acad Sci U S A*. Sep 23 2008;105(38):14347-52. doi:10.1073/pnas.0803873105

109. Allen P, Kang KT, Bischoff J. Rapid onset of perfused blood vessels after implantation of ECFCs and MPCs in collagen, PuraMatrix and fibrin provisional matrices. *J Tissue Eng Regen Med*. May 2015;9(5):632-6. doi:10.1002/term.1803

110. Chen X, Aledia AS, Popson SA, Him L, Hughes CC, George SC. Rapid anastomosis of endothelial progenitor cell-derived vessels with host vasculature is promoted by a high density of cotransplanted fibroblasts. *Tissue Eng Part A*. Feb 2010;16(2):585-94. doi:10.1089/ten.TEA.2009.0491

111. White SM, Hingorani R, Arora RP, Hughes CC, George SC, Choi B. Longitudinal in vivo imaging to assess blood flow and oxygenation in implantable engineered tissues. *Tissue Eng Part C Methods*. Sep 2012;18(9):697-709. doi:10.1089/ten.TEC.2011.0744

112. Lee KY, Mooney DJ. Hydrogels for tissue engineering. *Chem Rev*. Jul 2001;101(7):1869-79. doi:10.1021/cr000108x

113. Liu Y, Teoh SH, Chong MS, Yeow CH, Kamm RD, Choolani M, Chan JK. Contrasting effects of vasculogenic induction upon biaxial bioreactor stimulation of mesenchymal stem cells and endothelial progenitor cells cocultures in three-dimensional scaffolds under in vitro and in vivo paradigms for vascularized bone tissue engineering. *Tissue Eng Part A*. Apr 2013;19(7-8):893-904. doi:10.1089/ten.TEA.2012.0187

114. Zigdon-Giladi H, Michaeli-Geller G, Bick T, Lewinson D, Machtei EE. Human blood-derived endothelial progenitor cells augment vasculogenesis and osteogenesis. *J Clin Periodontol*. Jan 2015;42(1):89-95. doi:10.1111/jcpe.12325

115. Kim KL, Han DK, Park K, Song SH, Kim JY, Kim JM, Ki HY, Yie SW, Roh CR, Jeon ES, Kim DK, Suh W. Enhanced dermal wound neovascularization by targeted delivery of endothelial progenitor cells using an RGD-g-PLLA scaffold. *Biomaterials*. Aug 2009;30(22):3742-8. doi:10.1016/j.biomaterials.2009.03.053

116. Singh S, Wu BM, Dunn JC. Accelerating vascularization in polycaprolactone scaffolds by endothelial progenitor cells. *Tissue Eng Part A*. Jul 2011;17(13-14):1819-30. doi:10.1089/ten.TEA.2010.0708

117. Saif J, Schwarz TM, Chau DY, Henstock J, Sami P, Leicht SF, Hermann PC, Alcala S, Mulero F, Shakesheff KM, Heeschen C, Aicher A. Combination of injectable multiple growth factor-releasing scaffolds and cell therapy as an advanced modality to enhance tissue neovascularization. *Arterioscler Thromb Vasc Biol*. Oct 2010;30(10):1897-904. doi:10.1161/ATVBAHA.110.207928

118. Levengood SK, Poellmann MJ, Clark SG, Ingram DA, Yoder MC, Johnson AJ. Human endothelial colony forming cells undergo vasculogenesis within biphasic calcium phosphate bone tissue engineering constructs. *Acta Biomater*. Dec 2011;7(12):4222-8. doi:10.1016/j.actbio.2011.07.006

119. Qiu TG. Transplantation of human embryonic stem cell-derived retinal pigment epithelial cells (MA09-hRPE) in macular degeneration. *NPJ Regen Med*. 2019;4:19. doi:10.1038/s41536-019-0081-8

120. Duh EJ, Sun JK, Stitt AW. Diabetic retinopathy: current understanding, mechanisms, and treatment strategies. *JCI Insight*. Jul 20 2017;2(14)doi:10.1172/jci.insight.93751

121. Hubert L, Darbousset R, Panicot-Dubois L, Robert S, Sabatier F, Fallague K, Dignat-George F, Dubois C. Neutrophils recruit and activate human endothelial colony-forming cells at the site of vessel injury via P-selectin glycoprotein ligand-1 and L-selectin. *J Thromb Haemost*. Jul 2014;12(7):1170-81. doi:10.1111/jth.12551

122. Collett JA, Mehrotra P, Crone A, Shelley WC, Yoder MC, Basile DP. Endothelial colony-forming cells ameliorate endothelial dysfunction via secreted factors following ischemia-reperfusion injury. *Am J Physiol Renal Physiol*. May 1 2017;312(5):F897-F907. doi:10.1152/ajprenal.00643.2016

123. Li S, Tian Y, Huang X, Zhang Y, Wang D, Wei H, Dong J, Jiang R, Zhang J. Intravenous transfusion of endothelial colony-forming cells attenuates vascular degeneration after cerebral aneurysm induction. *Brain Res*. Dec 17 2014;1593:65-75. doi:10.1016/j.brainres.2014.09.077

124. Lin RZ, Moreno-Luna R, Li D, Jaminet SC, Greene AK, Melero-Martin JM. Human endothelial colony-forming cells serve as trophic mediators for mesenchymal stem cell engraftment via paracrine signaling. *Proc Natl Acad Sci U S A*. Jul 15 2014;111(28):10137-42. doi:10.1073/pnas.1405388111

125. Patel JI, Hykin PG, Gregor ZJ, Boulton M, Cree IA. Angiopoietin concentrations in diabetic retinopathy. *Br J Ophthalmol*. Apr 2005;89(4):480-3. doi:10.1136/bjo.2004.049940

126. Gavard J, Patel V, Gutkind JS. Angiopoietin-1 prevents VEGF-induced endothelial permeability by sequestering Src through mDia. *Dev Cell*. Jan 2008;14(1):25-36. doi:10.1016/j.devcel.2007.10.019

127. Thurston G, Rudge JS, Ioffe E, Zhou H, Ross L, Croll SD, Glazer N, Holash J, McDonald DM, Yancopoulos GD. Angiopoietin-1 protects the adult vasculature against plasma leakage. *Nat Med*. Apr 2000;6(4):460-3. doi:10.1038/74725

128. Ponta H, Sherman L, Herrlich PA. CD44: from adhesion molecules to signalling regulators. *Nat Rev Mol Cell Biol*. Jan 2003;4(1):33-45. doi:10.1038/nrm1004

129. Pietras A, Katz AM, Ekstrom EJ, Wee B, Halliday JJ, Pitter KL, Werbeck JL, Amankulor NM, Huse JT, Holland EC. Osteopontin-CD44 signaling in the glioma perivascular niche enhances cancer stem cell phenotypes and promotes aggressive tumor growth. *Cell Stem Cell*. Mar 6 2014;14(3):357-69. doi:10.1016/j.stem.2014.01.005

130. Cheng C, Yaffe MB, Sharp PA. A positive feedback loop couples Ras activation and CD44 alternative splicing. *Genes Dev*. Jul 1 2006;20(13):1715-20. doi:10.1101/gad.1430906

131. Zoller M. CD44: can a cancer-initiating cell profit from an abundantly expressed molecule? *Nat Rev Cancer*. Apr 2011;11(4):254-67. doi:10.1038/nrc3023

132. Ritter MR, Banin E, Moreno SK, Aguilar E, Dorrell MI, Friedlander M. Myeloid progenitors differentiate into microglia and promote vascular repair in a model of ischemic retinopathy. *J Clin Invest*. Dec 2006;116(12):3266-76. doi:10.1172/JCI29683

133. Chang KH, Chan-Ling T, McFarland EL, Afzal A, Pan H, Baxter LC, Shaw LC, Caballero S, Sengupta N, Li Calzi S, Sullivan SM, Grant MB. IGF binding protein-3 regulates hematopoietic stem cell and endothelial precursor cell function during vascular development. *Proc Natl Acad Sci U S A*. Jun 19 2007;104(25):10595-600. doi:10.1073/pnas.0702072104

134. Lofqvist C, Chen J, Connor KM, Smith AC, Aderman CM, Liu N, Pintar JE, Ludwig T, Hellstrom A, Smith LE. IGFBP3 suppresses retinopathy through suppression of oxygen-induced vessel loss and promotion of vascular regrowth. *Proc Natl Acad Sci U S A*. Jun 19 2007;104(25):10589-94. doi:10.1073/pnas.0702031104

135. Baxter RC. IGF binding proteins in cancer: mechanistic and clinical insights. *Nat Rev Cancer*. May 2014;14(5):329-41. doi:10.1038/nrc3720

136. Liu B, Lee KW, Li H, Ma L, Lin GL, Chandraratna RA, Cohen P. Combination therapy of insulin-like growth factor binding protein-3 and retinoid X receptor ligands synergize on prostate cancer cell apoptosis in vitro and in vivo. *Clin Cancer Res*. Jul 1 2005;11(13):4851-6. doi:10.1158/1078-0432.CCR-04-2160

137. Granata R, Trovato L, Garbarino G, Taliano M, Ponti R, Sala G, Ghidoni R, Ghigo E. Dual effects of IGFBP-3 on endothelial cell apoptosis and survival: involvement of the sphingolipid signaling pathways. *FASEB J*. Sep 2004;18(12):1456-8. doi:10.1096/fj.04-1618fje

138. Meyer-Schwickerath R, Pfeiffer A, Blum WF, Freyberger H, Klein M, Losche C, Rollmann R, Schatz H. Vitreous levels of the insulin-like growth factors I and II, and the insulin-like growth factor binding proteins 2 and 3, increase in neovascular eye disease. Studies in nondiabetic and diabetic subjects. *J Clin Invest*. Dec 1993;92(6):2620-5. doi:10.1172/JCI116877

139. Schmid MC, Bisoffi M, Wetterwald A, Gautschi E, Thalmann GN, Mitola S, Bussolino F, Cecchini MG. Insulin-like growth factor binding protein-3 is overexpressed in endothelial cells of mouse breast tumor vessels. *Int J Cancer*. Feb 20 2003;103(5):577-86. doi:10.1002/ijc.10874

140. Fraser HM, Lunn SF, Kim H, Duncan WC, Rodger FE, Illingworth PJ, Erickson GF. Changes in insulin-like growth factor-binding protein-3 messenger ribonucleic acid in endothelial cells of the human corpus luteum: a possible role in luteal development and rescue. *J Clin Endocrinol Metab*. Apr 2000;85(4):1672-7. doi:10.1210/jcem.85.4.6497

141. Zhang Q, Soderland C, Steinle JJ. Regulation of retinal endothelial cell apoptosis through activation of the IGFBP-3 receptor. *Apoptosis*. Mar 2013;18(3):361-8. doi:10.1007/s10495-012-0793-3

142. Jiang Y, Zhang Q, Steinle JJ. Intravitreal injection of IGFBP-3 restores normal insulin signaling in diabetic rat retina. *PLoS One*. 2014;9(4):e93788. doi:10.1371/journal.pone.0093788

143. Lofqvist C, Engstrom E, Sigurdsson J, Hard AL, Niklasson A, Ewald U, Holmstrom G, Smith LE, Hellstrom A. Postnatal head growth deficit among premature infants parallels retinopathy of prematurity and insulin-like growth factor-1 deficit. *Pediatrics*. Jun 2006;117(6):1930-8. doi:10.1542/peds.2005-1926

144. de Braganca AC, Volpini RA, Mehrotra P, Andrade L, Basile DP. Vitamin D deficiency contributes to vascular damage in sustained ischemic acute kidney injury. *Physiol Rep*. Jul 2016;4(13)doi:10.14814/phy2.12829

145. Chan AJ, Alikhan MA, Odobasic D, Gan PY, Khouri MB, Steinmetz OM, Mansell AS, Kitching AR, Holdsworth SR, Summers SA. Innate IL-17A-producing leukocytes promote acute kidney injury via inflammasome and Toll-like receptor activation. *Am J Pathol*. May 2014;184(5):1411-8. doi:10.1016/j.ajpath.2014.01.023

146. Mehrotra P, Patel JB, Ivancic CM, Collett JA, Basile DP. Th-17 cell activation in response to high salt following acute kidney injury is associated with progressive fibrosis and attenuated by AT-1R antagonism. *Kidney Int*. Oct 2015;88(4):776-84. doi:10.1038/ki.2015.200

147. Quintero-Fabian S, Arreola R, Becerril-Villanueva E, Torres-Romero JC, Arana-Argaez V, Lara-Riegos J, Ramirez-Camacho MA, Alvarez-Sanchez ME. Role of matrix metalloproteinases in angiogenesis and cancer. *Front Oncol*. 2019;9:1370. doi:10.3389/fonc.2019.01370

148. Yildirim N, Sahin A, Erol N, Kara S, Uslu S, Topbas S. The relationship between plasma MMP-9 and TIMP-2 levels and intraocular pressure elevation in diabetic patients after intravitreal triamcinolone injection. *J Glaucoma*. Jun-Jul 2008;17(4):253-6. doi:10.1097/IJG.0b013e31815c3a07

149. Gharagozlian S, Svennevig K, Bangstad HJ, Winberg JO, Kolset SO. Matrix metalloproteinases in subjects with type 1 diabetes. *BMC Clin Pathol*. Sep 16 2009;9:7. doi:10.1186/1472-6890-9-7

150. Noda K, Ishida S, Inoue M, Obata K, Oguchi Y, Okada Y, Ikeda E. Production and activation of matrix metalloproteinase-2 in proliferative diabetic retinopathy. *Invest Ophthalmol Vis Sci*. May 2003;44(5):2163-70. doi:10.1167/iovs.02-0662

151. Das A, McGuire PG, Eriqat C, Ober RR, DeJuan E, Jr., Williams GA, McLamore A, Biswas J, Johnson DW. Human diabetic neovascular membranes contain high levels of urokinase and metalloproteinase enzymes. *Invest Ophthalmol Vis Sci*. Mar 1999;40(3):809-13.

152. Berglin L, Sarman S, van der Ploeg I, Steen B, Ming Y, Itohara S, Seregard S, Kvanta A. Reduced choroidal neovascular membrane formation in matrix metalloproteinase-2-deficient mice. *Invest Ophthalmol Vis Sci*. Jan 2003;44(1):403-8. doi:10.1167/iovs.02-0180

153. Descamps FJ, Martens E, Kangave D, Struyf S, Geboes K, Van Damme J, Opdenakker G, Abu El-Asrar AM. The activated form of gelatinase B/matrix metalloproteinase-9 is associated with diabetic vitreous hemorrhage. *Exp Eye Res*. Aug 2006;83(2):401-7. doi:10.1016/j.exer.2006.01.017

154. Mohammad G, Kowluru RA. Novel role of mitochondrial matrix metalloproteinase-2 in the development of diabetic retinopathy. *Invest Ophthalmol Vis Sci*. Jun 1 2011;52(6):3832-41. doi:10.1167/iovs.10-6368

155. Mizutani M, Kern TS, Lorenzi M. Accelerated death of retinal microvascular cells in human and experimental diabetic retinopathy. *J Clin Invest*. Jun 15 1996;97(12):2883-90. doi:10.1172/JCI118746

156. Giebel SJ, Menicucci G, McGuire PG, Das A. Matrix metalloproteinases in early diabetic retinopathy and their role in alteration of the blood-retinal barrier. *Lab Invest*. May 2005;85(5):597-607. doi:10.1038/labinvest.3700251

157. Mohammad G, Vandooren J, Siddiquei MM, Martens E, Abu El-Asrar AM, Opdenakker G. Functional links between gelatinase B/matrix metalloproteinase-9 and prominin-1/CD133 in diabetic retinal vasculopathy and neuropathy. *Prog Retin Eye Res*. Nov 2014;43:76-91. doi:10.1016/j.preteyeres.2014.07.002

158. Abu El-Asrar AM, Siddiquei MM, Nawaz MI, De Hertogh G, Mohammad G, Alam K, Mousa A, Opdenakker G. Coexpression of heparanase activity, cathepsin L, tissue factor, tissue factor pathway inhibitor, and MMP-9 in proliferative diabetic retinopathy. *Mol Vis*. 2016;22:424-35.

159. Hollborn M, Stathopoulos C, Steffen A, Wiedemann P, Kohen L, Bringmann A. Positive feedback regulation between MMP-9 and VEGF in human RPE cells. *Invest Ophthalmol Vis Sci*. Sep 2007;48(9):4360-7. doi:10.1167/iovs.06-1234

160. Hawinkels LJ, Zuidwijk K, Verspaget HW, de Jonge-Muller ES, van Duijn W, Ferreira V, Fontijn RD, David G, Hommes DW, Lamers CB, Sier CF. VEGF release by MMP-9 mediated heparan sulphate cleavage induces colorectal cancer angiogenesis. *Eur J Cancer*. Sep 2008;44(13):1904-13. doi:10.1016/j.ejca.2008.06.031

161. Ebrahem Q, Chaurasia SS, Vasanji A, Qi JH, Klenotic PA, Cutler A, Asosingh K, Erzurum S, Anand-Apte B. Cross-talk between vascular endothelial growth factor and matrix metalloproteinases in the induction of neovascularization in vivo. *Am J Pathol*. Jan 2010;176(1):496-503. doi:10.2353/ajpath.2010.080642

162. Das A, McLamore A, Song W, McGuire PG. Retinal neovascularization is suppressed with a matrix metalloproteinase inhibitor. *Arch Ophthalmol*. Apr 1999;117(4):498-503. doi:10.1001/archopht.117.4.498

163. Barnett JM, McCollum GW, Fowler JA, Duan JJ, Kay JD, Liu RQ, Bingaman DP, Penn JS. Pharmacologic and genetic manipulation of MMP-2 and -9 affects retinal neovascularization in rodent models of OIR. *Invest Ophthalmol Vis Sci*. Feb 2007;48(2):907-15. doi:10.1167/iovs.06-0082

164. Lambert V, Wielockx B, Munaut C, Galopin C, Jost M, Itoh T, Werb Z, Baker A, Libert C, Krell HW, Foidart JM, Noel A, Rakic JM. MMP-2 and MMP-9 synergize in promoting choroidal neovascularization. *FASEB J*. Dec 2003;17(15):2290-2. doi:10.1096/fj.03-0113fje

165. Yeghiazarians Y, Honbo N, Imhof I, Woods B, Aguilera V, Ye J, Boyle AJ, Karliner JS. IL-15: a novel prosurvival signaling pathway in cardiomyocytes. *J Cardiovasc Pharmacol*. May 2014;63(5):406-11. doi:10.1097/FJC.0000000000000061

166. Karavelioglu E, Gonul Y, Kokulu S, Hazman O, Bozkurt F, Kocak A, Eser O. Anti-inflammatory and antiapoptotic effect of interleukine-18 binding protein on the spinal cord ischemia-reperfusion injury. *Inflammation*. Jun 2014;37(3):917-23. doi:10.1007/s10753-014-9811-7

167. Yang XF, Huang YX, Lan M, Zhang TR, Zhou J. Protective effects of leukemia inhibitory factor on retinal vasculature and cells in streptozotocin-induced diabetic mice. *Chin Med J (Engl)*. Jan 5 2018;131(1):75-81. doi:10.4103/0366-6999.221263

168. Au P, Daheron LM, Duda DG, Cohen KS, Tyrrell JA, Lanning RM, Fukumura D, Scadden DT, Jain RK. Differential in vivo potential of endothelial progenitor cells from human umbilical cord blood and adult peripheral blood to form functional long-lasting vessels. *Blood*. Feb 1 2008;111(3):1302-5. doi:10.1182/blood-2007-06-094318

169. Darland DC, D'Amore PA. TGF beta is required for the formation of capillary-like structures in three-dimensional cocultures of 10T1/2 and endothelial cells. *Angiogenesis*. 2001;4(1):11-20. doi:10.1023/a:1016611824696

170. Chen X, Aledia AS, Ghajar CM, Griffith CK, Putnam AJ, Hughes CC, George SC. Prevascularization of a fibrin-based tissue construct accelerates the formation of functional anastomosis with host vasculature. *Tissue Eng Part A*. Jun 2009;15(6):1363-71. doi:10.1089/ten.tea.2008.0314

171. Melero-Martin JM, Khan ZA, Picard A, Wu X, Paruchuri S, Bischoff J. In vivo vasculogenic potential of human blood-derived endothelial progenitor cells. *Blood*. Jun 1 2007;109(11):4761-8. doi:10.1182/blood-2006-12-062471

172. Foubert P, Matrone G, Souttou B, Lere-Dean C, Barateau V, Plouet J, Le Ricousse-Roussanne S, Levy BI, Silvestre JS, Tobelem G. Coadministration of endothelial and smooth muscle progenitor cells enhances the efficiency of proangiogenic cell-based therapy. *Circ Res*. Sep 26 2008;103(7):751-60. doi:10.1161/CIRCRESAHA.108.175083

173. Traktuev DO, Prater DN, Merfeld-Clauss S, Sanjeevaiah AR, Saadatzadeh MR, Murphy M, Johnstone BH, Ingram DA, March KL. Robust functional vascular network formation in vivo by cooperation of adipose progenitor and endothelial cells. *Circ Res*. Jun 19 2009;104(12):1410-20. doi:10.1161/CIRCRESAHA.108.190926

174. Kang KT, Lin RZ, Kuppermann D, Melero-Martin JM, Bischoff J. Endothelial colony forming cells and mesenchymal progenitor cells form blood vessels and increase blood flow in ischemic muscle. *Sci Rep*. Apr 10 2017;7(1):770. doi:10.1038/s41598-017-00809-1

175. Melero-Martin JM, De Obaldia ME, Kang SY, Khan ZA, Yuan L, Oettgen P, Bischoff J. Engineering robust and functional vascular networks in vivo with human adult and cord blood-derived progenitor cells. *Circ Res*. Jul 18 2008;103(2):194-202. doi:10.1161/CIRCRESAHA.108.178590

176. Kang KT, Allen P, Bischoff J. Bioengineered human vascular networks transplanted into secondary mice reconnect with the host vasculature and re-establish perfusion. *Blood*. Dec 15 2011;118(25):6718-21. doi:10.1182/blood-2011-08-375188

177. Kang KT, Coggins M, Xiao C, Rosenzweig A, Bischoff J. Human vasculogenic cells form functional blood vessels and mitigate adverse remodeling after ischemia reperfusion injury in rats. *Angiogenesis*. Oct 2013;16(4):773-84. doi:10.1007/s10456-013-9354-9

178. Lin RZ, Moreno-Luna R, Zhou B, Pu WT, Melero-Martin JM. Equal modulation of endothelial cell function by four distinct tissue-specific mesenchymal stem cells. *Angiogenesis*. Sep 2012;15(3):443-55. doi:10.1007/s10456-012-9272-2

179. Wang CH, Cherng WJ, Yang NI, Kuo LT, Hsu CM, Yeh HI, Lan YJ, Yeh CH, Stanford WL. Late-outgrowth endothelial cells attenuate intimal hyperplasia contributed by mesenchymal stem cells after vascular injury. *Arterioscler Thromb Vasc Biol*. Jan 2008;28(1):54-60. doi:10.1161/ATVBAHA.107.147256

180. Souidi N, Stolk M, Rudeck J, Strunk D, Schallmoser K, Volk HD, Seifert M. Stromal cells act as guardians for endothelial progenitors by reducing their immunogenicity after co-transplantation. *Stem Cells*. May 2017;35(5):1233-1245. doi:10.1002/stem.2573

181. Koike N, Fukumura D, Gralla O, Au P, Schechner JS, Jain RK. Tissue engineering: creation of long-lasting blood vessels. *Nature*. Mar 11 2004;428(6979):138-9. doi:10.1038/428138a

182. Darland DC, Massingham LJ, Smith SR, Piek E, Saint-Geniez M, D'Amore PA. Pericyte production of cell-associated VEGF is differentiation-dependent and is associated with endothelial survival. *Dev Biol*. Dec 1 2003;264(1):275-88. doi:10.1016/j.ydbio.2003.08.015

183. Hendrickx B, Verdonck K, Van den Berge S, Dickens S, Eriksson E, Vranckx JJ, Luttun A. Integration of blood outgrowth endothelial cells in dermal fibroblast sheets promotes full thickness wound healing. *Stem Cells*. Jul 2010;28(7):1165-77. doi:10.1002/stem.445

184. Liu Y, Teoh SH, Chong MS, Lee ES, Mattar CN, Randhawa NK, Zhang ZY, Medina RJ, Kamm RD, Fisk NM, Choolani M, Chan JK. Vasculogenic and osteogenesis-enhancing potential of human umbilical cord blood endothelial colony-forming cells. *Stem Cells*. Sep 2012;30(9):1911-24. doi:10.1002/stem.1164

185. Rossi E, Smadja D, Goyard C, Cras A, Dizier B, Bacha N, Lokajczyk A, Guerin CL, Gendron N, Planquette B, Mignon V, Bernabeu C, Sanchez O, Smadja DM. Co-injection of mesenchymal stem cells with endothelial progenitor cells accelerates muscle recovery in hind limb ischemia through an endoglin-dependent mechanism. *Thromb Haemost*. Oct 5 2017;117(10):1908-1918. doi:10.1160/TH17-01-0007

186. Hofmann NA, Ortner A, Jacamo RO, Reinisch A, Schallmoser K, Rohban R, Etchart N, Fruehwirth M, Beham-Schmid C, Andreeff M, Strunk D. Oxygen sensing mesenchymal progenitors promote neo-vasculogenesis in a humanized mouse model in vivo. *PLoS One*. 2012;7(9):e44468. doi:10.1371/journal.pone.0044468

187. Zhang Y, Liu Y, Liu H, Tang WH. Exosomes: biogenesis, biologic function and clinical potential. *Cell Biosci*. 2019;9:19. doi:10.1186/s13578-019-0282-2

188. Doyle LM, Wang MZ. Overview of extracellular vesicles, their origin, composition, purpose, and methods for exosome isolation and analysis. *Cells*. Jul 15 2019;8(7)doi:10.3390/cells8070727

189. Yanez-Mo M, Siljander PR, Andreu Z, Zavec AB, Borras FE, Buzas EI, Buzas K, Casal E, Cappello F, Carvalho J, Colas E, Cordeiro-da Silva A, Fais S, Falcon-Perez JM, Ghobrial IM, Giebel B, Gimona M, Graner M, Gursel I, Gursel M, Heegaard NH, Hendrix A, Kierulf P, Kokubun K, Kosanovic M, Kralj-Iglic V, Kramer-Albers EM, Laitinen S, Lasser C, Lener T, Ligeti E, Line A, Lipps G, Llorente A, Lotvall J, Mancek-Keber M, Marcilla A, Mittelbrunn M, Nazarenko I, Nolte-'t Hoen EN, Nyman TA, O'Driscoll L, Olivan M, Oliveira C, Pallinger E, Del Portillo HA, Reventos J, Rigau M, Rohde E, Sammar M, Sanchez-Madrid F, Santarem N, Schallmoser K, Ostenfeld MS, Stoorvogel W, Stukelj R, Van der Grein SG, Vasconcelos MH, Wauben MH, De Wever O. Biological properties of extracellular vesicles and their physiological functions. *J Extracell Vesicles*. 2015;4:27066. doi:10.3402/jev.v4.27066

190. Dellett M, Brown ED, Guduric-Fuchs J, O'Connor A, Stitt AW, Medina RJ, Simpson DA. MicroRNA-containing extracellular vesicles released from endothelial colony-forming cells modulate angiogenesis during ischaemic retinopathy. *J Cell Mol Med*. Dec 2017;21(12):3405-3419. doi:10.1111/jcmm.13251

191. Caruso S, Poon IKH. Apoptotic cell-derived extracellular vesicles: more than just debris. *Front Immunol*. 2018;9:1486. doi:10.3389/fimmu.2018.01486

192. Kusuma GD, Barabadi M, Tan JL, Morton DAV, Frith JE, Lim R. To protect and to preserve: novel preservation strategies for extracellular vesicles. *Front Pharmacol*. 2018;9:1199. doi:10.3389/fphar.2018.01199

193. Ge Q, Zhou Y, Lu J, Bai Y, Xie X, Lu Z. miRNA in plasma exosome is stable under different storage conditions. *Molecules*. Jan 27 2014;19(2):1568-75. doi:10.3390/molecules19021568

194. Sokolova V, Ludwig AK, Hornung S, Rotan O, Horn PA, Epple M, Giebel B. Characterisation of exosomes derived from human cells by nanoparticle tracking analysis and scanning electron microscopy. *Colloids Surf B Biointerfaces*. Oct 1 2011;87(1):146-50. doi:10.1016/j.colsurfb.2011.05.013

195. Witwer KW, Buzas EI, Bemis LT, Bora A, Lasser C, Lotvall J, Nolte-'t Hoen EN, Piper MG, Sivaraman S, Skog J, Thery C, Wauben MH, Hochberg F. Standardization of sample collection, isolation and analysis methods in extracellular vesicle research. *J Extracell Vesicles*. 2013;2doi:10.3402/jev.v2i0.20360

196. Rickwood D FT, Steensgaard J. *Centrifugation: essential data*. John Wiley & Sons Ltd; 1994.

197. Ford T, Graham J, Rickwood D. Iodixanol: a nonionic iso-osmotic centrifugation medium for the formation of self-generated gradients. *Anal Biochem*. Aug 1 1994;220(2):360-6. doi:10.1006/abio.1994.1350

198. Van Deun J, Mestdagh P, Sormunen R, Cocquyt V, Vermaelen K, Vandesompele J, Bracke M, De Wever O, Hendrix A. The impact of disparate isolation methods for extracellular vesicles on downstream RNA profiling. *J Extracell Vesicles*. 2014;3doi:10.3402/jev.v3.24858

199. Cantin R, Diou J, Belanger D, Tremblay AM, Gilbert C. Discrimination between exosomes and HIV-1: purification of both vesicles from cell-free supernatants. *J Immunol Methods*. Sep 30 2008;338(1-2):21-30. doi:10.1016/j.jim.2008.07.007

200. Konoshenko MY, Lekchnov EA, Vlassov AV, Laktionov PP. Isolation of extracellular vesicles: general methodologies and latest trends. *Biomed Res Int*. 2018;2018:8545347. doi:10.1155/2018/8545347

201. Weng Y, Sui Z, Shan Y, Hu Y, Chen Y, Zhang L, Zhang Y. Effective isolation of exosomes with polyethylene glycol from cell culture supernatant for in-depth proteome profiling. *Analyst*. Aug 7 2016;141(15):4640-6. doi:10.1039/c6an00892e

202. Li P, Kaslan M, Lee SH, Yao J, Gao Z. Progress in exosome isolation techniques. *Theranostics*. 2017;7(3):789-804. doi:10.7150/thno.18133

203. Sidhom K, Obi PO, Saleem A. A review of exosomal isolation methods: is size exclusion chromatography the best option? *Int J Mol Sci*. Sep 4 2020;21(18)doi:10.3390/ijms21186466

204. Thery C, Amigorena S, Raposo G, Clayton A. Isolation and characterization of exosomes from cell culture supernatants and biological fluids. *Curr Protoc Cell Biol*. Apr 2006;Chapter 3:Unit 3 22. doi:10.1002/0471143030.cb0322s30

205. Clayton A, Court J, Navabi H, Adams M, Mason MD, Hobot JA, Newman GR, Jasani B. Analysis of antigen presenting cell derived exosomes, based on immuno-magnetic isolation and flow cytometry. *J Immunol Methods*. Jan 1 2001;247(1-2):163-74. doi:10.1016/s0022-1759(00)00321-5

206. Boriachek K, Masud MK, Palma C, Phan HP, Yamauchi Y, Hossain MSA, Nguyen NT, Salomon C, Shiddiky MJA. Avoiding pre-Isolation step in exosome analysis: direct isolation and sensitive detection of exosomes using gold-loaded nanoporous ferric oxide nanozymes. *Anal Chem*. Mar 19 2019;91(6):3827-3834. doi:10.1021/acs.analchem.8b03619

207. Kim G, Yoo CE, Kim M, Kang HJ, Park D, Lee M, Huh N. Noble polymeric surface conjugated with zwitterionic moieties and antibodies for the isolation of exosomes from human serum. *Bioconjug Chem*. Oct 17 2012;23(10):2114-20. doi:10.1021/bc300339b

208. Sharma P, Ludwig S, Muller L, Hong CS, Kirkwood JM, Ferrone S, Whiteside TL. Immunoaffinity-based isolation of melanoma cell-derived exosomes from plasma of patients with melanoma. *J Extracell Vesicles*. 2018;7(1):1435138. doi:10.1080/20013078.2018.1435138

209. Ostenfeld MS, Jensen SG, Jeppesen DK, Christensen LL, Thorsen SB, Stenvang J, Hvam ML, Thomsen A, Mouritzen P, Rasmussen MH, Nielsen HJ, Orntoft TF, Andersen CL. miRNA profiling of circulating EpCAM(+) extracellular vesicles: promising biomarkers of colorectal cancer. *J Extracell Vesicles*. 2016;5:31488. doi:10.3402/jev.v5.31488

210. Ghosh A, Davey M, Chute IC, Griffiths SG, Lewis S, Chacko S, Barnett D, Crapoulet N, Fournier S, Joy A, Caissie MC, Ferguson AD, Daigle M, Meli MV, Lewis SM, Ouellette RJ. Rapid isolation of extracellular vesicles from cell culture and biological fluids using a synthetic peptide with specific affinity for heat shock proteins. *PLoS One*. 2014;9(10):e110443. doi:10.1371/journal.pone.0110443

211. Balaj L, Atai NA, Chen W, Mu D, Tannous BA, Breakefield XO, Skog J, Maguire CA. Heparin affinity purification of extracellular vesicles. *Sci Rep*. May 19 2015;5:10266. doi:10.1038/srep10266

212. Reiner AT, Witwer KW, van Balkom BWM, de Beer J, Brodie C, Corteling RL, Gabrielsson S, Gimona M, Ibrahim AG, de Kleijn D, Lai CP, Lotvall J, Del Portillo HA, Reischl IG, Riazifar M, Salomon C, Tahara H, Toh WS, Wauben MHM, Yang VK, Yang Y, Yeo RWY, Yin H, Giebel B, Rohde E, Lim SK. Concise review: developing best-practice models for the therapeutic use of extracellular vesicles. *Stem Cells Transl Med*. Aug 2017;6(8):1730-1739. doi:10.1002/sctm.17-0055

213. Contreras-Naranjo JC, Wu HJ, Ugaz VM. Microfluidics for exosome isolation and analysis: enabling liquid biopsy for personalized medicine. *Lab Chip*. Oct 25 2017;17(21):3558-3577. doi:10.1039/c7lc00592j

214. Kanwar SS, Dunlay CJ, Simeone DM, Nagrath S. Microfluidic device (ExoChip) for on-chip isolation, quantification and characterization of circulating exosomes. *Lab Chip*. Jun 7 2014;14(11):1891-900. doi:10.1039/c4lc00136b

215. Vaidyanathan R, Naghibosadat M, Rauf S, Korbie D, Carrascosa LG, Shiddiky MJ, Trau M. Detecting exosomes specifically: a multiplexed device based on alternating current electrohydrodynamic induced nanoshearing. *Anal Chem*. Nov 18 2014;86(22):11125-32. doi:10.1021/ac502082b

216. Zhang P, He M, Zeng Y. Ultrasensitive microfluidic analysis of circulating exosomes using a nanostructured graphene oxide/polydopamine coating. *Lab Chip*. Aug 2 2016;16(16):3033-42. doi:10.1039/c6lc00279j

217. Hisey CL, Dorayappan KDP, Cohn DE, Selvendiran K, Hansford DJ. Microfluidic affinity separation chip for selective capture and release of label-free ovarian cancer exosomes. *Lab Chip*. Oct 9 2018;18(20):3144-3153. doi:10.1039/c8lc00834e

218. Chen C, Skog J, Hsu CH, Lessard RT, Balaj L, Wurdinger T, Carter BS, Breakefield XO, Toner M, Irimia D. Microfluidic isolation and transcriptome analysis of serum microvesicles. *Lab Chip*. Feb 21 2010;10(4):505-11. doi:10.1039/b916199f

219. Lobb RJ, Becker M, Wen SW, Wong CS, Wiegmans AP, Leimgruber A, Moller A. Optimized exosome isolation protocol for cell culture supernatant and human plasma. *J Extracell Vesicles*. 2015;4:27031. doi:10.3402/jev.v4.27031

220. Alvarez ML, Khosroheidari M, Kanchi Ravi R, DiStefano JK. Comparison of protein, microRNA, and mRNA yields using different methods of urinary exosome isolation for the discovery of kidney disease biomarkers. *Kidney Int*. Nov 2012;82(9):1024-32. doi:10.1038/ki.2012.256

221. Rood IM, Deegens JK, Merchant ML, Tamboer WP, Wilkey DW, Wetzels JF, Klein JB. Comparison of three methods for isolation of urinary microvesicles to identify biomarkers of nephrotic syndrome. *Kidney Int*. Oct 2010;78(8):810-6. doi:10.1038/ki.2010.262

222. Taylor DD, Shah S. Methods of isolating extracellular vesicles impact down-stream analyses of their cargoes. *Methods*. Oct 1 2015;87:3-10. doi:10.1016/j.ymeth.2015.02.019

223. Vergauwen G, Dhondt B, Van Deun J, De Smedt E, Berx G, Timmerman E, Gevaert K, Miinalainen I, Cocquyt V, Braems G, Van den Broecke R, Denys H, De Wever O, Hendrix A. Confounding factors of ultrafiltration and protein analysis in extracellular vesicle research. *Sci Rep*. Jun 2 2017;7(1):2704. doi:10.1038/s41598-017-02599-y

224. Stranska R, Gysbrechts L, Wouters J, Vermeersch P, Bloch K, Dierickx D, Andrei G, Snoeck R. Comparison of membrane affinity-based method with size-exclusion chromatography for isolation of exosome-like vesicles from human plasma. *J Transl Med*. Jan 9 2018;16(1):1. doi:10.1186/s12967-017-1374-6

225. Boing AN, van der Pol E, Grootemaat AE, Coumans FA, Sturk A, Nieuwland R. Single-step isolation of extracellular vesicles by size-exclusion chromatography. *J Extracell Vesicles*. 2014;3doi:10.3402/jev.v3.23430

226. Lane RE, Korbie D, Trau M, Hill MM. Optimizing size exclusion chromatography for extracellular Vesicle enrichment and proteomic analysis from clinically relevant samples. *Proteomics*. Apr 2019;19(8):e1800156. doi:10.1002/pmic.201800156

227. Guan S, Yu H, Yan G, Gao M, Sun W, Zhang X. Characterization of urinary exosomes purified with size exclusion chromatography and ultracentrifugation. *J Proteome Res*. Jun 5 2020;19(6):2217-2225. doi:10.1021/acs.jproteome.9b00693

228. Gamez-Valero A, Monguio-Tortajada M, Carreras-Planella L, Franquesa M, Beyer K, Borras FE. Size-exclusion chromatography-based isolation minimally alters Extracellular Vesicles' characteristics compared to precipitating agents. *Sci Rep*. Sep 19 2016;6:33641. doi:10.1038/srep33641

229. Takov K, Yellon DM, Davidson SM. Comparison of small extracellular vesicles isolated from plasma by ultracentrifugation or size-exclusion chromatography: yield, purity and functional potential. *J Extracell Vesicles*. 2019;8(1):1560809. doi:10.1080/20013078.2018.1560809

230. Mol EA, Goumans MJ, Doevendans PA, Sluijter JPG, Vader P. Higher functionality of extracellular vesicles isolated using size-exclusion chromatography compared to ultracentrifugation. *Nanomedicine*. Aug 2017;13(6):2061-2065. doi:10.1016/j.nano.2017.03.011

231. Linares R, Tan S, Gounou C, Arraud N, Brisson AR. High-speed centrifugation induces aggregation of extracellular vesicles. *J Extracell Vesicles*. 2015;4:29509. doi:10.3402/jev.v4.29509

232. Livshits MA, Khomyakova E, Evtushenko EG, Lazarev VN, Kulemin NA, Semina SE, Generozov EV, Govorun VM. Isolation of exosomes by differential centrifugation: Theoretical analysis of a commonly used protocol. *Sci Rep*. Nov 30 2015;5:17319. doi:10.1038/srep17319

233. Navajas R, Corrales FJ, Paradela A. Serum exosome isolation by size-exclusion chromatography for the discovery and validation of preeclampsia-associated biomarkers. In: Brun V, Couté Y, eds. *Proteomics for Biomarker Discovery: Methods and Protocols*. Springer New York; 2019:39-50.

234. de Menezes-Neto A, Saez MJ, Lozano-Ramos I, Segui-Barber J, Martin-Jaular L, Ullate JM, Fernandez-Becerra C, Borras FE, Del Portillo HA. Size-exclusion chromatography as a stand-alone methodology identifies novel markers in mass spectrometry analyses of plasma-derived vesicles from healthy individuals. *J Extracell Vesicles*. 2015;4:27378. doi:10.3402/jev.v4.27378

235. Davis CN, Phillips H, Tomes JJ, Swain MT, Wilkinson TJ, Brophy PM, Morphew RM. The importance of extracellular vesicle purification for downstream analysis: A comparison of differential centrifugation and size exclusion chromatography for helminth pathogens. *PLoS Negl Trop Dis*. Feb 2019;13(2):e0007191. doi:10.1371/journal.pntd.0007191

236. Hong CS, Funk S, Muller L, Boyiadzis M, Whiteside TL. Isolation of biologically active and morphologically intact exosomes from plasma of patients with cancer. *J Extracell Vesicles*. 2016;5:29289. doi:10.3402/jev.v5.29289

237. Aqrawi LA, Galtung HK, Vestad B, Ovstebo R, Thiede B, Rusthen S, Young A, Guerreiro EM, Utheim TP, Chen X, Utheim OA, Palm O, Jensen JL. Identification of potential saliva and tear biomarkers in primary Sjogren's syndrome, utilising the extraction of extracellular vesicles and proteomics analysis. *Arthritis Res Ther*. Jan 25 2017;19(1):14. doi:10.1186/s13075-017-1228-x

238. Muller L, Hong CS, Stolz DB, Watkins SC, Whiteside TL. Isolation of biologically-active exosomes from human plasma. *J Immunol Methods*. Sep 2014;411:55-65. doi:10.1016/j.jim.2014.06.007

239. Kim JW, Wieckowski E, Taylor DD, Reichert TE, Watkins S, Whiteside TL. Fas ligand-positive membranous vesicles isolated from sera of patients with oral cancer induce apoptosis of activated T lymphocytes. *Clin Cancer Res*. Feb 1 2005;11(3):1010-20.

240. Guerreiro EM, Vestad B, Steffensen LA, Aass HCD, Saeed M, Ovstebo R, Costea DE, Galtung HK, Soland TM. Efficient extracellular vesicle isolation by combining cell media modifications, ultrafiltration, and size-exclusion chromatography. *PLoS One*. 2018;13(9):e0204276. doi:10.1371/journal.pone.0204276

241. Gardiner C, Di Vizio D, Sahoo S, Thery C, Witwer KW, Wauben M, Hill AF. Techniques used for the isolation and characterization of extracellular vesicles: results of a worldwide survey. *J Extracell Vesicles*. 2016;5:32945. doi:10.3402/jev.v5.32945

242. Benedikter BJ, Bouwman FG, Vajen T, Heinzmann ACA, Grauls G, Mariman EC, Wouters EFM, Savelkoul PH, Lopez-Iglesias C, Koenen RR, Rohde GGU, Stassen FRM. Ultrafiltration combined with size exclusion chromatography efficiently isolates extracellular vesicles from cell culture media for compositional and functional studies. *Sci Rep*. Nov 10 2017;7(1):15297. doi:10.1038/s41598-017-15717-7

243. Nordin JZ, Lee Y, Vader P, Mager I, Johansson HJ, Heusermann W, Wiklander OP, Hallbrink M, Seow Y, Bultema JJ, Gilthorpe J, Davies T, Fairchild PJ, Gabrielsson S, Meisner-Kober NC, Lehtio J, Smith CI, Wood MJ, El Andaloussi S. Ultrafiltration with size-exclusion liquid chromatography for high yield isolation of extracellular vesicles preserving intact biophysical and functional properties. *Nanomedicine*. May 2015;11(4):879-83. doi:10.1016/j.nano.2015.01.003

244. Cho S, Yang HC, Rhee WJ. Development and comparative analysis of human urine exosome isolation strategies. *Process Biochemistry*. 2020;88:197-203. doi:10.1016/j.procbio.2019.09.017

245. Wooff Y, Cioanca AV, Chu-Tan JA, Aggio-Bruce R, Schumann U, Natoli R. Small-medium extracellular vesicles and their miRNA cargo in retinal health and degeneration: mediators of homeostasis, and vehicles for targeted gene therapy. *Front Cell Neurosci*. 2020;14:160. doi:10.3389/fncel.2020.00160

246. Mighty J, Zhou J, Benito-Martin A, Sauma S, Hanna S, Onwumere O, Shi C, Muntzel M, Sauane M, Young M, Molina H, Cox D, Redenti S. Analysis of adult neural retina extracellular vesicle release, RNA transport and proteomic cargo. *Invest Ophthalmol Vis Sci*. Feb 7 2020;61(2):30. doi:10.1167/iovs.61.2.30

247. Zhou J, Benito-Martin A, Mighty J, Chang L, Ghoroghi S, Wu H, Wong M, Guariglia S, Baranov P, Young M, Gharbaran R, Emerson M, Mark MT, Molina H, Canto-Soler MV, Selgas HP, Redenti S. Retinal progenitor cells release extracellular vesicles containing developmental transcription factors, microRNA and membrane proteins. *Sci Rep*. Feb 12 2018;8(1):2823. doi:10.1038/s41598-018-20421-1

248. Zhou J, Flores-Bellver M, Pan J, Benito-Martin A, Shi C, Onwumere O, Mighty J, Qian J, Zhong X, Hogue T, Amponsah-Antwi B, Einbond L, Gharbaran R, Wu H, Chen B-J, Zheng Z, Tchaikovskaya T, Zhang X, Peinado H, Canto-Soler MV, Redenti S. Human retinal organoids release extracellular vesicles that regulate gene expression in target human retinal progenitor cells. *bioRxiv*. 2021:2021.02.10.430690. doi:10.1101/2021.02.10.430690

249. Nomura S, Shouzu A, Omoto S, Nishikawa M, Iwasaka T, Fukuhara S. Activated platelet and oxidized LDL induce endothelial membrane vesiculation: clinical significance of endothelial cell-derived microparticles in patients with type 2 diabetes. *Clin Appl Thromb Hemost*. Jul 2004;10(3):205-15. doi:10.1177/107602960401000302

250. Koga H, Sugiyama S, Kugiyama K, Watanabe K, Fukushima H, Tanaka T, Sakamoto T, Yoshimura M, Jinnouchi H, Ogawa H. Elevated levels of VE-cadherin-positive endothelial microparticles in patients with type 2 diabetes mellitus and coronary artery disease. *J Am Coll Cardiol*. May 17 2005;45(10):1622-30. doi:10.1016/j.jacc.2005.02.047

251. Tushuizen ME, Nieuwland R, Rustemeijer C, Hensgens BE, Sturk A, Heine RJ, Diamant M. Elevated endothelial microparticles following consecutive meals are associated with vascular endothelial dysfunction in type 2 diabetes. *Diabetes Care*. Mar 2007;30(3):728-30. doi:10.2337/dc06-1473

252. Mallat Z, Benamer H, Hugel B, Benessiano J, Steg PG, Freyssinet JM, Tedgui A. Elevated levels of shed membrane microparticles with procoagulant potential in the peripheral circulating blood of patients with acute coronary syndromes. *Circulation*. Feb 29 2000;101(8):841-3. doi:10.1161/01.cir.101.8.841

253. Preston RA, Jy W, Jimenez JJ, Mauro LM, Horstman LL, Valle M, Aime G, Ahn YS. Effects of severe hypertension on endothelial and platelet microparticles. *Hypertension*. Feb 2003;41(2):211-7. doi:10.1161/01.hyp.0000049760.15764.2d

254. Boulanger CM, Amabile N, Tedgui A. Circulating microparticles: a potential prognostic marker for atherosclerotic vascular disease. *Hypertension*. Aug 2006;48(2):180-6. doi:10.1161/01.HYP.0000231507.00962.b5

255. Biro E, Sturk-Maquelin KN, Vogel GM, Meuleman DG, Smit MJ, Hack CE, Sturk A, Nieuwland R. Human cell-derived microparticles promote thrombus formation in vivo in a tissue factor-dependent manner. *J Thromb Haemost*. Dec 2003;1(12):2561-8. doi:10.1046/j.1538-7836.2003.00456.x

256. Chou J, Mackman N, Merrill-Skoloff G, Pedersen B, Furie BC, Furie B. Hematopoietic cell-derived microparticle tissue factor contributes to fibrin formation during thrombus propagation. *Blood*. Nov 15 2004;104(10):3190-7. doi:10.1182/blood-2004-03-0935

257. Ogata N, Nomura S, Shouzu A, Imaizumi M, Arichi M, Matsumura M. Elevation of monocyte-derived microparticles in patients with diabetic retinopathy. *Diabetes Res Clin Pract*. Sep 2006;73(3):241-8. doi:10.1016/j.diabres.2006.01.014

258. Ogata N, Imaizumi M, Nomura S, Shozu A, Arichi M, Matsuoka M, Matsumura M. Increased levels of platelet-derived microparticles in patients with diabetic retinopathy. *Diabetes Res Clin Pract*. Jun 2005;68(3):193-201. doi:10.1016/j.diabres.2004.10.010

259. Barry OP, Pratico D, Lawson JA, FitzGerald GA. Transcellular activation of platelets and endothelial cells by bioactive lipids in platelet microparticles. *J Clin Invest*. May 1 1997;99(9):2118-27. doi:10.1172/JCI119385

260. Mause SF, von Hundelshausen P, Zernecke A, Koenen RR, Weber C. Platelet microparticles: a transcellular delivery system for RANTES promoting monocyte recruitment on endothelium. *Arterioscler Thromb Vasc Biol*. Jul 2005;25(7):1512-8. doi:10.1161/01.ATV.0000170133.43608.37

261. Tokarz A, Szuscik I, Kusnierz-Cabala B, Kapusta M, Konkolewska M, Zurakowski A, Georgescu A, Stepien E. Extracellular vesicles participate in the transport of cytokines and angiogenic factors in diabetic patients with ocular complications. *Folia Med Cracov*. 2015;55(4):35-48.

262. Amabile N, Guerin AP, Leroyer A, Mallat Z, Nguyen C, Boddaert J, London GM, Tedgui A, Boulanger CM. Circulating endothelial microparticles are associated with vascular dysfunction in patients with end-stage renal failure. *J Am Soc Nephrol*. Nov 2005;16(11):3381-8. doi:10.1681/ASN.2005050535

263. Chahed S, Leroyer AS, Benzerroug M, Gaucher D, Georgescu A, Picaud S, Silvestre JS, Gaudric A, Tedgui A, Massin P, Boulanger CM. Increased vitreous shedding of microparticles in proliferative diabetic retinopathy stimulates endothelial proliferation. *Diabetes*. Mar 2010;59(3):694-701. doi:10.2337/db08-1524

264. Martins B, Amorim M, Reis F, Ambrosio AF, Fernandes R. Extracellular vesicles and microRNA: putative role in diagnosis and treatment of diabetic retinopathy. *Antioxidants (Basel)*. Aug 4 2020;9(8)doi:10.3390/antiox9080705

265. Jansen F, Yang X, Hoyer FF, Paul K, Heiermann N, Becher MU, Abu Hussein N, Kebschull M, Bedorf J, Franklin BS, Latz E, Nickenig G, Werner N. Endothelial microparticle uptake in target cells is annexin I/phosphatidylserine receptor dependent and prevents apoptosis. *Arterioscler Thromb Vasc Biol*. Aug 2012;32(8):1925-35. doi:10.1161/ATVBAHA.112.253229

266. Wang J, Chen S, Ma X, Cheng C, Xiao X, Chen J, Liu S, Zhao B, Chen Y. Effects of endothelial progenitor cell-derived microvesicles on hypoxia/reoxygenation-induced endothelial dysfunction and apoptosis. *Oxid Med Cell Longev*. 2013;2013:572729. doi:10.1155/2013/572729

267. Deregibus MC, Cantaluppi V, Calogero R, Lo Iacono M, Tetta C, Biancone L, Bruno S, Bussolati B, Camussi G. Endothelial progenitor cell derived microvesicles activate an angiogenic program in endothelial cells by a horizontal transfer of mRNA. *Blood*. Oct 1 2007;110(7):2440-8. doi:10.1182/blood-2007-03-078709

268. Burger D, Vinas JL, Akbari S, Dehak H, Knoll W, Gutsol A, Carter A, Touyz RM, Allan DS, Burns KD. Human endothelial colony-forming cells protect against acute kidney injury: role of exosomes. *Am J Pathol*. Aug 2015;185(8):2309-23. doi:10.1016/j.ajpath.2015.04.010

269. Li X, Jiang C, Zhao J. Human endothelial progenitor cells-derived exosomes accelerate cutaneous wound healing in diabetic rats by promoting endothelial function. *J Diabetes Complications*. Aug 2016;30(6):986-92. doi:10.1016/j.jdiacomp.2016.05.009

270. Li X, Chen C, Wei L, Li Q, Niu X, Xu Y, Wang Y, Zhao J. Exosomes derived from endothelial progenitor cells attenuate vascular repair and accelerate reendothelialization by enhancing endothelial function. *Cytotherapy*. Feb 2016;18(2):253-62. doi:10.1016/j.jcyt.2015.11.009

271. Vinas JL, Burger D, Zimpelmann J, Haneef R, Knoll W, Campbell P, Gutsol A, Carter A, Allan DS, Burns KD. Transfer of microRNA-486-5p from human endothelial colony forming cell-derived exosomes reduces ischemic kidney injury. *Kidney Int*. Dec 2016;90(6):1238-1250. doi:10.1016/j.kint.2016.07.015

272. Zhang J, Chen C, Hu B, Niu X, Liu X, Zhang G, Zhang C, Li Q, Wang Y. Exosomes derived from human endothelial progenitor cells accelerate cutaneous wound healing by promoting angiogenesis through ERK1/2 signaling. *Int J Biol Sci*. 2016;12(12):1472-1487. doi:10.7150/ijbs.15514

273. Cantaluppi V, Gatti S, Medica D, Figliolini F, Bruno S, Deregibus MC, Sordi A, Biancone L, Tetta C, Camussi G. Microvesicles derived from endothelial progenitor cells protect the kidney from ischemia-reperfusion injury by microRNA-dependent reprogramming of resident renal cells. *Kidney Int*. Aug 2012;82(4):412-27. doi:10.1038/ki.2012.105

274. Vinas JL, Spence M, Gutsol A, Knoll W, Burger D, Zimpelmann J, Allan DS, Burns KD. Receptor-Ligand Interaction Mediates Targeting of Endothelial Colony Forming Cell-derived Exosomes to the Kidney after Ischemic Injury. *Sci Rep*. Nov 5 2018;8(1):16320. doi:10.1038/s41598-018-34557-7

275. Ranghino A, Cantaluppi V, Grange C, Vitillo L, Fop F, Biancone L, Deregibus MC, Tetta C, Segoloni GP, Camussi G. Endothelial progenitor cell-derived microvesicles improve neovascularization in a murine model of hindlimb ischemia. *Int J Immunopathol Pharmacol*. Jan-Mar 2012;25(1):75-85. doi:10.1177/039463201202500110

276. Gao W, Li F, Liu L, Xu X, Zhang B, Wu Y, Yin D, Zhou S, Sun D, Huang Y, Zhang J. Endothelial colony-forming cell-derived exosomes restore blood-brain barrier continuity in mice subjected to traumatic brain injury. *Exp Neurol*. Sep 2018;307:99-108. doi:10.1016/j.expneurol.2018.06.001

277. Zhou Y, Li P, Goodwin AJ, Cook JA, Halushka PV, Chang E, Fan H. Exosomes from endothelial progenitor cells improve the outcome of a murine model of sepsis. *Mol Ther*. May 2 2018;26(5):1375-1384. doi:10.1016/j.ymthe.2018.02.020

278. Jia Y, Zhu Y, Qiu S, Xu J, Chai Y. Exosomes secreted by endothelial progenitor cells accelerate bone regeneration during distraction osteogenesis by stimulating angiogenesis. *Stem Cell Res Ther*. Jan 11 2019;10(1):12. doi:10.1186/s13287-018-1115-7

279. Zhou Y, Li P, Goodwin AJ, Cook JA, Halushka PV, Chang E, Zingarelli B, Fan H. Exosomes from endothelial progenitor cells improve outcomes of the lipopolysaccharide-induced acute lung injury. *Crit Care*. Feb 13 2019;23(1):44. doi:10.1186/s13054-019-2339-3

280. Metin T, Dinc E, Gorur A, Erdogan S, Ertekin S, Sari AA, Tamer L, Celik Y. Evaluation of the plasma microRNA levels in stage 3 premature retinopathy with plus disease: preliminary study. *Eye (Lond)*. Feb 2018;32(2):415-420. doi:10.1038/eye.2017.193

281. Nunes DN, Dias-Neto E, Cardo-Vila M, Edwards JK, Dobroff AS, Giordano RJ, Mandelin J, Brentani HP, Hasselgren C, Yao VJ, Marchio S, Pereira CA, Passetti F, Calin GA, Sidman RL, Arap W, Pasqualini R. Synchronous down-modulation of miR-17 family members is an early causative event in the retinal angiogenic switch. *Proc Natl Acad Sci U S A*. Mar 24 2015;112(12):3770-5. doi:10.1073/pnas.1500008112

282. Wurdinger T, Tannous BA, Saydam O, Skog J, Grau S, Soutschek J, Weissleder R, Breakefield XO, Krichevsky AM. miR-296 regulates growth factor receptor overexpression in angiogenic endothelial cells. *Cancer Cell*. Nov 4 2008;14(5):382-93. doi:10.1016/j.ccr.2008.10.005

283. Takata H, Kato M, Denda K, Kitamura N. A hrs binding protein having a Src homology 3 domain is involved in intracellular degradation of growth factors and their receptors. *Genes Cells*. Jan 2000;5(1):57-69. doi:10.1046/j.1365-2443.2000.00303.x

284. Ewan LC, Jopling HM, Jia H, Mittar S, Bagherzadeh A, Howell GJ, Walker JH, Zachary IC, Ponnambalam S. Intrinsic tyrosine kinase activity is required for vascular endothelial growth factor receptor 2 ubiquitination, sorting and degradation in endothelial cells. *Traffic*. Sep 2006;7(9):1270-82. doi:10.1111/j.1600-0854.2006.00462.x

285. Stern KA, Visser Smit GD, Place TL, Winistorfer S, Piper RC, Lill NL. Epidermal growth factor receptor fate is controlled by Hrs tyrosine phosphorylation sites that regulate Hrs degradation. *Mol Cell Biol*. Feb 2007;27(3):888-98. doi:10.1128/MCB.02356-05

286. Bache KG, Raiborg C, Mehlum A, Stenmark H. STAM and Hrs are subunits of a multivalent ubiquitin-binding complex on early endosomes. *J Biol Chem*. Apr 4 2003;278(14):12513-21. doi:10.1074/jbc.M210843200

287. Folkerth RD. Descriptive analysis and quantification of angiogenesis in human brain tumors. *J Neurooncol*. Oct-Nov 2000;50(1-2):165-72. doi:10.1023/a:1006499824379

288. Ye P, Liu J, He F, Xu W, Yao K. Hypoxia-induced deregulation of miR-126 and its regulative effect on VEGF and MMP-9 expression. *Int J Med Sci*. 2014;11(1):17-23. doi:10.7150/ijms.7329

289. Wang H, Bloom O, Zhang M, Vishnubhakat JM, Ombrellino M, Che J, Frazier A, Yang H, Ivanova S, Borovikova L, Manogue KR, Faist E, Abraham E, Andersson J, Andersson U, Molina PE, Abumrad NN, Sama A, Tracey KJ. HMG-1 as a late mediator of endotoxin lethality in mice. *Science*. Jul 9 1999;285(5425):248-51. doi:10.1126/science.285.5425.248

290. Yang H, Ochani M, Li J, Qiang X, Tanovic M, Harris HE, Susarla SM, Ulloa L, Wang H, DiRaimo R, Czura CJ, Wang H, Roth J, Warren HS, Fink MP, Fenton MJ, Andersson U, Tracey KJ. Reversing established sepsis with antagonists of endogenous high-mobility group box 1. *Proc Natl Acad Sci U S A*. Jan 6 2004;101(1):296-301. doi:10.1073/pnas.2434651100

291. Suda K, Kitagawa Y, Ozawa S, Saikawa Y, Ueda M, Ebina M, Yamada S, Hashimoto S, Fukata S, Abraham E, Maruyama I, Kitajima M, Ishizaka A. Anti-high-mobility group box chromosomal protein 1 antibodies improve survival of rats with sepsis. *World J Surg*. Sep 2006;30(9):1755-62. doi:10.1007/s00268-005-0369-2

292. Huang W, Tang Y, Li L. HMGB1, a potent proinflammatory cytokine in sepsis. *Cytokine*. Aug 2010;51(2):119-26. doi:10.1016/j.cyto.2010.02.021

293. Liu Y, Zhuang GB, Zhou XZ. HMBG1 as a driver of inflammatory and immune processes in the pathogenesis of ocular diseases. *J Ophthalmol*. 2018;2018:5195290. doi:10.1155/2018/5195290

294. Nogueira-Machado JA, Volpe CM, Veloso CA, Chaves MM. HMGB1, TLR and RAGE: a functional tripod that leads to diabetic inflammation. *Expert Opin Ther Targets*. Aug 2011;15(8):1023-35. doi:10.1517/14728222.2011.575360

295. Klune JR, Dhupar R, Cardinal J, Billiar TR, Tsung A. HMGB1: endogenous danger signaling. *Mol Med*. Jul-Aug 2008;14(7-8):476-84. doi:10.2119/2008-00034.Klune

296. El-Asrar AM, Nawaz MI, Kangave D, Geboes K, Ola MS, Ahmad S, Al-Shabrawey M. High-mobility group box-1 and biomarkers of inflammation in the vitreous from patients with proliferative diabetic retinopathy. *Mol Vis*. 2011;17:1829-38.

297. El-Asrar AM, Missotten L, Geboes K. Expression of high-mobility groups box-1/receptor for advanced glycation end products/osteopontin/early growth response-1 pathway in proliferative vitreoretinal epiretinal membranes. *Mol Vis*. Feb 17 2011;17:508-18.

298. Abu El-Asrar AM, Alam K, Garcia-Ramirez M, Ahmad A, Siddiquei MM, Mohammad G, Mousa A, De Hertogh G, Opdenakker G, Simo R. Association of HMGB1 with oxidative stress markers and regulators in PDR. *Mol Vis*. 2017;23:853-871.

299. Mohammad G, Jomar D, Siddiquei MM, Alam K, Abu El-Asrar AM. High-mobility group box-1 protein mediates the regulation of signal transducer and activator of transcription-3 in the diabetic retina and in human retinal muller cells. *Ophthalmic Res*. 2017;57(3):150-160. doi:10.1159/000448115

300. Liu L, Jiang Y, Steinle JJ. Inhibition of HMGB1 protects the retina from ischemia-reperfusion, as well as reduces insulin resistance proteins. *PLoS One*. 2017;12(5):e0178236. doi:10.1371/journal.pone.0178236

301. Jiang S, Chen X. HMGB1 siRNA can reduce damage to retinal cells induced by high glucose in vitro and in vivo. *Drug Des Devel Ther*. 2017;11:783-795. doi:10.2147/DDDT.S129913

302. Abu El-Asrar AM, Mohammad G, Nawaz MI, Siddiquei MM. High-mobility group box-1 modulates the expression of inflammatory and angiogenic signaling pathways in diabetic retina. *Curr Eye Res*. 2015;40(11):1141-52. doi:10.3109/02713683.2014.982829

303. Jiang Y, Steinle JJ. HMGB1 inhibits insulin signalling through TLR4 and RAGE in human retinal endothelial cells. *Growth Factors*. Aug 2018;36(3-4):164-171. doi:10.1080/08977194.2018.1539393

304. Zhang W, Wang Y, Kong Y. Exosomes derived from mesenchymal stem cells modulate miR-126 to ameliorate hyperglycemia-induced retinal inflammation via targeting HMGB1. *Invest Ophthalmol Vis Sci*. Jan 2 2019;60(1):294-303. doi:10.1167/iovs.18-25617

305. Bartel DP. MicroRNAs: genomics, biogenesis, mechanism, and function. *Cell*. Jan 23 2004;116(2):281-97. doi:10.1016/s0092-8674(04)00045-5

306. Chistiakov DA, Orekhov AN, Bobryshev YV. The role of miR-126 in embryonic angiogenesis, adult vascular homeostasis, and vascular repair and its alterations in atherosclerotic disease. *J Mol Cell Cardiol*. Aug 2016;97:47-55. doi:10.1016/j.yjmcc.2016.05.007

307. d'Audigier C, Susen S, Blandinieres A, Mattot V, Saubamea B, Rossi E, Nevo N, Lecourt S, Guerin CL, Dizier B, Gendron N, Caetano B, Gaussem P, Soncin F, Smadja DM. Egfl7 Represses the Vasculogenic Potential of Human Endothelial Progenitor Cells. *Stem Cell Rev Rep*. Feb 2018;14(1):82-91. doi:10.1007/s12015-017-9775-8

308. Fish JE, Santoro MM, Morton SU, Yu S, Yeh RF, Wythe JD, Ivey KN, Bruneau BG, Stainier DY, Srivastava D. miR-126 regulates angiogenic signaling and vascular integrity. *Dev Cell*. Aug 2008;15(2):272-84. doi:10.1016/j.devcel.2008.07.008

309. Wang S, Aurora AB, Johnson BA, Qi X, McAnally J, Hill JA, Richardson JA, Bassel-Duby R, Olson EN. The endothelial-specific microRNA miR-126 governs vascular integrity and angiogenesis. *Dev Cell*. Aug 2008;15(2):261-71. doi:10.1016/j.devcel.2008.07.002

310. Karar J, Maity A. PI3K/AKT/mTOR pathway in angiogenesis. *Front Mol Neurosci*. 2011;4:51. doi:10.3389/fnmol.2011.00051

311. Alique M, Bodega G, Giannarelli C, Carracedo J, Ramirez R. MicroRNA-126 regulates Hypoxia-Inducible Factor-1alpha which inhibited migration, proliferation, and angiogenesis in

replicative endothelial senescence. *Sci Rep*. May 14 2019;9(1):7381. doi:10.1038/s41598-019-43689-3

312. Cheng L, Yu H, Yan N, Lai K, Xiang M. Hypoxia-inducible factor-1α target genes contribute to retinal neuroprotection. *Front Cell Neurosci*. 2017;11:20. doi:10.3389/fncel.2017.00020

313. Vadlapatla RK, Vadlapudi AD, Mitra AK. Hypoxia-inducible factor-1 (HIF-1): a potential target for intervention in ocular neovascular diseases. *Curr Drug Targets*. Jul 2013;14(8):919-35. doi:10.2174/13894501113149990015

314. Ito Y, Hart JR, Ueno L, Vogt PK. Oncogenic activity of the regulatory subunit p85beta of phosphatidylinositol 3-kinase (PI3K). *Proc Natl Acad Sci U S A*. Nov 25 2014;111(47):16826-9. doi:10.1073/pnas.1420281111

315. Sessa R, Seano G, di Blasio L, Gagliardi PA, Isella C, Medico E, Cotelli F, Bussolino F, Primo L. The miR-126 regulates angiopoietin-1 signaling and vessel maturation by targeting p85beta. *Biochim Biophys Acta*. Oct 2012;1823(10):1925-35. doi:10.1016/j.bbamcr.2012.07.011

316. Maehama T, Dixon JE. The tumor suppressor, PTEN/MMAC1, dephosphorylates the lipid second messenger, phosphatidylinositol 3,4,5-trisphosphate. *J Biol Chem*. May 29 1998;273(22):13375-8. doi:10.1074/jbc.273.22.13375

317. Jansen F, Yang X, Hoelscher M, Cattelan A, Schmitz T, Proebsting S, Wenzel D, Vosen S, Franklin BS, Fleischmann BK, Nickenig G, Werner N. Endothelial microparticle-mediated transfer of MicroRNA-126 promotes vascular endothelial cell repair via SPRED1 and is abrogated in glucose-damaged endothelial microparticles. *Circulation*. Oct 29 2013;128(18):2026-38. doi:10.1161/CIRCULATIONAHA.113.001720

318. Asgeirsdottir SA, van Solingen C, Kurniati NF, Zwiers PJ, Heeringa P, van Meurs M, Satchell SC, Saleem MA, Mathieson PW, Banas B, Kamps JA, Rabelink TJ, van Zonneveld AJ, Molema G. MicroRNA-126 contributes to renal microvascular heterogeneity of VCAM-1 protein expression in acute inflammation. *Am J Physiol Renal Physiol*. Jun 15 2012;302(12):F1630-9. doi:10.1152/ajprenal.00400.2011

319. Gustavsson C, Agardh CD, Zetterqvist AV, Nilsson J, Agardh E, Gomez MF. Vascular cellular adhesion molecule-1 (VCAM-1) expression in mice retinal vessels is affected by both hyperglycemia and hyperlipidemia. *PLoS One*. Sep 13 2010;5(9):e12699. doi:10.1371/journal.pone.0012699

320. Iliaki E, Poulaki V, Mitsiades N, Mitsiades CS, Miller JW, Gragoudas ES. Role of alpha 4 integrin (CD49d) in the pathogenesis of diabetic retinopathy. *Invest Ophthalmol Vis Sci*. Oct 2009;50(10):4898-904. doi:10.1167/iovs.08-2013

321. Matsumoto K, Sera Y, Ueki Y, Inukai G, Niiro E, Miyake S. Comparison of serum concentrations of soluble adhesion molecules in diabetic microangiopathy and macroangiopathy. *Diabet Med*. Oct 2002;19(10):822-6. doi:10.1046/j.1464-5491.2002.00799.x

322. Limb GA, Hickman-Casey J, Hollifield RD, Chignell AH. Vascular adhesion molecules in vitreous from eyes with proliferative diabetic retinopathy. *Invest Ophthalmol Vis Sci*. Sep 1999;40(10):2453-7.

323. Harris TA, Yamakuchi M, Ferlito M, Mendell JT, Lowenstein CJ. MicroRNA-126 regulates endothelial expression of vascular cell adhesion molecule 1. *Proc Natl Acad Sci U S A*. Feb 5 2008;105(5):1516-21. doi:10.1073/pnas.0707493105

324. Yan T, Liu Y, Cui K, Hu B, Wang F, Zou L. MicroRNA-126 regulates EPCs function: implications for a role of miR-126 in preeclampsia. *J Cell Biochem*. Sep 2013;114(9):2148-59. doi:10.1002/jcb.24563

325. Zhang Q, Kandic I, Kutryk MJ. Dysregulation of angiogenesis-related microRNAs in endothelial progenitor cells from patients with coronary artery disease. *Biochem Biophys Res Commun*. Feb 4 2011;405(1):42-6. doi:10.1016/j.bbrc.2010.12.119

326. Zernecke A, Bot I, Djalali-Talab Y, Shagdarsuren E, Bidzhekov K, Meiler S, Krohn R, Schober A, Sperandio M, Soehnlein O, Bornemann J, Tacke F, Biessen EA, Weber C. Protective role of CXC receptor 4/CXC ligand 12 unveils the importance of neutrophils in atherosclerosis. *Circ Res*. Feb 1 2008;102(2):209-17. doi:10.1161/CIRCRESAHA.107.160697

327. Zernecke A, Bidzhekov K, Noels H, Shagdarsuren E, Gan L, Denecke B, Hristov M, Koppel T, Jahantigh MN, Lutgens E, Wang S, Olson EN, Schober A, Weber C. Delivery of microRNA-126 by apoptotic bodies induces CXCL12-dependent vascular protection. *Sci Signal*. Dec 8 2009;2(100):ra81. doi:10.1126/scisignal.2000610

328. Mikkola HK, Gekas C, Orkin SH, Dieterlen-Lievre F. Placenta as a site for hematopoietic stem cell development. *Exp Hematol*. Sep 2005;33(9):1048-54. doi:10.1016/j.exphem.2005.06.011

329. Ottersbach K, Dzierzak E. Analysis of the mouse placenta as a hematopoietic stem cell niche. *Methods Mol Biol*. 2009;538:335-46. doi:10.1007/978-1-59745-418-6_17

330. Robin C, Bollerot K, Mendes S, Haak E, Crisan M, Cerisoli F, Lauw I, Kaimakis P, Jorna R, Vermeulen M, Kayser M, van der Linden R, Imanirad P, Verstegen M, Nawaz-Yousaf H, Papazian N, Steegers E, Cupedo T, Dzierzak E. Human placenta is a potent hematopoietic niche containing hematopoietic stem and progenitor cells throughout development. *Cell Stem Cell*. Oct 2 2009;5(4):385-95. doi:10.1016/j.stem.2009.08.020

331. Stanimirovic DB, Friedman A. Pathophysiology of the neurovascular unit: disease cause or consequence? *J Cereb Blood Flow Metab*. Jul 2012;32(7):1207-21. doi:10.1038/jcbfm.2012.25

332. Storkebaum E, Quaegebeur A, Vikkula M, Carmeliet P. Cerebrovascular disorders: molecular insights and therapeutic opportunities. *Nat Neurosci*. Oct 26 2011;14(11):1390-7. doi:10.1038/nn.2947

333. Shen Q, Goderie SK, Jin L, Karanth N, Sun Y, Abramova N, Vincent P, Pumiglia K, Temple S. Endothelial cells stimulate self-renewal and expand neurogenesis of neural stem cells. *Science*. May 28 2004;304(5675):1338-40. doi:10.1126/science.1095505

334. Garrigue P, Hache G, Bennis Y, Brige P, Stalin J, Pellegrini L, Velly L, Orlandi F, Castaldi E, Dignat-George F, Sabatier F, Guillet B. Erythropoietin Pretreatment of Transplanted Endothelial Colony-Forming Cells Enhances Recovery in a Cerebral Ischemia Model by Increasing Their Homing Ability: A SPECT/CT Study. *J Nucl Med*. Nov 2016;57(11):1798-1804. doi:10.2967/jnumed.115.170308

335. Otani A, Kinder K, Ewalt K, Otero FJ, Schimmel P, Friedlander M. Bone marrow-derived stem cells target retinal astrocytes and can promote or inhibit retinal angiogenesis. *Nat Med*. Sep 2002;8(9):1004-10. doi:10.1038/nm744

336. Otani A, Dorrell MI, Kinder K, Moreno SK, Nusinowitz S, Banin E, Heckenlively J, Friedlander M. Rescue of retinal degeneration by intravitreally injected adult bone marrow–derived lineage-negative hematopoietic stem cells. *Journal of Clinical Investigation*. 2004;114(6):765-774. doi:10.1172/jci200421686

337. Zagrean AM, Hermann DM, Opris I, Zagrean L, Popa-Wagner A. Multicellular Crosstalk Between Exosomes and the Neurovascular Unit After Cerebral Ischemia. Therapeutic Implications. *Front Neurosci*. 2018;12:811. doi:10.3389/fnins.2018.00811

338. Xiao S, Bucher F, Wu Y, Rokem A, Lee CS, Marra KV, Fallon R, Diaz-Aguilar S, Aguilar E, Friedlander M, Lee AY. Fully automated, deep learning segmentation of oxygen-induced retinopathy images. *JCI Insight*. Dec 21 2017;2(24)doi:10.1172/jci.insight.97585

339. Zudaire E, Gambardella L, Kurcz C, Vermeren S. A computational tool for quantitative analysis of vascular networks. *PLoS One*. 2011;6(11):e27385. doi:10.1371/journal.pone.0027385

340. Usui Y, Westenskow PD, Kurihara T, Aguilar E, Sakimoto S, Paris LP, Wittgrove C, Feitelberg D, Friedlander MS, Moreno SK, Dorrell MI, Friedlander M. Neurovascular crosstalk between interneurons and capillaries is required for vision. *J Clin Invest*. Jun 2015;125(6):2335-46. doi:10.1172/JCI80297

341. Srinivasan S, Yeri A, Cheah PS, Chung A, Danielson K, De Hoff P, Filant J, Laurent CD, Laurent LD, Magee R, Moeller C, Murthy VL, Nejad P, Paul A, Rigoutsos I, Rodosthenous R, Shah RV, Simonson B, To C, Wong D, Yan IK, Zhang X, Balaj L, Breakefield XO, Daaboul G, Gandhi R, Lapidus J, Londin E, Patel T, Raffai RL, Sood AK, Alexander RP, Das S, Laurent LC. Small RNA Sequencing across Diverse Biofluids Identifies Optimal Methods for exRNA Isolation. *Cell*. Apr 4 2019;177(2):446-462 e16. doi:10.1016/j.cell.2019.03.024

342. Srinivasan S, Treacy R, Herrero T, Olsen R, Leonardo TR, Zhang X, DeHoff P, To C, Poling LG, Fernando A, Leon-Garcia S, Knepper K, Tran V, Meads M, Tasarz J, Vuppala A, Park S, Laurent CD, Bui T, Cheah PS, Overcash RT, Ramos GA, Roeder H, Ghiran I, Parast M, Consortium PS, Breakefield XO, Lueth AJ, Rust SR, Dufford MT, Fox AC, Hickok DE, Burchard J, Boniface JJ, Laurent LC. Discovery and Verification of Extracellular miRNA Biomarkers for Non-invasive Prediction of Pre-eclampsia in Asymptomatic Women. *Cell Rep Med*. May 19 2020;1(2)doi:10.1016/j.xcrm.2020.100013

343. Schwarzenbach H, da Silva AM, Calin G, Pantel K. Data Normalization Strategies for MicroRNA Quantification. *Clin Chem*. Nov 2015;61(11):1333-42. doi:10.1373/clinchem.2015.239459

344. Endzelins E, Berger A, Melne V, Bajo-Santos C, Sobolevska K, Abols A, Rodriguez M, Santare D, Rudnickiha A, Lietuvietis V, Llorente A, Line A. Detection of circulating miRNAs: comparative analysis of extracellular vesicle-incorporated miRNAs and cell-free miRNAs in whole plasma of prostate cancer patients. *BMC Cancer*. Nov 9 2017;17(1):730. doi:10.1186/s12885-017-3737-z

345. Price ND, Trent J, El-Naggar AK, Cogdell D, Taylor E, Hunt KK, Pollock RE, Hood L, Shmulevich I, Zhang W. Highly accurate two-gene classifier for differentiating gastrointestinal stromal tumors and leiomyosarcomas. *Proc Natl Acad Sci U S A*. Feb 27 2007;104(9):3414-9. doi:10.1073/pnas.0611373104

346. Trajkovic K, Hsu C, Chiantia S, Rajendran L, Wenzel D, Wieland F, Schwille P, Brugger B, Simons M. Ceramide triggers budding of exosome vesicles into multivesicular endosomes. *Science*. Feb 29 2008;319(5867):1244-7. doi:10.1126/science.1153124

347. Kosaka N, Iguchi H, Yoshioka Y, Takeshita F, Matsuki Y, Ochiya T. Secretory mechanisms and intercellular transfer of microRNAs in living cells. *J Biol Chem*. Jun 4 2010;285(23):17442-52. doi:10.1074/jbc.M110.107821

348. Li J, Liu K, Liu Y, Xu Y, Zhang F, Yang H, Liu J, Pan T, Chen J, Wu M, Zhou X, Yuan Z. Exosomes mediate the cell-to-cell transmission of IFN-alpha-induced antiviral activity. *Nat Immunol*. Aug 2013;14(8):793-803. doi:10.1038/ni.2647

349. Smith LE. Pathogenesis of retinopathy of prematurity. *Growth Horm IGF Res*. Jun 2004;14 Suppl A:S140-4. doi:10.1016/j.ghir.2004.03.030

350. Stahl A, Connor KM, Sapieha P, Chen J, Dennison RJ, Krah NM, Seaward MR, Willett KL, Aderman CM, Guerin KI, Hua J, Lofqvist C, Hellstrom A, Smith LE. The mouse retina as an angiogenesis model. *Invest Ophthalmol Vis Sci*. Jun 2010;51(6):2813-26. doi:10.1167/iovs.10-5176

351. Blanks JC, Johnson LV. Vascular atrophy in the retinal degenerative rd mouse. *J Comp Neurol*. Dec 22 1986;254(4):543-53. doi:10.1002/cne.902540407

352. Gargini C, Terzibasi E, Mazzoni F, Strettoi E. Retinal organization in the retinal degeneration 10 (rd10) mutant mouse: a morphological and ERG study. *J Comp Neurol*. Jan 10 2007;500(2):222-38. doi:10.1002/cne.21144

353. Eadie BD, Etminan M, Carleton BC, Maberley DA, Mikelberg FS. Association of repeated intravitreous bevacizumab injections with risk for glaucoma surgery. *JAMA Ophthalmol*. Apr 1 2017;135(4):363-368. doi:10.1001/jamaophthalmol.2017.0059

354. Li Z, Xu R, Zhu X, Li Y, Wang Y, Xu W. MicroRNA-23a-3p improves traumatic brain injury through modulating the neurological apoptosis and inflammation response in mice. *Cell Cycle*. Jan 2020;19(1):24-38. doi:10.1080/15384101.2019.1691763

355. Zhao H, Tao Z, Wang R, Liu P, Yan F, Li J, Zhang C, Ji X, Luo Y. MicroRNA-23a-3p attenuates oxidative stress injury in a mouse model of focal cerebral ischemia-reperfusion. *Brain Res*. Dec 10 2014;1592:65-72. doi:10.1016/j.brainres.2014.09.055

356. He Y, Cai Y, Pai PM, Ren X, Xia Z. The causes and consequences of miR-503 dysregulation and Its impact on cardiovascular disease and cancer. Review. *Frontiers in Pharmacology*. 2021-March-08 2021;12(174)doi:10.3389/fphar.2021.629611

357. Sun SL, Shu YG, Tao MY. miR-503 inhibits proliferation, migration, and angiogenesis of glioma by acting on VEGFA through targeting LRIG2. *Cancer Manag Res*. 2019;11:10599-10608. doi:10.2147/CMAR.S222681

358. Wei L, Sun C, Zhang Y, Han N, Sun S. miR-503-5p inhibits colon cancer tumorigenesis, angiogenesis, and lymphangiogenesis by directly downregulating VEGF-A. *Gene Ther*. Jun 12 2020;doi:10.1038/s41434-020-0167-3

359. Zhou B, Ma R, Si W, Li S, Xu Y, Tu X, Wang Q. MicroRNA-503 targets FGF2 and VEGFA and inhibits tumor angiogenesis and growth. *Cancer Lett*. Jun 10 2013;333(2):159-69. doi:10.1016/j.canlet.2013.01.028

360. Yang HK, Chen H, Mao F, Xiao QG, Xie RF, Lei T. Downregulation of LRIG2 expression inhibits angiogenesis of glioma via EGFR/VEGF-A pathway. *Oncol Lett*. Oct 2017;14(4):4021-4028. doi:10.3892/ol.2017.6671

361. Lange C, Storkebaum E, de Almodovar CR, Dewerchin M, Carmeliet P. Vascular endothelial growth factor: a neurovascular target in neurological diseases. *Nat Rev Neurol*. Aug 2016;12(8):439-54. doi:10.1038/nrneurol.2016.88